Non-Orthogonal Multiple Access for 5G: Design and Performance Enhancement

by

Yuanwei Liu

Doctor of Philosophy

School of Electronic Engineering and Computer Science
Queen Mary University of London
United Kingdom

May 2016

TO MY FAMILY

Acknowledgments

Foremost, I would like to express my sincere gratitude to my supervisors, Dr. Maged Elkashlan and Dr. Akram Alomainy, for their continuous support of my Ph.D research. Special thanks to my primary supervisor, Dr. Maged Elkashlan, who provided valuable technical guidance and constructive suggestions on my research works and directions. During the past three years, working with Maged is a wonderful experience. His wide knowledge, strong research enthusiasm and hard-working attitude have inspired me during all my PhD period, and will have a profound effect on my future carrier. I am extremely lucky to have such a nice supervisor as well as an interesting friend. I could not have imagined having a better supervisor and mentor for my Ph.D research.

I would like to thank all my collaborators: Dr. Tran Trung Duy, Dr. Trung Q. Duong, Dr. Syed Ali Raza Zaidi, Dr. S. Ali Mousavifar, Prof. Cyril Leung, Prof. Zhiguo Ding, Prof. Jinhong Yuan, Prof. H. Vincent Poor, Prof. Jinho Choi, Dr. Qi Sun, Dr. Chih-Lin I, Dr. Yue Gao, Prof. Lajos Hanzo, Prof. George K. Karagiannidis, Prof. Arumugam Nallanathan, Prof. Qiang Ni, Prof. Xin Sun, Dr. Kok Keong Chai, Dr. Yue Chen, and Dr. Jesus Alonso-Zarate for their helpful suggestions and comments on my research. I would like to special thank Dr. Trung Q. Duong for hosting my visit in Queen's University Belfast. I also would like to special thank Prof. Zhiguo Ding for hosting my visit in Lancaster University.

I would also like to thank Dr. Nan Wang, Dr. Yue Liu, Dr. Dan Zhao, Dr. Xinyue Wang, Dr. Yun Li, Jie Deng, Dr. Gareth Tyson, Dr. Dantong Liu, Dr. Lifeng Wang, Dr. Yansha Deng, Dr. Zhiyuan Shi, Dr. Zhijin Qin, Jingjing Zhao, Hanxiao Wang, Liumeng Song, Anqi He, Xiuxian Lao, Bingyu Xu, Tianhao Guo, Jingze Yang, Yanru Wang, Yuhang Dai, Yuan Ma, Xingjian Zhang, Fenyu Jiang, Aini Li, Yuhui Yao, and all my colleges and friends in network group, antenna group, and computer vision group

at Queen Mary University of London, for their constant encouragement and kind help. I really have had a wonderful memories in my Ph.D life and study.

Last and the most importantly, I would like to express my deepest gratitude to my beloved family, especially my parents, who always unconditionally support me at any time. Meanwhile, this thesis is specially dedicated to my deeply loved grandmother, and may her soul rest in peace.

Abstract

Spectrum scarcity is one of the most important challenges in wireless communications networks due to the sky-rocketing growth of multimedia applications. As the latest member of the multiple access family, non-orthogonal multiple access (NOMA) has been recently proposed for 3GPP Long Term Evolution (LTE) and envisioned to be a key component of the 5th generation (5G) mobile networks for its potential ability on spectrum enhancement. The feature of NOMA is to serve multiple users at the same time/frequency/code, but with different power levels, which yields a significant spectral efficiency gain over conventional orthogonal multiple access (OMA). This thesis provides a systematic treatment of this newly emerging technology, from the basic principles of NOMA, to its combination with simultaneously information and wireless power transfer (SWIPT) technology, to apply in cognitive radio (CR) networks and Heterogeneous networks (HetNets), as well as enhancing the physical layer security and addressing the fairness issue.

First, this thesis examines the application of SWIPT to NOMA networks with spatially randomly located users. A new cooperative SWIPT NOMA protocol is proposed, in which near NOMA users that are close to the source act as energy harvesting relays in the aid of far NOMA users. Three user selection schemes are proposed to investigate the effect of locations on the performance. Besides the closed-form expressions in terms of outage probability and throughput, the diversity gain of the considered networks is determined.

Second, when considering NOMA in CR networks, stochastic geometry tools are used to evaluate the outage performance of the considered network. New closed-form expressions are derived for the outage probability. Diversity order of NOMA users has been analyzed based on the derived outage probability, which reveals important design insights

regarding the interplay between two power constraints scenarios.

Third, a new promising transmission framework is proposed, in which massive multiple-input multiple-output (MIMO) is employed in macro cells and NOMA is adopted in small cells. For maximizing the biased average received power at mobile users, a massive MIMO and NOMA based user association scheme is developed. Analytical expressions for the spectrum efficiency of each tier are derived using stochastic geometry. It is confirmed that NOMA is capable of enhancing the spectrum efficiency of the network compared to the OMA based HetNets.

Fourth, this thesis investigates the physical layer security of NOMA in large-scale networks with invoking stochastic geometry. Both single-antenna and multiple-antenna aided transmission scenarios are considered, where the base station (BS) communicates with randomly distributed NOMA users. In addition to the derived exact analytical expressions for each scenario, some important insights such as secrecy diversity order and large antenna array property are obtained by carrying the asymptotic analysis.

Fifth and last, the fundamental issues of fairness surrounding the joint power allocation and dynamic user clustering are addressed in MIMO-NOMA systems in this thesis. A two-step optimization approach is proposed to solve the formulated problem. Three efficient suboptimal algorithms are proposed to reduce the computational complexity. To further improve the performance of the worst user in each cluster, power allocation coefficients are optimized by using bi-section search. Important insights are concluded from the generated simulate results.

Table of Contents

List of Figures

List of Tables

List of Abbreviations

AN	Artificial Noise
AF	Amplify-and-Forward
AWGN	Additive White Gaussian Noise
BS	Base Station
BF	Beamforming
BPP	Binomial Point Process
CDMA	Code Division Multiple Access
CF	Compress-and-Forward
CoMP	Coordinated Multipoint
CR	Cognitive Radio
C-RAN	Cloud-based Radio Access Networks
CS	Compressive Sensing
CSI	Channel State Information
CSIT	Channel State Information at the Transmitter
CDF	Cumulative Distribution Function
D2D	Device-to-Device
DF	Decode-and-Forward
DPC	Dirty-Paper Coding
FCC	Federal Communications Commission
FD	Full-Duplex
FDMA	Frequency Division Multiple Access

HCPP	Hard Core Point Process
HetNets	Heterogeneous Networks
HPPPs	Homogeneous Poisson Point Processes
i.i.d.	Independent and Identically Distributed
IoT	Internet of Things
LTE	Long Term Evolution
LUs	Legitimate Users
MA	Multiple Access
M2M	Machine-to-Machine
mmWave	Millimeter Wave
MRC	Maximal Ratio Combining
MIMO	Multi-Input and Multi-Output
MISO	Multiple-input Single-output
MUSA	Multi-User Shared Access
NNNF	Nearest Near user and Nearest Far user
NNFF	Nearest Near user and Farthest Far user
NOMA	Non-Orthogonal Multiple Access
OFDMA	Orthogonal Frequency Division Multiple access
OMA	Orthogonal Multiple Access
PA	Power Allocation
PDMA	Pattern Division Multiple Access
PN	Primary Network
PCP	Poisson Cluster Process
PLS	Physical Layer Secerity
PPP	Poisson Point Process
PR	Primary Receiver
PT	Primary Transmitter
PU	Primary User

PDF	Probability Density Function
P2P	Peer-to-Peer
QoS	Quality of Service
RB	Resource Block
RF	Radio Frequency
RNRF	Random Near user and Random Far user
SC	Superposition Coding
SCMA	Sparse Code Multiple Access
SDN	Software Defined Networks
SIC	Successive Interference Cancellation
SN	Secondary Network
SR	Secondary Receiver
ST	Secondary Transmitter
SU	Secondary User
SISO	Single Input Single Output
SNR	Signal-to-Noise Ratio
SINR	Signal-to-Interference-Plus-Noise Ratio
SOP	Secrecy Outage Probability
SWIPT	Simultaneous Wireless Information and Power Transfer

TDMA	Time Division Multiple Access
TPC	Transmit Precoding
WNV	Wireless Network Visualization
WPT	Wireless Power Transfer
ZF	Zero-forcing
ZFBF	Zero-forcing Beamforming
1G	First Generation
2G	Second Generation
3G	Third Generation
3GPP	Third Generation Partnership Project
4G	Fourth-Generation
5G	Fifth-Generation

Chapter 1

Introduction

1.1 Background

1.1.1 On the way to 5G

As the long-term evolution (LTE) system is reaching maturity and the fourth generation (4G) has commercially deployed, a certain number of researchers have pondered over the ways and means for the coming fifth generation (5G) cellular network. The 5G networks is with high expectation on making substantial breakthrough beyond the previous four generations, especially on the provision of at least 1,000 times higher system capacity, 10 times higher spectrum efficiency and 10 times lower energy efficiency per service than 4G networks [1]. Towards these direction, several key technologies and approaches such as ultra-densification, millimeter wave (mmWave), massive multiple-input multiple-output (MIMO), device-to-device (D2D) and machine-to-machine (M2M) communication, full-duplex (FD) communication, energy harvesting, cloud-based radio access networks (C-RAN), wireless network visualization (WNV), and software defined networks (SDN) were identified by researchers.

1.1.2 Multiple Access Techniques for 5G

Apart from the aforementioned approaches, multiple access (MA) technology is also regarded as one of the most fundamental aspect in physical layer, which have significantly varied in each generation wireless networks and affected the definition of technical feature to a large extent. Looking back on the development of the MA formats, in the first generation (1G), the MA is frequency division multiple access (FDMA), which is an analog frequency modulation based technology. From the secondary generation (2G), the MA began to transform into a digital modulation format—time division multiple access (TDMA) by exploiting time multiplexing. Then the code division multiple access (CDMA), which was proposed by Qualcomm [2], became the dominant MA standard in the third generation (3G) networks. In an effort to overcome the limitations of CDMA which is not capable of supporting high-speed data rates, orthogonal frequency division multiple access (OFDMA) was dominantly adopted in 4G networks [3].

Due to the fact that the unprecedented expansion of new Internet-enabled smart devices, applications and services is expediting the development of the 5G networks, the MA technology is also required to be reconsidered. Non-orthogonal multiple access (NOMA), which has been recently proposed for 3GPP Long Term Evolution (LTE) [4, 5], is expected to have a superior spectral efficiency. It has also been pointed out that NOMA has the potential to be integrated with existing MA paradigms, since it exploits the new dimension of the power domain. The key idea of NOMA is to ensure that multiple users can be served within a given resource slot (e.g., time/frequrecy/code), by applying successive interference cancellation (SIC), which is fundamentally different from conventional orthogonal MA technologies (e.g., FDMA/TDMA/CDMA/OFDMA). The motivation behind this approach lies in the fact that NOMA can use spectrum more efficiently by opportunistically exploring users' channel conditions [6] and is capable of serving multiple users with different quality of service (QoS) requirements in the same resource slot.

1.2 Motivation and Contributions

As a promising candidate for future 5G systems, the NOMA transmission mainly exhibits the following main advantages.

- **High spectrum efficiency**: Spectrum efficiency, is one of the well accepted performance metrics in wireless networks. NOMA exhibits a high spectrum efficiency to improve the sum system throughput, which is attributed to the fact that NOMA allows one resource block (RB) (e.g., time/frequecy/code) to be occupied by multiple users [7].

- **Fairness-throughput tradeoff**: One key feature of NOMA is to allocate more power to the weak user, which is different from the conventional popular power allocation (PA) policies such as water filling PA[1] [4]. By doing so, NOMA is capable of guaranteeing a good tradeoff between the fairness among users and system throughput.

- **Ultra-high connectivity**: The future 5G systems are envisioned to support the connection of billions of smart devices (e.g., Internet of Things (IoT)). The existence of NOMA offers a promising approach to efficiently solve this non-trivial task by fully exploiting the non-orthogonal characteristic. More specifically, unlike convectional orthogonal multiple access (OMA) which requires equal number of RBs to support these equal number devices, NOMA is able to serve them with occupying much less RBs.

- **Good compatibility**: From the theoretic perspective, NOMA can be an "add-on" technique to any exiting OMA techniques (e.g., TDMA/FDMA/CDMA/OFDMA), due to the fact that it exploits a new power dimension. Also, with the mature development of superposition coding (SC) and SIC technologies both in theory and practice, it is very promising that NOMA is capable of achieving good compatibility

[1]Note that the advantage of water filling PA strategy is that it can achieve the optimal system throughput but with lower user fairness.

with the existing MA techniques.

- **Open flexibility**: Compared to other existing techniques for MA, such as multi-user shared access (MUSA), pattern division multiple access (PDMA), sparse code multiple access (SCMA) [8], NOMA provides an easy-understanding and low complexity design [4]. In fact, the fundamental principle of the aforementioned MA schemes and NOMA are very similar, which is to allocate multiple users in a single RB. Taking the comparison of NOMA and SCMA as an example, SCMA can be regarded as a developed technologies of NOMA which integrates appropriate sparse coding, modulation and subcarrier allocation.

Motivated by the advantages aforementioned, and along with the recent developments on NOMA, this thesis spans the system design and performance enhancement of NOMA. More particularly, the research of this thesis first investigates novel system designs with integrating NOMA with recent advanced technologies such as simultaneous wireless information and power transfer (SWIPT), cognitive radio (CR), and heterogeneous networks (HetNets) for further performance enhancement. Then it focuses on addressing two important issues of NOMA—physical layer security issue and fairness issue in MIMO-NOMA systems. The specific motivations and contributions of this dissertation are summarized in the following.

1.2.1 Cooperative NOMA with Simultaneous Wireless Information and Power Transfer

One important advantage of the NOMA concept is that it can squeeze a user with better channel conditions into a channel that is occupied by a user with worse channel conditions [6]. For example, consider a downlink scenario in which there are two groups of users: 1) near users, which are close to the base station (BS) and often have better channel conditions; and 2) far users, which are close to the edge of the cell controlled by the BS and therefore often have worse channel conditions. While the spectral efficiency

of NOMA is superior compared to that of OMA [5, 9], the fact that the near users co-exist with the far users causes performance degradation to the far users. In order to improve the reliability of the far users, an efficient method was proposed in [10] by applying cooperative transmission to NOMA. The key idea of this cooperative NOMA scheme is that the users that are close to the BS are used as relays to help the far users with poor channel conditions. The advantage of implementing cooperative transmission in NOMA systems is that successive interference cancelation is used at the near users and hence the information of the far users is known by these near users. In this case, it is natural to consider the use of the near users as decode-and-forward (DF) relays to transmit information to the far users.

In Chapter 3, this setting was considered, but with the additional feature that the near users are energy constrained and hence harvest energy from their received radio frequency (RF) signals. To improve the reliability of the far NOMA users without draining the near users' batteries, the application of SWIPT to NOMA is considered, where SWIPT is performed at the near NOMA users. Therefore, the aforementioned two communication concepts, cooperative NOMA and SWIPT, can be naturally linked together, and a new spectral and energy efficient wireless MA protocol, namely, the cooperative SWIPT NOMA protocol, is proposed in Chapter 3. In order to investigate the impact of the locations of randomly deployed users on the performance of the proposed protocol, tools from stochastic geometry are used. Particularly, users are spatially randomly deployed in two groups via homogeneous Poisson point processes (PPPs). Here, the near users are grouped together and randomly deployed in an area close to the BS. The far users are in the other group and are deployed close to the edge of the cell controlled by the BS.

Since NOMA is co-channel interference limited, it is important to combine NOMA with conventional OMA technologies and realize a new hybrid MA network. For example, first users can be grouped in pairs to perform NOMA, and then conventional time/frequency/code division MA is applied to serve the different user pairs. Note that

this hybrid MA scheme can effectively reduce the system complexity since fewer users are grouped together for the implementation of NOMA. Based on the proposed protocol and the considered stochastic geometric model, a natural question arises: which near NOMA user should help which far NOMA user? To investigate the performance of one pair of selected NOMA users, three opportunistic user selection schemes are proposed, based on locations of users to perform NOMA in Chapter 3.

1.2.2 NOMA in Large-Scale Underlay Cognitive Radio Networks

Spectrum efficiency is of significant importance and becomes one of the main design targets for future 5G networks. One important approach to improve spectrum efficiency is the paradigm of underlay CR networks, which was proposed in [11] and has rekindled increasing interest in using spectrum more efficiently. The key idea of underlay CR networks is that each secondary user (SU) is allowed to access the spectrum of the primary users (PUs) as long as the SU meets a predetermined interference threshold constraint in the primary network (PN).

Motivated by this, in Chapter 4, the application of NOMA in underlay CR networks is considered, with using additional power control at the secondary base station (BS) to improve the spectral efficiency. Stochastic geometry is used to model a large-scale CR network with a large number of randomly deployed primary transmitters (PTs) and primary receivers (PRs). In order to characterize the performance of the considered network, new closed-form expressions of the outage probability are derived using stochastic-geometry. More importantly, by carrying out the diversity analysis, new insights are obtained under the two scenarios with different power constraints: 1) fixed transmit power of the PTs, and 2) transmit power of the PTs being proportional to that of the secondary base station. A pivotal conclusion is reached that by carefully designing target data rates and power allocation coefficients of users, NOMA can outperform conventional OMA in underlay CR networks.

1.2.3 NOMA in Massive MIMO aided HetNets

HetNets, massive MIMO and millimeter wave (mmWave) as the "big three" technologies [12], laid the fundamental structure for emerging 5G communication systems. It is believed that the novel structure design—by introducing NOMA based small cells in massive MIMO enabled HetNets—can be a new highly rewarding candidate, which will contribute to the design of a more promising 5G system due to the following key advantages: 1) In NOMA based HetNets, with employing higher BS densities, BSs are capable of accessing the served users closer, which can increase the signal to interference and noise ratio (SINR) by intelligently tracking the multi-category interference, such as inter/intra-tier interference and intra-BS interference. 2) With applying NOMA in the single-antenna based small cells, the complex precoding/cluster design for MIMO-NOMA systems can be avoided. 3) NOMA is capable of dealing with the fairness issue by allocating more power to weak users, which is of great significance for HetNets when investigating efficient resource allocation in the sophisticated multi-tier networks.

Motivated by the aforementioned potential benefits, in Chapter 5, a novel hybrid HetNets framework is proposed, with NOMA based small cells and massive MIMO aided macro cells to further enhance the performance of existing HetNets design. For maximizing the biased average received power at mobile users, a massive MIMO and NOMA based user association scheme is developed. In an effort to evaluate the performance of the proposed framework, analytical expressions for the spectrum efficiency of each tier are derived using stochastic geometry. The performance gap of NOMA based and OMA based HetNets is confirmed.

1.2.4 Security Enhancement to NOMA in Large-Scale Networks

It is currently noted that wireless networks are confronted with security issues since the broadcast nature of the wireless medium is susceptible to potential security threats such as eavesdropping and impersonation. The concept of physical layer security (PLS),

which was proposed by Wyner as early as 1975 from an information-theoretical perspective [13], has sparked of wide-spread recent interest. Compared with convectional networks, the major specialties of PLS in NOMA networks are: NOMA users with weak channel conditions are subject to the interference from the superposed signals while users with strong channel condition are capable of canceling this part of interference. As such, the weak one of NOMA users is more susceptible to security threats.

Motivated to enhance the PLS of NOMA, in Chapter 6, the scenario of large-scale networks where a BS supports randomly roaming NOMA users is considered. An eavesdropper-exclusion zone is introduced around the BS for improving the secrecy performance of the large-scale networks considered in which no eavesdroppers are allowed to roam. Specifically, both a single-antenna scenario and a multiple-antenna scenario at the BS are considered. 1) For the single-antenna scenario, M NOMA users are randomly roaming in a finite disc (user zone) with the quality-order of their channel conditions known at the BS. 2) For the multiple-antenna scenario, beamforming is invoked at the BS for generating artificial noise (AN). New exact expressions of the security outage probability are derived for both single-antenna and multiple-antenna aided scenarios. It is demonstrated that the security performance of the NOMA networks can be improved by invoking the protected zone and by generating artificial noise at the BS.

1.2.5 Fairness of MIMO-NOMA systems

The multiple antenna techniques is of significant importance for each generation of MA systems, since it brings an extra dimension — spatial domain for further performance improvements. However, the distinct characteristics (e.g., channel ordering and power allocation) inevitably necessitate the redesign of the multiple antenna NOMA systems. To solve this problem, a cluster based MIMO-NOMA structure was designed in [14], but with considering fixed power allocation and the same number of users in each cluster. Also, due to the fact that NOMA is based on SIC technique, users could achieve unequal rates with different power allocation. As such, fairness is an important issue for NOMA

in each application scenarios [15].

Motivated by this, in Chapter 7, a dynamic user allocation and power optimization problem is investigated by considering the fairness issue in cluster-based MIMO-NOMA systems. In order to solve this optimization problem, three sub-optimal algorithms are proposed to realize different tradeoffs of complexity and throughput of the worst user. In addition, for each given user clustering case, the power allocation coefficients are optimized for the users in each cluster by adopting a bisection search based algorithm. It is worth noting that top-down B algorithm can achieve a good tradeoff between complexity and throughput compared to top-down A and bottom up algorithms.

1.3 Related Works

In this section, the related works of this thesis surrounding NOMA and other emerging technologies are discussed.

1.3.1 Non-orthogonal multiple access

NOMA techniques have received remarkable attention both in the world of academia and industry. In this subsection, the related works of NOMA are introduced from the single antenna NOMA, multiple antenna NOMA and cooperative NOMA.

1.3.1.1 NOMA in Single-Antenna systems

Regarding downlink scenarios, in [7], a two-user NOMA downlink transmission which adopted SIC receivers was proposed. With taking further practical consideration on the key link adaptation functionalities of the LTE, the system-level performance was evaluated in [5, 16]. Ding *et al.* [9] investigated the performance of the NOMA downlink for randomly roaming users. It was shown that NOMA is indeed capable of achieving

a better performance than their traditional OMA counter parts. Xu *et al.* [17] developed a new evaluation criterion to examine the performance gain of NOMA over OMA from the view of information theory. More specifically, considering a simple two-user single-antenna scenarios with Gaussian broadcasting (BC), the comparison of TDMA and NOMA in terms of capacity region and two rate regions was shown in [17]. By considering the user fairness of a NOMA system, a user-power allocation optimization problem was addressed by Timotheou and Krikidis [15]. Regarding uplink NOMA scenarios, an uplink NOMA transmission scheme was proposed in [18], and its performance was evaluated systematically. As an investigating extension of [18], a novel iterative multiuser detection and decoding strategy was designed to further enhance the performance of uplink NOMA transmission in [19]. In an effort to lower the implementation complexity, Chen *et al.* [20] considered to apply a user-pairing based suboptimal policy for facilitating the uplink NOMA transmission. In [21], Zhang *et al.* proposed a novel power control strategy for uplink NOMA transmission and theoretically investigated the outage probability and the delay-limited sum rate.

1.3.1.2 NOMA in Multiple-Antenna systems

While the aforementioned NOMA works focus on single-antenna scenarios, to further improve the performance of NOMA systems, multiple antennas were introduced in NOMA. The application of multiple antenna techniques in NOMA has attached substantial interests from both academia [14, 22–31] and industry [7, 22, 32, 33]. For MISO-NOMA scenarios, Choi [24] proposed a two-stage multicast beamforming with SC method for downlink transmission, in which a zero-forcing (ZF) beamforming was employed to avoid inter-group/cluster interference first, and then the optimal beamforming vectors was considered to minimize the total transmitting power within each group/cluster. By exploiting receive beamforming at the side of NOMA users for suppressing the interference, Higuchi and Benjebbour [22] investigated a less restrictive beamforming design at the BS compared with ZF for both the downlink and uplink

transmissions. In [26], Hanif *et al.* solved the downlink sum rate maximization problem with obtaining the complex precoding vectors, under the vector-based decoding constraints which guaranteed SIC is able to be performed at better users.

For MIMO-NOMA scenarios, Higuchi and Kishiyama [32] proposed a novel scheme which simultaneously applying open loop-type random beamforming and the intra-beam SIC for downlink NOMA transmission. However, the random beamforming may bring uncertainties for the quality of service (QoS) at users' side, which will degrade the system performance. To overcome this issue, in [14], Ding *at el* proposed a precoding and detection matrix design for a cluster-based downlink MIMO-NOMA scenario with fixed power allocation. By adopting this design, the considered MIMO-NOMA systems can be decomposed into several independent single-input single-output (SISO) NOMA channels and such conventional NOMA can be applied. Furthermore, in order to establish a more general framework both considering downlink and uplink MIMO-NOMA transmission and seek larger diversity gain, a more sophisticated approach which combined with signal alignment (SA) was proposed in [25]. Stochastic geometry tools are invoked to model NOMA users and interferers to capture the impact of the locations. Note that the existing works on NOMA design always relied on assuming different channel conditions of users, which is, nevertheless, a strong assumption. Motivated by confronting this challenge and enabling NOMA can be applied in more general scenarios, Ding *at el* [28] designed a precoding and detection approach which is capable of establishing significantly different channel gains for users in IoT scenarios. Sun *et al.* [23] first investigated an power optimization problem for maximizing the ergodic capacity and showed that the proposed MIMO-NOMA schemes is able to achieve significantly better performance than OMA. In an effort to further lower the decoding complexity at users, a layered transmission MIMO-NOMA scheme was proposed by Choi [27] by investigating an optimal power allocation problem. It was demonstrated that with invoking layered transmission scheme, the sum rates still grow linearly with the antenna number, which is similar to the conventional MIMO. In [34], Ding and Poor employed the clustering MIMO-NOMA

design and decomposed the channels of massive-MIMO-NOMA into a number of SISO-NOMA channel. A one-bit feedback scheme for the designed massive-MIMO-NOMA systems was proposed to lower the implementation complexity.

1.3.1.3 NOMA and cooperative transmission

The recent research works associated to NOMA with cooperative relaying systems are based on two common relay protocols, namely, amplify-and-forward (AF) relay protocol and DF relay protocol. For AF relaying, Men and Ge investigated the outage performance of the systems in single antenna AF relay aided NOMA downlink transmission scenarios, while both the BS and the users were equipped with single antenna in [35] and multiple antenna in [36]. It also illustrated the potential gains of NOMA over OMA in both two scenarios. Regarding the DF relaying protocol, apart form the well integration with the cooperative NOMA protocol which is proposed by in [10], a DF based two-stage relaying protocol was proposed in [37].

Apart from extending the transmission coverage of wireless networks, another key aspect of cooperative communication is to generate spatial diversity for combating the deleterious fading. Coordinate multi-point (CoMP) transmission, as an effective approach to mitigate the interference, is particularly capable of improving the performance of the users at the edge of the cell. In [38], Choi first attempted to employe NOMA into CoMP transmission system for spectral efficiency improvement. A new coordinated superposition coding scheme with the aid of Alamouti code was proposed. In an effort to explore more efficient design approach, Tian *et al.* [39] proposed a novel opportunistic NOMA transmission scheme in CoMP system and showed the effectiveness compared with the convectional joint-transmission NOMA. In [40], Kim and Lee considered a coordinated direct and relay transmission scheme, where the BS communicated with a near user and a relay simultaneously with invoking NOMA technique during the first phase, while communicated with a far user with the aid of the relay. In [41], Vien *et al.* proposed a NOMA based power allocation for a downlink CRAN scenario, which can be also regarded as a

coordinated transmission scenario where all the BSs are controlled by a cloud.

1.3.2 Other Related Emerging Technologies

In this subsection, the related works of other emerging technologies applied in this thesis are introduced, such as underlay cognitive radio (CR) networks, massive MIMO aided Hetnets, RF wireless power transfer and PLS.

1.3.2.1 Underlay Cognitive Radio Networks

The underlay CR is like an intelligent interference controlling paradigm, in which SUs are permitted to access the spectrum allocated to PUs as long as the interference power constraint is satisfied [42]. In [43], an underlay CR network taking into account the spatial distribution of the SU relays and PUs was considered and its performance was evaluated by using stochastic geometry tools. In [6], a new CR inspired NOMA scheme was proposed and the impact of user pairing was examined, by focusing on a simple scenario with only one PT.

Since point-to-point communications in CR networks is well established in the existing literature, recent research on CR mainly focused on cooperative relaying. In [44], a scenario with a single source-destination pair, assisted by a group of cognitive relay nodes, is considered. In [45], considering a relay selection criterion, the outage probability of cognitive relay networks is evaluated. Note that the aforementioned works mainly consider single primary transmitter and receiver. For the multiple primary transmitters and receivers case, the outage performance of cognitive relay networks with single antenna and MIMO is investigated in [46] and [47].

1.3.2.2 Massive MIMO and Hetnets

The massive MIMO regime enable to equip tens of hundreds/thousands antennas at a BS, and hence is capable of offering an unprecedented level of freedom to serve multiple mobile users. The core idea of HetNets is to establish closer BS-user link by densely overlaying small cells. By doing so, the promising benefits such as lower power consumption, higher throughput and enhanced spatial reuse of spectrum can be experienced. Aiming to fully take advantages of both massive MIMO and HetNets, several research contributions have been made [48–50]. In [48], the interference coordination issue of massive MIMO enabled HetNets was addressed by utilizing the spatial blanking of macro cells. In [49], the authors investigated a joint user association and interference management optimization problem in massive MIMO HetNets. By applying stochastic geometry model, the spectrum efficiency of uplink massive MIMO aided HetNets was evaluated in [50].

Regarding NOMA systems related to HetNets, in an effort to intelligently cope with the interference from multi-layers, in [51], Xu *et al.* proposed a cooperative NOMA scheme in HetNets and minimized the inter-user interference with the aid of dirty paper coding (DPC) precoding. The distinct power disparity between the macro BSs and pico BSs was investigated.

1.3.2.3 RF Wireless Power Transfer

Recently, harvesting energy from ambient RF signals has received increasing attention due to its convenience in providing energy self-sufficiency to a low power communication system [52]. With recent advances in the technology of low power devices both in industry [53] and academia [54, 55], it is expected that harvesting energy from RF signals will provide a practically realizable solution for future applications, especially for networks with low power devices such as wireless sensor network nodes [56, 57].

SWIPT, which was initially proposed in [58], has rekindled the interest of researchers

to explore more energy efficient networks. In [58], it was assumed that both information and energy could be extracted from the same radio frequency signals at the same time, which does not hold in practice. Motivated by this issue, two practical receiver architectures, namely time switching (TS) receiver and power splitting (PS) receiver, were proposed in a MIMO system in [59]. Since point-to-point communication systems with SWIPT are well established in the existing literature, recent research on SWIPT has focused on two common cooperative relaying systems: AF and DF. On one hand, for AF relaying, a TS-based relaying protocol and a PS-based relaying protocol were proposed in [60]. On the other hand, for DF relaying, a new antenna switching SWIPT protocol was proposed in [61] to lower the implementation complexity. Additionally, a novel wireless energy harvesting DF relaying protocol was proposed in [62] for underlay CR networks to enable secondary users can harvest energy from the primary users. In [63], the application of SWIPT to DF cooperative networks with randomly deployed relays was investigated using stochastic geometry in a cooperative scenario with multiple source nodes and a single destination. A scenario in which multiple source-destination pairs are randomly deployed and communicate with each other via a single energy harvesting relay was considered in [64].

Regarding NOMA systems related with SWIPT, in [65], the uplink NOMA transmission considering energy constrained users which can harvest energy from the BS with adopting "*harvest-then-transmit*" protocol. The results demonstrate that NOMA can provide considerable improvements in terms of system throughput, fairness and energy efficiency.

1.3.2.4 Physical Layer Security

Given the broadcast nature of wireless transmissions, the concept of PLS, which was proposed by Wyner as early as 1975 from an information-theoretical perspective [13], has sparked of wide-spread recent interest. To elaborate, PLS has been considered from a practical perspective in [66, 66–70]. Specifically, robust beamforming transmission

in conjunction with applying AN for mitigating the impact of imperfect channel state information (CSI) in MIMO wiretap channels was proposed by Mukherjee and Swindlehurst [66]. Ding *et al.* [67] invoked relay-aided cooperative diversity for increasing the capacity of the desired link. More particularly, the impact of eavesdroppers on the diversity and multiplexing gains was investigated both in single-antenna and multiple-antenna scenarios. Additionally, the tradeoffs between secure performance and reliability in the presence of eavesdropping attacks was identified by Zou *et al.* [69]. The PLS in large-scale networks was investigated in [71], where both the legitimate and the eavesdropping nodes positions were modeled using stochastic geometry. Furthermore, the PLS of D2D communication in large-scale cognitive radio networks was investigated by Liu *et al.* [70] with invoking a wireless power transfer model, where the positions of the power beacons, the legitimate and the eavesdropping nodes were modeled using stochastic geometry. Liu *et al.* [68] considered the security enhancement benefits of cognitive relay-aided networks and proposed several relay and jammer selection and techniques.

Recently, various physical layer techniques, such as cooperative jamming [72] and AN [73] aided solutions were proposed for improving the PLS, even if the eavesdroppers have better channel conditions than the legitimate receivers. A popular technique is to generate AN at the transmitter for degrading the eavesdroppers' reception, which was proposed by Goel and Negi in [73]. In contrast to the traditional view, which regards noise and interference as a detrimental effect, generating AN at the transmitter is capable of improving the security, because it degrades the channel conditions of eavesdroppers without affecting those of the legitimate receivers. An AN-based multi-antenna aided secure transmission scheme affected by colluding eavesdroppers was considered by Zhou and McKay [74] for the scenarios associated both with perfect and imperfect CSI at both the transmitter and receiver. As a further development, the secrecy enhancement achieved in wireless Ad Hoc networks was investigated by Zhang *et al.* [75], with the aid of both beamforming and sectoring techniques. Regarding NOMA systems related to PLS, Zhang *et al.* in [76] investigated the PLS of SISO-NOMA networks, in which the

secrecy sum rate of the networks were maximized with a predefined QoS requirement. The optimal power allocation was obtained as closed-form expressions.

1.4 Dissertation Organization

The remainder of this thesis is organized as follows. Chapter 2 introduces some fundamental concepts such as basic principles of NOMA, wireless power transfer, cognitive radio, massive MIMO, HetNets, physical layer security, and stochastic geometry. Chapter 3 investigates the application of SWIPT in NOMA networks. Chapter 4 introduces NOMA in underlay large-scale cognitive radio networks. Chapter 5 proposes a novel hybrid HetNets design where NOMA is adopted in small cells and massive MIMO is employed in macro cells. Chapter 6 examines the enhancement of physical layer security in large-scale NOMA networks. Chapter 7 investigates the fairness issue of cluster-based MIMO-NOMA systems. Chapter 8 concludes this thesis and discusses the promising future research directions.

1.5 Author's Publications

- Journal Papers

    1. **Y. Liu**, Z. Ding, M. Elkashlan, and H. V. Poor, "Cooperative non-orthogonal multiple access with simultaneous wireless information and power transfer", *IEEE Journal on Selected Areas in Communications*, vol. 34, no. 4, Apr. 2016.

    2. **Y. Liu**, M. Elkashlan, Z. Ding, and G. K. Karagiannidis, "Fairness of User Clustering in MIMO Non-orthogonal Multiple Access Systems", *IEEE Communication Letter*; vol. 20, no. 7, pp. 1465-1468, July 2016.

    3. **Y. Liu**, Z. Ding, M. Elkashlan, and J. Yuan, "Non-orthogonal Multiple Access

in Large-Scale Underlay Cognitive Radio Networks", *IEEE Transactions on Vehicular Technology*; accepted to appear.

4. **Y. Liu**, S. A. Mousavifar, Y. Deng, C. Leung, and M. Elkashlan, "Wireless Energy Harvesting in a Cognitive Relay Network", *IEEE Transactions on Wireless Communications*, vol. 15, no. 4, pp. 2498-2508, Apr. 2016.

5. **Y. Liu**, L. Wang, S. A. R. Zaidi, M. Elkashlan, and T. Q. Duong, "Secure D2D communication in large-scale cognitive cellular networks: a wireless power transfer model", *IEEE Transactions on Communications*; vol. 64, no. 1, pp. 329-342, Jan. 2016.

6. **Y. Liu**, L. Wang, T. T. Duy, M. Elkashlan, and T. Q. Duong, "Relay selection for security enhancement in cognitive relay networks", *IEEE Wireless Communications Letters*; vol. 4, no. 1, pp. 46-49, Feb. 2015.

7. **Y. Liu**, L. Wang, M. Elkashlan, T. Q. Duong, and A. Nallanathan, "Two-Way Relay Networks with Wireless Power Transfer: Design and Performance Analysis", *IET Communications*; June 2016.

8. J. Zhao, **Y. Liu**, K. K. Chai, Y. Chen, and M. Elkashlan, "Many-to-Many Matching with Externalities for Device-to-Device Communications", *IEEE Wireless Communications Letters*; (under review).

9. **Y. Liu**, Z. Qin, M. Elkashlan, Y. Gao, and L. Hanzo, "Enhancing the Physical Layer Security of Non-orthogonal Multiple Access in Large-scale Networks", *IEEE Transactions on Wireless Communications*; (under review).

10. Z. Qin, **Y. Liu**, Y. Gao, M. Elkashlan, and A. Nallanathan, "Throughput Analysis of Wireless Powered Cognitive Radio Networks with Compressive Sensing and Matrix Completion", *IEEE Transactions on Communications*; (revision).

11. Z. Ding, **Y. Liu**, J. Choi, Q. Sun, M. Elkashlan, Chih-Lin I, and H. V. Poor, "Application of Non-orthogonal Multiple Access in LTE and 5G Networks", *IEEE Communication Magazine*; (revision).

12. Z. Song, **Y. Liu**, Q. Ni, M. Elkashlan, and X. Sun, "Exploiting Spectral-Energy Efficiency Tradeoff with Fairness in Non-Orthogonal Multiple Access Networks", *IEEE Communications Letters*; (revision).

- Conference Papers

1. **Y. Liu**, Z. Qin, M. Elkashlan, Y. Gao, and A. Nallanathan, "Non-orthogonal Multiple Access in Massive MIMO Aided Heterogeneous Networks", in *Proc. IEEE Global Telecommunications Conf. (GLOBECOM'16)*, Washington DC, USA, Dec. 2016.

2. J. Zhao, **Y. Liu**, K. K. Chai, Y. Chen, M. Elkashlan, and J. Alonso-Zarate, "NOMA-based D2D Communications: Towards 5G", in *Proc. IEEE Global Telecommunications Conf. (GLOBECOM'16)*, Washington DC, USA, Dec. 2016.

3. Z. Qin, **Y. Liu**, Z. Ding, Y. Gao and M. Elkashlan, "Physical Layer Security for 5G Non-orthogonal Multiple Access in Large-scale Networks", in *Proc. IEEE Int. Communications Conf. (ICC'16)*, Kuala Lumpur, Malaysia, May 2016.

4. Z. Qin, **Y. Liu**, Y. Gao, M. Elkashlan, and A. Nallanathan, "Throughput analysis for compressive spectrum sensing with wireless power transfer", in *Proc. IEEE Global Telecommunications Conf. (GLOBECOM'15)*, San Diego CA, USA, December 2015.

5. **Y. Liu**, Z. Ding, M. Elkashlan, and H. V. Poor, "Cooperative non-orthogonal multiple access in 5G system with SWIPT", in *Proc. European Signal Processing Conf. (EUSIPCO15)*, Nice, France, August 2015. **(Invited Paper)**

6. **Y. Liu**, L. Wang, S. A. R. Zaidi, M. Elkashlan, and T. Q. Duong, "Secure D2D communication in large-scale cognitive cellular networks with wireless power transfer", in *Proc. IEEE Int. Communications Conf. (ICC'15)*, London, UK, June 2015.

7. **Y. Liu**, L. Wang, M. Elkashlan, T. Q. Duong, and A. Nallanathan, "Two-way relaying networks with wireless power transfer: Policies design and throughput analysis", in *Proc. IEEE Global Telecommunications Conf. (GLOBECOM'14)*, Austin TX, USA, December 2014.

8. S. A. Mousavifar, **Y. Liu**, C. Leung, M. Elkashlan, and T. Q. Duong, "Wireless energy harvesting and spectrum sharing in cognitive radio", in *Proc. IEEE Veh. Technol. Conf. (VTC-Fall'14)*, Vancouver, Canada, September 2014.

Chapter 2

Fundamental Concepts

In this chapter, the technical knowledge used in this thesis is provided. The basic principles of NOMA is first introduced, which includes several fundamental background of NOMA, especially the cooperative NOMA and the MIMO-NOMA design, which lays a solid foundation for the technical works in Chapters 3 and 7, respectively. Then the concept of RF wireless power transfer, CR, massive MIMO and HetNets, and PLS are introduced, which provided technical guidelines for the works in in Chapter 3–6, respectively. Last a powerful modeling tool, namely, stochastic geometry is described in an effort to offer a complete understanding for the related technical works in Chapter 3 to Chapter 6.

2.1 Basic principles of NOMA

The fundamental concept of NOMA is to realize the multiple access technologies from the power domain (as shown in Fig. 2.1(a)). Unlike the conventional multiple access technologies, NOMA is capable of bringing a new power dimension to perform multiplexing in the existing time/freaquecy/code domain. In other words, NOMA can be regarded as an "add-on" technique, which provides the very promising potential to be

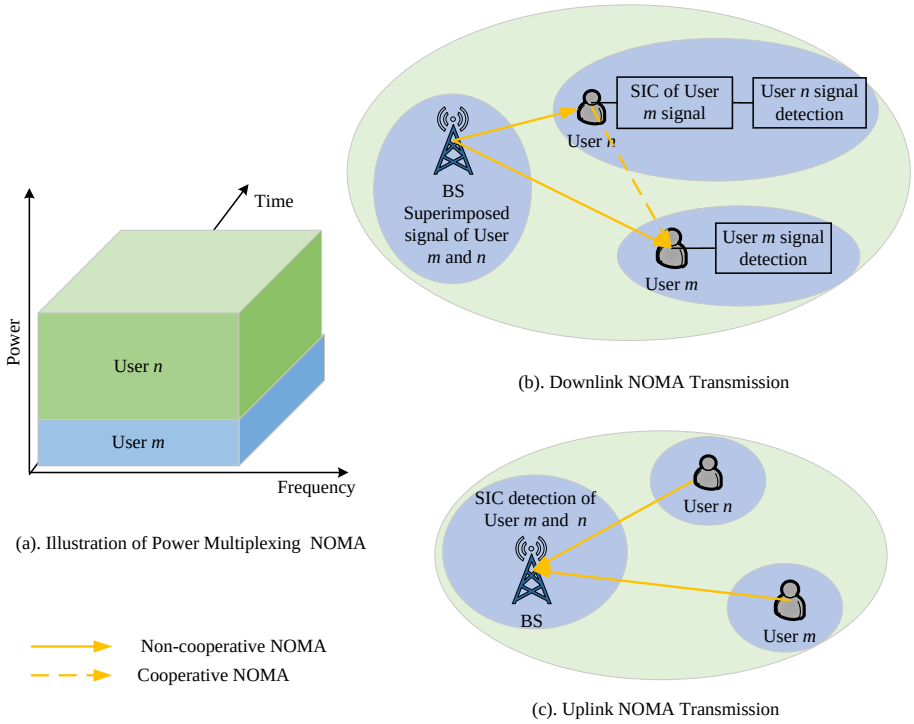

Figure 2.1: Illustration of NOMA transmission.

well integrated with the existing MA paradigms.

2.1.1 Key Technologies of NOMA

The key enabling technologies for NOMA is based on two principles, namely, SC and SIC. In fact, these two technologies are not new and the roots of them can be found in many existing literature [77–91].

As the two main technologies SC and SIC continue to mature both in theoretical and practical aspects, NOMA is able to be applied in the next generation networks without considering the implementation issues. By invoking SC technique, the BS transmits the combination of superposition coded signals of all users' messages. Without loss of generality, the channel gains of users are with respect to a particular ordering (e.g., increasing order or decreasing order). In the traditional OMA schemes, one of the popular power allocation policy is water filling policy. However, in NOMA, users with

poor channel conditions are supposed to allocate more power. By doing so, it can ensure that the users with poor channel condition can decode the message of themselves by treating other users' messages as noise. For those users which are in good channel conditions, SIC technologies can be applied to enable subtract the interference from other users with poorer channel conditions.

2.1.1.1 Superposition Coding

As first proposed by Cover as early as in 1972 [77], the elegant idea of SC is regarded as one of the fundamental building blocks of coding schemes to achieve the capacity on a scalar Gaussian broadcast channel [78]. More particularly, it was theoretically demonstrated that SC is capable of achieving the capacities of Gaussian BC channel capacity by Bergmans [79] and of achieving the capacities of the general degraded broadcast channel capacity by Gallager [92]. The fundamental concept of SC is that it is able to encode a user with poor channel condition at a lower rate and then superimpose the signal of a user with better channel condition on it. Due to the solid foundation laid on the information perspective, researchers begin to apply SC technologies to enormous channels, such as interference channels [80], relay channels [81], multiple access channels [82], and wiretap channels [83]. While the aforementioned contributions sufficiently motivate the use of SC from theoretic perspective, another breakthrough which have been made on SC is to bring this technique from theory to practice [84, 93]. Specifically, Vanka *et al.* [84] designed an experimental platform using a software-radio system to investigate the performance of SC. The set of achievable rate pairs under a packet-error constraint was determined.

2.1.1.2 Successive Interference Cancelation

Aiming to improve the network capacity with efficient managing interference, SIC is regarded as a promising technology for performing interference cancelation in wireless

networks. SIC technique achieves interference cancelation with the following procedure: it enables the user with stronger link to decode the user with weaker link first. Then, it regenerates the signal of weaker user at the stronger user side and subtract the interference. At last the stronger user decodes its information without suffering the interference from the weaker user. It is demonstrated that SIC is capable of reaching the region boundaries of Shannon capacity, both in terms of the broadcast channel and multiple access networks. Additionally, one main advantage of SIC is that it requires low hardware complexity design at the receiver side [85]. As such, SIC has been widely studied and various version was been employed in practical systems such as CDMA [86] and vertical-bell laboratories layered space-time (V-BLAST) [87]. Furthermore, SIC has been exploited in several practical scenarios, such as multi-user MIMO networks [88], multi-hop networks [89], random access systems [90], and stochastic geometry modeled large-scale networks [91]. Another important development on SIC is that it has been implemented in some commercial systems, e.g., IEEE 802.15.4.

2.1.2 Investigating NOMA from Information Theorematic Perspective

When realizing the penitential advantages of a new multiple access technology, it is quite significant to investigate the performance gain from the standpoint of information theory perspective (e.g., capacity region). In fact, the concept of NOMA is a special case of the development of SC for the BC channel. Some existing works have laid a solid foundation for identifying the capacity region of the BC channel of NOMA. Particularly, by using SC, the capacity region of a degraded discrete memoryless BS was established by Cover [77]. As an extension of [77], Bergmans found the Gaussian BC capacity region in single-antenna scenarios [94].

Inspired by [77], [94], several researchers began to explore the potential performance gain from the perspective [17, 95, 96]. Xu *et al.* [17] developed a new evaluation criterion to examine the performance gain of NOMA over OMA from the view of information theory. More specifically, considering a simple two user single-antenna scenarios with

Gaussian BC, the comparison of TDMA and NOMA in terms of capacity region and two rate regions was shown in [17]. The analytical results show that NOMA can outperform TDMA both in terms of individual rates and sum rates. In [95], Shieh and Huang focused on examining the capacity region of downlink NOMA with being based on systematically designing practical schemes and investigated the promising gains of NOMA over OMA with designing practical encoders and decoders. Furthermore, by proposing to form relaying broadcast channels (RBC) into NOMA for performance enhancement, So and Sung [96] examined the achievable capacity region of RBC with invoking several relaying stratifies, such as DF relaying, compress-and-forward (CF) relaying with/without DPC.

2.1.3 Mathematical demonstration of NOMA

For better illustrating the relationship between NOMA and OMA from the information theoretic aspect, an analytical demonstration is provided with examining the high signal-noise ratio (SNR) performance. Consider a two user case of downlink NOMA transmission, first h_m and h_n are denoted as the channel coefficients of the user m and user n, ρ as the transmit SNR at the BS and assume that $|h_m|^2 < |h_n|^2$ without loss of generality. According to the Shannon Capacity theorem, the obtaining throughput in the context of OMA can be expressed as $\frac{1}{2}\log_2\left(1+\rho|h_m|^2\right)$ and $\frac{1}{2}\log_2\left(1+\rho|h_m|^2\right)$, respectively. Regarding to NOMA, the obtaining throughput are given by $\log_2\left(1+\frac{\rho\alpha_m|h_m|^2}{1+\rho\alpha_n|h_m|^2}\right)$ and $\log\left(1+\rho\alpha_n|h_n|^2\right)$, where α_m and α_n are the power allocation coefficients which satisfies $\alpha_m > \alpha_n$ and $\alpha_m + \alpha_n = 1$. At high SNR approximation, the sum throughput of OMA and NOMA are $\frac{1}{2}\log_2\left(\rho|h_m|^2\right)+\frac{1}{2}\log_2\left(\rho|h_n|^2\right) = \log_2\left(\rho\sqrt{|h_m|^2|h_n|^2}\right)$ and $\log_2\left(\rho|h_n|^2\right)$, respectively. As such, it is noted that in high SNR region, the sum throughput of NOMA significantly outperform OMA, especially for the scenarios when the channel conditions of two users are largely different. On the stand point of mathematically thinking, the performance improvements brought by NOMA is mainly due to the fact that the resource (e.g., time/frequence) splitting factor $\frac{1}{2}$ that outside of the logarithm, is more damaging than the power allocation inside of the logarithm.

2.1.4 Downlink and Uplink NOMA Transmission

Downlink NOMA transmission employees the SC technique at the BS for sending combination signals and the SIC technique at users for interference cancelation. More specifically, as shown in Fig. 2.1(b), at the side of strong user (User n), the interference of the superimposed signal can be cancelled with employing SIC technique. While at the side of weak user (User m), it will decode the message by treating User n as interference. This thesis focuses on the downlink NOMA transmission scenarios (in Chapters 3–8). This is attributes to the fact that a downlink version of NOMA transmission, namely, multiuser superposition transmission (MUST), has been already included in the long-term evolution advanced (LTE-A) standards, which is more promising as a candidate for 5G.

Unlike the downlink NOMA transmission, the uplink NOMA transmission requires that the BS should send controlling signals to multiple users for power allocation first. Then multiple users transmit their own information to the BS in the same orthogonal resource block (RB) resource (as shown in Fig. 2.1(c)). With the aid of SIC technique, the BS decodes all the messages of users following increasing/decreasing decoding order.

2.1.5 Cooperative NOMA Transmission

The core idea of cooperative NOMA is to regard strong NOMA users as several DF relays to help weak NOMA users. Still taking the two user downlink transmission in Fig. 2.1(b) as an example. The cooperative NOMA requires two time slots for transmission. The first slot, namely, direct transmission phase, is the same as the non-cooperative NOMA (as shown in Fig. 2.1(b) with solid line). During the second time slot which is called cooperative phase, User n will forward the decoded message to user m with invoking DF relaying protocol (as shown in Fig. 2.1(b) with dash line). Proposed by Ding *et al.* [10], this novel concept sparked interests to researchers since the cooperative NOMA fully exploits the penitential benefits of SIC and DF decoding. In this thesis, the design

of Chapter 3 is based on cooperative NOMA

Compared with the conventional NOMA, the key advantages of the cooperative NOMA transmission can be summarized as follows. 1) Technique integration: with applying SIC technology in NOMA, the message of the weak user has already been decoded at the side of strong user. As such, it is natural to consider the use of DF relay protocol; 2) Better fairness: one key feature of cooperative NOMA is that the reliability of the weak user is significantly improved. As a consequence, the fairness of the NOMA transmission can be guarantied; and 3) High diversity gain: cooperative NOMA is capable of achieving higher diversity gain for the weak NOMA user, which is an effective approach to overcome the multi-path fading.

2.1.6 NOMA in Multi-Antenna Systems

Compared to the SISO system, invoking multiple antennas at the BS can be used to improve the SNR with the aid of beamforming or increase the system throughput with the aid of spatial multiplexing. The two well-acceptable multi-antenna NOMA technologies are NOMA with beamforming and NOMA with spatial multiplexing [4], which are introduced in the following.

NOMA with BF provide an effective approach to improve the spectral efficiency by exploiting the power domain and spatial domain. One of the popular multiple antenna NOMA design considering the beamforming is to establish a cluster-based structure. More particularly, all users are considered to be divided into several different clusters. In each cluster, the spatial channels of users are highly correlated. As shown in Fig. 2.2, the NOMA users all associated into M clusters and each cluster is consists of L_m users, where $m \in \{1, 2, ..., M\}$. In this case, appropriate beams for the corresponding clusters can be designed. With applying effective precoding design, it is able to guarantee that the beam associated to the particular cluster is orthogonal to the channels of users in all the other clusters. By doing so, the inter-cluster interference can be efficiently suppressed.

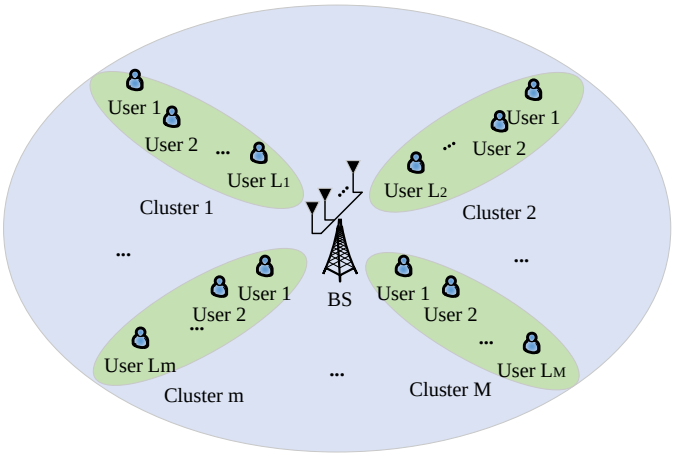

Figure 2.2: Illustration of NOMA with beamforming in a cluster-based MIMO architecture.

Then take a deeper look at the users in each cluster, due to the existing differences of channel conditions among users, it becomes the conventional NOMA scenarios. Thus, SIC can be invoked to manage the intra-cluster interference between users in the same cluster. In Chapter 7, this cluster-based MIMO-NOMA structure design is adopted.

NOMA with spatial multiplexing (SM) is capable of increasing the system throughput and spatial multiplexing gain through equipping multiple antennas at both the transmitters and receivers. In other words, unlike NOMA with BF, all the scenarios considered in NOMA with SM should be the MIMO-NOMA scenarios. Essentially, NOMA with SM is a combination of NOMA and MIMO. As such, the scaling property of linearly growing relationship between achievable rate and minimum number of transmitter/receiver (M) should still exist.

2.2 RF Wireless Power Transfer

One of the key objective of future 5G networks is to maximize energy efficiency of wireless networks, especially for the energy-constrained wireless devices. Energy harvesting (EH) is an effective means to prolong the life of a wireless network, and has recently received remarkable attention since it is increasingly contributing to green communication. How-

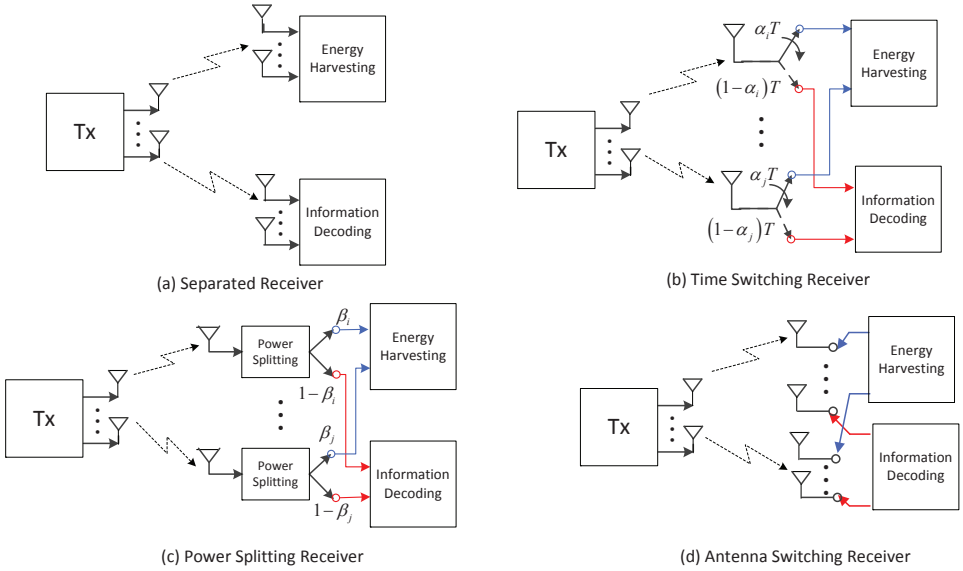

Figure 2.3: Illustration of the existing SWIPT receivers.

ever, the traditional energy harvesting techniques such as water, solar, wind, vibration and thermoelectric effects, depend on the locations, environments, and time. Different from the conventional EH techniques, RF wireless power transfer (WPT) provides a more flexible approach for powering the energy constraint devices. Another motivation behind this approach lies in the fact that most devices are surrounded by RF signals, as a consequence, even harmful signals (e.g., noise and interference) can be regarded as the penitential energy harvesting source. These potential advantages of WPT aforementioned have recently attracted considerable attention by researchers to study this field [59, 60, 70, 97–99].

SWIPT has been developed as a more promising RF WPT techniques for its potential ability to enable information and energy to transmit in the same waveform [59]. Due to the fact that it is not possible to extract information and energy from the same radio frequency signals at the same time. More practical energy and information receiver structures are necessitated. The four well-accepted receiver structure designs are summarized in [100], namely, separated, time switching, power splitting and antenna switching receivers (as shown in Fig. 2.3). Among them, separated and antenna switching receivers exploits separation of information and energy from spacial domain. While time switching

and power splitting receivers separates information and energy from time domain and power domain. In Chapter 3, a power splitting receiver based architecture is applied in a DF relay system.

2.3 Cognitive Radio Networks

The last decade has witnessed the rapid explosion of the wireless devices all over the world, which gives rise to the increasing demand for wireless spectrum resource. As reported by Federal Communications Commission (FCC), there are significant temporal and spatial variations in the allocated spectrum. Given this fact, CR, first coined by Mitola [101], has rekindled the interest to solve the spectrum scarcity problem. The basic concept of CR is that at a certain time or geographic region, the unlicensed users are allowed to access to the licensed spectrum intelligently. With applying different approaches by secondary users (SUs) to access the spectrum of primary users (PUs), CR is mainly categorized into three paradigms, namely, interweave, overlay, and underlay [102], from different standpoints to manage interference: 1) The interweave CR can be regarded as an interference avoiding paradigm, in which SUs are required to sense the temporary voids on space-frequency domain of PUs before they access [103–108]. The concurrent transmission of SUs and PUs is not allowed in interweave paradigm. 2) The overlay paradigm is essentially an interference mitigating technique. With the aid of some encoding techniques (e.g. DPC), overlay CR ensures that cognitive user is capable of transiting simultaneously with non-cognitive user [102]. Additionally, SUs are able to operate as a rely to forward the information of PUs' to PU receivers. 3) The underlay CR is like an intelligent interference controlling paradigm, in which SUs are permitted to access the spectrum allocated to PUs as long as the interference power constraint is satisfied [42].

In this thesis, the underlay CR scenarios are considered in Chapter 4. Taking a simple example to illustrate the basic concept of underlay CR. As shown in Fig. 2.4,

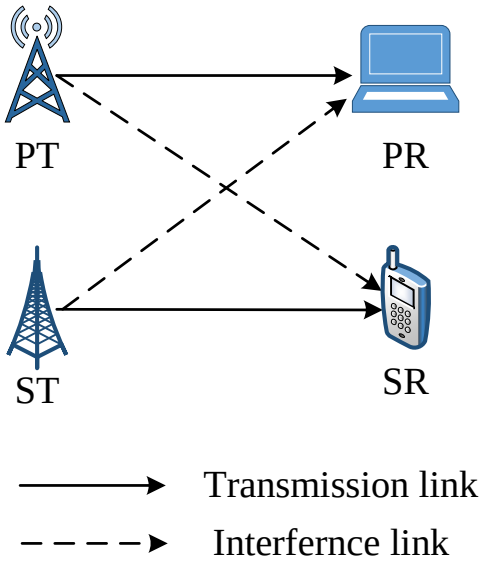

Figure 2.4: Illustration of underlay cognitive radio networks.

a primary transmitter (PT) communicates with a primary receiver (PR). At the same time, a pair of SUs can reuse the same frequency. More precisely, a secondary transmitter (ST) is able to transmit information to a secondary receiver (SR) as long as satisfying a predetermined interference constraint to PR. Note that SR will also suffer interference from PT in this underlay paradigm.

2.4 Massive MIMO

Massive MIMO is considered as one of the "big three" technologies [12] in 5G systems for its significant ability for improving the received SNR and spectrum efficiencies. It is evidently shown that massive MIMO is capable of increasing the capacity more than 10 times as well as improve energy efficiency radiated 100 times [109]. Compared to the conventional MIMO which is limited by the number of antennas, massive MIMO is able to provide many potential advantages in terms of offering large multiplexing gains, high data rates, more stable link reliability and better tradeoff between spectral and energy efficiency. For example, with applying zero forcing (ZF) transmit precoding (TPC) with equal power allocation, the averaged received power at the served user can be improved

as

$$P_r = G_M P_t L/N, \tag{2.1}$$

where $G_M = M - N + 1$ is the array gain obtained at users [110, 111], P_t is the transmit power of the BS, L is large-scale path loss.

The potential benefits of massive MIMO sparked the interest of researchers to attempt the massive MIMO transmission into NOMA. In [34], Ding and Poor employed the clustering MIMO-NOMA design and decomposed the channels of massive-MIMO-NOMA into a number of SISO-NOMA channel. A one-bit feedback scheme for the designed massive-MIMO-NOMA systems was proposed to lower the implementation complexity.

2.5 Heterogeneous Networks

Dense HetNets, as one of "big three" 5G technologies [12], is capable of significantly improving the network capacity. The core idea of HetNets is essentially to move BSs closer to the served users and as such the spectrum across geographical fields can be densely reoccupied. Actually, the multi-layer HetNets layout has been envisaged in the LTE-A by involving the small cells (e.g., picocells, femtocells, relays) underlaying marco cells in the cellular networks, which further determines the dominant role of HetNets in future wirless networks. Fig. 2.5 illustrates a three-tier HetNets which include one marco cell, several pico cells and femto cells. It is noted that each BS has its own coverage.

Due to the sparsity of marco cells and small cells, users will surfer the inter-layer interference as well as the intra-layer interference. As such, it necessitates to intelligently determine users to associate which tier BS. One recent popular user association strategy is based on the maximum average received power of each tier. By doing so, a user is allowed to access any tier BS which can provide the best coverage [112]. This is particularly important useful in a hybrid HetNets while adopts different technologies

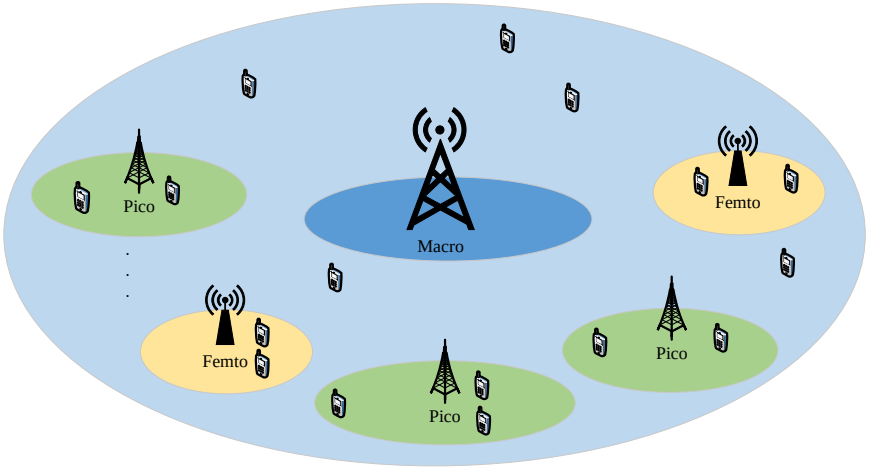

Figure 2.5: Illustration of a three-tier HetNets.

in different tier (e.g., massive MIMO in marco cells and single antenna in small cells). In Chapter 5, this average received power based flexible user association approach is employed.

2.6 Physical Layer Security

The broadcast nature of the wireless medium makes that it is susceptible to the security threats of eavesdropping. PLS, which was proposed by Wyner as early as 1975 from an information-theoretical perspective [13], has aroused wide concern as an appealing approach to achieve secure transmission. Different from the traditional approaches which design cryptographic protocols in the upper layer, PLS aims to exploit characteristics of wireless channels in physical layer for transmitting confidential messages. Triggered by the rapid development of wireless networks, the idea of PLS has been considered from a practical perspective in many scenarios [66–69, 113].

A basic wiretap channel is that a transmission sends the secrecy information to a legitimate receiver in the presence of eavesdroppers who intend to maliciously obtain the messages. The key idea of achieving perfect secrecy in wiretap channel is to ensure that the quality of the main channel is better than that of the eavesdropper's channel. The

secrecy capacity is given by [114]

$$I_s = [I_M - I_E]^+, \tag{2.2}$$

where I_M is the capacity of the main channel, I_E is the capacity of the eavesdropper's channel, and $[x]^+ = \max\{x, 0\}$. Due to the characteristic of physical layer security, related research works mainly towards to two directions, increasing the main channel quality (e.g., establish closer link) and decreasing the eavesdropper's channel quality (e.g., generating friendly jamming signals [72] or artificial noise [73]). More efficient approaches to enhance physical layer security is further discussed in Chapter 6.

2.7 Stochastic Geometry Approaches for Large-Scale Networks

While the aforementioned sections mainly focus on introducing fundamental scenarios, this section presents a powerful mathematical and statistical tool, namely, stochastic geometry for modeling and analyzing wireless networks. Unlike the traditional topology approaches which always ignore the density and mobility of nodes, stochastic geometry is capable of capturing the topological randomness of the networks and hence can provide tractable analytical results for the average network behaviors according to some distributions [115]. This is particularly essential in large-scale networks which consist of a large number of randomly deployed nodes (e.g., BSs, mobile users, etc.) whose channels and locations are with high uncertainty. Fig. 2.6 is an example of stochastic geometry model, which shows the spatial distribution of a wireless powered secure D2D communication scenario [70].

The stochastic geometry based model is to assume the spatial distribution of networks obeys a certain point process, such as the Binomial point process (BPP), the Poisson cluster process (PCP), the Hard core point process (HCPP) and the Poisson

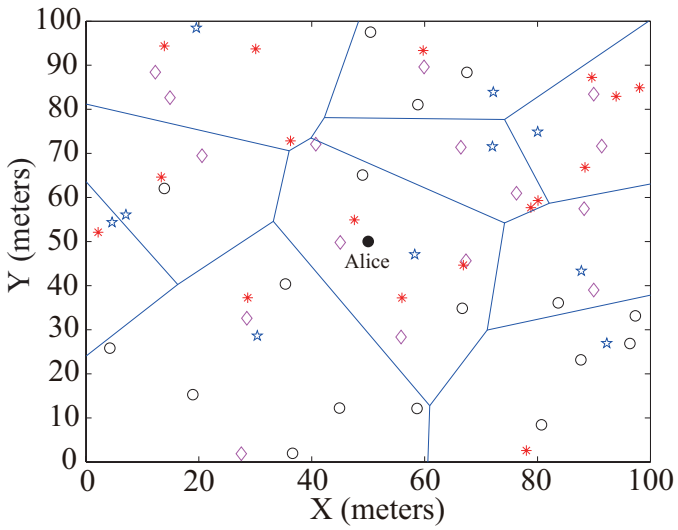

Figure 2.6: An example of stochastic geometry model considering that a wireless powered secure D2D communication scenarios. A part of a network captures the spatial distributions of the transmitter (Alice), power beacons (pink diamonds), legitimate receiver (empty circles), BSs (blue five-pointed stars), and eavesdroppers (red stars) follow homogeneous PPP.

point process (PPP) [116]. Among them, PPP is a commonly-used process in the existing literature considering large-scale wireless networks. Note that the PPP can be either a homogeneous PPP which has a constant points' density or a heterogeneous PPP which has a various points' density. A useful property of PPP is the probability generating functional, which is capable of calculating the products of PPP as [117]

$$\mathbb{E}\left[\prod_{x\in\Phi} F(x)\right] = \exp\left[-\int_{\mathbb{R}^n} (1-F(x))\,\Lambda(dx)\right], \tag{2.3}$$

where Φ represents the point process and Λ is the intensity measure.

In Chapter 3, 4, 5, and 6, stochastic geometry approaches are used to model the considered large-scale networks in different scenarios, all PPPs in this thesis are modeled to follow the independent homogeneous PPPs.

Chapter 3

Cooperative Non-Orthogonal Multiple Access with Simultaneous Wireless Information and Power Transfer

This chapter is organized as follows. The main contributions are first introduced in Section 3.1. In Section 3.2, the network model for studying cooperative SWIPT NOMA is presented. In Section 3.3, new analytical expressions are derived for the outage probability, diversity gain, and throughput when the proposed selection schemes are used. Numerical results are presented in Section 3.4, which is followed by conclusion in Sections 3.5.

3.1 Introduction

The application of SWIPT is considered in NOMA networks. On the standpoint of joint tackling spectrum efficiency and energy efficiency, an incentive user cooperation NOMA protocol was proposed, by regarding near users as energy harvesting relays for improving reliability of far users. To further investigate the effect of locations of users on performance, three opportunistic user selection schemes are proposed as follows: 1) random near user and random far user (RNRF) selection, where both the near and far users are randomly selected from the two groups; 2) nearest near user and nearest far user (NNNF) selection, where a near user and a far user closest to the BS are selected from the two groups; and 3) nearest near user and farthest far user (NNFF) selection, where a near user which is closest to the BS is selected and a far user which is farthest from the BS is selected. The insights obtained from these opportunistic user selection schemes provide guidance for the design of dynamic user clustering algorithms, a topic beyond the scope of this work. The primary contributions of this chapter are summarized as follows.

- A new SWIPT NOMA protocol to improve the reliability of the far users with the help of the near users without consuming extra energy is proposed. With this in mind, three user selection schemes are proposed by opportunistically taking into account the users' locations.

- Closed-form expressions for the outage probability at the near and far users are derived, when considering the three proposed user selection schemes. In addition, the delay-sensitive throughput based on the outage probabilities of the near and far users are analyzed.

- The diversity gain of the three proposed selection schemes for the near and far users are derived. It is concluded that all three schemes have the same diversity order. For the far users, it is worth noting that the diversity gain of the proposed cooperative SWIPT NOMA is the same as that of a conventional cooperative network

without radio frequency energy harvesting.

- Comparing RNRF, NNNF, and NNFF, it is confirmed that NNNF achieves the lowest outage probability and the highest throughput for both the near and far users.

3.2 Network Model

Considering a network with a single source S (i.e., the BS) and two groups of randomly deployed users $\{\mathrm{A_i}\}$ and $\{\mathrm{B_i}\}$. It is assumed that the users in group $\{\mathrm{B_i}\}$ are deployed within disc D_{B} with radius $R_{D_{\mathrm{B}}}$. The far users $\{\mathrm{A_i}\}$ are deployed within ring D_{A} with radius $R_{D_{\mathrm{C}}}$ and $R_{D_{\mathrm{A}}}$(assuming $R_{D_{\mathrm{C}}} \gg R_{D_{\mathrm{B}}}$), as shown in Fig. 3.1. Note that the BS is located at the origin of both the disc D_{B} and the ring D_{A}. The locations of the near and far users are modeled as homogeneous PPPs Φ_κ ($\kappa \in \{\mathrm{A}, \mathrm{B}\}$) with densities λ_{Φ_κ}. Here the near users are uniformly distributed within the disc and the far users are uniformly distributed within the ring. The number of users in R_{D_κ}, denoted by N_κ, follows a Poisson distribution $\Pr(N_\kappa = k) = (\mu_\kappa^k/k!)e^{-\mu_\kappa}$, where μ_κ is the mean number of users, i.e., $\mu_{\mathrm{A}} = \pi\left(R_{D_{\mathrm{A}}}^2 - R_{D_{\mathrm{C}}}^2\right)\lambda_{\Phi_{\mathrm{A}}}$ and $\mu_{\mathrm{B}} = \pi R_{D_{\mathrm{B}}}^2 \lambda_{\Phi_{\mathrm{B}}}$. All channels are assumed to be quasi-static Rayleigh fading, where the channel coefficients are constant for each transmission block but vary independently between different blocks. In the proposed network, the users in $\{\mathrm{B_i}\}$ are considered as energy harvesting relays that harvest energy from the BS and forward the information to $\{\mathrm{A_i}\}$ using the harvested energy as their transmit powers. The DF strategy is applied at $\{\mathrm{B_i}\}$ and the cooperative NOMA system consists of two phases, detailed in the following. In this work, without loss of generality, it is assumed that the two phases have the same transmission periods, the same as in [60, 63, 64]. It is worth pointing out that dynamic time allocation for the two phases may further improve the performance of the proposed cooperative NOMA scheme, but consideration of this issue is beyond the scope of the chapter.

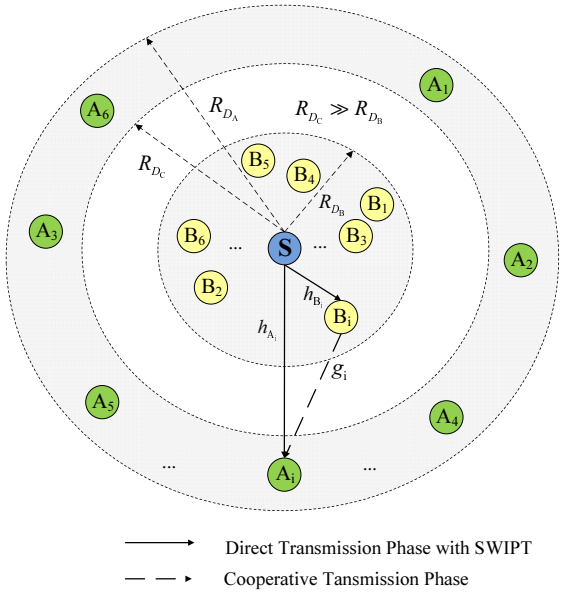

Figure 3.1: An illustration of a downlink SWIPT NOMA system with a base station S (blue circle). The spatial distributions of the near users (yellow circles) and the far users (green circles) follow homogeneous PPPs. $\{\mathrm{B_i}\}$ are within disc D_B with radius R_{D_B}. $\{\mathrm{A_i}\}$ are within ring D_A with radius R_{D_C} and R_{D_A}.

3.2.1 Phase 1: Direct Transmission

Prior to transmission, the two users denoted by $\mathrm{A_i}$ and $\mathrm{B_i}$, are selected to perform NOMA, where the selection criterion will be discussed in the next section. During the first phase, the BS sends two messages $p_{i1}x_{i1} + p_{i2}x_{i2}$ to two selected users $\mathrm{A_i}$ and $\mathrm{B_i}$ based on NOMA [9], where p_{i1} and p_{i2} are the power allocation coefficients and x_{i1} and x_{i2} are the messages of $\mathrm{A_i}$ and $\mathrm{B_i}$. The observation at $\mathrm{A_i}$ is given by

$$y_{\mathrm{A_i},1} = \sqrt{P_\mathrm{S}} \sum_{k\in\{1,2\}} p_{ik}x_{ik} \frac{h_{\mathrm{A_i}}}{\sqrt{1+d_{\mathrm{A_i}}^{\alpha}}} + n_{\mathrm{A_i},1}, \tag{3.1}$$

where P_{S} is the transmit power at the BS, $h_{\mathrm{A_i}}$ models the small-scale Rayleigh fading from the BS to $\mathrm{A_i}$ with $h_{\mathrm{A_i}} \sim \mathcal{CN}(0,1)$[1], $n_{\mathrm{A_i},1}$ is additive Gaussian white noise (AWGN) at $\mathrm{A_i}$ with variance $\sigma^2_{\mathrm{A_i}}$, $d_{\mathrm{A_i}}$ is the distance between BS and $\mathrm{A_i}$, and α is the path loss exponent.

It is assumed that $|p_{i1}|^2 > |p_{i2}|^2$ with $|p_{i1}|^2 + |p_{i2}|^2 = 1$. The received SINR at $\mathrm{A_i}$ to detect x_{i1} is given by

$$\gamma^{x_{i1}}_{\mathrm{S,A_i}} = \frac{\rho|h_{\mathrm{A_i}}|^2|p_{i1}|^2}{\rho|p_{i2}|^2|h_{\mathrm{A_i}}|^2 + 1 + d^{\alpha}_{\mathrm{A_i}}}, \tag{3.2}$$

where $\rho = \frac{P_{\mathrm{S}}}{\sigma^2}$ is the transmit SNR (assuming $\sigma^2_{\mathrm{A_i}} = \sigma^2_{\mathrm{B_i}} = \sigma^2$).

Consider that the near users have rechargeable storage ability [60, 118] and power splitting (as shown in Fig. 2.3) is applied to perform SWIPT. From the implementation point of view, this rechargeable storage unit can be a supercapacitor or a short-term high-efficiency battery [61]. The power splitting approach is applied as explained in the following: the observation at $\mathrm{B_i}$ is divided into two parts. One part is used for information decoding by directing the observation flow to the detection circuit and the remaining part is used for energy harvesting to powers $\mathrm{B_i}$ for helping $\mathrm{A_i}$. Thus, the received signal

$$y_{\mathrm{B_i},1} = \sqrt{P_{\mathrm{S}}} \sum_{k\in\{1,2\}} p_{ik}x_{ik}\frac{\sqrt{1-\beta_i}h_{\mathrm{B_i}}}{\sqrt{1+d^{\alpha}_{\mathrm{B_i}}}} + n_{\mathrm{B_i},1}, \tag{3.3}$$

where β_i is the power splitting coefficient, $h_{\mathrm{B_i}}$ models the small-scale Rayleigh fading from the BS to $\mathrm{B_i}$ with $h_{\mathrm{B_i}} \sim \mathcal{CN}(0,1)$, $n_{\mathrm{B_i}}$ is AWGN at $n_{\mathrm{B_i},1}$ with variance $\sigma^2_{\mathrm{B_i}}$, and $d_{\mathrm{B_i}}$ is the distance between the BS and $\mathrm{B_i}$. The bounded path loss model is used to ensure that the path loss is always larger than one even for small distances [63].

Applying NOMA, SIC [119] is carried out at $\mathrm{B_i}$. Particularly, $\mathrm{B_i}$ first decodes the message of $\mathrm{A_i}$, then subtracts this component from the received signal to detect its own

[1] $\mathcal{CN}(x,y)$ refers to the distribution with the mean value of x and the variance value of y.

information. Therefore, the received SINR at $\mathrm{B_i}$ to detect x_{i1} of $\mathrm{A_i}$ is given by

$$\gamma_{\mathrm{S,B_i}}^{x_{i1}} = \frac{\rho|h_{\mathrm{B_i}}|^2|p_{i1}|^2(1-\beta_i)}{\rho|h_{\mathrm{B_i}}|^2|p_{i2}|^2(1-\beta_i)+1+d_{\mathrm{B_i}}^{\alpha}}. \tag{3.4}$$

The received SNR at $\mathrm{B_i}$ to detect x_{i2} of $\mathrm{B_i}$ is given by

$$\gamma_{\mathrm{S,B_i}}^{x_{i2}} = \frac{\rho|h_{\mathrm{B_i}}|^2|p_{i2}|^2(1-\beta_i)}{1+d_{\mathrm{B_i}}^{\alpha}}. \tag{3.5}$$

The power splitting coefficient β_i is used to determine the amount of harvested energy. Based on (3.4), the data rate supported by the channel from the BS to $\mathrm{B_i}$ for decoding x_{i1} is given by

$$R_{x_{i1}} = \frac{1}{2}\log\left(1+\frac{\rho|h_{\mathrm{B_i}}|^2|p_{i1}|^2(1-\beta_i)}{\rho|h_{\mathrm{B_i}}|^2|p_{i2}|^2(1-\beta_i)+1+d_{\mathrm{B_i}}^{\alpha}}\right). \tag{3.6}$$

It is assumed that the energy required to receive/process information is negligible compared to the energy required for information transmission [60, 70]. In this work, the dynamic power splitting protocol is applied, which means that the power splitting coefficient β_i is a variable and opportunistically tuned to support the relay transmission. The aim is to first guarantee the detection of the message of the far NOMA user, $\mathrm{A_i}$, at the near NOMA user $\mathrm{B_i}$, then $\mathrm{B_i}$ can harvest the remaining energy. In this case, based on (3.6), in order to ensure that $\mathrm{B_i}$ can successfully decode the information of $\mathrm{A_i}$, a rate is assumed as follows, i.e., $R_1 = R_{x_{i1}}$. Therefore, the power splitting coefficient is set as follows:

$$\beta_i = \max\left\{0, 1-\frac{\tau_1\left(1+d_{\mathrm{B_i}}^{\alpha}\right)}{\rho\left(|p_{i1}|^2-\tau_1|p_{i2}|^2\right)|h_{\mathrm{B_i}}|^2}\right\}, \tag{3.7}$$

where $\tau_1 = 2^{2R_1}-1$. Here $\beta_i = 0$ means that all the energy is used for information decoding and no energy remains for energy harvesting.

Based on (3.3), the energy harvested at $\mathrm{B_i}$ is given by

$$E_{\mathrm{B_i}} = \frac{T\eta P_{\mathrm{S}}\beta_i |h_{\mathrm{B_i}}|^2}{2\left(1+d_{\mathrm{B_i}}^{\alpha}\right)}, \tag{3.8}$$

where T is the time period for the entire transmission including the direct transmission phase and the cooperative transmission phase, and η is the energy harvesting coefficient. It is assumed that the two phases have the same transmission period, and therefore, the transmit power at $\mathrm{B_i}$ can be expressed as follows:

$$P_t = \frac{\eta P_{\mathrm{S}}\beta_i |h_{\mathrm{B_i}}|^2}{1+d_{\mathrm{B_i}}^{\alpha}}. \tag{3.9}$$

3.2.2 Phase 2: Cooperative Transmission

During this phase, $\mathrm{B_i}$ forwards x_{i1} to $\mathrm{A_i}$ by using the harvested energy during the direct transmission phase. In this case, $\mathrm{A_i}$ observes

$$y_{\mathrm{A_i},2} = \frac{\sqrt{P_t}x_{i1}g_{\mathrm{i}}}{\sqrt{1+d_{\mathrm{C_i}}^{\alpha}}} + n_{\mathrm{A_i},2}, \tag{3.10}$$

where g_{i} models the small-scale Rayleigh fading from $\mathrm{B_i}$ to $\mathrm{A_i}$ with $g_{\mathrm{i}} \sim \mathcal{CN}(0,1)$, $n_{\mathrm{A_i},2}$ is AWGN at $\mathrm{A_i}$ with variance $\sigma^2_{\mathrm{A_i}}$, $d_{\mathrm{C_i}} = \sqrt{d^2_{\mathrm{A_i}} + d^2_{\mathrm{B_i}} - 2d_{\mathrm{A_i}}d_{\mathrm{B_i}}\cos(\theta_i)}$ is the distance between $\mathrm{B_i}$ and $\mathrm{A_i}$, and θ_i denotes the angle $\angle \mathrm{A_iSB_i}$ (as shown in Fig. 3.1).

Based on (3.9) and (3.10), the received SNR for $\mathrm{A_i}$ to detect x_{i1} forwarded from $\mathrm{B_i}$ is given by

$$\gamma^{x_{i1}}_{\mathrm{A_i},\mathrm{B_i}} = \frac{P_t|g_i|^2}{\left(1+d_{\mathrm{C_i}}^{\alpha}\right)\sigma^2} = \frac{\eta\rho\beta_i|h_{\mathrm{B_i}}|^2|g_i|^2}{\left(1+d_{\mathrm{C_i}}^{\alpha}\right)\left(1+d_{\mathrm{B_i}}^{\alpha}\right)}. \tag{3.11}$$

At the end of this phase, $\mathrm{A_i}$ combines the signals from the BS and $\mathrm{B_i}$ using maximal-ratio combining (MRC). Combining the SNR of the direct transmission phase (3.2) and the SINR of the cooperative transmission phase (3.11), the received SINR at $\mathrm{A_i}$ is

obtained as follows:

$$\gamma_{\mathrm{A_i,MRC}}^{x_{i1}} = \frac{\rho|h_{\mathrm{A_i}}|^2|p_{i1}|^2}{\rho|h_{\mathrm{A_i}}|^2|p_{i2}|^2+1+d_{\mathrm{A_i}}^{\alpha}} + \frac{\eta\rho\beta_i|h_{\mathrm{B_i}}|^2|g_i|^2}{\left(1+d_{\mathrm{B_i}}^{\alpha}\right)\left(1+d_{\mathrm{C_i}}^{\alpha}\right)}. \tag{3.12}$$

3.3 Non-Orthogonal Multiple Access with User Selection

In this section, the performance of three user selection schemes are characterized in the following.

3.3.1 RNRF Selection Scheme

In this scheme, the BS randomly selects a near user $\mathrm{B_i}$ and a far user $\mathrm{A_i}$. This selection scheme provides a fair opportunity for each user to access the source with the NOMA protocol. The advantage of this user selection scheme is that it does not require the knowledge of instantaneous channel state information (CSI). To make meaningful conclusions, in the rest of the chapter, only the case $\beta_i > 0$ is focused on in this chapter and the number of near users and far users satisfy $N_B \geq 1$ and $N_A \geq 1$, respectively.

3.3.1.1 Outage Probability of the Near Users of RNRF

In the NOMA protocol, an outage of $\mathrm{B_i}$ can occur for two reasons. The first is that $\mathrm{B_i}$ cannot detect x_{i1}. The second is that $\mathrm{B_i}$ can detect x_{i1} but cannot detect x_{i2}. To guarantee that the NOMA protocol can be implemented, the condition $|p_{i1}|^2-|p_{i2}|^2\tau_1 > 0$ should be satisfied [9]. Based on this, the outage probability of $\mathrm{B_i}$ can be expressed as follows:

$$P_{\mathrm{B_i}} = \Pr\left(\frac{\rho|h_{\mathrm{B_i}}|^2|p_{i1}|^2}{\rho|h_{\mathrm{B_i}}|^2|p_{i2}|^2+1+d_{\mathrm{B_i}}^{\alpha}} < \tau_1\right) + \Pr\left(\frac{\rho|h_{\mathrm{B_i}}|^2|p_{i1}|^2}{\rho|h_{\mathrm{B_i}}|^2|p_{i2}|^2+1+d_{\mathrm{B_i}}^{\alpha}} > \tau_1, \gamma_{\mathrm{S,B_i}}^{x_{i2}} < \tau_2\right), \tag{3.13}$$

where $\tau_2 = 2^{2R_2} - 1$ with R_2 being the target rate at which $\mathrm{B_i}$ can detect x_{i2}.

The following theorem provides the outage probability of the near users in RNRF for an arbitrary choice of α.

Theorem 1. Conditioned on the PPPs, the outage probability of the near users $\mathrm{B_i}$ can be approximated as follows:

$$P_{\mathrm{B_i}} \approx \frac{1}{2}\sum_{n=1}^{N} \omega_N \sqrt{1-{\phi_n}^2}\left(1-e^{-c_n \varepsilon_{\mathrm{A}_i}}\right)(\phi_n+1), \tag{3.14}$$

if $\varepsilon_{\mathrm{A}_i} \geq \varepsilon_{\mathrm{B}_i}$, otherwise $P_{\mathrm{B_i}} = 1$, where $\varepsilon_{\mathrm{A}_i} = \frac{\tau_1}{\rho\left(|p_{i1}|^2 - |p_{i2}|^2\tau_1\right)}$ and $\varepsilon_{\mathrm{B}_i} = \frac{\tau_2}{\rho|p_{i2}|^2}$, N is a parameter to ensure a complexity-accuracy tradeoff, $c_n = 1 + \left(\frac{R_{D_\mathrm{B}}}{2}(\phi_n+1)\right)^{\alpha}$, $\omega_N = \frac{\pi}{N}$, and $\phi_n = \cos\left(\frac{2n-1}{2N}\pi\right)$.

Proof. Define $X_i = \frac{|h_{\mathrm{A_i}}|^2}{1+d_{\mathrm{A_i}}^{\alpha}}$, $Y_i = \frac{|h_{\mathrm{B_i}}|^2}{1+d_{\mathrm{B_i}}^{\alpha}}$, and $Z_i = \frac{|g_i|^2}{1+d_{\mathrm{C_i}}^{\alpha}}$. Substituting (3.4) and (3.5) into (3.13), the outage probability of the near users is given by

$$P_{\mathrm{B_i}} = \Pr\left(Y_i < \varepsilon_{\mathrm{A}_i}\right) + \Pr\left(Y_i > \varepsilon_{\mathrm{A}_i}, \varepsilon_{\mathrm{A}_i} < \varepsilon_{\mathrm{B}_i}\right). \tag{3.15}$$

If $\varepsilon_{\mathrm{A}_i} < \varepsilon_{\mathrm{B}_i}$, the outage probability at the near users is always one.

For the case $\varepsilon_{\mathrm{A}_i} \geq \varepsilon_{\mathrm{B}_i}$, note that the users are deployed in D_B and D_A according to homogeneous PPPs. Therefore, the NOMA users are modeled as independently and identically distributed (i.i.d.) points in D_B and D_A, denoted by W_{κ_i} ($\kappa \in \{\mathrm{A}, \mathrm{B}\}$), which contain the location information about $\mathrm{A_i}$ and $\mathrm{B_i}$, respectively. The probability density functions (PDFs) of $W_{\mathrm{A_i}}$ and $W_{\mathrm{B_i}}$ are given by

$$f_{W_{\mathrm{B_i}}}(\omega_{\mathrm{B_i}}) = \frac{\lambda_{\Phi_\mathrm{B}}}{\mu_\mathrm{B}} = \frac{1}{\pi R_{D_\mathrm{B}}^2}, \tag{3.16}$$

and

$$f_{W_{\mathrm{A_i}}}\left(\omega_{\mathrm{A_i}}\right)=\frac{\lambda_{\Phi_{\mathrm{A}}}}{\mu_{\mathrm{A}}}=\frac{1}{\pi\left(R_{D_{\mathrm{A}}}^{2}-R_{D_{\mathrm{C}}}^{2}\right)}, \tag{3.17}$$

respectively.

Therefore, for the case $\varepsilon_{\mathrm{A}_i}\geq\varepsilon_{\mathrm{B}_i}$, the cumulative distribution function (CDF) of Y_i is given by

$$\begin{aligned}F_{Y_i}\left(\varepsilon\right)=&\int\limits_{D_{\mathrm{B}}}\left(1-e^{-\left(1+d_{\mathrm{B_i}}^{\alpha}\right)\varepsilon}\right)f_{W_{\mathrm{B_i}}}\left(\omega_{\mathrm{B_i}}\right)d\omega_{\mathrm{B_i}}\\=&\frac{2}{R_{D_{\mathrm{B}}}^{2}}\int_{0}^{R_{D_{\mathrm{B}}}}\left(1-e^{-(1+r^{\alpha})\varepsilon}\right)rdr.\end{aligned} \tag{3.18}$$

For many communication scenarios $\alpha>2$, and it is challenging to obtain exact closed-from expressions for the above. In this case, Gaussian-Chebyshev quadrature [120] can be applied to find the approximation of (3.18) as follows:

$$F_{Y_i}\left(\varepsilon\right)\approx\frac{1}{2}\sum_{n=1}^{N}\omega_N\sqrt{1-\phi_n{}^2}\left(1-e^{-c_n\varepsilon}\right)\left(\phi_n+1\right). \tag{3.19}$$

Applying $\varepsilon_{\mathrm{A}_i}\rightarrow\varepsilon$ into (3.19), (3.14) is obtained, and the proof of the theorem is completed. □

Corollary 1. For the special case $\alpha=2$, the outage probability of $\mathrm{B_i}$ can be obtained as follows:

$$P_{\mathrm{B_i}}|_{\alpha=2}=1-\frac{e^{-\varepsilon_{\mathrm{A}_i}}}{R_{D_{\mathrm{B}}}^{2}\varepsilon_{\mathrm{A}_i}}+\frac{e^{-\left(1+R_{D_{\mathrm{B}}}^{2}\right)\varepsilon_{\mathrm{A}_i}}}{R_{D_{\mathrm{B}}}^{2}\varepsilon_{\mathrm{A}_i}}, \tag{3.20}$$

if $\varepsilon_{\mathrm{A}_i}\geq\varepsilon_{\mathrm{B}_i}$, otherwise $P_{\mathrm{B_i}}|_{\alpha=2}=1$.

Proof. Based on (3.18), when $\alpha=2$ and after some manipulations, the following expres-

sion can be easily obtained

$$F_{Y_i}(\varepsilon)|_{\alpha=2} = 1 - \frac{e^{-\varepsilon}}{R_{D_\mathrm{B}}^2 \varepsilon} + \frac{e^{-\left(1+R_{D_\mathrm{B}}^2\right)\varepsilon}}{R_{D_\mathrm{B}}^2 \varepsilon}. \tag{3.21}$$

Applying $\varepsilon_{\mathrm{A}_i} \to \varepsilon$ into (3.21), (3.20) can be obtained. The proof is complete. □

3.3.1.2 Outage Probability of the Far Users of RNRF

With the proposed cooperative SWIPT NOMA protocol, outage experienced by $\mathrm{A_i}$ can occur in two situations. The first is when $\mathrm{B_i}$ can detect x_{i1} but the overall received SNR at $\mathrm{A_i}$ cannot support the targeted rate. The second is when neither $\mathrm{A_i}$ nor $\mathrm{B_i}$ can detect x_{i1}. Based on this, the outage probability can be expressed as follows:

$$P_{\mathrm{A_i}} = \Pr\left(\gamma_{\mathrm{A_i,MRC}}^{x_{i1}} < \tau_1, \gamma_{\mathrm{S,B_i}}^{x_{i1}}\Big|_{\beta_i=0} > \tau_1\right) + \Pr\left(\gamma_{\mathrm{S,A_i}}^{x_{i1}} < \tau_1, \gamma_{\mathrm{S,B_i}}^{x_{i1}}\Big|_{\beta_i=0} < \tau_1\right). \tag{3.22}$$

The following theorem provides the outage probability of the far users in RNRF for an arbitrary choice of α.

Theorem 2. Conditioned on the PPPs, and assuming $R_{D_\mathrm{C}} \gg R_{D_\mathrm{B}}$, the outage probability of $\mathrm{A_i}$ can be approximated as follows:

$$\begin{aligned} P_{\mathrm{A_i}} \approx{}& \zeta_1 \sum_{n=1}^{N} (\phi_n + 1) \sqrt{1 - {\phi_n}^2} c_n \sum_{k=1}^{K} \sqrt{1 - \psi_k^2} s_k (1 + s_k^\alpha)^2 \\ &\times \sum_{m=1}^{M} \sqrt{1 - \varphi_m^2} e^{-\left(1+s_k^\alpha\right)t_m} \chi_{t_m} \left(\ln \frac{\chi_{t_m}(1 + s_k^\alpha)}{\eta\rho} c_n + 2c_0\right) \\ &+ a_1 \sum_{n=1}^{N} \sqrt{1 - {\phi_n}^2} c_n (\phi_n + 1) \sum_{k=1}^{K} \sqrt{1 - {\psi_k}^2} (1 + s_k^\alpha) s_k, \end{aligned} \tag{3.23}$$

where M and K are parameters to ensure a complexity-accuracy tradeoff, $\zeta_1 = -\frac{\varepsilon_{\mathrm{A}_i} R_{D_{\mathrm{B_i}}} \omega_N \omega_K \omega_M}{8\left(R_{D_{\mathrm{A_i}}} + R_{D_{\mathrm{C_i}}}\right)\eta\rho}$, $\chi_{t_m} = \tau_1 - \frac{\rho t_m |p_{i1}|^2}{\rho t_m |p_{i2}|^2 + 1}$, $t_m = \frac{\varepsilon_{\mathrm{A}_i}}{2}(\varphi_m + 1)$, $\omega_M = \frac{\pi}{M}$, $\varphi_m = \cos\left(\frac{2m-1}{2M}\pi\right)$, $s_k = \frac{R_{D_\mathrm{A}} - R_{D_\mathrm{C}}}{2}(\psi_k + 1) + R_{D_\mathrm{C}}$, $\omega_K = \frac{\pi}{K}$, $\psi_k = \cos\left(\frac{2k-1}{2K}\pi\right)$, $c_0 = -\frac{\varphi(1)}{2} - \frac{\varphi(2)}{2}$, and $a_1 = \frac{\omega_K \omega_N \varepsilon_{\mathrm{A}_1}^2}{2\left(R_{D_\mathrm{A}} + R_{D_\mathrm{C}}\right)}$.

Proof. See Appendix A.1. □

Corollary 2. For the special case $\alpha = 2$, the outage probability of $\mathrm{A_i}$ can be simplified as follows:

$$\begin{aligned} P_{\mathrm{A_i}}|_{\alpha=2} \approx \zeta_2 \sum_{k=1}^{K} \sqrt{1-\psi_k^2} s_k \left(1+s_k^2\right)^2 \sum_{m=1}^{M} \sqrt{1-\varphi_m^2} \\ \times \chi_{t_m} e^{-\left(1+s_k^2\right)t_m} \left(\ln \frac{\chi_{t_m}\left(1+s_k^2\right)}{\eta\rho} c_n + b_0 \right) \\ + \left(1 - \frac{e^{-\left(1+R_{D_\mathrm{C}}^2\right)\varepsilon_{\mathrm{A}_i}}}{\varepsilon_{\mathrm{A}_i}\left(R_{D_\mathrm{A}}^2 - R_{D_\mathrm{C}}^2\right)} + \frac{e^{-\left(1+R_{D_\mathrm{A}}^2\right)\varepsilon_{\mathrm{A}_i}}}{\varepsilon_{\mathrm{A}_i}\left(R_{D_\mathrm{A}}^2 - R_{D_\mathrm{C}}^2\right)} \right) \\ \times \left(1 - \frac{e^{-\varepsilon_{\mathrm{A}_i}}}{R_{D_\mathrm{B}}^2 \varepsilon_{\mathrm{A}_i}} + \frac{e^{-\left(1+R_{D_\mathrm{B}}^2\right)\varepsilon_{\mathrm{A}_i}}}{R_{D_\mathrm{B}}^2 \varepsilon_{\mathrm{A}_i}} \right), \end{aligned} \tag{3.24}$$

where $\zeta_2 = -\frac{\omega_K \omega_M \varepsilon_{\mathrm{A}_i}\left(R_{D_\mathrm{B}}^2+2\right)}{8\left(R_{D_\mathrm{A}}+R_{D_\mathrm{C}}\right)\eta\rho}$ *and* $b_0 = \frac{\left(1+R_{D_\mathrm{B}}^2\right)^2 \ln\left(1+R_{D_\mathrm{B}}^2\right)}{2R_{D_\mathrm{B}}^2} + \left(R_{D_\mathrm{B}}^2+2\right)\left(c_0 - \frac{1}{4}\right)$.

Proof. See Appendix B. □

3.3.1.3 Diversity Analysis of RNRF

To obtain further insights into the derived outage probability, a diversity analysis of both the near and far users of RNRF is provided.

Near users: For the near users, based on the analytical results, high SNR approximations is carried out as follows. When $\varepsilon \to 0$, a high SNR approximation of (3.19) with $1 - e^{-x} \approx x$ is given by

$$F_{Y_i}(\varepsilon) \approx \frac{1}{2} \sum_{n=1}^{N} \omega_N \sqrt{1-\phi_n{}^2} c_n \varepsilon_{\mathrm{A}_i} (\phi_n + 1). \tag{3.25}$$

The diversity gain is defined as follows:

$$d = -\lim_{\rho\to\infty} \frac{\log P(\rho)}{\log \rho}. \tag{3.26}$$

Substituting (3.25) into (3.26), the diversity gain for the near users is obtained as one, which means that using NOMA with energy harvesting will not decrease the diversity gain.

Far users: For the far users, substituting (3.23) into (3.26), the diversity gain is obtained as

$$\begin{aligned} d &= -\lim_{\rho\to\infty} \frac{\log\left(-\frac{1}{\rho^2}\log\frac{1}{\rho}\right)}{\log\rho} \\ &= -\lim_{\rho\to\infty} \frac{\log\log\rho - \log\rho^2}{\log\rho} = 2. \end{aligned} \tag{3.27}$$

As can be seen from (3.27), the diversity gain of RNRF is two, which is the same as that of the conventional cooperative network [121]. This result indicates that using NOMA with an energy harvesting relay will not affect the diversity gain. In addition, it is seen that at high SNRs, the dominant factor for the outage probability is $\frac{1}{\rho^2}\ln\rho$. Therefore it is concluded that the outage probability of using NOMA with SWIPT decays at a rate of $\frac{\ln SNR}{SNR^2}$. However, for a conventional cooperative system without energy harvesting, a faster decreasing rate of $\frac{1}{SNR^2}$ can be achieved.

3.3.1.4 System Throughput in Delay-Sensitive Transmission Mode of RNRF

In this chapter, the delay-sensitive throughput is been focused on. In this mode, the transmitter sends information at a fixed rate and the throughput is determined by evaluating the outage probability.

Based on the analytical results for the outage probability of the near and far users,

the system throughput of RNRF in the delay-sensitive transmission mode is given by

$$R_{\tau_{\mathrm{RNRF}}} = (1 - P_{\mathrm{A_i}})\, R_1 + (1 - P_{\mathrm{B_i}})\, R_2, \tag{3.28}$$

where $P_{\mathrm{A_i}}$ and $P_{\mathrm{B_i}}$ are obtained from (3.23) and (3.14), respectively.

3.3.2 NNNF Selection Scheme

In this subsection, the performance of NNNF is characterized, which exploits the users' CSI opportunistically. First a user within the disc D_{B} which has the shortest distance to the BS is selected as the near NOMA user (denoted by $\mathrm{B_{i^*}}$). This is because the near users also act as energy harvesting relays to help the far users. The NNNF scheme can enable the selected near user to harvest more energy. Then a user within the ring D_{A} which has the shortest distance to the BS is selected as the far NOMA user (denoted by $\mathrm{A_{i^*}}$). One advantage of the NNNF scheme is that it can minimize the outage probability of both the near and far users.

3.3.2.1 Outage Probability of the Near Users of NNNF

Using the same definition of the outage probability as the near users of NOMA, the outage probability of the near users of NNNF is characterized.

The following theorem provides the outage probability of the near users of NNNF for an arbitrary choice of α.

Theorem 3. Conditioned on the PPPs, the outage probability of $\mathrm{B_{i^*}}$ can be approximated as follows:

$$P_{\mathrm{B_{i^*}}} \approx b_1 \sum_{n=1}^{N} \sqrt{1 - {\phi_n}^2} \left(1 - e^{-(1+c_{n*}^{\alpha})\varepsilon_{\mathrm{A}_i}}\right) c_{n*} e^{-\pi\lambda_{\Phi_{\mathrm{B}}} c_{n*}^2}, \tag{3.29}$$

if $\varepsilon_{\mathrm{A}_i} \geq \varepsilon_{\mathrm{B}_i}$, otherwise $P_{\mathrm{B_{i^*}}} = 1$, where $c_{n*} = \frac{R_{D_{\mathrm{B}}}}{2}(\phi_n + 1)$, $b_1 = \frac{\xi_{\mathrm{B}}\omega_N R_{D_{\mathrm{B}}}}{2}$, and $\xi_{\mathrm{B}} =$

$\frac{2\pi\lambda_{\Phi_{\mathrm{B}}}}{1-e^{-\pi\lambda_{\Phi_{\mathrm{B}}}R_{D_{\mathrm{B}}}^2}}$.

Proof. Similar to (3.15), the outage probability of $\mathrm{B}_{\mathrm{i}^*}$ can be expressed as follows:

$$P_{\mathrm{B}_{\mathrm{i}^*}} = \Pr\left(Y_{i^*} < \varepsilon_{\mathrm{A}_i} \middle| N_{\mathrm{B}} \geq 1\right) = F_{Y_{i^*}}\left(\varepsilon_{\mathrm{A}_i}\right), \tag{3.30}$$

where $Y_{i^*} = \frac{\left|h_{\mathrm{B}_{\mathrm{i}}}\right|^2}{1+d_{\mathrm{B}_{\mathrm{i}^*}}^{\alpha}}$ and $d_{\mathrm{B}_{\mathrm{i}^*}}$ is the distance from the nearest $\mathrm{B}_{\mathrm{i}^*}$ to the BS.

The CDF of Y_{i^*} can be written as follows:

$$F_{Y_{i^*}}(\varepsilon) = \int_0^{R_{D_{\mathrm{B}}}} \left(1 - e^{-\left(1+r_{\mathrm{B}}^{\alpha}\right)\varepsilon}\right) f_{d_{\mathrm{B}_{\mathrm{i}^*}}}(r_{\mathrm{B}})\, dr_{\mathrm{B}}, \tag{3.31}$$

where $f_{d_{\mathrm{B}_{\mathrm{i}^*}}}$ is the PDF of the shortest distance from $\mathrm{B}_{\mathrm{i}^*}$ to the BS.

The probability $\Pr\left\{d_{\mathrm{B}_{\mathrm{i}^*}} > r \middle| N_{\mathrm{B}} \geq 1\right\}$ conditioned on $N_{\mathrm{B}} \geq 1$ is the event that there is no point located in the disc. Therefore this probability can be expressed as follows:

$$\begin{aligned}
&\Pr\left\{d_{\mathrm{B}_{\mathrm{i}^*}} > r \middle| N_{\mathrm{B}} \geq 1\right\} \\
=&\frac{\Pr\left\{d_{\mathrm{B}_{\mathrm{i}^*}} > r\right\} - \Pr\left\{d_{\mathrm{B}_{\mathrm{i}^*}} > r, N_{\mathrm{B}} = 0\right\}}{\Pr\left\{N_{\mathrm{B}} \geq 1\right\}} \\
=&\frac{e^{-\pi\lambda_{\Phi_{\mathrm{B}}}r^2} - e^{-\pi\lambda_{\Phi_{\mathrm{B}}}R_{D_{\mathrm{B}}}^2}}{1 - e^{-\pi\lambda_{\Phi_{\mathrm{B}}}R_{D_{\mathrm{B}}}^2}}.
\end{aligned} \tag{3.32}$$

Then the corresponding PDF of $\mathrm{B}_{\mathrm{i}^*}$ is given by

$$f_{d_{\mathrm{B}_{\mathrm{i}^*}}}(r_{\mathrm{B}}) = \xi_{\mathrm{B}} r_{\mathrm{B}} e^{-\pi\lambda_{\Phi_{\mathrm{B}}}r_{\mathrm{B}}^2}. \tag{3.33}$$

Substituting (3.33) into (3.31), the following expression is obtained

$$F_{Y_{i^*}}(\varepsilon) = \xi_{\mathrm{B}} \int_0^{R_{D_{\mathrm{B}}}} \left(1 - e^{-\left(1+r_{\mathrm{B}}^{\alpha}\right)\varepsilon}\right) r_{\mathrm{B}} e^{-\pi\lambda_{\Phi_{\mathrm{B}}}r_{\mathrm{B}}^2} dr_{\mathrm{B}}. \tag{3.34}$$

Applying the Gaussian-Chebyshev quadrature approximation to (3.19), the following

expression is obtained

$$F_{Y_{i^*}}(\varepsilon) \approx \frac{\xi_{\mathrm{B}}\omega_N R_{D_{\mathrm{B}}}}{2} \sum_{n=1}^{N} \sqrt{1-\phi_n{}^2} \left(1 - e^{-(1+c_{n*}^{\alpha})\varepsilon}\right) c_{n*} e^{-\pi\lambda_{\Phi_{\mathrm{B}}} c_{n*}^2}. \tag{3.35}$$

Applying $\varepsilon_{\mathrm{A}_i} \to \varepsilon$, the approximate outage probability of $\mathrm{B_{i^*}}$ is obtained in (3.29). □

Based on (3.34) and after some manipulations, the following corollary can be obtained.

Corollary 3. For the special case $\alpha = 2$, the outage probability of $\mathrm{B_{i^*}}$ can be expressed as follows:

$$P_{\mathrm{B_{i^*}}}\big|_{\alpha=2} = \frac{\xi_{\mathrm{B}}\left(e^{-R_{D_{\mathrm{B}}}^2\left(\pi\lambda_{\Phi_{\mathrm{B}}}+\varepsilon_{\mathrm{A}_i}\right)-\varepsilon_{\mathrm{A}_i}} - e^{-\varepsilon_{\mathrm{A}_i}}\right)}{2\left(\pi\lambda_{\Phi_{\mathrm{B}}}+\varepsilon_{\mathrm{A}_i}\right)} - \frac{\xi_{\mathrm{B}}\left(e^{-\pi\lambda_{\Phi_{\mathrm{B}}}R_{D_{\mathrm{B}}}^2}-1\right)}{2\pi\lambda_{\Phi_{\mathrm{B}}}}, \tag{3.36}$$

if $\varepsilon_{\mathrm{A}_i} \geq \varepsilon_{\mathrm{B}_i}$, *otherwise* $P_{\mathrm{B_{i^*}}}\big|_{\alpha=2} = 1$.

3.3.2.2 Outage Probability of the Far Users of NNNF

Using the same definition of the outage probability for the far users of NOMA, and similar to (3.22), the outage probability of the far users in NNNF can be characterized. The following theorem provides the outage probability of the far users in NNNF for an arbitrary choice of α.

Theorem 4. Conditioned on the PPPs and assuming $R_{D_{\mathrm{C}}} \gg R_{D_{\mathrm{B}}}$, the outage proba-

bility of $\mathrm{A}_{\mathrm{i}^*}$ can be approximated as follows:

$$
\begin{aligned}
P_{\mathrm{A}_{\mathrm{i}^*}} \approx\ & \varsigma^* \sum_{n=1}^{N} \sqrt{1-{\phi_n}^2}\left(1+c_{n*}^{\alpha}\right) c_{n*} e^{-\pi\lambda_{\Phi_{\mathrm{B}}} c_{n*}^2} \\
& \times \sum_{k=1}^{K} \sqrt{1-\psi_k^2}(1+s_k^{\alpha})^2 s_k e^{-\pi\lambda_{\Phi_{\mathrm{A}}}\left(s_k^2-R_{D_{\mathrm{C}}}^2\right)} \sum_{m=1}^{M} \sqrt{1-\varphi_m^2} \\
& \times e^{-\left(1+s_k^{\alpha}\right)t_m} \chi_{t_m}\left(\ln \frac{\chi_{t_m}\left(1+s_k^{\alpha}\right)\left(1+c_{n*}^{\alpha}\right)}{\eta\rho} + 2c_0\right) \\
& + b_2 b_3 \sum_{k=1}^{K} \sqrt{1-{\psi_k}^2}(1+s_k^{\alpha}) s_k e^{-\pi\lambda_{\Phi_{\mathrm{A}}} s_k^2} \\
& \times \sum_{n=1}^{N}\left(\sqrt{1-{\phi_n}^2}\left(1+c_{n*}^{\alpha}\right) c_{n*} e^{-\pi\lambda_{\Phi_{\mathrm{B}}} c_{n*}^2}\right),
\end{aligned} \tag{3.37}
$$

where $\varsigma^* = -\frac{\xi_{\mathrm{B}}\xi_{\mathrm{A}}\omega_N\omega_K\omega_M\varepsilon_{\mathrm{A}_i} R_{D_{\mathrm{B}}}\left(R_{D_{\mathrm{A}}}-R_{D_{\mathrm{C}}}\right)}{8\eta\rho}$, $b_2 = \frac{\xi_{\mathrm{A}} e^{\pi\lambda_{\Phi_{\mathrm{A}}} R_{D_{\mathrm{C}}}^2}\omega_K\varepsilon_{\mathrm{A}_i}}{R_{D_{\mathrm{A}}}+R_{D_{\mathrm{C}}}}$, and $b_3 = \frac{\xi_{\mathrm{B}}\omega_N R_{D_{\mathrm{B}}}\varepsilon_{\mathrm{A}_i}}{2}$.

Proof. See Appendix A.3. □

Corollary 4. For the special case $\alpha = 2$, the outage probability of $\mathrm{A}_{\mathrm{i}^*}$ can be simplified as

$$
\begin{aligned}
& P_{\mathrm{A}_{\mathrm{i}^*}}\big|_{\alpha=2} \approx \varsigma^* \sum_{n=1}^{N} \sqrt{1-{\phi_n}^2}\left(1+c_{n*}^2\right) c_{n*} e^{-\pi\lambda_{\Phi_{\mathrm{B}}} c_{n*}^2} \sum_{k=1}^{K} \sqrt{1-\psi_k^2}\left(1+s_k^2\right)^2 s_k e^{-\pi\lambda_{\Phi_{\mathrm{A}}}\left(s_k^2-R_{D_{\mathrm{C}}}^2\right)} \\
& \times \sum_{m=1}^{M} \sqrt{1-\varphi_m^2}\left(e^{-\left(1+s_k^2\right)t_m}\chi_{t_m}\left(\ln\frac{\chi_{t_m}\left(1+s_k^2\right)\left(1+c_{n*}^2\right)}{\eta\rho}+2c_0\right)\right) \\
& + \left(\frac{e^{-\varepsilon_{\mathrm{A}_i}}}{\pi\lambda_{\Phi_{\mathrm{A}}}+\varepsilon_{\mathrm{A}_i}}\left(e^{-R_{D_{\mathrm{A}}}^2\left(\pi\lambda_{\Phi_{\mathrm{A}}}+\varepsilon_{\mathrm{A}_i}\right)} - e^{-R_{D_{\mathrm{C}}}^2\left(\pi\lambda_{\Phi_{\mathrm{A}}}+\varepsilon_{\mathrm{A}_i}\right)}\right) - \frac{\left(e^{-\pi\lambda_{\Phi_{\mathrm{A}}}R_{D_{\mathrm{A}}}^2} - e^{-\pi\lambda_{\Phi_{\mathrm{A}}}R_{D_{\mathrm{C}}}^2}\right)}{\pi\lambda_{\Phi_{\mathrm{A}}}}\right) \\
& \times \frac{\xi_{\mathrm{A}} e^{\pi\lambda_{\Phi_{\mathrm{A}}}R_{D_{\mathrm{C}}}^2}\xi_{\mathrm{B}}}{4}\left(\frac{e^{-R_{D_{\mathrm{B}}}^2\left(\pi\lambda_{\Phi_{\mathrm{B}}}+\varepsilon_{\mathrm{A}_i}\right)-\varepsilon_{\mathrm{A}_i}} - e^{-\varepsilon_{\mathrm{A}_i}}}{\pi\lambda_{\Phi_{\mathrm{B}}}+\varepsilon_{\mathrm{A}_i}} - \frac{e^{-\pi\lambda_{\Phi_{\mathrm{B}}}R_{D_{\mathrm{B}}}^2}-1}{\pi\lambda_{\Phi_{\mathrm{B}}}}\right).
\end{aligned} \tag{3.38}
$$

Proof. For the special case $\alpha = 2$, after some manipulations, (A.3.11) can be expressed

as follows:

$$F_{X_{i^*}}(\varepsilon)\big|_{\alpha=2} = -\frac{\xi_{\mathrm{A}}\left(e^{\pi\lambda_{\Phi_{\mathrm{A}}}\left(R_{D_{\mathrm{C}}}^2-R_{D_{\mathrm{A}}}^2\right)}-1\right)}{2\pi\lambda_{\Phi_{\mathrm{A}}}} + \frac{\xi_{\mathrm{A}}e^{\pi\lambda_{\Phi_{\mathrm{A}}}R_{D_{\mathrm{C}}}^2}e^{-\varepsilon}}{2\left(\pi\lambda_{\Phi_{\mathrm{A}}}+\varepsilon\right)}\left(e^{-R_{D_{\mathrm{A}}}^2\left(\pi\lambda_{\Phi_{\mathrm{A}}}+\varepsilon\right)}-e^{-R_{D_{\mathrm{C}}}^2\left(\pi\lambda_{\Phi_{\mathrm{A}}}+\varepsilon\right)}\right). \tag{3.39}$$

Based on (A.3.10), combining (3.39) and (3.36), and setting $\alpha = 2$ into (A.3.9), (3.38) can be obtained. The proof is complete. □

3.3.2.3 Diversity Analysis of NNNF

Similarly, diversity analysis of both the near and far users of NNNF is provided.

Near users: For the near users, based on the analytical results, the high SNR approximation is carried out as follows. When $\varepsilon \to 0$, a high SNR approximation of (3.29) with $1 - e^{-x} \approx x$ is given by

$$P_{\mathrm{B}_{\mathrm{i}^*}} \approx b_1\varepsilon_{\mathrm{A}_i}\sum_{n=1}^{N}\left(\sqrt{1-{\phi_n}^2}\left(1+c_{n*}^{\alpha}\right)c_{n*}e^{-\pi\lambda_{\Phi_{\mathrm{B}}}c_{n*}^2}\right). \tag{3.40}$$

Substituting (3.40) into (3.26), the diversity gain for the near users of NNNF is obtained as one, which indicates that using NNNF will not affect the diversity gain.

Far users: For the far users, substituting (3.37) into (3.26), the diversity gain is obtained as still two. This indicates that NNNF will not affect the diversity gain.

3.3.2.4 System Throughput in Delay-Sensitive Transmission Mode of NNNF

Based on the analytical results for the outage probability of the near and far users, the system throughput of NNNF in the delay-sensitive transmission mode is given by

$$R_{\tau_{\mathrm{NNNF}}} = \left(1-P_{\mathrm{A}_{\mathrm{i}^*}}\right)R_1 + \left(1-P_{\mathrm{B}_{\mathrm{i}^*}}\right)R_2, \tag{3.41}$$

where $P_{\mathrm{A_{i^*}}}$ and $P_{\mathrm{B_{i^*}}}$ are obtained from (3.37) and (3.29), respectively.

3.3.3 NNFF Selection Scheme

In this scheme, first a user within disc D_{B} which has the shortest distance to the BS is selected as a near NOMA user. Then a user within ring D_{A} which has the farthest distance to the BS is selected as a far NOMA user (denoted by $\mathrm{A_{i'}}$). The use of this selection scheme is inspired by an interesting observation described in [9] that NOMA can offer a larger performance gain over conventional MA when user channel conditions are more distinct.

3.3.3.1 Outage Probability of the Near Users of NNFF

Since the same criterion for the near users is used, the outage probabilities of near nears for an arbitrary α and the special case $\alpha = 2$ are the same as those expressed in (3.29) and (3.36), respectively.

3.3.3.2 Outage Probability of the Far Users of NNFF

Using the same definition of the outage probability of the far users, and similar to (3.22), the outage probability of the far users of NNFF can be characterized. The following theorem provides the outage probability of the far user of NNFF for an arbitrary choice of α.

Theorem 5. Conditioned on the PPPs and assuming $R_{D_{\mathrm{C}}} \gg R_{D_{\mathrm{B}}}$, the outage proba-

bility of $\mathrm{A}_{\mathrm{i}'}$ can be approximated as follows:

$$
\begin{aligned}
P_{\mathrm{A}_{\mathrm{i}'}} \approx\ & \varsigma^* \sum_{n=1}^{N} \sqrt{1-{\phi_n}^2}\,(1+c_{n*}^{\alpha})\,c_{n*} e^{-\pi\lambda_{\Phi_{\mathrm{B}}} c_{n*}^2} \\
& \times \sum_{k=1}^{K} \sqrt{1-\psi_k^2}(1+s_k^{\alpha})^2 s_k e^{-\pi\lambda_{\Phi_{\mathrm{A}}}\left(R_{D_{\mathrm{A}}}^2 - s_k^2\right)} \sum_{m=1}^{M} \sqrt{1-\varphi_m^2} \\
& \times e^{-\left(1+s_k^{\alpha}\right)t_m} \chi_{t_m} \left(\ln \frac{\chi_{t_m}\left(1+s_k^{\alpha}\right)\left(1+c_{n*}^{\alpha}\right)}{\eta\rho} + 2c_0 \right) \\
& + b_3 b_4 \sum_{k=1}^{K} \sqrt{1-{\psi_k}^2}(1+s_k^{\alpha}) s_k e^{\pi\lambda_{\Phi_{\mathrm{A}}} s_k^2} \\
& \times \sum_{n=1}^{N} \left(\sqrt{1-{\phi_n}^2}\,(1+c_{n*}^{\alpha})\,c_{n*} e^{-\pi\lambda_{\Phi_{\mathrm{B}}} c_{n*}^2} \right),
\end{aligned} \tag{3.42}
$$

where $b_4 = \frac{\xi_{\mathrm{A}} e^{-\pi\lambda_{\Phi_{\mathrm{A}}} R_{D_{\mathrm{A}}}^2} \omega_K \varepsilon_{\mathrm{A}_i}}{R_{D_{\mathrm{A}}} + R_{D_{\mathrm{C}}}}$.

Proof. See Appendix A.4. □

Corollary 5. For the special case $\alpha = 2$, after some manipulations, the outage probability of $\mathrm{A}_{\mathrm{i}'}$ can be simplified as

$$
\begin{aligned}
P_{\mathrm{A}_{\mathrm{i}'}}\big|_{\alpha=2} \approx\ & \varsigma^* \sum_{n=1}^{N} \sqrt{1-{\phi_n}^2}\left(1+c_{n*}^2\right) c_{n*} e^{-\pi\lambda_{\Phi_{\mathrm{B}}} c_{n*}^2} \sum_{k=1}^{K} \sqrt{1-\psi_k^2}\left(1+s_k^2\right)^2 s_k e^{-\pi\lambda_{\Phi_{\mathrm{A}}}\left(R_{D_{\mathrm{A}}}^2 - s_k^2\right)} \\
& \times \sum_{m=1}^{M} \sqrt{1-\varphi_m^2} \left(e^{-\left(1+s_k^2\right)t_m} \chi_{t_m} \left(\ln \frac{\chi_{t_m}\left(1+s_k^2\right)\left(1+c_{n*}^2\right)}{\eta\rho} + 2c_0 \right) \right) \\
& + \frac{\xi_{\mathrm{A}} e^{-\pi\lambda_{\Phi_{\mathrm{A}}} R_{D_{\mathrm{A}}}^2}}{2} \left(\frac{e^{\pi\lambda_{\Phi_{\mathrm{A}}} R_{D_{\mathrm{A}}}^2} - e^{\pi\lambda_{\Phi_{\mathrm{A}}} R_{D_{\mathrm{C}}}^2}}{\pi\lambda_{\Phi_{\mathrm{A}}}} - \frac{e^{-\varepsilon_{\mathrm{A}_i}}}{\pi\lambda_{\Phi_{\mathrm{A}}} - \varepsilon_{\mathrm{A}_i}} \left(e^{R_{D_{\mathrm{A}}}^2\left(\pi\lambda_{\Phi_{\mathrm{A}}} - \varepsilon_{\mathrm{A}_i}\right)} - e^{R_{D_{\mathrm{C}}}^2\left(\pi\lambda_{\Phi_{\mathrm{A}}} - \varepsilon_{\mathrm{A}_i}\right)} \right) \right) \\
& \times \frac{\xi_{\mathrm{B}}}{2} \left(\frac{\left(e^{-R_{D_{\mathrm{B}}}^2\left(\pi\lambda_{\Phi_{\mathrm{B}}} + \varepsilon_{\mathrm{A}_i}\right) - \varepsilon_{\mathrm{A}_i}} - e^{-\varepsilon_{\mathrm{A}_i}} \right)}{\left(\pi\lambda_{\Phi_{\mathrm{B}}} + \varepsilon_{\mathrm{A}_i}\right)} - \frac{\left(e^{-\pi\lambda_{\Phi_{\mathrm{B}}} R_{D_{\mathrm{B}}}^2} - 1 \right)}{\pi\lambda_{\Phi_{\mathrm{B}}}} \right).
\end{aligned} \tag{3.43}
$$

3.3.3.3 Diversity Analysis

Similarly, diversity analysis of both the near and far uses in NNFF are provided.

Near users: Since the same criterion for selecting a near user is used, the diversity

gain is one, which is the same as for NNNF.

Far users: Substituting (3.42) into (3.26), the diversity gain is obtained as still two. Therefore, it is concluded that using opportunistic user selection schemes (NNNF and NNFF) based on distances will not affect the diversity gain.

3.3.3.4 System Throughput in Delay-Sensitive Transmission Mode of NNFF

Based on the analytical results for the outage probability of the near and far users, the system throughput of NNFF in the delay-sensitive transmission mode is given by

$$R_{\tau_{\mathrm{NNFF}}} = \left(1 - P_{\mathrm{A_{i'}}}\right) R_1 + \left(1 - P_{\mathrm{B_{i^*}}}\right) R_2, \tag{3.44}$$

where $P_{\mathrm{A_{i'}}}$ and $P_{\mathrm{B_{i^*}}}$ are obtained from (3.42) and (3.29), respectively.

3.4 Numerical Results

In this section, numerical results are presented to facilitate the performance evaluations (including the outage probability of the near and the far users and the delay sensitive throughput) of the proposed cooperative SWIPT NOMA protocol. In the considered network, it is assumed that the energy conversion efficiency of SWIPT is $\eta = 0.7$ and the power allocation coefficients of NOMA is $|p_{i1}|^2 = 0.8$, $|p_{i1}|^2 = 0.2$. In the following figures, red, blue and black color lines are used to represent the RNRF, NNNF and NNFF user selection schemes, respectively.

3.4.1 Outage Probability of the Near Users

In this subsection, the outage probability achieved by the near users with different choices of density and path loss coefficients for the three user selection schemes is demonstrated. Note that the same user selection criterion is applied for the near users of NNNF and

NNFF, NNN(F)F is used to represent these two selection schemes in Fig. 3.2, Fig. 3.3, and Fig. 3.4.

Fig. 3.2 plots the outage probability of the near users versus SNR with different path loss coefficients for both RNRF and NNN(F)F. The solid red and blue curves are for the special case $\alpha = 2$ of RNRF and NNN(F)F, corresponding to the analytical results derived in (3.20) and (3.36), respectively. The dashed red and blue curves are for an arbitrary choice of α, corresponding to the analytical results derived in (3.14) and (3.29), respectively. Monte Carlo simulation results are marked as "•" to verify the derivation. The figure shows precise agreement between the simulation and analytical curves. One can observe that by performing NNNF and NNFF (which refers to as NNN(F)F in the figure), lower outage probability is achieved than with RNRF since shorter distances mean lower path loss and leads to better performance. The figure also demonstrates that as α increases, outage will occur more frequently because of higher path loss. For NNNF and NNFF, the performance is very close for different values of α. This is because the bounded path loss model (i.e. $1 + d_{\mathrm{i}}^{\alpha} > 1$) is used to ensure that the path loss is always larger than one. When selecting the nearest near user, d_{i} will approach zero and the path loss will approach one, which makes the performance difference of the three selection schemes insignificant. It is worth noting that all curves have the same slopes, which indicates that the diversity gains of the schemes are the same. This phenomenon validates the insights obtained from the analytical results derived in (3.26). Fig. 3.2 also shows that if the choices of rates for users are incorrect (i.e., $R_1 = 0.5$ and $R_2 = 1$ in this figure), the outage probability of the near users will be always one, which verifies the analytical results in (3.14) and (3.29).

Fig. 3.3 plots the outage probability of the near users versus their density with different values of $R_{D_{\mathrm{B}}}$. RNRF is also shown in the figure as a benchmark for comparison. Several observations are drawn as follows: 1) The outage probabilities of RNRF and NNN(F)F decrease with decreasing $R_{D_{\mathrm{B}}}$ because path loss is reduced; 2) The outage probability of NNN(F)F decreases as the density of the near users increases. This is due

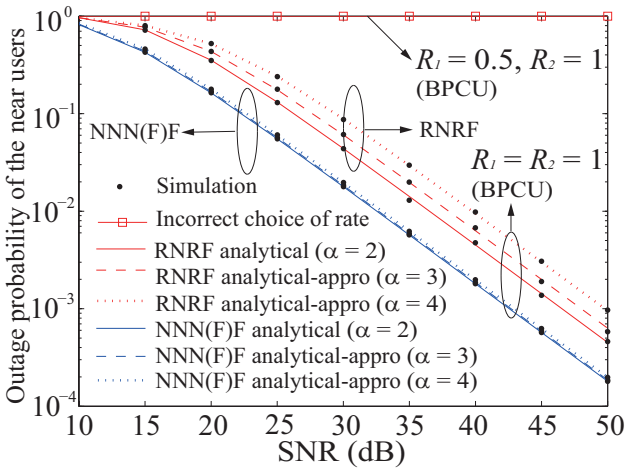

Figure 3.2: Outage probability of the near users versus SNR with different α, where $R_{D_\mathrm{B}} = 2\ m$, and $\lambda_{\Phi_\mathrm{B}} = 1$.

to the multiuser diversity gain, since there is an increasing number of the near users; 3) The outage probability of RNRF is a constant, i.e., independent of the density of near users, and is the outage ceiling of the NNN(F)F. This is due to the fact that no opportunistic user selection is carried out for RNRF; and 4) An outage floor exits even if the density of the near users goes to infinity. This is due to the bounded path loss model used in this chapter. When the number of the near users exceeds a threshold, the selected near user will be very close to the source, which makes the path loss approach one.

Fig. 3.4 plots the outage probability of the near users versus the rate of the near users and far users for both RNRF and NNN(F)F. One can observe that the outage of the near users occurs more frequently as the rate of the far user, R_1, increases. This is because in the proposed protocol, the near user $\mathrm{B_i}$ needs to first decode x_{i1} which is intended to the far user $\mathrm{A_i}$, and then decode its own message. Therefore increasing R_1 makes it harder to decode x_{i1}, which will lead to increased outages. An important observation is that incorrect choices of R_1 and R_2 will make the outage probability always one. Particularly, for the choice of R_1, it should satisfy the condition $(|p_{i1}|^2 - |p_{i2}|^2\tau_1 > 0)$ in order to ensure that successive interference cancelation can be implemented. For the

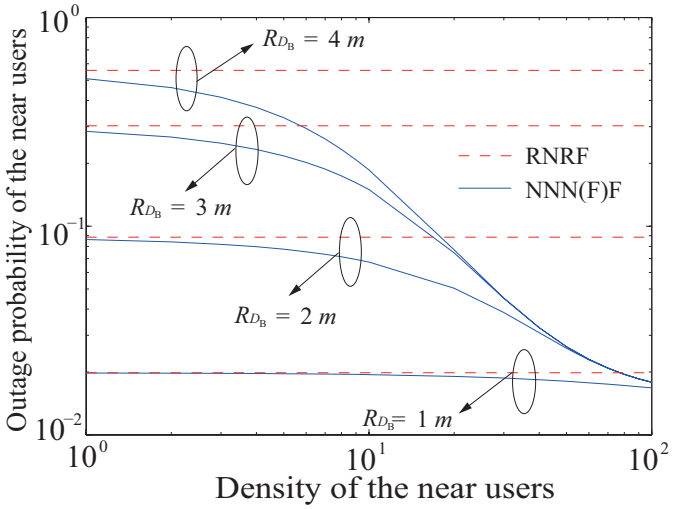

Figure 3.3: Outage probability of the near users versus density with different R_{D_B}, where $\lambda_{\Phi_B} = 1$, and $SNR = 30$ dB.

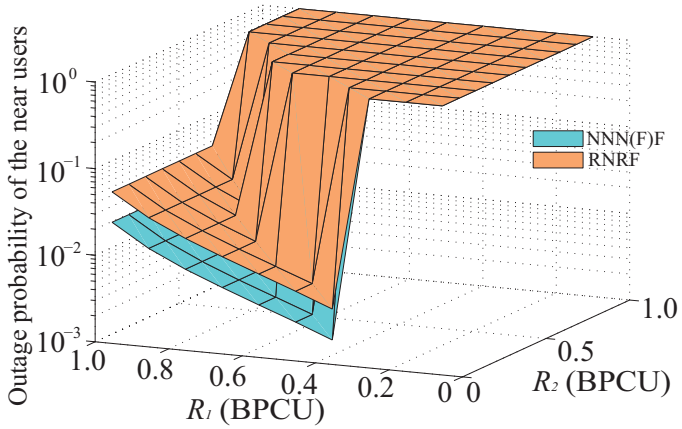

Figure 3.4: Outage probability of the near users versus R_1 and R_2, where $\alpha = 2, R_{D_B} = 2$ m, and $SNR = 30$ dB.

choice of R_2, it should satisfy the condition that the split energy for detecting x_{i1} is also sufficient to detect x_{i2} ($\varepsilon_{A_i} \geq \varepsilon_{B_i}$).

3.4.2 Outage Probability of the Far Users

In this subsection, it is demonstrated that the outage probability of the far users with different choices of the density, path loss coefficients, and user zone of the three user

selection schemes.

Fig. 3.5 plots the outage probability of the far users versus SNR with different path loss coefficients of RNRF, NNNF, and NNFF. The dashed red, blue, and black curves circled together and pointed by $\alpha = 2$, are the analytical approximations for the special case of RNRF, NNNF, and NNFF, which are obtained from (3.24), (3.38) and (3.43), respectively. The dashed red, blue, and black curves circled together and pointed by $\alpha = 3$, are the analytical approximations for an arbitrary choice of α of RNRF, NNNF, and NNFF, which are obtained from (3.23), (3.37) and (3.42), respectively. The solid marked lines are used to represent the Monte Carlo simulation results for each case. As can be observed from the figure, the simulation and the analytical approximation are very close, particularly in the high SNR region. Several observations can be drawn as follows: 1) NNNF achieves the lowest outage probability among the three selection schemes since both the near and far users have the smallest path loss; 2) NNFF achieves lower outage than RNRF, which indicates that the distance of the near users has more impact than that of the far users; 3) it is clear that all of the curves in Fig. 3.5 have the same slopes, which indicates that the diversity gains of the far users for the three schemes are the same. In the diversity analysis, it is shown that the diversity gain of the three selection schemes is two. The simulation validates the analytical results and indicates that the achievable diversity gain is the same for different user selection schemes.

Fig. 3.6 plots the outage probability of the far users versus R_1 with different $R_{D_{\mathrm{C}}}$ and $R_{D_{\mathrm{B}}}$. One can observe that the outage probabilities of the three schemes increase as R_1 increases. This is because increasing R_1 will make the threshold of decoding higher, which in turn leads to more outage. It can also be observed that increasing the radius of the user zone for the far users will deteriorate the outage performance. The reason is that the path loss of the far users becomes larger.

Fig. 3.7 plots the outage probability of the far users versus SNR for both cooperative NOMA and non-cooperative NOMA. Several observations can be drawn as follows: 1) by using an energy constrained relay to perform cooperative NOMA transmission, the

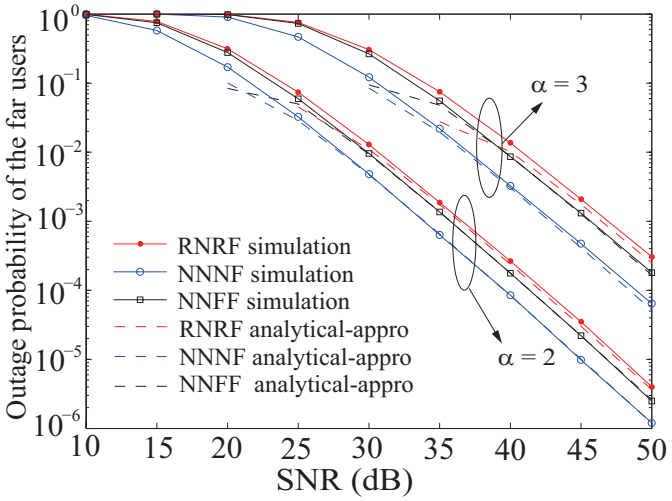

Figure 3.5: Outage probability of the far users with different α, $R_1 = 0.3$ bit per channel use (BPCU), $R_{D_\mathrm{A}} = 10\ m$, $R_{D_\mathrm{B}} = 2\ m$, $R_{D_\mathrm{C}} = 8\ m$, $\lambda_{\Phi_\mathrm{A}} = 1$, and $\lambda_{\Phi_\mathrm{B}} = 1$.

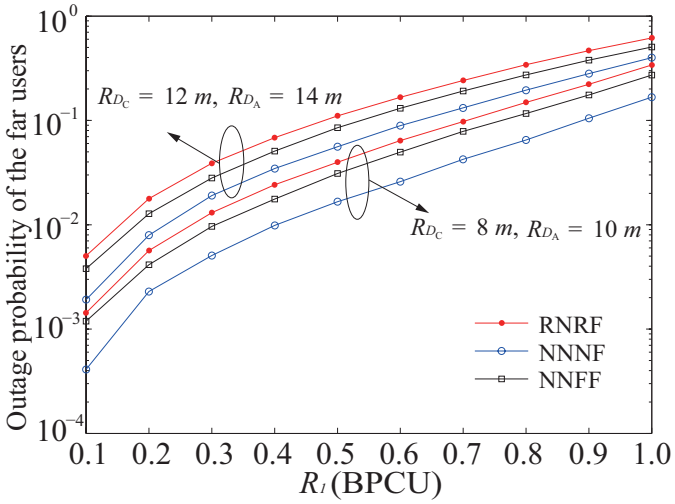

Figure 3.6: Outage probability of the far users versus R_1, where $\alpha = 2$, $R_{D_\mathrm{B}} = 2\ m$, and $SNR = 30$ dB.

outage probability of the far users has a larger slope than that of non-cooperative NOMA, for all user selection schemes. This is due to the fact that cooperative NOMA can achieve a larger diversity gain and guarantees more reliable reception for the far users in the high SINR region; 2) NNNF achieves the lowest outage probability among these three selection schemes both for cooperative NOMA and non-cooperative NOMA because of its smallest path loss; 3) it is worth noting that NNFF has higher outage probability

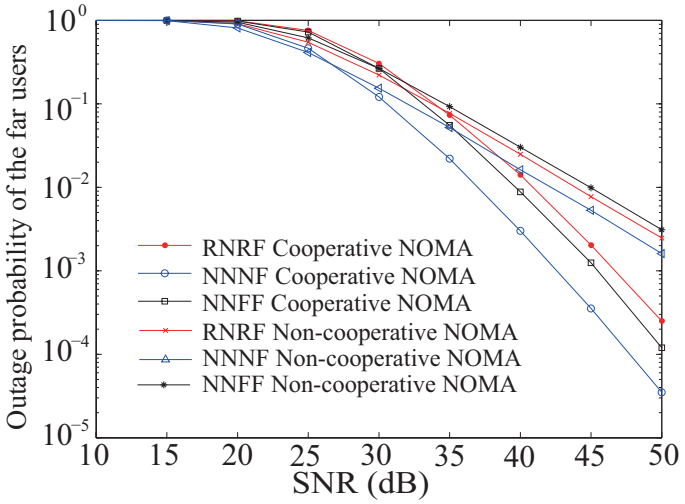

Figure 3.7: Comparison of outage probability with non-cooperative NOMA, $\alpha = 3$, $R_1 = 0.3$ BPCU, $R_{D_\mathrm{A}} = 10$ m, $R_{D_\mathrm{B}} = 2$ m, $R_{D_\mathrm{C}} = 8$ m, $\lambda_{\Phi_\mathrm{A}} = 1$, and $\lambda_{\Phi_\mathrm{B}} = 1$.

than RNRF in non-cooperative NOMA, however, it achieves lower outage probability than RNRF in cooperative NOMA. This phenomenon indicates that it is very helpful and necessary to apply cooperative NOMA in NNFF due to the largest performance gain over non-cooperative NOMA.

3.4.3 Throughput in Delay-Sensitive Transmission Mode

Fig. 3.8 plots the system throughput versus SNR with different targeted rates. One can observe that NNNF achieves the highest throughput since it has the lowest outage probability among three selection schemes. The figure also demonstrates the existence of the throughput ceilings in the high SNR region. This is due to the fact that the outage probability is approaching zero and the throughput is determined only by the targeted data rate. It is worth noting that increasing R_2 from $R_2 = 0.5$ BPCU to $R_2 = 1$ BPCU can improve the throughput; however, for the case $R_2 = 2$ BPCU, the throughput is lowered. This is because, in the latter case, the energy remaining for information decoding is not sufficient for message detection of the near user, and hence an outage occurs, which in turn affects the throughput. Therefore, it is seen that it

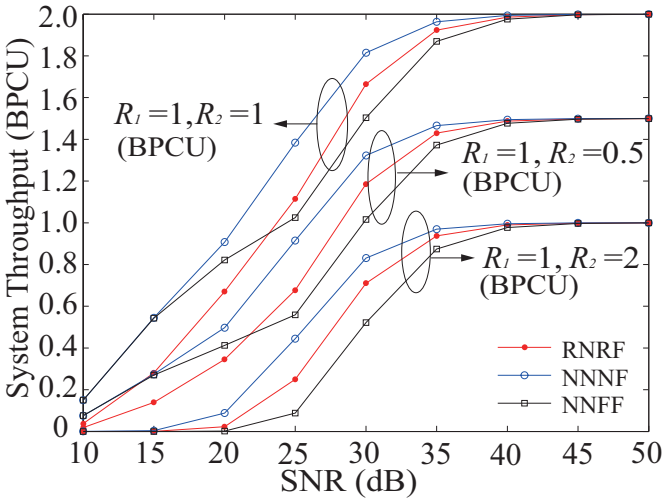

Figure 3.8: System throughput in delay-sensitive mode versus SNR with different rate, $\alpha = 2$, $R_{D_\mathrm{A}} = 10\ m$, $R_{D_\mathrm{B}} = 2\ m$, $R_{D_\mathrm{C}} = 8\ m$, $\lambda_{\Phi_\mathrm{A}} = 1$, and $\lambda_{\Phi_\mathrm{B}} = 1$.

is important to select appropriate transmission rates when designing practical NOMA downlink transmission systems.

3.5 Summary

In this chapter, the application of SWIPT to NOMA has been considered. A novel cooperative SWIPT NOMA protocol with three different user selection criteria has been proposed. Stochastic geometric approach is used to provide a complete framework to model the locations of users and evaluate the performance of the proposed user selection schemes. Closed-form results have been derived in terms of outage probability and delay-sensitive throughput to determine the system performance. The diversity gain of the three user selection schemes has also been characterized and proved to be the same as that of a conventional cooperative network. For the proposed protocol, the decreasing rate of the outage probability of far users is $\frac{\ln SNR}{SNR^2}$ while it is $\frac{1}{SNR^2}$ for a conventional cooperative network. Numerical results have been presented to validate the analysis. It is concluded that by carefully choosing the parameters of the network, (e.g., transmission

rate or power splitting coefficient), acceptable system performance can be guaranteed even if the users do not use their own batteries to power the relay transmission.

Chapter 4

Non-orthogonal Multiple Access in Large-Scale Underlay Cognitive Radio Networks

This chapter is organized as follows. The main contributions are firstly introduced in Section 4.1. In Section 4.2, the considered CR NOMA scenarios is presented with using scholastic geometry. In Section 4.3, new analytical expressions are derived for the outage probability and diversity order are derived. Section 4.5 gives the numerical results of the considered framework. Finally, Section 4.6 concludes this chapter.

4.1 Introduction

The application of NOMA in underlay CR networks uses additional power control at the secondary BS to improve the spectral efficiency. Stochastic geometry is used to model a large-scale CR network with a large number of randomly deployed PTs and PRs. Consider a practical system design as follows: 1) All the SUs, PTs, and PRs are randomly deployed based on the considered stochastic geometry model; 2) Each SU

suffers interference from other NOMA SUs as well as the PTs; and 3) The secondary BS must satisfy a predefined power constraint threshold to avoid interference at the PRs. New closed-form expressions of the outage probability of the NOMA users are derived to evaluate the performance of the considered CR NOMA network. Moreover, considering two different power constraints at the PTs, diversity order[1] analysis is carried out with providing important insights: 1) When the transmit power of the PTs is fixed, the m-th user among all ordered NOMA user experiences a diversity order of m; and 2) When the the transmit power of the PTs is proportional to that of the secondary BS, an asymptotic error floor exists for the outage probability.

4.2 Network Model

As shown in 4.1, consider a large-scale underlay spectrum sharing scenario consisting of the PN and the secondary network (SN). In the SN, a secondary BS is located at the center of a disc, denoted by $\mathcal{D}$ with radius R_D as its coverage. The M randomly deployed secondary users are uniformly distributed within the disc which is the user zone for NOMA. The secondary BS communicates with all SUs within the disc by applying the NOMA transmission protocol. It is worthy pointing out that the power of the secondary transmitter is constrained in order to limit the interference at the PRs. In the PN, a random number of PTs and PRs is distributed in an infinite two dimensional plane. The spatial topology of all the PTs and PRs are modeled using homogeneous PPPs, denoted by Φ_b and Φ_ℓ with density λ_b and λ_ℓ, respectively. All channels are assumed to be quasi-static Rayleigh fading where the channel coefficients are constant for each transmission block but vary independently between different blocks.

According to underlay CR, the transmit power P_t at the secondary BS is constrained

[1]Diversity order is defined as the slope for the outage provability curve decreasing with the signal-to-noise-ratio (SNR). It measures the number of independent fading paths over which the data is received. In NOMA networks, since users' channels are ordered and SIC is applied at each receiver, it is of importance to investigate the diversity order.

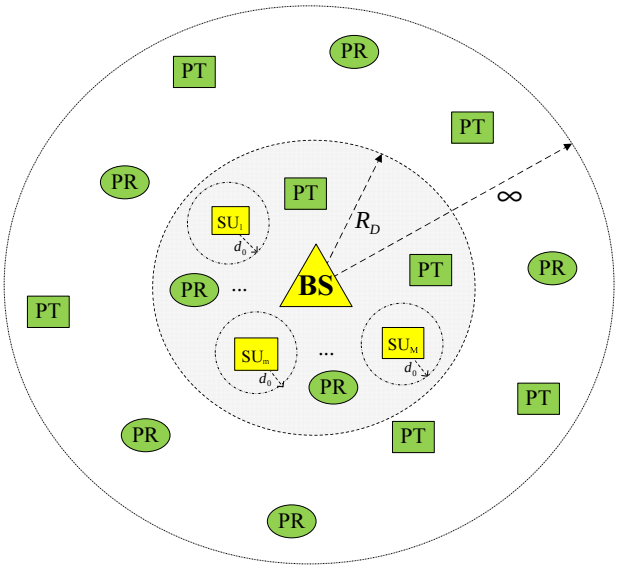

Figure 4.1: Illustration of the considered NOMA CR networks, where PT is primary transmitter, PR is primary receiver, SU is secondary user, and BS is base station. Here, d_0, R_D, and ∞ are the radius of the guard zone for secondary users, the user zone (disc $\mathcal{D}$) for the secondary users, and the infinite two dimensional plane for primary users.

as follows:

$$P_t = \min\left\{\frac{I_p}{\max\limits_{\ell\in\Phi_\ell}|g_\ell|^2}, P_s\right\}, \tag{4.1}$$

where I_p is the maximum permissible interference power at the PRs, P_s is maximum transmission power at the secondary BS, $|g_\ell|^2 = |\hat{g}_\ell|^2 L(d_\ell)$ is the overall channel gain

from the secondary BS to PRs ℓ. Here, $\hat{g}_\ell$ is small-scale fading with $\hat{g}_\ell \sim \mathcal{CN}(0,1)$, $L\left(d_\ell\right) = \frac{1}{1+d_\ell^\alpha}$ is large-scale path loss, d_ℓ is the distance between the secondary BS and the PRs, and α is the path loss exponent. A bounded path loss model is used to ensure the path loss is always larger than one even for small distances [9, 122].

According to NOMA, the BS sends a combination of messages to all NOMA users, and the observation at the m-th secondary user is given by

$$y_m = h_m \sum_{n=1}^{M} \sqrt{a_n P_t} x_n + n_m, \tag{4.2}$$

where n_m is the AWGN at the m-th user with variance σ^2, a_n is the power allocation coefficient for the n-th SU with $\sum_{n=1}^{M} a_n = 1$, x_n is the information for the n-th user, and h_m is the channel coefficient between the m-th user and the secondary BS.

For the SUs, they also observe the interferences of the randomly deployed PTs in the PN. Usually, when the PTs are close to the secondary NOMA users, they will cause significant interference. To overcome this issue, an interference guard zone D_0 is introduced to each secondary NOMA user with radius of d_0, which means that there is no interference from PTs allowed inside this zone [123]. It is assumed that $d_0 \geq 1$ in this chapter. The interference links from the PTs to the SUs are dominated by the path loss and is given by

$$I_B = \sum_{b \in \Phi_b} L\left(d_b\right), \tag{4.3}$$

where $L(d_b) = 1/(1+d_b^\alpha)$ is the large-scale path loss and d_b is the distance from the PTs to the SUs.

Without loss of generality, all the channels of SUs are assumed to follow the order as $|h_1|^2 \leq |h_2|^2 \leq \cdots \leq |h_M|^2$. The power allocation coefficients are assumed to follow the order as $a_1 \geq a_2 \geq \cdots \geq a_M$. According to the NOMA principle, SIC is carried out at the receivers [119]. It is assumed that $1 \leq j \leq m < i$. In this case, the m-th

user can decode the message of the j-th user and treats the message for the i-th user as interference. Specifically, the m-th user first decodes the messages of all the $(m-1)$ users, and then successively subtracts these messages to obtain its own information. Therefore, the received SINR for the m-th user to decode the information of the j-th user is given by

$$\gamma_{m,j} = \frac{|h_m|^2 \gamma_t a_j}{|h_m|^2 \gamma_t \sum\limits_{i=j+1}^{M} a_i + \rho_b I_B + 1}, \tag{4.4}$$

where $\gamma_t = \min\left\{\frac{\rho_p}{\max\limits_{\ell\in\Phi_\ell}|g_\ell|^2}, \rho_s\right\}$, $\rho_p = \frac{I_p}{\sigma^2}, \rho_s = \frac{P_s}{\sigma^2}, \rho_b = \frac{P_B}{\sigma^2}$, and P_B is the transmit power of the PTs, $|h_m|^2$ is the overall ordered channel gain from the secondary BS to the m-th SU. For the case $m = j$, it indicates the m-th user decodes the message of itself. Note that the SINR for the M-th SU is $\gamma_{M,M} = \frac{|h_M|^2 \gamma_t a_M}{\rho_b I_B + 1}$.

4.3 Outage Probability

In this section, exact analysis of the considered networks in terms of outage probability is provided. In NOMA, an outage occurs if the m-th user can not detect any of the j-th user's message, where $j \leq m$ due to the SIC. Denote $X_m = \frac{|h_m|^2 \gamma_t}{\rho_b I_B + 1}$. Based on (4.4), the CDF of X_m is given by

$$F_{X_m}(\varepsilon) = \Pr\left\{\frac{|h_m|^2 \gamma_t}{\rho_b I_B + 1} < \varepsilon\right\}. \tag{4.5}$$

Denote $\varepsilon_j = \tau_j / \left(a_j - \tau_j \sum_{i=j+1}^{M} a_i\right)$ for $j < M$, $\tau_j = 2^{R_j} - 1$, R_j is the target data rate for the j-th user, $\varepsilon_M = \tau_M / a_M$, and $\varepsilon_m^{\max} = \max\{\varepsilon_1, \varepsilon_2, ..., \varepsilon_m\}$.

The outage probability at the m-th user can be expressed as follows:

$$P_m = \Pr\{X_m < \varepsilon_m^{\max}\} = F_{X_m}(\varepsilon_m^{\max}), \tag{4.6}$$

where the condition $a_j - \tau_j \sum_{i=j+1}^{M} a_i > 0$ should be satisfied due to applying NOMA, otherwise the outage probability will always be one [9].

It is necessary to calculate the CDF of X_m conditioned on I_B and γ_t. Rewrite (4.5) as follows:

$$F_{X_m|I_B,\gamma_t}(\varepsilon) = F_{|h_m|^2}\left(\frac{(\rho_b I_B + 1)\,\varepsilon}{\gamma_t}\right), \tag{4.7}$$

where $F_{|h_m|^2}$ is the CDF of h_m. Based on order statistics [124] and applying binomial expansion, the CDF of the ordered channels has a relationship with the unordered channels as follows:

$$F_{|h_m|^2}(y) = \psi_m \sum_{p=0}^{M-m} \binom{M-m}{p} \frac{(-1)^p}{m+p} \left(F_{|\tilde{h}|^2}(y)\right)^{m+p}, \tag{4.8}$$

where $y = \frac{(\rho_b I_B+1)\varepsilon}{\gamma_t}$, $\psi_m = \frac{M!}{(M-m)!(m-1)!}$, and $\left|\tilde{h}\right|^2 = \left|\hat{h}\right|^2 L(d)$ is the unordered channel gain of an arbitrary SU. Here, $\hat{h}$ is the small-scale fading coefficient with $\hat{h} \sim \mathcal{CN}(0,1)$, $L(d) = \frac{1}{1+d^\alpha}$ is the large-scale path loss, and d is a random variable representing the distance from the secondary BS to an arbitrary SU.

Then using the assumption of homogenous PPP and applying the polar coordinates, $F_{|\tilde{h}|^2}(y)$ is expressed as follows:

$$F_{|\tilde{h}|^2}(y) = \frac{2}{R_D^2} \int_0^{R_D} \left(1 - e^{-(1+r^\alpha)y}\right) r dr. \tag{4.9}$$

Note that it is challenging to obtain an insightful expression for the unordered CDF. As such, the Gaussian-Chebyshev quadrature [120] is applied in this chapter to find an approximation for (4.9) as

$$F_{|\tilde{h}|^2}(y) \approx \sum_{n=0}^{N} b_n e^{-c_n y}, \tag{4.10}$$

where N is a complexity-accuracy tradeoff parameter, $b_n = -\omega_N \sqrt{1-\phi_n^2}\,(\phi_n + 1)$, $b_0 =$

$-\sum_{n=1}^{N} b_n$, $c_n = 1 + \left(\frac{R_D}{2}\left(\phi_n + 1\right)\right)^{\alpha}$, $\omega_N = \frac{\pi}{N}$, and $\phi_n = \cos\left(\frac{2n-1}{2N}\pi\right)$.

Substituting (4.10) into (4.8) and applying the multinomial theorem, the following express is obtained

$$F_{|h_m|^2}(y) = \psi_m \sum_{p=0}^{M-m} \binom{M-m}{p} \frac{(-1)^p}{m+p} \sum_{q_0+\cdots+q_N=m+p} \binom{m+p}{q_0+\cdots+q_N} \left(\prod_{n=0}^{N} b_n^{q_n}\right) e^{-\sum_{n=0}^{N} q_n c_n y}. \tag{4.11}$$

where $\binom{m+p}{q_0+\cdots+q_N} = \frac{(m+p)!}{q_0!\cdots q_N!}$. Based on (4.11), the CDF of X_m can be expressed as follows:

$$\begin{aligned} F_{X_m}(\varepsilon_j) =& \int_0^{\infty}\int_0^{\infty} F_{|h_m|^2}\left(\frac{(\rho_b x+1)\varepsilon_j}{z}\right) f_{I_B}(x)\, f_{\gamma_t}(z)\, dxdz \\ =& \psi_m \sum_{p=0}^{M-m} \binom{M-m}{p} \frac{(-1)^p}{m+p} \sum_{q_0+\cdots+q_N=m+p} \binom{m+p}{q_0+\cdots+q_N} \left(\prod_{n=0}^{N} b_n^{q_n}\right) \\ & \times \underbrace{\int_0^{\infty} e^{-\frac{\varepsilon_j}{z}\sum_{n=0}^{N} q_n c_n} \underbrace{\int_0^{\infty} e^{-\frac{x\rho_b\varepsilon_j}{z}\sum_{n=0}^{N} q_n c_n} f_{I_B}(x)dx}_{Q_2} f_{\gamma_t}(z)dz}_{Q_1}, \end{aligned} \tag{4.12}$$

where f_{γ_t} is the PDF of γ_t. Q_2 in (4.12) is expressed as follows:

$$Q_2 = \int_0^{\infty} e^{-x\frac{\rho_b\varepsilon_j}{z}\sum_{n=0}^{N} q_n c_n} f_{I_B}(x)dx = E_{\Phi_b}\left\{e^{-\frac{x\rho_b\varepsilon_j}{z}\sum_{n=0}^{N} q_n c_n}\right\} = L_{I_B}\left(\frac{\rho_b\varepsilon_j}{z}\sum_{n=0}^{N} q_n c_n\right). \tag{4.13}$$

In this case, the Laplace transformation of the interferences from the PT can be expressed as [123]

$$\begin{aligned} L_{I_B}(s) &= \exp\left(-\lambda_b\pi\left[\left(e^{-sd_0^{-\alpha}}-1\right)d_0^2 + s^{\delta}\gamma\left(1-\delta, sd_0^{-\alpha}\right)\right]\right) \\ &= \exp\left(-\lambda_b\pi\left[\left(e^{-sd_0^{-\alpha}}-1\right)d_0^2 + s^{\delta}\underbrace{\int_0^{sd_0^{-\alpha}} t^{-\delta}e^{-t}dt}_{\Theta}\right]\right), \end{aligned} \tag{4.14}$$

where $\delta = \frac{2}{\alpha}$ and $\gamma(\cdot)$ is the lower incomplete Gamma function.

To obtain an insightful expression, Gaussian-Chebyshev quadrature is used to approximate the lower incomplete Gamma function in (4.14), Θ can be expressed as follows:

$$\Theta \approx s^{1-\delta} \sum_{l=1}^{L} \beta_l e^{-t_l s d_0^{-\alpha}}, \tag{4.15}$$

where L is a complexity-accuracy tradeoff parameter, $\beta_l = \frac{1}{2} d_0^{2-\alpha} \omega_L \sqrt{1-\theta_l^2} t_l^{-\delta}$, $t_l = \frac{1}{2}(\theta_l + 1)$, $\omega_L = \frac{\pi}{L}$, and $\theta_l = \cos\left(\frac{2l-1}{2L}\pi\right)$. Substituting (4.15) into (4.14), the Laplace transformation is approximated as follows:

$$L_{I_B}(s) \approx e^{-\lambda_b \pi \left(\left(e^{-s d_0^{-\alpha}} - 1 \right) d_0^2 + s \sum\limits_{l=1}^{L} \beta_l e^{-t_l s d_0^{-\alpha}} \right)}. \tag{4.16}$$

Substituting (4.16) into (4.12), Q_2 is given by

$$Q_2 = e^{-\lambda_b \pi \left(\left(e^{-\frac{\rho_b \varepsilon_j d_0^{-\alpha}}{z} \sum\limits_{n=0}^{N} q_n c_n} - 1 \right) d_0^2 + \frac{\rho_b \varepsilon_j}{z} \sum\limits_{n=0}^{N} q_n c_n \sum\limits_{l=1}^{L} \beta_l e^{-\frac{t_l \rho_b \varepsilon_j}{z d_0^{\alpha}} \sum\limits_{n=0}^{N} q_n c_n} \right)}. \tag{4.17}$$

The following theorem provides the PDF of γ_t.

Theorem 6. *Consider the use of the composite channel model with Rayleigh fading and path loss, the PDF of the effective power of the secondary BS is given by*

$$f_{\gamma_t}(x) = e^{-a_\ell \rho_s^\delta e^{-\frac{\rho_p}{x}}} Dirac(x - \rho_s) + \left(\frac{\rho_p}{x} + \delta \right) a_\ell x^{\delta - 1} e^{-a_\ell x^\delta e^{-\frac{\rho_p}{x}} - \frac{\rho_p}{x}} U(\rho_s - x), \tag{4.18}$$

where $a_\ell = \frac{\delta \pi \lambda_\ell \Gamma(\delta)}{\rho_p^\delta}$, $U(\cdot)$ *is the unit step function, and* $Dirac(\cdot)$ *is the impulse function.*

Proof. The CDF of γ_t is given by

$$\begin{aligned} F_{\gamma_t}(x) &= \Pr\left\{\min\left\{\frac{\rho_p}{\max\limits_{\ell\in\Phi_\ell}|g_\ell|^2}, \rho_s\right\} \le x\right\} \\ &= \Pr\left\{\max_{\ell\in\Phi_\ell}|g_\ell|^2 \ge \max\left\{\frac{\rho_p}{x}, \frac{\rho_p}{\rho_s}\right\}\right\} + \Pr\left\{\max_{\ell\in\Phi_\ell}|g_\ell|^2 \le \frac{\rho_p}{\rho_s}, \rho_s \le x\right\} \\ &= 1 - U(\rho_s - x)\underbrace{\Pr\left\{\max_{\ell\in\Phi_\ell}|g_\ell|^2 \ge \frac{\rho_p}{x}\right\}}_{\Omega}. \end{aligned} \tag{4.19}$$

Denote $\bar{\Omega} = 1 - \Omega$, $\bar{\Omega}$ is expressed as follows:

$$\begin{aligned} \bar{\Omega} &= \Pr\left\{\max_{\ell\in\Phi_\ell}|g_\ell|^2 \le \frac{\rho_p}{x}\right\} = E_{\Phi_\ell}\left\{\prod_{\ell\in\Phi_\ell}\Pr\left\{|\hat{g}_\ell|^2 \le \frac{(1+d_\ell^\alpha)\rho_p}{x}\right\}\right\} \\ &= E_{\Phi_\ell}\left\{\prod_{\ell\in\Phi_\ell} F_{|\hat{g}_\ell|^2}\left(\frac{(1+d_\ell^\alpha)\rho_p}{x}\right)\right\}. \end{aligned} \tag{4.20}$$

Applying the generating function, (4.20) is rewritten as follows:

$$\bar{\Omega} = \exp\left[-\lambda_\ell \int\limits_{R^2}\left(1 - F_{|\hat{g}_\ell|^2}\left((1+d_\ell^\alpha)\mu\right)\right) r dr\right] = \exp\left[-2\pi\lambda_\ell e^{-\mu}\int_0^\infty r e^{-\mu r^\alpha} dr\right]. \tag{4.21}$$

Applying [125, Eq. (3.326.2)], the following expression is obtained

$$\Omega = 1 - \bar{\Omega} = 1 - e^{-\frac{e^{-\mu}\delta\pi\lambda_\ell\Gamma(\delta)}{\mu^\delta}}, \tag{4.22}$$

where $\Gamma(\cdot)$ is Gamma function. Substituting (4.22) into (4.19), the following expression is obtained

$$F_{\gamma_t}(x) = 1 - U(\rho_s - x)\, e^{-e^{-\frac{\rho_p}{x}} x^\delta a_\ell}. \tag{4.23}$$

By taking the derivative of $F_{\gamma_t}(x)$ in (4.23), the PDF of γ_t is obtained in (4.18). The

proof is complete.

□

Substituting (4.18) and (4.17) into (4.12), Q_1 is expressed as follows:

$$Q_1 = e^{-a_\ell \rho_s^\delta e^{-\frac{\rho_p}{\rho_s}} - \frac{\varepsilon_j \sum_{n=0}^{N} q_n c_n}{\rho_s} - \lambda_b \pi \left(\left(e^{-\frac{\rho_b \varepsilon_j}{\rho_s d_0^\alpha} \sum_{n=0}^{N} q_n c_n} - 1 \right) d_0^2 + \frac{\rho_b \varepsilon_j}{\rho_s} \sum_{n=0}^{N} q_n c_n \sum_{l=1}^{L} \beta_l e^{-\frac{t_l \rho_b \varepsilon_j}{\rho_s d_0^\alpha} \sum_{n=0}^{N} q_n c_n} \right)} + \underbrace{\int_0^{\rho_s} a_\ell \left(\frac{\rho_p}{z} + \delta \right) z^{\delta-1} e^{-a_\ell z^\delta e^{-\frac{\rho_p}{z}} - \frac{\rho_p + \varepsilon_j \sum_{n=0}^{N} q_n c_n}{z}} Q_2 dz}_{\Psi}. \tag{4.24}$$

Note that it is very challenging to solve the integral Ψ in (4.24), therefore, the Gaussian-Chebyshev quadrature is applied to approximate the integral as follows:

$$\Psi \approx \sum_{k=1}^{K} \eta_k e^{-\frac{\rho_p + \varepsilon_j \sum_{n=0}^{N} q_n c_n}{\rho_s s_k} - \lambda_b \pi \left(\left(e^{-\frac{\rho_b \varepsilon_j}{\rho_s s_k d_0^\alpha} \sum_{n=0}^{N} q_n c_n} - 1 \right) d_0^2 + \frac{\rho_b \varepsilon_j}{\rho_s s_k} \sum_{n=0}^{N} q_n c_n \sum_{l=1}^{L} \beta_l e^{-\frac{t_l \rho_b \varepsilon_j}{\rho_s s_k d_0^\alpha} \sum_{n=0}^{N} q_n c_n} \right)}, \tag{4.25}$$

where K is a complexity-accuracy tradeoff parameter, $\omega_K = \frac{\pi}{K}$, $\varphi_k = \cos\left(\frac{2k-1}{2K}\pi\right)$, $s_k = \frac{1}{2}(\varphi_k + 1)$, and $\eta_k = \frac{\omega_K}{2}\sqrt{1-\varphi_k^2}\left(\frac{\rho_p}{\rho_s s_k} + \delta\right) a_\ell \rho_s^\delta s_k^{\delta-1} e^{-a_\ell \rho_s^\delta s_k^\delta e^{-\frac{\rho_p}{\rho_s s_k}}}$.

Substituting (4.24) and (4.25) into (4.12) and applying $\varepsilon_{\max} \to \varepsilon_j$, based on (4.6), the

closed-form expression of the outage probability is obtained at the m-th user as follows:

$$P_m = \psi_m \sum_{p=0}^{M-m} \binom{M-m}{p} \frac{(-1)^p}{m+p} \sum_{q_0+\cdots+q_N=m+p} \binom{m+p}{q_0+\cdots+q_N} \left(\prod_{n=0}^{N} b_n^{q_n}\right)$$
$$\times \left[e^{-a_\ell \rho_s^\delta e^{-\frac{\rho_p}{\rho_s}} - \frac{\varepsilon_{\max} \sum_{n=0}^{N} q_n c_n}{\rho_s} - \lambda_b \pi \left(\left(e^{-\frac{\rho_b \varepsilon_{\max}}{\rho_s d_0^\alpha} \sum_{n=0}^{N} q_n c_n} - 1 \right) d_0^2 + \frac{\rho_b \varepsilon_{\max}}{\rho_s} \sum_{n=0}^{N} q_n c_n \sum_{l=1}^{L} \beta_l e^{-\frac{t_l \rho_b \varepsilon_{\max}}{\rho_s d_0^\alpha} \sum_{n=0}^{N} q_n c_n} \right)} \right.$$
$$\left. + \sum_{k=1}^{K} \eta_k e^{-\frac{\rho_p + \varepsilon_{\max} \sum_{n=0}^{N} q_n c_n}{\rho_s s_k} - \lambda_b \pi \left(\left(e^{-\frac{\rho_b \varepsilon_{\max}}{\rho_s s_k d_0^\alpha} \sum_{n=0}^{N} q_n c_n} - 1 \right) d_0^2 + \frac{\rho_b \varepsilon_{\max}}{\rho_s s_k} \sum_{n=0}^{N} q_n c_n \sum_{l=1}^{L} \beta_l e^{-\frac{t_l \rho_b \varepsilon_{\max}}{\rho_s s_k d_0^\alpha} \sum_{n=0}^{N} q_n c_n} \right)} \right]. \tag{4.26}$$

4.4 Diversity Analysis

Based on the analytical results for the outage probability in (4.26), it is aimed to provide asymptotic diversity analysis for the ordered NOMA users. The diversity order of the user's outage probability is defined as

$$d = -\lim_{\rho_s \to \infty} \frac{\log P_m(\rho_s)}{\log \rho_s}. \tag{4.27}$$

4.4.1 Fixed Transmit Power at Primary Transmitters

In this case, the diversity with the fixed transmit SNR at the PTs (ρ_b) is examined, while the transmit SNR of secondary BS (ρ_s) and the maximum permissible interference constraint at the PRs (ρ_p) go to the infinity. Particularly, it is assumed that ρ_p is proportional to ρ_s, i.e. $\rho_p = \kappa \rho_s$, where κ is a positive scaling factor. This assumption applies to the scenario where the PRs can tolerate a large amount of interference from the secondary BS and the target data rate is relatively small in the PN. Denote $\gamma_{t^*} = \frac{\gamma_t}{\rho_s} = min\left\{\frac{\kappa}{\max\limits_{\ell \in \Phi_\ell} |g_\ell|^2}, 1\right\}$, similar to (4.8), the ordered CDF has the relationship with

unordered CDF as

$$F^{\infty}_{X_m|I_B,\gamma_{t^*}}(y^*) = \psi_m \sum_{p=0}^{M-m} \binom{M-m}{p} \frac{(-1)^p}{m+p} \left(F^{\infty}_{|\tilde{h}|^2}(y^*) \right)^{m+p}, \tag{4.28}$$

where $y^* = \frac{(\rho_b I_B+1)\varepsilon_j}{\rho_s \gamma_{t^*}}$. When $\rho_s \to \infty$, it is observed that $y^* \to 0$. In order to investigate an insightful expression to obtain the diversity order, Gaussian-Chebyshev quadrature and $1 - e^{-y^*} \approx y^*$ are used to approximate (4.9) as

$$F^{\infty}_{|\tilde{h}|^2}(y^*) \approx \sum_{n=1}^{N} \chi_n y^*, \tag{4.29}$$

where $\chi_n = \omega_N \sqrt{1-\phi_n^2}\,(\phi_n + 1)\, c_n$. Substituting (4.29) into (4.28), since $y^* \to 0$, the following expression is obtained

$$F^{\infty}_{X_m|I_B,\gamma_{t^*}}(\varepsilon_j) = \xi \left(\frac{(\rho_b I_B + 1)\,\varepsilon_j}{\rho_s \gamma_{t^*}} \right)^m + o\left(\left(\frac{(\rho_b I_B + 1)\,\varepsilon_j}{\rho_s \gamma_{t^*}} \right)^m \right), \tag{4.30}$$

where $\xi = \frac{\psi_m \left(\sum_{n=1}^{N} \chi_n \right)^m}{m}$ and $o(x)$ refers the high order expression of x. Based on (4.6), (4.11), and (4.30), the asymptotic outage probability is given by

$$P^{\infty}_{m_F} \approx \frac{1}{\rho_s^m} \underbrace{\int_0^{\infty} \int_0^{\infty} \xi \left(\frac{(\rho_b x + 1)\,\varepsilon_{\max}}{z} \right)^m f_{I_B}(x)\, f_{\gamma_{t^*}}(z)\, dx dz}_{C}, \tag{4.31}$$

where $f_{\gamma_{t^*}}$ the PDF of γ_{t^*}. Since C is a constant independent of ρ_s, (4.31) can be expressed as follows:

$$P^{\infty}_{m_F} = \frac{1}{\rho_s^m} C + o\left({\rho_s}^{-m} \right), \tag{4.32}$$

Substituting (4.32) into (4.27), the diversity order of this case is obtained as m. This can be explained as follows. Note that SIC is applied at the ordered SUs. For the first user with the poorest channel gain, no interference cancelation is operated at the receiver,

therefore its diversity gain is one. While for the m-th user, since the interferences from all the other $(m-1)$ users are canceled, it obtains a diversity of m.

4.4.2 Transmit Power of Primary Transmitters Proportional to that of Secondary Ones

In this case, the diversity with the transmit SNR at the PTs (ρ_b) is proportional to the transmit SNR of secondary BS (ρ_s) is examined. Particularly, it is assumed that $\rho_b = \nu\rho_s$, where ν is a positive scaling factor. It is still assumed that ρ_p is proportional to ρ_s. Applying $\rho_s \to \infty$, $\rho_p = \kappa\rho_s$ and $\rho_b = \nu\rho_s$ to (4.26), the asymptotic outage probability of the m-th user in this case is obtained as follows:

$$\begin{aligned} P_{m_P}^{\infty} \approx & \psi_m \sum_{p=0}^{M-m} \binom{M-m}{p} \frac{(-1)^p}{m+p} \sum_{q_0+\cdots+q_N=m+p} \binom{m+p}{q_0+\cdots+q_N} \left(\prod_{n=0}^{N} b_n^{q_n}\right) \\ & \times \Bigg[e^{-a_\ell^\infty e^{-\kappa} - \lambda_b \pi \left(\left(e^{-\frac{\nu\varepsilon_{\max}}{d_0^\alpha} \sum_{n=0}^{N} q_n c_n} - 1 \right) d_0^2 + \nu\varepsilon_{\max} \sum_{n=0}^{N} q_n c_n \sum_{l=1}^{L} \beta_l e^{-\frac{t_l \nu\varepsilon_{\max}}{d_0^\alpha} \sum_{n=0}^{N} q_n c_n} \right)} \\ & + \sum_{k=1}^{K} \eta_k^\infty e^{-\frac{\kappa}{s_k} - \lambda_b \pi \left(\left(e^{-\frac{\nu\varepsilon_{\max}}{s_k d_0^\alpha} \sum_{n=0}^{N} q_n c_n} - 1 \right) d_0^2 + \frac{\nu\varepsilon_{\max}}{s_k} \sum_{n=0}^{N} q_n c_n \sum_{l=1}^{L} \beta_l e^{-\frac{t_l \nu\varepsilon_{\max}}{s_k d_0^\alpha} \sum_{n=0}^{N} q_n c_n} \right)} \Bigg]. \end{aligned} \tag{4.33}$$

where $a_\ell^\infty = \frac{\delta\pi\lambda_\ell\Gamma(\delta)}{\kappa^\delta}$ and $\eta_k^\infty = \frac{\omega_K}{2}\sqrt{1-\varphi_k^2}\left(\frac{\kappa}{s_k}+\delta\right) a_\ell^\infty s_k^{\delta-1} e^{-a_\ell^\infty s_k^\delta e^{-\frac{\kappa}{s_k}}}$.

It is observed that $P_{m_P}^{\infty}$ is a constant independent of ρ_s. Substituting (4.33) into (4.27), it is obtained that asymptotically there is an error floor for the outage probability of SUs.

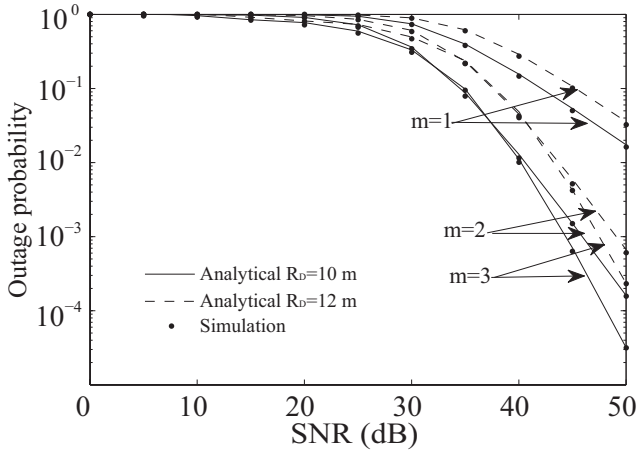

(a) For different user zone, with $\lambda_b = 10^{-3}$, $\lambda_\ell = 10^{-3}$, $\kappa = 1$, $\alpha = 4$, $\rho_b = 20$ dB, and $M = 3$.

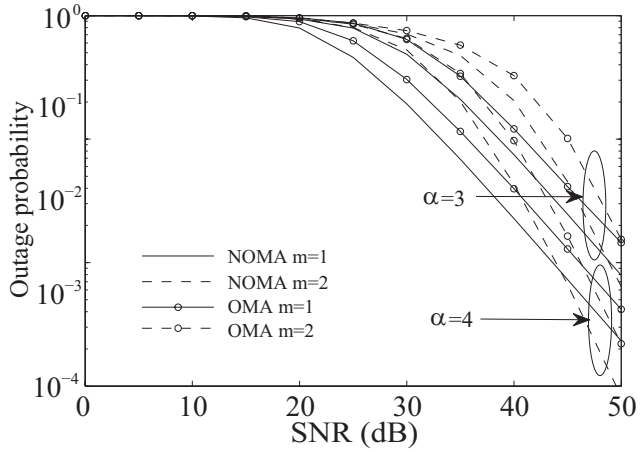

(b) For different α, with $\lambda_b = 10^{-3}$, $\lambda_\ell = 10^{-3}$, $\kappa = 1$, $R_D = 5$ m, $\rho_b = 20$ dB, and $M = 2$.

Figure 4.2: Outage probability of the m-th user versus ρ_s of the first scenario.

4.5 Numerical Results

In this section, numerical results are presented to verify the accuracy of the analysis as well as to obtain more important insights for NOMA in large-scale CR networks. In the considered network, the radius of the guard zone is assumed to be $d_0 = 2$ m. The Gaussian-Chebyshev parameters are chosen with $N = 5$, $K = 10$, and $L = 10$. Monte Carlo simulation results are marked as "•" to verify the derivation.

Fig. 4.2 plots the outage probability of the m-th user for the first scenario when ρ_b

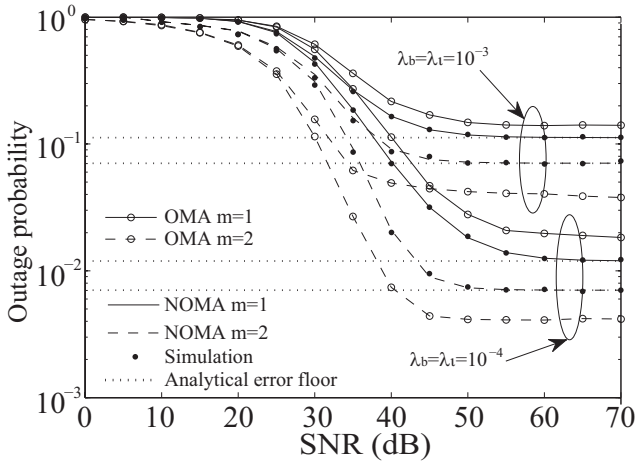

(a) For different density of PTs and PRs, with $\alpha = 4$, $\kappa = 1$, $\nu = 1$, $R_D = 10$ m, $\rho_b = \nu\rho_s$, and $M = 2$.

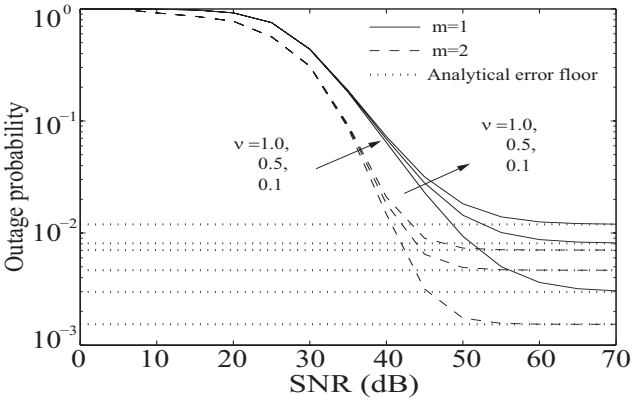

(b) For different ν, with $\alpha = 4$, $\lambda_b = 10^{-4}$, $\lambda_\ell = 10^{-4}$, $\kappa = 0.5$, $R_D = 10$ m, $\rho_b = \nu\rho_s$, and $M = 2$.

Figure 4.3: Outage probability of the m-th user versus ρ_s of the second scenario.

is fixed and ρ_p is proportional to ρ_s. In Fig. 4.2(a), the power allocation coefficients are $a_1 = 0.5$, $a_2 = 0.4$ and $a_3 = 0.1$. The target data rate for each user is assumed to be all the same as $R_1 = R_2 = R_3 = 0.1$ bit per channel use (BPCU). The dashed and solid curves are obtained from the analytical results derived in (4.26). Several observations can be drawn as follows: 1) Reducing the coverage of the secondary users zone $\mathcal{D}$ can achieve a lower outage probability because of a smaller path loss. 2) The ordered users with different channel conditions have different decreasing slope because of different diversity orders, which verifies the derivation of (4.31). In Fig. 4.2(b), the power allocation

coefficients are $a_1 = 0.8$ and $a_2 = 0.2$. The target rate is $R_1 = 1$ and $R_2 = 3$ BPCU. The performance of a conventional OMA is also shown in the figure as a benchmark for comparison. It can be observed that for different values of the path loss, NOMA can achieve a lower outage probability than the conventional OMA.

Fig. 4.3 plots the outage probability of the m-th user for the second scenario when both ρ_b and ρ_p are proportional to ρ_s. The power allocation coefficients are $a_1 = 0.8$ and $a_2 = 0.2$. The target rates are $R_1 = R_2 = 0.1$ BPCU. The dashed and solid curves are obtained from the analytical results derived in (4.26). One observation is that error floors exist in both Figs. 4.3(a) and 4.3(b), which verifies the asymptotic results in (4.33). Another observation is that user two ($m = 2$) outperforms user one ($m = 1$). The reason is that for user two, by applying SIC, the interference from user one is canceled. While for user one, the interference from user two still exists. In Fig. 4.3(a), it is shown that the error floor become smaller when λ_b and λ_ℓ decrease, which is due to less interference from PTs and the relaxed interference power constraint at the PRs. It is also worth noting that with these system parameters, NOMA outperforms OMA for user one while OMA outperforms NOMA for user two, which indicates the importance of selecting appropriate power allocation coefficients and target data rates for NOMA. In Fig. 4.3(b), it is observed that the error floors become smaller as ν decreases. This is due to the fact that smaller ν means a lower transmit power of PTs, which in turn reduces the interference at SUs.

4.6 Summary

In this chapter, NOMA in large-scale underlay cognitive radio networks with randomly deployed users have been studied. Stochastic geometry tools were used to evaluate the outage performance of the considered network. New closed-form expressions were derived for the outage probability. Diversity order of NOMA users has been analyzed in two situations based on the derived outage probability. An important future direction

is to optimize the power allocation coefficients to further improve the performance gap between NOMA and conventional MA in CR networks.

Chapter 5

Non-orthogonal Multiple Access in Massive MIMO Aided Heterogeneous Networks

This chapter is organized as follows. The main contributions of this work is first introduced in 5.1. Then the proposed novel hybrid framework with NOMA and massive MIMO based HetNets is presented in 5.2. Following a flexible average received power based user association approach is described in Section 5.3. Section 5.4 presents the analytical results in terms of spectrum efficiency. Section 5.5 shows the numerical results of the proposed framework. Section 5.6 concludes this chapter.

5.1 Introduction

A novel hybrid HetNets framework is proposed, with NOMA based small cells and massive MIMO aided macro cells to further enhance the performance of existing HetNets design. In this framework, a downlink K-tier HetNets is considered, where macro BSs are equipped with large antenna arrays with linear zero-forcing beamforming (ZFBF)

capability to serve multiple single-antenna users simultaneously, and small cells BSs are equipped with single antenna each to serve two single-antenna users simultaneously with NOMA transmission. A stochastic geometry approach is adopted to model the considered K-tier HetNets. Based on the proposed framework, the primary contributions can be summarized as follows: 1) The flexible biased association to address the impact of NOMA and massive MIMO on the maximum biased received power is considered; 2) The exact analytical expressions of the NOMA based small cells in term of spectrum efficiency are derived; and 3) It is shown that NOMA based small cells are capable of achieving higher spectrum efficiency compared to conventional OMA based small cells, which demonstrates the benefits of the proposed framework.

5.2 Network Model

5.2.1 System Description

In this chapter, the downlink transmission scenarios are been focused on. A K-tier HetNets model is considered, where the first tier represents the macro cells and the other tiers represent the small cells such as pico cells and femto cells. The positions of macro BSs and all the k-th tier ($k \in \{2, \cdots, K\}$) BSs are modeled as homogeneous PPPs Φ_1 and Φ_k and with density λ_1 and λ_k, respectively. Motivated by the fact that it is common to overlay a high-power macro cell with successively denser and lower power small cell, it is considered to apply massive MIMO technologies to macro cells and NOMA transmission to small cells in this work. As shown in Fig. 5.1, in macro cells, macro BSs are considered to equipped with M antennas, each macro BS transmit signals to N users over the same resource block (e.g., time/frequency/code). It is assumed that $M \gg N > 1$ and the linear ZFBF technique is applied at each macro BS with assigning equal power to N data streams [110]. In small cells, each small cell BS is considered to be equipped with single antenna. Consider to adopt user pairing in each tier of small cells to implement NOMA for lowering the system complexity. All users are considered to be

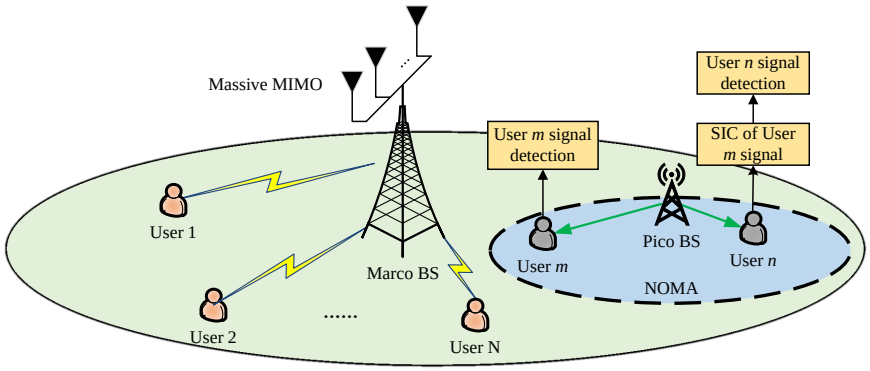

Figure 5.1: Illustration of NOMA and massive MIMO based hybrid HetNets.

equipped with single antenna each as well. All channel are assumed to undergo quasi-static Rayleigh fading, where the channel coefficients are constant for each transmission block but independent between different blocks.

5.2.2 Massive MIMO and NOMA Based User Association

In this work, a user is allowed to access any tier BS, which can provide the best coverage [112]. It is considered that the flexible user association is based on the maximum average received power of both macro cells and small cells.

5.2.2.1 Average received power in massive MIMO aided macro cells

In macro cells, since the macro BS is equipped with multiple antennas, users in macro cells can experience large array gains. Adopting ZFBF transmission scheme, the array gain obtained at macro users is given by $G_M = M - N + 1$ [110, 111]. As a result, the average received power that users connect with macro BS ℓ (where $\ell \in \Phi_1$) is given by

$$P_{r,1} = G_M P_1 L\left(d_{\ell,1}\right)/N, \tag{5.1}$$

where P_1 is the transmit power of the macro BSs, $L\left(d_{\ell,1}\right) = \eta d_{\ell,1}^{-\alpha_1}$ is large-scale path loss, $d_{\ell,1}$ is the distance between users and macro BSs, η is the frequency dependent

factor, and α_1 is the path loss exponent of macro cells.

5.2.2.2 Average received power in NOMA based small cells

Different from the convectional user association of OMA based small cells, NOMA exploits the power sparsity for multiple access by allocating different power to different users. More precisely, as shown in Fig. 5.1, the k-th tier BS sends a combination signals of User m and User n with allocating power $a_{m,k}$ and $a_{n,k}$ to each user. Here, the power allocation should satisfy $a_{m,k} > a_{n,k}$ and $a_{m,k} + a_{n,k} = 1$. Due to the random spatial topology of the stochastic geometry model, the space information of users are not pre-determined. The user association policy for the NOMA based small cells is based on assuming the typical user as far user first. As such, in the i-th tier small cell, the averaged received power that users connect with the i-th tier BS j (where $j \in \Phi_i$) is given by

$$P_{r,i} = a_{n,i} P_i L\left(d_{j,i}\right) B_i, \tag{5.2}$$

where P_i is the transmit power of i-th tier BS, $L\left(d_{j,i}\right) = \eta d_{j,i}^{-\alpha_i}$ is large-scale path loss, $d_{j,i}$ is the distance between the user and the i-th tier BS, α_i is the path loss exponent of the i-th tier small cells, and B_i is the bias factor. Here, the bias factor (e.g. $B_i > 1$) is used to extend the cell coverage. It is noted that the biasing factor B_i is useful for offloading data traffic in HetNets [112].

5.2.3 Downlink Transmission

5.2.3.1 Massive MIMO aided macro cell transmission

Without loss of generality, it is assumed that a typical user is located at the origin of an infinite two-dimension plane. Based on (5.1) and (5.2), the received SINR that a typical user connects with a macro BS at a random distance $d_{o,1}$ can be expressed as

$$\gamma_{r,1} = \frac{\frac{P_1}{N} h_{o,1} L\left(d_{o,1}\right)}{I_{M,1} + I_{S,1} + \sigma^2}, \tag{5.3}$$

where $I_{M,1} = \sum_{\ell \in \Phi_1 \setminus B_{o,1}} \frac{P_1}{N} h_{\ell,1} L\left(d_{\ell,1}\right)$ is the interference from macro cells, $I_{S,1} = \sum_{i=2}^{K} \sum_{j \in \Phi_i} P_i h_{j,i} L\left(d_{j,i}\right)$ is the interference from small cells, σ^2 is the AWGN power, $h_{o,1}$ is the small-scale fading coefficient between the typical user and the connected macro BS, $h_{\ell,1}$ and $d_{\ell,1}$ are the small-scale fading coefficients and distance between a typical user and connected macro BS ℓ except the serving macro BS $B_{o,1}$, respectively, $h_{j,i}$ and $d_{j,i}$ are the small-scale fading coefficients and distance between a typical user and connected i-th tier small cell BS j, respectively. Here, $h_{o,1}$ follows Gamma distribution with parameters $(M - N + 1, 1)$, $h_{\ell,1}$ follows Gamma distribution with parameters $(N, 1)$, and $h_{j,i}$ follows exponential distribution with unit mean.

5.2.3.2 NOMA based small cell transmission

In small cells, without loss of generality, it is considered that each small cell BS has already associated one user in the previous round of user association process. With applying NOMA protocol, the aim is to squeeze a typical user into the same small cell to improve the spectral efficiency, which is one key feature of NOMA [4]. For simplicity, it is assumed that the distances between the existing users and the connected small cell BSs are the same as R_k. It is assumed that the distance between the typical user and the connected small cell BS is x, which is a random value. Since it is not pre-determined that the typical user is a near user n or a far user m. Denote d_{o,k_m} and d_{o,k_n} are the distance between the k-th tier small cell BS and user m and user n, respectively. As such, two possible cases can happen in the following.

Near user case: In the first case, it is considered that the typical user is a near user n ($x \leq R_k$), as such, it can be expressed as $d_{o,k_m} = R_k$. In this case, the interference from the existing user can be canceled. As such, the received SINR that a typical user

n connects with the k-th tier small cell can be expressed as

$$\gamma_{k_n} = \frac{a_{n,k} P_k g_{o,k} L\left(d_{o,k_n}\right)}{I_{M,k} + I_{S,k} + \sigma^2}, \tag{5.4}$$

where $L\left(d_{o,k_n}\right) = \eta d_{o,k_n}^{-\alpha_i}$, $I_{M,k} = \sum_{\ell \in \Phi_1} \frac{P_1}{N} g_{\ell,1} L\left(d_{\ell,1}\right)$ is the interference from macro cells, $I_{S,k} = \sum_{i=2}^{K} \sum_{j \in \Phi_i \setminus B_{o,k}} P_i g_{j,i} L\left(d_{j,i}\right)$ is the interference from small cells, $g_{o,k}$ and d_{o,k_n} is the small-scale fading coefficients and distance between the typical user and the connected k-th tier BS, $g_{\ell,1}$ and $d_{\ell,1}$ are the small-scale fading coefficients and distance between a typical user and connected macro BS ℓ, respectively, $g_{j,i}$ and $d_{j,i}$ are the small-scale fading coefficients and distance between a typical user and connected i-th tier small cell BS j except the serving BS $B_{o,k}$, respectively. Here, $g_{o,k}$ and $g_{j,i}$ follow exponential distributions with unit mean. $g_{\ell,1}$ follows Gamma distribution with parameters $(N, 1)$.

For the existing far user m^*, it will directly decode its own message by treating the message of user n as interference. Therefore, the received SINR that for the existing user m^* in the k-th tier small cell can be expressed as

$$\gamma_{k_{m^*}} = \frac{a_{m,k} P_k g_{o,k} L\left(R_k\right)}{I_{k,n} + I_{M,k} + I_{S,k} + \sigma^2}, \tag{5.5}$$

where $I_{k,n} = a_{n,k} P_k g_{o,k} L\left(R_k\right)$ is the intra-BS interference from the connected k-th tier BS with superposition information of user n, and $L\left(R_k\right) = \eta {R_k}^{-\alpha_k}$.

Far user case: In the second case, it is considered that the typical user is a far user m ($x > R_k$), then $d_{o,k_n} = R_k$ can be expressed. As such, received SINR that user m connects with the k-th tier small cell can be expressed as

$$\gamma_{k_m} = \frac{a_{m,k} P_k g_{o,k} L\left(d_{o,k_m}\right)}{I_{k,n^*} + I_{M,k} + I_{S,k} + \sigma^2}, \tag{5.6}$$

where $I_{k,n^*} = a_{n,k} P_k g_{o,k} L\left(d_{o,k_m}\right)$ is the interference from the BS with superposition the information of existing user n^* of the k-th tier small cell with $L\left(d_{o,k_m}\right) = \eta d_{o,k_m}^{-\alpha_k}$, d_{o,k_n} is the distance between the typical user m and the connected k-th tier BS.

Regarding the existing near user n^*, it is capable of cancelling interference from the typical user m by applying SIC technique. Therefore, the received SINR of user n^* is given by

$$\gamma_{k_{n^*}} = \frac{a_{n,k} P_k g_{o,k} L\left(R_k\right)}{I_{M,k} + I_{S,k} + \sigma^2}. \tag{5.7}$$

5.3 User Association Probability

As described in Section II-B, the user association of this proposed framework is based on maximizing the biased average received power at users. As such, based on (5.1) and (5.2), the user association of macro cells and small cells are given in the following.

Using the similar method as Lemma 1 of [112], the user association probability that a typical user connects with macro BSs can be calculated as

$$A_1 = 2\pi\lambda_1 \int_0^\infty r \exp\left[-\pi \sum_{i=2}^{K} \lambda_i \left(\frac{a_{n,i} P_i B_i N}{P_1 G_M r^{-\alpha_1}}\right)^{\delta_i} - \pi\lambda_1 r^2\right] dr, \tag{5.8}$$

where $\delta_i = \frac{2}{\alpha_i}$.

The user association probability that a typical user connects with small cell BSs in the k-th tier can be calculated as

$$A_k = 2\pi\lambda_k \int_0^\infty r \exp\left[-\pi \sum_{i=2}^{K} \lambda_i \left(\frac{P_i B_i r^{\alpha_k}}{P_k B_k}\right)^{\delta_i} - \pi\lambda_1 \left(\frac{P_1 G_M r^{\alpha_k}}{N a_{n,k} P_k B_k}\right)^{\delta_1}\right] dr, \tag{5.9}$$

where $\delta_1 = \frac{2}{\alpha_1}$.

The PDF of the distance between a typical user and the connected macro BS is

considered. Based on (5.8), the following expression is obtained

$$f_{d_{o,1}}(x) = \frac{2\pi\lambda_1 x}{A_1} \exp\left[-\pi \sum_{i=2}^{K} \lambda_i \left(\frac{a_{n,i} P_i B_i N}{P_1 G_M x^{-\alpha_1}}\right)^{\delta_i} - \pi\lambda_1 x^2\right]. \tag{5.10}$$

Then the PDF of the distance between a typical user and the connected k-th tier small cell BS is to be calculated. Based on (5.9), the following expression is obtained

$$f_{d_{o,k}}(x) = \frac{2\pi\lambda_k x}{A_k} \exp\left[-\pi \sum_{i=2}^{K} \lambda_i \left(\frac{P_i B_i x^{\alpha_k}}{P_k B_k}\right)^{\delta_i} - \pi\lambda_1 \left(\frac{P_1 G_M x^{\alpha_k}}{N a_{n,k} P_k B_k}\right)^{\delta_1}\right]. \tag{5.11}$$

5.4 Spectrum Efficiency Evaluation

In an effort to evaluate the spectrum efficiency of the proposed NOMA and massive MIMO based HetNets framework, the achievable ergodic rate of each tier is to be calculated in the following subsections.

5.4.1 Achievable Ergodic Rate of Small Cells

The aim of this work is to apply NOMA transmission in small cells to further improve the spectrum efficiency. Recall that the distance order between the connected BS and the two users are not predetermined (as aforementioned in Section 5.2), as such, in this subsection, the achievable ergodic rate of small cell both for the near user case and far user case are calculated in *Lemma 1* and *Lemma 2* in the following respectively.

Lemma 1. *Conditioned on the HPPPs, the achievable ergodic rate of the k-th tier small cell for the near user case can be expressed as follows:*

$$\tau_k^n = \frac{1}{\ln 2} \int_0^{\frac{a_{m,k}}{a_{n,k}}} \frac{1 - F_{k_{m^*}}(z)}{1+z} dz + \frac{1}{\ln 2} \int_0^{\infty} \frac{1 - F_{k_n}(z)}{1+z} dz, \tag{5.12}$$

where $F_{k_n}(z)$ and $F_{k_{m^*}}(z)$ are given in the following equations:

$$F_{k_n}(z) = 1 - \frac{2\pi\lambda_k}{A_k}\int_0^{R_k} x \exp\left(\Lambda(x) - \frac{\sigma^2 z x^{\alpha_k}}{a_{n,k}P_k\eta} - \Theta\left(\frac{z x^{\alpha_k}}{a_{n,k}P_k\eta}\right)\right) dx, \tag{5.13}$$

and

$$\begin{aligned} F_{k_{m^*}}(z) =& 1 - \frac{2\pi\lambda_k}{A_k}\int_0^{R_k} x \exp\left[-\frac{\sigma^2 z {R_k}^{\alpha_k}}{(a_{m,k} - a_{n,k}z)P_k\eta}\right. \\ & \left. -\Theta\left(\frac{z {R_k}^{\alpha_k}}{(a_{m,k} - a_{n,k}z)P_k\eta}\right) + \Lambda(x)\right] dx. \end{aligned} \tag{5.14}$$

Here $\Lambda(x) = -\pi\sum_{i=2}^{K}\lambda_i\left(\frac{P_i B_i x^{\alpha_k}}{P_k B_k}\right)^{\delta_i} - \pi\lambda_1\left(\frac{P_1 G_M x^{\alpha_k}}{N a_{n,k} P_k B_k}\right)^{\delta_1}$ *and* $\Theta(s)$ *in* (5.13) *and* (5.14) *is given by*

$$\begin{aligned} \Theta(s) =& \lambda_1\pi\delta_1\sum_{p=1}^{N}\binom{N}{p}\left(s\frac{P_1}{N}\eta\right)^p\left(-s\frac{P_1}{N}\eta\right)^{\delta_1 - p} \\ & \times B\left(-s\frac{P_1}{N}\eta[\omega_{1,k}(x)]^{-\alpha_1}; p - \delta_1, 1 - N\right) \\ & + s\sum_{i=2}^{K}\frac{\lambda_i 2\pi P_i\eta(\omega_{i,k}(x))^{2-\alpha_i}}{\alpha_i(1-\delta_i)} \\ & \times {}_2F_1\left(1, 1-\delta_i; 2-\delta_i; -sP_i\eta(\omega_{i,k}(x))^{-\alpha_i}\right), \end{aligned} \tag{5.15}$$

where $\omega_{1,k}(x) = \left(\frac{P_1 G_M}{a_{n,k}P_k B_k N}\right)^{\frac{\delta_1}{2}} x^{\frac{\alpha_k}{\alpha_1}}$ *and* $\omega_{i,k}(x) = \left(\frac{P_i B_i}{P_k B_k}\right)^{\frac{\delta_i}{2}} x^{\frac{\alpha_k}{\alpha_i}}$ *are the nearest distance allowed between the typical user associated to the k-th tier small cell and the macro cell BS, and between the typical user and the i-th tier small cell BS, respectively.* $B(\cdot;\cdot,\cdot)$ *and* ${}_2F_1(\cdot,\cdot;\cdot;\cdot)$ *are the the incomplete Beta function [125, Eq. (8.319)] and Gauss hypergeometric function [125, Eq. (9.142)], respectively.*

Proof. For small cells, the achievable ergodic rate of near user case for the k-th tier can be expressed as

$$\begin{aligned} \tau_k^n &= E\left\{\log_2\left(1 + \gamma_{k_{m^*}}\right) + \log_2\left(1 + \gamma_{k_n}\right)\right\} \\ &= \frac{1}{\ln 2}\int_0^{\infty}\frac{1 - F_{k_{m^*}}(z)}{1+z}dz + \frac{1}{\ln 2}\int_0^{\infty}\frac{1 - F_{k_n}(z)}{1+z}dz. \end{aligned} \tag{5.16}$$

First it is required to obtain the expressions for $F_{k_n}(z)$. Based on (5.4), the following expression can be obtained

$$\begin{aligned} F_{k_n}(z) =& \int_0^{R_k} \Pr\left[\frac{a_{n,k}P_k g_{o,k}\eta x^{-\alpha_k}}{I_{M,k}+I_{S,k}+\sigma^2} \leq z\right] f_{d_{o,k}}(x)\,dx \\ =& 1-\int_0^{R_k} \exp\left(-\frac{\sigma^2 z x^{\alpha_k}}{a_{n,k}P_k\eta}\right)\mathcal{L}_{I_{k*}}\left(\frac{z x^{\alpha_k}}{a_{n,k}P_k\eta}\right) f_{d_{o,k}}(x)\,dx, \end{aligned} \tag{5.17}$$

where it is denoted that $I_{k*} = I_{M,k} + I_{S,k}$. Then turn to the attention to the laplace transform of I_{k*} with utilizing it as $\mathcal{L}_{I_{k*}}(s) = \mathcal{L}_{I_{M,k}}(s)\,\mathcal{L}_{I_{S,k}}(s)$. Then these two parts are derived in the following:

$$\begin{aligned} \mathcal{L}_{I_{M,k}}(s) &= E_{I_{M,k}}\left[\exp\left(-s\sum_{\ell\in\Phi_1}\frac{P_1}{N}g_{\ell,1}L(d_{\ell,1})\right)\right] \\ &= E_{\Phi_1}\left[\prod_{\ell\in\Phi_1} E_{g_{\ell,1}}\left[\exp\left(-s\frac{P_1}{N}g_{\ell,1}\eta d_{\ell,1}^{-\alpha_1}\right)\right]\right] \\ &\overset{(a)}{=} \exp\left(-\lambda_1 2\pi\int_{\omega_{i,1}(x)}^{\infty}\left(1-E_{g_{\ell,1}}\left[e^{-\frac{sP_1 g_{\ell,1}\eta}{Nr^{\alpha_1}}}\right]\right) r dr\right), \end{aligned} \tag{5.18}$$

where (a) is obtained with the aid of invoking generating functional of PPP. Recall that the $g_{\ell,1}$ follows Gamma distribution with parameter $(N,1)$. With the aid of Laplace transform for the Gamma distribution, $E_{g_{\ell,1}}\left[\exp\left(-s\frac{P_1}{N}g_{\ell,1}\eta r^{-\alpha_1}\right)\right] = \mathcal{L}_{g_{\ell,1}}\left(s\frac{P_1}{N}\eta r^{-\alpha_1}\right) = \left(1+s\frac{P_1}{N}\eta r^{-\alpha_1}\right)^{-N}$ is obtained. As such, (5.18) can be rewritten as

$$\mathcal{L}_{I_{M,k}}(s) = \exp\left(-\lambda_1 2\pi\int_{\omega_{1,k}(x)}^{\infty}\left(1-\left(1+\frac{sP_1\eta}{Nr^{\alpha_1}}\right)^{-N}\right) r dr\right). \tag{5.19}$$

Applying binomial expression and after some mathematical manipulations, the Laplace transform of $I_{M,k}$ is obtained as

$$\begin{aligned} \mathcal{L}_{I_{M,k}}(s) =& \exp\left[-\lambda_1\pi\delta_1\sum_{p=1}^{N}\binom{N}{p}\left(s\frac{P_1}{N}\eta\right)^p\left(-s\frac{P_1}{N}\eta\right)^{\delta_1-p}\right. \\ &\left.\times B\left(-s\frac{P_1}{N}\eta[\omega_{i,1}(x)]^{-\alpha_1}; p-\delta_1, 1-N\right)\right], \end{aligned} \tag{5.20}$$

where $B(\cdot;\cdot,\cdot)$ is the is the incomplete Beta function. Following the similar procedure to obtain (5.20), with the aid of [125, Eq. (3.324)], $I_{s,k}$ can be expressed as

$$\mathcal{L}_{I_{S,k}}(s) = \exp\left[-s\sum_{i=2}^{K}\frac{\lambda_i 2\pi P_i \eta(\omega_{i,k}(x))^{2-\alpha_i}}{\alpha_i(1-\delta_i)} \times {}_2F_1\left(1,1-\delta_i;2-\delta_i;-sP_i\eta(\omega_{i,k}(x))^{-\alpha_i}\right)\right], \tag{5.21}$$

where ${}_2F_1(\cdot,\cdot;\cdot;\cdot)$ is the is the Gauss hypergeometric function. Then combining (5.20) and (5.21), the Laplace transform of I_{k*} can be obtained as $\mathcal{L}_{I_{k*}}(s) = \exp(-\Theta(s))$, where $\Theta(s)$ is given in (5.15). Then plugging (5.11) and $\mathcal{L}_{I_{k*}}(s)$ into (5.17), the CDF of $F_{k_n}(z)$ can be obtained in (5.13). Then turn to the attention to derive the CDF of $F_{k_{m^*}}(z)$. Based on (5.5), $F_{k_{m^*}}(z)$ can be obtained as

$$F_{k_{m^*}}(z) = \int_0^{R_k} f_{d_{o,k}}(x)\Pr\left[(a_{m,k}-a_{n,k}z)g_{o,k} \le \frac{\left(I_{M,k}+I_{S,k}+\sigma^2\right)z}{P_k\eta {R_k}^{-\alpha_k}}\right]dx. \tag{5.22}$$

Note that for the case $z \ge \frac{a_{m,k}}{a_{n,k}}$, it is easy to observe that $F_{k_{m^*}}(z) = 1$. For the case $z \le \frac{a_{m,k}}{a_{n,k}}$, following the similar procedure of deriving (5.13),the following expression can be obtained

$$F_{k_{m^*}}(z) = 1 - \int_0^{R_k}\exp\left(-\frac{\sigma^2 z {R_k}^{\alpha_k}}{(a_{m,k}-a_{n,k}z)P_k\eta}\right)L_{I_{k*}}\left(\frac{z{R_k}^{\alpha_k}}{(a_{m,k}-a_{n,k}z)P_k\eta}\right)f_{d_{o,k}}(x)\,dx. \tag{5.23}$$

Plugging $L_{I_{k*}}(s)$ into (5.23), combining the two cases aforementioned, the following expression is obtained

$$F_{k_{m^*}}(z) = 1 - U\left(\frac{a_{m,k}}{a_{n,k}} - z\right) \times \int_0^{R_k}\exp\left[-\frac{\sigma^2 z {R_k}^{\alpha_k}}{(a_{m,k}-a_{n,k}z)P_k\eta} - \Theta\left(\frac{z{R_k}^{\alpha_k}}{(a_{m,k}-a_{n,k}z)P_k\eta}, R_k\right)\right]f_{d_{o,k}}(x)\,dx, \tag{5.24}$$

where $U(\cdot)$ is the unit step function. Substituting (5.23) and the (5.13) into (5.16), the

ergodic rate of small cell for the near user case is obtained. The proof is complete.

□

Lemma 2. *Conditioned on the HPPPs, the achievable ergodic rate of the k-th tier small cell for the far user case can be expressed as follows:*

$$\tau_k^f = \frac{1}{\ln 2}\int_0^{\infty}\frac{1-F_{k_{n^*}}(z)}{1+z}dz + \frac{1}{\ln 2}\int_0^{\frac{a_{m,k}}{a_{n,k}}}\frac{1-F_{k_m}(z)}{1+z}dz, \tag{5.25}$$

where $F_{k_n}(z)$ *and* $F_{k_{m^*}}(z)$ *are given in the following equations:*

$$\begin{aligned} F_{k_m}(z) =& 1 - \frac{2\pi\lambda_k}{A_k}\int_{R_k}^{\infty} \times \exp\left[-\frac{\sigma^2 z x^{\alpha_k}}{P_k\eta\left(a_{m,k}-a_{n,k}z\right)}\right. \\ & \left. -\Theta\left(\frac{z x^{\alpha_k}}{P_k\eta\left(a_{m,k}-a_{n,k}z\right)}\right)+\Lambda(x)\right]dx, \end{aligned} \tag{5.26}$$

and

$$F_{k_{n^*}}(z) = 1 - \frac{2\pi\lambda_k}{A_k}\int_{R_k}^{\infty}\exp\left[\Lambda(x) - \frac{\sigma^2 z {R_k}^{\alpha_k}}{P_k\eta a_{n,k}} - \Theta\left(\frac{z{R_k}^{\alpha_k}}{P_k\eta a_{n,k}}\right)\right]dx. \tag{5.27}$$

Proof. The proof procedure is similar to the approach of obtaining (5.12), which is detailed introduced above. □

Combining (5.12) and (5.25), a general case for the achievable ergodic rate of the k-th tier small cell is obtained as

$$\tau_k = \tau_k^n + \tau_k^f. \tag{5.28}$$

5.4.2 Achievable Ergodic Rate of Macro cells

In massive MIMO aided macro cells, the achievable ergodic rate can be significantly improved due to multiple-antenna array gains, but with undertaking more power consumption and high complexity. In order to evaluate the spectrum efficiency of the whole system, a tractable lower bound of throughput of macro cell is derived in the following

theorem.

Theorem 7. *Conditioned on the HPPPs, the lower bound achievable ergodic rate of macro cells can be expressed as follows:*

$$\tau_{1,L} = \log_2\left(1 + \frac{P_1 G_M \eta}{N\int_0^\infty \left(Q_1\left(x\right) + \sigma^2\right) x^{\alpha_1} f_{d_{o,1}}\left(x\right) dx}\right), \tag{5.29}$$

where $f_{d_{o,1}}\left(x\right)$ *is given in* (5.10), $Q_1\left(x\right) = \frac{2P_1\eta\pi\lambda_1}{\alpha_1 - 2}x^{2-\alpha_1} + \sum_{i=2}^{K} 2\pi\lambda_i\left(\frac{P_i\eta}{\alpha_i - 2}\right)\left[\omega_{i,1}\left(x\right)\right]^{2-\alpha_i}$, *and* $\omega_{i,1}\left(x\right) = \left(\frac{a_{n,i}P_iB_iN}{P_1G_M}\right)^{\frac{\delta_i}{2}} x^{\frac{\alpha_1}{\alpha_i}}$ *Here* $\omega_{i,1}\left(x\right)$ *is denoted as the nearest distance allowed between i-th tier small cell BS and the typical user associated to the macro cell.*

Proof. With the aid of Jensen's inequality, the lower bound of the achievable ergodic rate of the macro cell can be obtained as

$$E\left\{\log_2\left(1 + \gamma_{r,1}\right)\right\} \geq \tau_{1,L} = \log_2\left(1 + \left(E\left\{\left(\gamma_{r,1}\right)^{-1}\right\}\right)^{-1}\right) \tag{5.30}$$

By invoking the law of large numbers, the following approximation $h_{o,1} \approx G_M$ can hold. Then $\tau_{1,L}$ can be approximated as follows:

$$\begin{aligned} E\left\{\left(\gamma_{r,1}\right)^{-1}\right\} &\approx \frac{N}{P_1 G_M \eta} E\left\{\left(I_{M,1} + I_{S,1} + \sigma^2\right) x^{\alpha_1}\right\} \\ &= \frac{N}{P_1 G_M \eta}\int_0^\infty \left(E\left\{I_{M,1} + I_{S,1}\right\} + \sigma^2\right) x^{\alpha_1} f_{d_{o,1}}\left(x\right) dx. \end{aligned} \tag{5.31}$$

Then turn to the attention to the expectation, denote $Q_1\left(x\right) = E\left\{I_{M,1} + I_{S,1}\right\}$, with the aid of Campbell's Theorem, the following expression is obtained

$$\begin{aligned} Q_1\left(x\right) &= E\left\{\sum_{\ell \in \Phi_1 \setminus B_{o,1}} \frac{P_1}{N} h_{\ell,1} L\left(d_{\ell,1}\right)\right\} + E\left\{\sum\nolimits_{i=2}^{K}\sum\nolimits_{j \in \Phi_i} P_i h_{j,i} L\left(d_{j,i}\right)\right\} \\ &= \frac{2P_1\eta\pi\lambda_1}{\alpha_1 - 2}x^{2-\alpha_1} + \sum_{i=2}^{K} 2\pi\lambda_i\left(\frac{P_i\eta}{\alpha_i - 2}\right)\left[\omega_{i,1}\left(x\right)\right]^{2-\alpha_i}, \end{aligned} \tag{5.32}$$

The proof is complete. □

5.4.3 Spectrum Efficiency

Based on the analysis of last two subsection, a tractable lower bound of spectrum efficiency is given by

$$\tau_{SE,L} = A_1 N \tau_{1,L} + \sum\nolimits_{k=2}^{K} A_k \tau_k, \tag{5.33}$$

where $N\tau_1$ and $A_k\tau_k$ are the low bound spectrum efficiency of macro cells and exact spectrum efficiency of the k-th tier small cells, respectively.

5.5 Numerical Results

In this section, numerical results are presented to facilitate the performance evaluations of NOMA in the considered massive MIMO aided K-tier HetNets. The BS density of macro cells is set to be $\lambda_1 = \left(500^2 \times \pi\right)^{-1}$. The considered network is assumed to operate at a carrier frequency of 1 GHz. The noise figure is $N_f = 10$ dB, hence the noise power is $\sigma^2 = -170 + 10 \times \log_{10}(BW) + N_f = -90$ dBm. The path loss exponent for macro cells and k-th tier small cells are $\alpha_1 = 3.5$ and $\alpha_k = 4$, respectively. The power allocation coefficients of NOMA are $a_{m,k} = 0.6$ and $a_{n,k} = 0.4$. The distance between small cells and an existing user is $R_k = 50$ m. Monte Carlo simulations are provided to verify the accuracy of the analysis.

Fig. 5.2 shows the effect of M and bias factor on user association probability, where the tiers of HetNets are set to be $K = 3$, including macro cells and two tiers small cells. The curves representing macro cells and small cells are from (5.8) and (5.9), respectively. One can observe that as the number of antennas at macro BS increases, more users are likely to associate to macro cells. This is because that the massive MIMO aided macro cells are capable of providing larger array gain, which in turns enhance the average received power for the connected users. Another observation is that increasing the bias factor can encourage more users connect to the small cells, which is an efficient method to

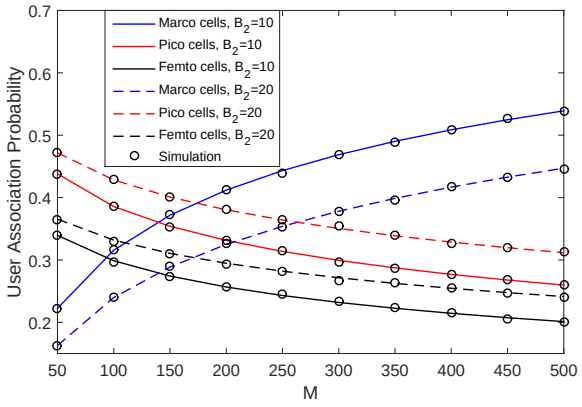

Figure 5.2: User association probability of the considered network, with $K = 3$, $N = 15$, $P_1 = 40$ dBm, $P_2 = 30$ dBm and $P_3 = 20$ dBm, $\lambda_2 = \lambda_3 = 20 \times \lambda_1$, and $B_3 = 20B_2$.

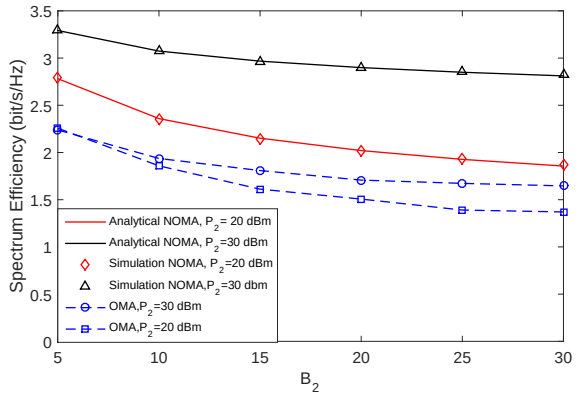

Figure 5.3: Comparison of NOMA based and OMA based small cells in terms of spectrum efficiency, with $K = 2$, $M = 200$, $N = 15$, $\lambda_2 = 20 \times \lambda_1$, and $P_1 = 40$ dBm.

extend the coverage of small cells or control loading balance among each tier of HetNets. It is also noted that regarding small cells, the Femto cells can associate with more users than Pico cells. This attributes to the fact that Femto cell BSs have higher transmit power than Pico cell BSs.

Fig. 5.3 plots the spectrum efficiency of NOMA based and OMA based small cells versus bias factor with different transmit power of small cell BSs, respectively. The solid curves representing the performance of NOMA based small cells are from (5.28). One can observe is that the spectrum efficiency of small cells decreases as the bias factor

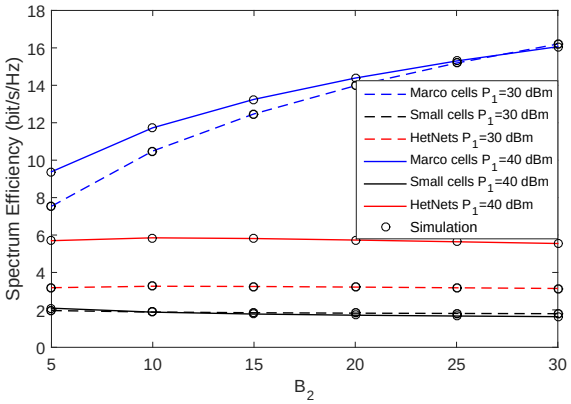

Figure 5.4: Spectrum efficiency of the proposed framework, with $K = 2$, $M = 50$, $N = 5$, $P_2 = 20$ dBm, $\lambda_2 = 100 \times \lambda_1$.

increases. This behavior can be explained as follows: larger bias factor makes more macro users with low SINR are associated to small cells, which in turn degrades the spectrum efficiency of small cells. It is also worth noting that the performance of NOMA based small cells outperforms the conventional OMA based small cells, which in turn can enhance the spectrum efficiency of the whole HetNets. What is worth pointing out is that optimizing the power allocation between two NOMA users can further enlarge the performance gap over the OMA based scheme [15], which is out of the scope of this chapter.

Fig. 5.4 illustrates the spectrum efficiency versus bias factor with different transmit power of small cell BSs. The curves representing the spectrum efficiency of small cells, macro cells and HetNets are from (5.28), (5.29) and (5.33), respectively. The performance of conventional OMA based small cells is illustrated as a benchmark to demonstrate the effectiveness of the proposed framework. One can observe that macro cells can achieve higher spectrum efficiency compared to small cells. This is attributed to the fact that macro BSs are able to serve multiple users simultaneously with offering promising array gains to each user. It is also noted that the spectrum efficiency of macro cells improves as bias factor increases. The reason is again that more low SINR macro cell users are associated to small cells, which in turn makes the spectrum efficiency of macro cells enhance.

5.6 Summary

In this chapter, a novel hybrid massive MIMO and NOMA based HetNets framework has been designed. A flexible massive MIMO and NONA based user association scheme was considered. Stochastic geometry was employed to model the networks and evaluate the corresponding performance. Analytical expressions for spectrum efficiency of the netowrks were derived. It has been demonstrated that NOMA based small cells were able to well-coexist with the current HetNets structure and were capable of achieving higher spectrum efficiency. A promising future direction is to optimize the power allocation among NOMA users to further enhance the spectrum efficiency of the proposed framework.

Chapter 6

Enhancing the Physical Layer Security of Non-orthogonal Multiple Access in Large-scale Networks

This chapter is organized as follows. The main contributions of this work is first introduced in 6.1. In Section 6.2, a single-antenna transmission scenario is investigated in random wireless networks, where channel ordering of the NOMA users is relied on. New expressions are derived in the exact secrecy outage probability (SOP) analysis and diversity order analysis. In Section 6.3, a multiple-antenna transmission scenario is investigated, which relies on generating AN at the BS. New expressions are derived both by the exact analysis and large scale antenna array analysis. The numerical results are presented in Section 6.4 for verifying the proposed analysis, which is followed by the conclusions in Section 6.5.

6.1 Introduction

The security enhancement of NOMA systems from the perspective of physical layer is investigated in this chapter. Consider the scenario of large-scale networks, where a BS supports randomly roaming NOMA users. In order to avoid sophisticated high-complexity message detection at the receivers, a user pairing technique is adopted for ensuring that only two users share a specific orthogonal resource slot [6], which can be readily separated by low-complexity SIC. A random number of eavesdroppers are randomly positioned on an infinite two-dimensional plane according to a homogeneous PPP. Both the locations and the CSI of the eavesdroppers are assumed to be unknown at the BS. An eavesdropper-exclusion zone is introduced around the BS for improving the secrecy performance of the large-scale networks considered in which no eavesdroppers are allowed to roam. This 'disc' was referred to as a protected zone in [75, 126, 127]. Specifically, both a single-antenna scenario and a multiple-antenna scenario at the BS are considered. 1) For the single-antenna scenario, M NOMA users are randomly roaming in an finite disc (user zone) with the quality-order of their channel conditions known at the BS. For example, the m-th NOMA user is channel-quality order of m. In this case, the m-th user is paired with the n-th user for transmission within the same resource slot; 2) For the multiple-antenna scenario, beamforming is invoked at the BS for generating AN, since beamforming achieves the maximum secrecy capacity for MISO channels [128]. In order to reduce the complexity of channel ordering of MISO channels for NOMA, the circular cell is partitioned into an an internal disc and an external ring. One user is selected from the internal disc and another is selected from the external ring to be paired together for transmission within the same resource slot using a NOMA protocol. The primary contributions of this chapter are as follows:

- The secrecy performance of large-scale NOMA networks is investigated both for a single-antenna aided and a multiple-antenna assisted scenario at the BS. A protected zone synonymously referred to as the eavesdropper-exclusion area, is invoked in both scenarios for improving the PLS. Additionally, it is proposed to generate

AN at the BS in the multiple-antenna aided scenario for further enhancing the secrecy performance.

- For the single-antenna scenario, the exact analytical expressions of the secrecy outage probability (SOP) of the selected pair of NOMA users are derived, when relying on channel ordering. Then the secrecy diversity analysis is further extended on and the expressions of asymptotic SOP are derived. The results derived confirm that: 1) for the selected pair, the m-th user is capable of attaining a secrecy diversity order of m; 2) the secrecy diversity order is determined by the one associated with the worse channel condition between the paired users.

- For the multiple-antenna scenario, the exact analytical expressions of the SOP are derived in conjunction with AN generated at the BS. To gain further insights, it is assumed having a large antenna array and the expressions of SOP is derived, when the number of antennas tends to infinity. The results derived confirm that increasing the number of antennas has no effect on the received SINR at the eavesdroppers, when the BS is equipped with a large antenna array.

- It is shown that: 1) the SOP can be reduced both by extending the protected zone and by generating AN at the BS; 2) the asymptotic SOP results of the large antenna array analysis is capable of closely approximating the exact secrecy outage provability; 3) there is an optimal desired signal-power and AN power sharing ratio, which minimizes the SOP in the multi-antenna scenario.

6.2 Physical Layer Security in Random Wireless Networks with Channel Ordering

As shown in Fig. 6.1, this work focus the attention on a secure downlink communication scenario. In the scenario considered, a BS communicates with M legitimate users (LUs) in the presence of eavesdroppers (Es). Many existing contention on NOMA have demon-

strated that it is an effective approach to pair two users together in a single resource slot in order to reduce the implementation complexity [6, 7]. Hence, in this treatise, it is assumed that the M users are divided into $M/2$ orthogonal pairs. For each pair, the NOMA transmission protocol is invoked. The Es would interpret the signal, but without trying to modify it. It is assumed that BS is located at the center of a disc, denoted by $\mathcal{D}$, which has a coverage radius of R_D (which is defined as the user zone for NOMA [9]). The M randomly roaming LUs are uniformly distributed within the disc. A random number of Es is distributed in an infinite two-dimensional plane. The spatial distribution of all Es is modeled using a homogeneous PPP, which is denoted by Φ_e associated with the density λ_e. It is assumed that the Es can be detected, provided that they are close enough to BS. Therefore, an E-exclusion area having a radius of r_p is introduced. Additionally, all channels are assumed to impose quasi-static Rayleigh fading, where the channel coefficients are constant for each transmission block, but vary independently between different blocks.

Without loss of generality, it is assumed that all the channels between the BS and LUs obey $|h_1|^2 \leq \cdots |h_m|^2 \leq \cdots |h_n|^2 \leq \cdots |h_M|^2$, where $|h_m|^2$ and $|h_n|^2$ represent the ordered channel gain of the m-th user and the n-th user, respectively. Both the the small-scale fading and the path loss are incorporated into the ordered channel gain. Again, it is assumed that the m-th user and the n-th user ($m < n$) are paired for transmission in the same resource slot. With loss of generality, this work focus the attention on a single selected pair of users in the rest of the work. In the NOMA transmission protocol, more power should be allocated to the user suffering from worse channel condition [4, 7]. Therefore, the power allocation coefficients satisfy the conditions that $a_m \geq a_n$ and $a_m + a_n = 1$. SIC is invoked for detecting the stronger user first [119]. Based on the aforementioned assumptions, the instantaneous SINR of the m-th user and the SNR of the n-th user can be written as:

$$\gamma_{B_m} = \frac{a_m |h_m|^2}{a_n |h_m|^2 + \frac{1}{\rho_b}}, \tag{6.1}$$

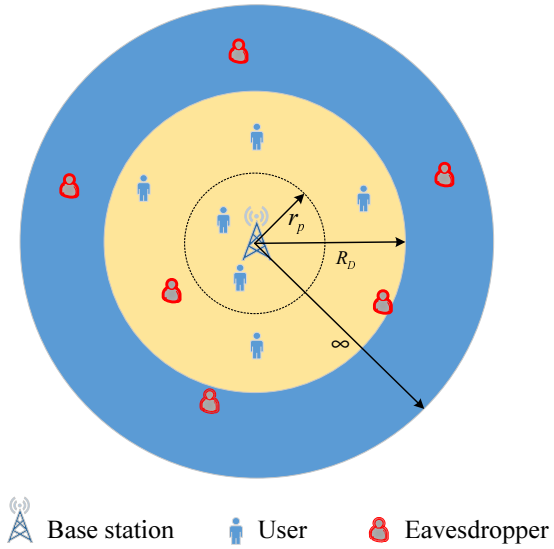

Figure 6.1: Network model for secure NOMA transmission in single-antenna scenario, where r_p, R_D, and ∞ is the radius of the E-exclusion area, NOMA user zone $\mathcal{D}$ (the disc with yellow color), and an infinite two dimensional plane for Es, respectively.

and

$$\gamma_{B_n} = \rho_b a_n |h_n|^2, \tag{6.2}$$

respectively. The convenient concept of transmit SNR $\rho_b = \frac{P_T}{\sigma_b^2}$ is introduced, where P_T is the transmit power at the BS and σ_b^2 is the variance of the AWGN at the LUs, noting that this is not a physically measurable quantity owing to their geographic separation. In order to ensure that the m-th user can successfully decode the message of the n-th user, the condition of $a_m \geq \left(2^{R_m} - 1\right) a_n$ should be satisfied. Additionally, a bounded path loss model is used for guaranteeing that there is a practical path-loss, which is higher than one even for small distances.

Consider the worst-case scenario of large-scale networks, in which the Es are assumed to have strong detection capabilities. Specifically, by applying multiuser detection techniques, the multiuser data stream received from BS can be distinguished by the Es. Under this assumption, the most detrimental E is not necessarily the nearest one, but the one having the best channel to BS. Therefore, the instantaneous SNR of detecting the information of the m-th user and the n-th user at the most detrimental E can be expressed as follows:

$$\gamma_{E_\kappa} = \rho_e a_\kappa \max_{e \in \Phi_e, d_e \geq r_p} \left\{ |g_e|^2 L\left(d_e\right) \right\}. \tag{6.3}$$

It is assumed that $\kappa \in \{m, n\}$, $\rho_e = \frac{P_A}{\sigma_e^2}$ is the transmit SNR with σ_e^2 being the variance of the AWGN at Es. Additionally, g_e is defined as the small-scale fading coefficient associated with $g_e \sim \mathcal{CN}(0, 1)$, $L\left(d_e\right) = \frac{1}{d_e^\alpha}$ is the path loss, and d_e is the distance from Es to BS.

6.2.1 New Channel Statistics

In this subsection, several new channel statistics for LUs and Es are derived, which will be used for deriving the secrecy outage probability in the next section.

Lemma 3. Assuming M randomly located NOMA users in the disc of Fig. 6.1, the

cumulative distribution function (CDF) $F_{\gamma_{B_n}}$ of the n-th LU is given by

$$F_{\gamma_{B_n}}(x) = \varphi_n \sum_{p=0}^{M-n} \binom{M-n}{p} \frac{(-1)^p}{n+p} \sum_{\tilde{S}_n^p} \binom{n+p}{q_0+\cdots+q_K} \left(\prod_{K=0}^{K} b_k^{q_k} \right) e^{-\sum\limits_{k=0}^{K} q_k c_k \frac{x}{\rho_b a_n}}, \tag{6.4}$$

where K is a complexity-vs-accuracy tradeoff parameter, $b_k = -\omega_K \sqrt{1-\phi_k^2}\,(\phi_k+1)$, $b_0 = -\sum\limits_{k=1}^{K} b_k$, $c_k = 1 + \left[\frac{R_D}{2}(\phi_k+1)\right]^{\alpha}$, $\omega_K = \frac{\pi}{K}$, *and* $\phi_k = \cos\left(\frac{2k-1}{2K}\pi\right)$, $\tilde{S}_n^p = \left\{ (q_0, q_1, \cdots, q_K) | \sum\limits_{i=0}^{K} q_i = n+p \right\}$, $\binom{n+p}{q_0+\cdots+q_K} = \frac{(n+p)!}{q_0!\cdots q_K!}$ and $\varphi_n = \frac{M!}{(M-n)!(n-1)!}$.

Proof. See Appendix B.1. □

Lemma 4. Assuming M randomly positioned NOMA users in the disc of Fig. 6.1, the CDF $F_{\gamma_{B_m}}$ of the m-th LU is given by

$$F_{\gamma_{B_m}}(x) = U\left(x - \frac{a_m}{a_n}\right) + U\left(\frac{a_m}{a_n} - x\right) \varphi_m \sum_{p=0}^{M-m} \binom{M-m}{p} \frac{(-1)^p}{m+p} \sum_{\tilde{S}_m^p} \binom{m+p}{q_0+\cdots+q_K} \left(\prod_{k=0}^{K} b_k^{q_k} \right) e^{-\sum\limits_{k=0}^{K} q_k c_k \frac{x}{(a_m - a_n x)\rho_b}}. \tag{6.5}$$

where $U(x)$ is the unit step function formulated as $U(x) = \begin{cases} 1, x > 0 \\ 0, x \le 0 \end{cases}$, and $\tilde{S}_m^p = \left\{ (q_0, q_1, \cdots, q_K) | \sum\limits_{i=0}^{K} q_i = m+p \right\}$.

Proof. Based on (6.1), the CDF of $F_{\gamma_{B_m}}(x)$ can be expressed as

$$F_{\gamma_{B_m}}(x) = \Pr\left\{ \frac{a_m |h_m|^2}{a_n |h_m|^2 + \frac{1}{\rho_b}} < x \right\} = \begin{cases} \underbrace{\Pr\left\{ |h_m|^2 < \frac{x}{(a_m - a_n x)\rho_b} \right\}}_{\Phi_m}, x < \frac{a_m}{a_n} \\ 1, x \ge \frac{a_m}{a_n} \end{cases}. \tag{6.6}$$

To derive the CDF of $F_{\gamma_{B_m}}(x)$, Φ_m can be expressed as

$$\Phi_m = F_{|h_m|^2}\left(\frac{x}{(a_m - a_n x)\,\rho_b}\right). \tag{6.7}$$

Based on (B.1.5), interchanging the parameters $m \to n$ and applying $y = \frac{x}{(a_m - a_n x)\rho_b}$, the following expression is obtained

$$\Phi_m = \varphi_m \sum_{p=0}^{M-m} \binom{M-m}{p} \frac{(-1)^p}{m+p} \sum_{\tilde{S}_m^p} \binom{m+p}{q_0 + \cdots + q_K} \left(\prod_{k=0}^{K} b_k^{q_k}\right) e^{-\sum\limits_{k=0}^{K} q_k c_k \frac{x}{(a_m - a_n x)\rho_b}}. \tag{6.8}$$

By substituting (6.8) into (6.6), with the aid of the unit step function, the CDF of $F_{\gamma_{B_m}}(x)$ can be obtained. The proof is complete. □

Lemma 5. *Assuming that the eavesdroppers obey the PPP distribution and the E-exclusion zone has a radius of r_p, the probability density function (PDF) $f_{\gamma_{E_\kappa}}$ of the most detrimental E (where $\kappa \in \{m, n\}$) is given by*

$$f_{\gamma_{E_\kappa}}(x) = \mu_{\kappa 1} e^{-\frac{\mu_{\kappa 1}\Gamma(\delta, \mu_{\kappa 2} x)}{x^\delta}} \left(\frac{\mu_{\kappa 2}^\delta e^{-\mu_{\kappa 2} x}}{x} + \frac{\delta \Gamma(\delta, \mu_{\kappa 2} x)}{x^{\delta+1}}\right), \tag{6.9}$$

where $\mu_{\kappa 1} = \delta \pi \lambda_e (\rho_e a_\kappa)^\delta, \mu_{\kappa 2} = \frac{r_p^\alpha}{\rho_e a_\kappa}$, $\delta = \frac{2}{\alpha}$ and $\Gamma(\cdot, \cdot)$ is the upper incomplete Gamma function.

Proof. To derive the PDF of $f_{\gamma_{E_\kappa}}(x)$, it is required to compute the CDF of $F_{\gamma_{E_\kappa}}$ firstly as

$$\begin{aligned} F_{\gamma_{E_\kappa}}(x) =& \Pr\{\gamma_{E_\kappa} \le x\} = E_{\Phi_e}\left\{\prod_{e \in \Phi_e, d_e \ge r_p} \Pr\left\{|g_e|^2 \le \frac{x d_e^\alpha}{\rho_e a_\kappa}\right\}\right\} \\ =& E_{\Phi_e}\left\{\prod_{e \in \Phi_e, d_e \ge r_p} F_{|g_e|^2}\left(\frac{x d_e^\alpha}{\rho_e a_\kappa}\right)\right\}. \end{aligned} \tag{6.10}$$

By applying the generating functional given by [115], (6.10) can be rewritten as

$$\begin{aligned} F_{\gamma_{E_\kappa}}(x) &= \exp\left[-\lambda_e \int_{R^2} \left(1 - F_{|g_e|^2}\left(\frac{x d_e^\alpha}{\rho_e a_\kappa}\right)\right) r dr\right] \\ &= \exp\left[-2\pi\lambda_e \int_{r_p}^{\infty} r e^{-\frac{x}{\rho_e a_\kappa} r^\alpha} dr\right]. \end{aligned} \tag{6.11}$$

By applying [125, Eq. (3.381.9)], it is arrived at:

$$F_{\gamma_{E_\kappa}}(x) = e^{-\frac{\delta\pi\lambda_e(\rho_e a_\kappa)^\delta \Gamma\left(\delta, \frac{x r_p^\alpha}{\rho_e a_\kappa}\right)}{x^\delta}}. \tag{6.12}$$

By taking the derivative of the CDF $F_{\gamma_{E_\kappa}}(x)$ in (6.12), the PDF γ_{E_κ} is obtained in (6.9). The proof is complete. □

6.2.2 Secrecy Outage Probability

In this work, the SOP is used as the secrecy performance metric. Additionally, the secrecy rate of the m-th and of the n-th user can be expressed as

$$I_m = [\log_2(1 + \gamma_{B_m}) - \log_2(1 + \gamma_{E_m})]^+, \tag{6.13}$$

and

$$I_n = [\log_2(1 + \gamma_{B_n}) - \log_2(1 + \gamma_{E_n})]^+, \tag{6.14}$$

respectively, where $[x]^+ = \max\{x, 0\}$. Given the expected secrecy rate R_m and R_n for the m-th and n-th users, a secrecy outage event is declared, when the instantaneous secrecy rate drops below R_m and R_n, respectively. Based on (6.13), the SOP for the m-th user is given by

$$P_m(R_m) = \Pr\{I_m < R_m\} = \int_0^\infty f_{\gamma_{E_m}}(x) F_{\gamma_{B_m}}\left(2^{R_m}(1 + x) - 1\right) dx. \tag{6.15}$$

Based on the assumption of $a_m \geq \left(2^{R_m}-1\right)a_n$, it is considered that the SOP under the condition that the connection between BS and LUs can be established. Upon using the results of **Lemma 4** and **Lemma 5**, as well as substituting (6.5) and (6.9) into (6.15), after some further mathematical manipulations, the SOP of the m-th user can be expressed according to the following theorem:

Theorem 8. *Assuming that the LUs position obeys the PPP for the ordered channels of the LUs, the SOP of the m-th user is given by*

$$P_m\left(R_m\right) = 1 - e^{-\frac{\mu_{m1}\Gamma\left(\delta,\tau_m\mu_{m2}\right)}{{\tau_m}^{\delta}}} + \varphi_m \sum_{p=0}^{M-m}\binom{M-m}{p}\frac{(-1)^p}{m+p}\sum_{\tilde{S}_m^p}\binom{m+p}{q_0+\cdots+q_K}\left(\prod_{k=0}^{K} b_k^{q_k}\right)$$
$$\times \int_0^{\tau_m} \mu_{m1}\left(\frac{\mu_{m2}^{\delta}e^{-\mu_{m2}x}}{x} + \frac{\delta\Gamma\left(\delta,\mu_{m2}x\right)}{x^{\delta+1}}\right) e^{-\frac{\mu_{m1}\Gamma\left(\delta,\mu_{m2}x\right)}{x^{\delta}} - \sum\limits_{k=0}^{K} q_k c_k \frac{2^{R_m}(1+x)-1}{\left(a_m - a_n\left(2^{R_m}(1+x)-1\right)\right)\rho_b}} dx. \tag{6.16}$$

where $\tau_m = \frac{1}{2^{R_m}(1-a_m)} - 1$.

Similarly, for the n-th user, based on (6.14), the SOP is given by

$$P_n\left(R_n\right) = \Pr\left\{I_n < R_n\right\} = \int_0^{\infty} f_{\gamma_{E_n}}\left(x\right) F_{\gamma_{B_n}}\left(2^{R_n}\left(1+x\right)-1\right) dx. \tag{6.17}$$

Upon using the results of **Lemma 3** and **Lemma 5**, and substituting (6.4) and (6.9) into (6.17), after some further mathematical manipulations, the SOP of the n-th user can be expressed with the aid of the following theorem:

Theorem 9. *Assuming that the LUs position obeys the PPP for the ordered channels of the LUs, the SOP of the n-th user is given by*

$$P_n\left(R_n\right) = \varphi_n \sum_{p=0}^{M-n}\binom{M-n}{p}\frac{(-1)^p}{n+p}\sum_{\tilde{S}_n^p}\binom{n+p}{q_0+\cdots+q_K}\left(\prod_{K=0}^{K} b_k^{q_k}\right)$$
$$\times \int_0^{\infty} \mu_{n1}\left(\frac{\mu_{n2}^{\delta}e^{-\mu_{n2}x}}{x} + \frac{\delta\Gamma\left(\delta,\mu_{n2}x\right)}{x^{\delta+1}}\right) e^{-\frac{\mu_{n1}\Gamma\left(\delta,\mu_{n2}x\right)}{x^{\delta}} - \sum\limits_{k=0}^{K} q_k c_k \frac{2^{R_n}(1+x)-1}{\rho_b a_n}} dx. \tag{6.18}$$

In this chapter, it is considered that the secrecy outage occurs in the m-th user and the n-th user are independent. In other words, the SOP of the m-th user has on effect on the SOP of the n-th user and vice versa. As a consequence, the SOP for the selected user pair is defined as that of either the m-th user or the n-th user outage. Hence, based on (6.16) and (6.18), the SOP of the selected user pair is given by

$$P_{mn} = 1 - (1 - P_m)(1 - P_n). \tag{6.19}$$

6.2.3 Secrecy Diversity Order Analysis

In order to derive the secrecy diversity order to gain further insights into the system's operation in the high-SNR regime, the following new analytical framework is introduced. Again, as the worst-case scenario, it is assumed that Es have a powerful detection capability. The asymptotic behavior is analyzed, usually when the SNR of the channels between the BS and LUs is sufficiently high, i.e., when the BS's transmit SNR obeys $\rho_b \to \infty$, while the SNR of the channels between BS and Es is set to arbitrary values. It is noted that for the E-transmit SNR of $\rho_e \to \infty$, the probability of successful eavesdropping will tend to unity. The secrecy diversity order can be defined as follows:

$$d_s = -\lim_{\rho_b \to \infty} \frac{\log P^{\infty}}{\log \rho_b}, \tag{6.20}$$

where P^{∞} is the asymptotic SOP. The diversity order analysis is commenced by characterizing the CDF of the LUs $F^{\infty}_{\gamma_{B_m}}$ and $F^{\infty}_{\gamma_{B_n}}$ in the high-SNR regime. When $y \to 0$, based on (B.1.3) and the approximation of $1 - e^{-y} \approx y$, the asymptotic unordered CDF of $\left|\tilde{h}_n\right|^2$ is obtained as follows:

$$F^{\infty}_{\left|\tilde{h}_n\right|^2}(y) \approx \frac{2y}{R_D^2} \int_0^{R_D} (1 + r^{\alpha})\, r dr = y\ell, \tag{6.21}$$

where $\ell = 1 + \frac{2R_D^{\alpha}}{\alpha+2}$.

Substituting (6.21) into (B.1.2), the asymptotic unordered CDF of $\left|\tilde{h}_n\right|^2$ is given by

$$F^{\infty}_{|h_n|^2}(y) = \varphi_n \sum_{p=0}^{M-n} \binom{M-n}{p} \frac{(-1)^p}{n+p} (y\ell)^{n+p} \approx \frac{\varphi_n}{n} (y\ell)^n. \tag{6.22}$$

Based on (B.1.1), the following expression can be obtained

$$F^{\infty}_{\gamma_{B_n}}(x) = \varphi_n \sum_{p=0}^{M-n} \binom{M-n}{p} \frac{(-1)^p}{n+p} \left(\frac{x\ell}{\rho_b a_n}\right)^{n+p} \approx \frac{\varphi_n}{n} \left(\frac{x\ell}{\rho_b a_n}\right)^n. \tag{6.23}$$

Based on (6.7) and (6.22), it is arrived at:

$$\Phi^{\infty}_m = \varphi_m \sum_{p=0}^{M-m} \binom{M-m}{p} \frac{(-1)^p}{m+p} \left(\frac{x\ell}{(a_m - a_n x)\,\rho_b}\right)^{m+p} \approx \frac{\varphi_m}{m} \left(\frac{x\ell}{(a_m - a_n x)\,\rho_b}\right)^m. \tag{6.24}$$

Substituting (6.24) into (6.6), the asymptotic CDF of γ_{B_m} can be expressed as

$$F^{\infty}_{\gamma_{B_m}}(x) = U\left(x - \frac{a_m}{a_n}\right) + U\left(\frac{a_m}{a_n} - x\right) \Phi^{\infty}_m, \tag{6.25}$$

where Φ^{∞}_m is given in (6.24).

Based on (6.17), the CDF of $F_{\gamma_{B_n}}$ can be replaced by the asymptotic $F^{\infty}_{\gamma_{B_n}}$ of (6.23). After some manipulations, it is arrived at the asymptotic SOP of the n-th user formulated by the following theorem.

Theorem 10. *Assuming that the LUs position obeys the PPP for the ordered channels of the LUs, the asymptotic SOP of the n-th user is given by*

$$P^{\infty}_n(R_n) = G_n(\rho_b)^{-D_n} + o\left(\rho_b^{-D_n}\right), \tag{6.26}$$

where $G_n = \frac{\varphi_n Q_1}{n}$, $Q_1 = \int_0^{\infty} \mu_{n1} e^{-\frac{\mu_{n1}\Gamma(\delta, \mu_{n2} x)}{x^{\delta}}} \left(\frac{\mu^{\delta}_{n2} e^{-\mu_{n2} x}}{x} + \frac{\delta \Gamma(\delta, \mu_{n2} x)}{x^{\delta+1}}\right) \left(\frac{\left(2^{R_n}(1+x)-1\right)\ell}{a_n}\right)^n dx$, and $D_n = n$.

Similarly, based on (6.15), the CDF of $F_{\gamma_{B_m}}$ can be replaced by the asymptotic $F^{\infty}_{\gamma_{B_m}}$ of (6.25). Additionally, the asymptotic SOP of the m-th user can be formulated by the following theorem.

Theorem 11. *Assuming that the LUs position obeys the PPP for the ordered channels of the LUs, the asymptotic SOP for the m-th user is given by*

$$P_m^{\infty}\left(R_n\right) = G_m(\rho_b)^{-D_m} + o\left(\rho_b^{-D_m}\right), \tag{6.27}$$

where $G_m = \frac{\varphi_m Q_2}{m}$,
$Q_2 = \int_0^{\tau_m} \mu_{m1} e^{-\frac{\mu_{m1}\Gamma(\delta,\mu_{m2}x)}{x^{\delta}}} \left(\frac{\mu_{m2}^{\delta} e^{-\mu_{m2}x}}{x} + \frac{\delta\Gamma(\delta,\mu_{m2}x)}{x^{\delta+1}}\right) \left(\frac{\left(2^{R_m}(1+x)-1\right)\ell}{(a_m - a_n(2^{R_m}(1+x)-1))}\right)^m dx$, and
$D_m = m$.

Substituting (6.26) and (6.27) into (6.19), the asymptotic SOP for the user pair can be expressed as

$$P_{mn}^{\infty} = P_m^{\infty} + P_n^{\infty} - P_m^{\infty} P_n^{\infty} \approx P_m^{\infty} G_m(\rho_b)^{-D_m}. \tag{6.28}$$

Based on **Theorem 11** and **Theorem 10**, and upon substituting (6.26) and (6.27) into (6.20), it is arrived at the following proposition.

Proposition 1. *For $m < n$, the secrecy diversity order can be expressed as*

$$d_s = -\lim_{\rho_b \to \infty} \frac{\log\left(P_m^{\infty} + P_n^{\infty} - P_m^{\infty} P_n^{\infty}\right)}{\log \rho_b} = m. \tag{6.29}$$

Remark 1. *The results of* (6.29) *indicate that the secrecy diversity order and the asymptotic SOP for the user pair considered are determined by the m-th user.*

Remark 1 provides insightful guidelines for improving the SOP of the networks considered by invoking user pairing among of the M users. Since the SOP of a user pair is determined by that of the one having a poor channel, it is efficient to pair the user having the best channel and the second best channel for the sake of achieving an increased secrecy diversity order.

6.3 Enhancing Security with the aid of Artificial Noise

In order to further improve the secrecy performance, let us now consider the employment of multiple antennas at BS for generating AN in order to degrade the Es' SNR. More particularly, the BS is equipped with N_A antennas, while all LUs and Es are equipped with a single antenna each. The superposed information of NOMA is masked by superimposing AN on Es with the aid of the BS. It is assumed that the CSI of LUs are known at BS. Since the AN is in the null space of the intended LU's channel, it will not impose any effects on LUs. However, it can significantly degrade the channel and hence the capacity of Es. More precisely, the key idea of using AN as proposed in [129] can be described as follows: an orthogonal basis of C^{N_A} is generated at BS for user κ, (where $\kappa \in \{m, n\}$) as a $(N_A \times N_A)$ element precoding matrix $\mathbf{U}_\kappa = [\mathbf{u}_\kappa, \mathbf{V}_\kappa]$, where $\mathbf{u}_\kappa = \mathbf{h}_\kappa^\dagger / \|\mathbf{h}_\kappa\|^1$, and $\mathbf{V}_\kappa$ is of size $N_A \times (N_A - 1)$. Here, $\mathbf{h}_\kappa \in \mathrm{C}^{1\times N_A}$ is denoted as the intended channel between the BS and user κ. As such, $\mathbf{u}_\kappa \in \mathrm{C}^{N_A \times 1}$. It is noted that each column of $\mathbf{V}_\kappa$ is orthogonal to $\mathbf{u}_\kappa$. Beamforming is applied at the BS for generating AN. As such, the transmitted superposed information, which is masked by AN at the BS is given by

$$\sum_{\kappa\in\{m,n\}} \sqrt{a_\kappa}\mathbf{x}_\kappa = \sum_{\kappa\in\{m,n\}} \sqrt{a_\kappa}\left(\mathbf{u}_\kappa s_\kappa + \mathbf{V}_\kappa \mathbf{t}_\kappa\right), \tag{6.30}$$

where s_κ is the information-bearing signal with a variance of σ_s^2, and $\mathbf{t}_\kappa$ is the AN signal. Here the $(N_A - 1)$ elements of $\mathbf{t}_\kappa$ are independent identically distributed (i.i.d.) complex Gaussian random variables with a variance of σ_a^2. As such, the overall power per transmission is $P_T = P_S + P_A$, where $P_S = \theta P_T = \sigma_s^2$ is the transmission power of the desired information-bearing signal, while $P_A = (1-\theta) P_T = (N_A - 1)\sigma_a^2$ is the transmission power of the AN. Here θ represents the power sharing coefficients between the information-bearing signal and AN. To reduce the complexity of channel ordering in this MISO system when applying the NOMA protocol, as shown in Fig. 6.2, the disc D is divided into two regions, namely, D_1 and D_2, respectively. Here, D_1 is an internal

[1] † is the conjugate transpose operator

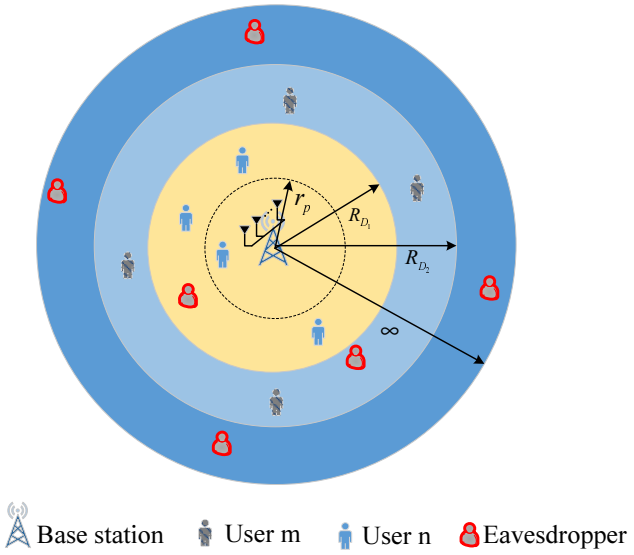

Figure 6.2: Network model for secure NOMA transmission using AN in multiple-antenna scenario, where r_p, R_{D_1}, R_{D_2}, and ∞ is the radius of the E-exclusion zone, NOMA user zone for user n, NOMA user zone for user m, and an infinite two dimensional plane for eavesdroppers, respectively.

disc with radius R_{D_1}, and the group of user n is located in this region. D_2 is an external ring spanning the radius distance from R_{D_1} to R_{D_2}, and the group of user m is located in this region. In this scenario, channel ordering is unnecessary at the BS, since in this case the path loss is the dominant channel impairment. For simplicity, it is assumed that

user n and user m are the selected user from each group in the rest of this chapter. The cell-center user n is assumed to be capable of cancelling the interference of the cell-edge user m using SIC techniques. User n and user m are randomly selected[2] in each region for pairing them for NOMA. The combined signal at user m is given by

$$\begin{aligned}\mathbf{y}_m &= \frac{\mathbf{h}_m\mathbf{u}_m\sqrt{a_m}s_m}{\sqrt{1+d_m^\alpha}} + \frac{\mathbf{h}_m\mathbf{u}_n\sqrt{a_n}s_n}{\sqrt{1+d_m^\alpha}} + \frac{\mathbf{h}_m\mathbf{V}_n\sqrt{a_n}\mathbf{t}_n}{\sqrt{1+d_m^\alpha}} + n_m \\ &= \underbrace{\frac{\|\mathbf{h}_m\|\sqrt{a_m}s_m}{\sqrt{1+d_m^\alpha}}}_{\textbf{Signal part}} + \underbrace{\frac{\left|\mathbf{h}_m\frac{\mathbf{h}_n^\dagger}{\|\mathbf{h}_n\|}\right|\sqrt{a_n}s_n}{\sqrt{1+d_m^\alpha}} + \frac{\mathbf{h}_m\mathbf{V}_n\sqrt{a_n}\mathbf{t}_n}{\sqrt{1+d_m^\alpha}} + n_m}_{\textbf{Interference and noise part}},\end{aligned} \tag{6.31}$$

where n_m is a Gaussian noise vector at user m, while d_m is the distance between the BS and user m. Substituting (6.30) into (6.31), the received SINR at user m is given by

$$\gamma_{B_m}^{AN} = \frac{a_m\sigma_s^2\|\mathbf{h}_m\|^2}{a_n\sigma_s^2\left|\mathbf{h}_m\frac{\mathbf{h}_n^\dagger}{\|\mathbf{h}_n\|}\right|^2 + a_n\sigma_a^2\|\mathbf{h}_m\mathbf{V}_n\|^2 + 1 + d_m^\alpha}, \tag{6.32}$$

where the variance of n_m is normalized to unity. As such, the transmit SNR at BS can be expressed as $\rho_t = P_T$.

Since SIC is applied at user n, the interference arriving from user m can be detected and subtracted firstly. The aggregate signal at user n is given by

$$\begin{aligned}\mathbf{y}_n &= \frac{\mathbf{h}_n\mathbf{u}_n\sqrt{a_n}s_n}{\sqrt{1+d_n^\alpha}} + \frac{\mathbf{h}_n\mathbf{V}_m\sqrt{a_m}\mathbf{t}_m}{\sqrt{1+d_n^\alpha}} + n_n \\ &= \underbrace{\frac{\|\mathbf{h}_n\|\sqrt{a_n}s_n}{\sqrt{1+d_n^\alpha}}}_{\textbf{Signal part}} + \underbrace{\frac{\mathbf{h}_n\mathbf{V}_m\sqrt{a_m}\mathbf{t}_m}{\sqrt{1+d_n^\alpha}} + n_n}_{\textbf{Interference and noise part}},\end{aligned} \tag{6.33}$$

where n_n is the Gaussian noise at user n, while d_n is the distance between the BS and user n. The received SINR at user n is given by

$$\gamma_{B_n}^{AN} = \frac{a_n\sigma_s^2\|\mathbf{h}_n\|^2}{a_m\sigma_a^2\|\mathbf{h}_n\mathbf{V}_m\|^2 + 1 + d_n^\alpha}, \tag{6.34}$$

[2]Dynamic user selection schemes are capable of further improving the performance of the framework considered, but they are beyond the scope of this work.

where the variance of $\mathbf{n}_n$ is normalized to unity. The signal observed by Es is given by

$$\begin{aligned}\mathbf{y}_e &= \sum_{\kappa\in\{m,n\}} \frac{\mathbf{h}_e\sqrt{a_\kappa}\mathbf{x}_\kappa}{\sqrt{d_e^\alpha}} + n_e \\ &= \underbrace{\frac{\mathbf{h}_e\frac{\mathbf{h}_m^\dagger}{\|\mathbf{h}_m\|}\sqrt{a_m}s_m}{\sqrt{d_e^\alpha}}}_{\textbf{Signal part } m} + \underbrace{\frac{\mathbf{h}_e\frac{\mathbf{h}_n^\dagger}{\|\mathbf{h}_n\|}\sqrt{a_n}s_n}{\sqrt{d_e^\alpha}}}_{\textbf{Signal part } n} + \underbrace{\frac{\mathbf{h}_e\mathbf{V}_m\sqrt{a_m}\mathbf{t}_m}{\sqrt{d_e^\alpha}} + \frac{\mathbf{h}_e\mathbf{V}_n\sqrt{a_n}\mathbf{t}_n}{\sqrt{d_e^\alpha}} + n_e}_{\textbf{Interference and noise part}},\end{aligned} \tag{6.35}$$

where n_e is the Gaussian noises at Es, while $\mathbf{h}_e \in \mathrm{C}^{1\times N_A}$ is the channel vector between the BS and Es. Similar to the single-antenna scenario, again, it is assumed that the Es have a strong detection capability and hence they unambiguously distinguish the messages of user m and user n. The received SINR of the most detrimental E associated with detecting user κ is given by

$$\gamma_{E_\kappa}^{AN} = a_\kappa\sigma_s^2 \max_{e\in\Phi_e, d_e\geq r_p}\left\{\frac{X_{e,\kappa}}{I_e^{AN}+d_e^\alpha}\right\}, \tag{6.36}$$

where the variance of n_e is normalized to unity, and $X_{e,\kappa} = \left|\mathbf{h}_e\frac{\mathbf{h}_\kappa^\dagger}{\|\mathbf{h}_\kappa\|}\right|^2$ as well as $I_e^{AN} = a_m\sigma_a^2\|\mathbf{h}_e\mathbf{V}_m\|^2 + a_n\sigma_a^2\|\mathbf{h}_e\mathbf{V}_n\|^2$.

6.3.1 New Channel Statistics

In this subsection, several new channel statistics for LUs and Es in the presence of AN are derived, which will be used for deriving the SOP in the next subsection.

Lemma 6. *Assuming that user m is randomly positioned in the ring D_2 of Fig. 6.2, for*

the case of $\theta \neq \frac{1}{N_A}$, *the CDF of* $F_{B_m}^{AN}$ *is given by* (6.37)

$$F_{B_m}^{AN}(x) = 1 - e^{-\frac{\nu x}{a_n}} \sum_{p=0}^{N_A-1} \frac{(\nu x)^p}{p!} \sum_{q=0}^{p} \binom{p}{q} a_n^{q-p} \underbrace{a_1 \left(\frac{\Gamma(q+1)}{\left(\nu x + \frac{1}{P_S}\right)^{q+1}} - \sum_{l=0}^{N_A-2} \frac{\left(\frac{N_A-1}{P_A} - \frac{1}{P_S}\right)^l}{\frac{l!\left(\nu x + \frac{N_A-1}{P_A}\right)^{q+l+1}}{\Gamma(q+l+1)}} \right)}_{\mathrm{I}(\theta)}$$
$$\times \sum_{u=0}^{p-q} \binom{p-q}{u} \frac{\gamma\left(u+\delta, \frac{\nu x}{a_n} R_{D_2}^{\alpha}\right) - \gamma\left(u+\delta, \frac{\nu x}{a_n} R_{D_1}^{\alpha}\right)}{\left(\frac{\nu x}{a_n}\right)^{u+\delta}}, \tag{6.37}$$

where $\gamma(\cdot,\cdot)$ is the lower incomplete Gamma function, $\Gamma(\cdot)$ is the Gamma function, $a_1 = \delta\left(1 - \frac{P_A}{(N_A-1)P_S}\right)^{1-N_A} / \left(\left(R_{D_2}^2 - R_{D_1}^2\right) P_S\right)$, and $\nu = \frac{a_n}{a_m P_S}$.

For the case of $\theta = \frac{1}{N_A}$, the CDF of $F_{B_m}^{AN}$ is given by (6.37) upon substituting $\mathrm{I}(\theta)$ by $\mathrm{I}^*(\theta)$, where $\mathrm{I}^*(\theta) = \frac{a_2 \Gamma(q+N_A)}{\left(\nu x + \frac{1}{P_S}\right)^{q+N_A}} \sum_{u=0}^{p-q} \binom{p-q}{u}$ and $a_2 = \frac{\delta}{\left(R_{D_2}^2 - R_{D_1}^2\right) P_S{}^{N_A} (N_A-1)!}$.

Proof. See Appendix B.2. □

Lemma 7. *Assuming that user n is randomly positioned in the disc* D_1 *of Fig. 6.2, the CDF of* $F_{B_n}^{AN}$ *is given by*

$$F_{B_n}^{AN}(x) = 1 - b_2 e^{-\frac{\vartheta x}{a_m}} \sum_{p=0}^{N_A-1} \frac{\vartheta^p x^p}{p!} \sum_{q=0}^{p} \binom{p}{q} \frac{\Gamma(N_A - 1 + q)}{\left(\vartheta x + \frac{N_A-1}{P_A}\right)^{N_A-1+q}} a_m^{p-q}$$
$$\times \sum_{u=0}^{p-q} \binom{p-q}{u} \frac{a_m^{u+\delta} \gamma\left(u+\delta, \frac{\vartheta x}{a_m} R_{D_1}^{\alpha}\right)}{(\vartheta x)^{u+\delta}}, \tag{6.38}$$

where $b_2 = \frac{\delta}{R_{D_1}^2 \Gamma(N_A-1)\left(\frac{P_A}{N_A-1}\right)^{N_A-1}}$ and $\vartheta = \frac{a_m}{a_n P_S}$.

Proof. See Appendix B.3. □

Lemma 8. *Assuming that the distribution of Es obeys a PPP and that the E-exclusion zone has a radius of* r_p, *the PDF of* $f_{\gamma_{E_\kappa}^{AN}}$ *(where* $\kappa \in \{m, n\}$*) is given by*

$$f_{\gamma_{E_\kappa}^{AN}}(x) = -e^{\Theta_\kappa \Psi_{\kappa 1}} \left(\frac{\left(\mu_{\kappa 2}^{AN}\right)^{\delta} e^{-x\mu_{\kappa 2}^{AN}}}{x} \Psi_{\kappa 1} + \frac{\delta \Theta_\kappa \Psi_{\kappa 1}}{x} + \Theta_\kappa \Psi_{\kappa 2} \right), \tag{6.39}$$

where $\Theta_\kappa = \frac{\Gamma\left(\delta, x\mu_{\kappa 2}^{AN}\right)}{x^\delta}$, $\Gamma(\cdot,\cdot)$ is the upper incomplete Gamma function, $\Psi_{\kappa 1} = \Omega \frac{1}{\left(\frac{x}{a_\kappa P_S}+\tau_i\right)^j}$,

$\Psi_{\kappa 2} = \Omega \frac{1}{\left(\frac{x}{a_\kappa P_S}+\tau_i\right)^j}\left(\frac{j}{\left(\frac{x}{a_\kappa P_S}+\tau_i\right)}\frac{1}{a_\kappa P_S}\right)$,

$\Omega = (-1)^{N_A}\mu_{\kappa 1}^{AN}\prod_{i=1}^{2}\tau_i^{N_A-1}\sum_{i=1}^{2}\sum_{j=1}^{N_A-1} a_{N_A-j,N_A-1}(2\tau_i - L)^{j-(2N_A-2)}$, $L = \tau_1 + \tau_2, \tau_1 = \frac{N_A-1}{a_m P_A}, \tau_2 = \frac{N_A-1}{a_n P_A}$, $a_{N_A-j,N_A-1} = \binom{2N_A-j-3}{N_A-j-1}$, $\mu_{\kappa 1}^{AN} = \pi\lambda_e\delta(a_\kappa P_S)^\delta$, and $\mu_{\kappa 2}^{AN} = \frac{r_p^\alpha}{a_\kappa P_S}$.

Proof. See Appendix B.4. □

6.3.2 Secrecy Outage Probability

In this subsection, the SOP of a multiple-antenna aided scenario is investigated relying on AN. Using the results of **Lemma 6** and **Lemma 8**, based on (6.15), the SOP of user m is expressed using the following theorem:

Theorem 12. *Assuming that the LUs and Es distribution obey PPPs and that AN is generated at the BS, for the case $\theta \neq \frac{1}{N_A}$, the SOP of user m is given by*

$$P_m^{AN}(R_m) = \int_0^\infty -e^{\Theta_m\Psi_{m1}}\left(\frac{\left(\mu_{m2}^{AN}\right)^\delta e^{-x\mu_{m2}^{AN}}}{x}\Psi_{m1} + \frac{\delta\Theta_m\Psi_{m1}}{x} + \Theta_m\Psi_{m2}\right)\times \underbrace{\left(1 - a_1^*\sum_{p=0}^{N_A-1}\frac{\iota_m^p}{p!}\sum_{q=0}^{p}\binom{p}{q}a_n^q\left(\frac{\Gamma(q+1)}{\left(a_n\iota_{m*}+\frac{1}{P_S}\right)^{q+1}} - \sum_{l=0}^{N_A-2}\frac{\frac{1}{l!}\left(\frac{N_A-1}{P_A}-\frac{1}{P_S}\right)^l\Gamma(q+l+1)}{\left(a_n\iota_{m*}+\frac{N_A-1}{P_A}\right)^{q+l+1}}\right)\mathrm{T}_1^*\right)}_{\mathrm{K}(\theta)} dx, \tag{6.40}$$

where $a_1^* = \frac{\delta e^{-\iota_{m*}}\left(1-\frac{P_A}{(N_A-1)P_S}\right)^{1-N_A}}{\left(R_{D_2}^2 - R_{D_1}^2\right)P_S}$, $\mathrm{T}_1^* = \sum_{u=0}^{p-q}\binom{p-q}{u}\frac{\gamma\left(u+\delta,\iota_{m*}R_{D_2}^\alpha\right)-\gamma\left(u+\delta,\iota_{m*}R_{D_1}^\alpha\right)}{\iota_{m*}^{u+\delta}}$, and $\iota_{m*} = \frac{\nu\left(2^{R_m}(1+x)-1\right)}{a_n}$.

For the case of $\theta = \frac{1}{N_A}$, the SOP for user m is given by (6.40) upon substituting $\mathrm{K}(\theta)$ with $\mathrm{K}^*(\theta)$, where $\mathrm{K}^*(\theta) = 1 - a_2^*\sum_{p=0}^{N_A-1}\frac{\iota_{m*}^p}{p!}\sum_{q=0}^{p}\binom{p}{q}\frac{\Gamma(q+N_A)a_n^q}{\left(a_n\iota_{m*}+\frac{1}{P_S}\right)^{q+N_A}}\sum_{u=0}^{p-q}\binom{p-q}{u}\mathrm{T}_1^*$, and $a_2^* = \frac{\delta e^{-\iota_{m*}}}{\left(R_{D_2}^2 - R_{D_1}^2\right)P_S{}^{N_A}(N_A-1)!}$.

Similarly, using the results of **Lemma 7** and **Lemma 8**, as well as (6.17), the SOP of user n is expressed by the following theorem:

Theorem 13. *Assuming that the LUs and Es distribution obey PPPs and that AN is generated at the BS, the SOP of user n is given by*

$$P_n^{AN}(R_n) = \int_0^{\infty} -e^{\Theta_n \Psi_{n1}} \left(\frac{\left(\mu_{n2}^{AN}\right)^{\delta} e^{-x\mu_{n2}^{AN}}}{x} \Psi_{n1} + \frac{\delta \Theta_n \Psi_{n1}}{x} + \Theta_n \Psi_{n2} \right) \times \left(1 - b_2 e^{-\iota_n} \sum_{p=0}^{N_A-1} \frac{\iota_{n*}}{p!} \sum_{q=0}^{p} \binom{p}{q} \frac{\Gamma(N_A - 1 + q)\, a_m^q}{\left(a_m \iota_{n*} + \frac{N_A-1}{P_A}\right)^{N_A-1+q}} \sum_{u=0}^{p-q} \binom{p-q}{u} \frac{\gamma\left(u+\delta, \iota_{n*} R_{D_1}^{\alpha}\right)}{\iota_{n*}^{u+\delta}} \right) dx, \tag{6.41}$$

where $\iota_{n*} = \frac{\vartheta\left(2^{R_n}(1+x)-1\right)}{a_m}$.

Based on (6.40) and (6.41), the SOP for the selected user pair can be expressed as

$$P_{mn}^{AN} = 1 - \left(1 - P_m^{AN}\right)\left(1 - P_n^{AN}\right). \tag{6.42}$$

6.3.3 Large Antenna Array Analysis

In this subsection, the system's asymptotic behavior is investigated when the BS is equipped with large antenna arrays. It is noted that for the exact SOP derived in (6.40) and (6.41), as N_A increases, the number of summations in the equations will increase exponentially, which imposes an excessive complexity. Motivated by this, the work seeks good approximations for the SOP associated with a large N_A. With the aid of the theorem of large values, the following approximations can be obtained: $\lim_{N_A\to\infty} \|\mathbf{h}_n\|^2 \to N_A$, $\lim_{N_A\to\infty} \|\mathbf{h}_m\|^2 \to N_A$, $\lim_{N_A\to\infty} \|\mathbf{h}_n \mathbf{V}_m\|^2 \to N_A - 1$, and $\lim_{N_A\to\infty} \|\mathbf{h}_m \mathbf{V}_n\|^2 \to N_A - 1$.

The asymptotic CDF of user n for $N_A \to \infty$ is first derived. Based on (6.34), the asymptotic CDF of $F_{B_n,\infty}^{AN}$ can be first derived as

$$F_{B_n,\infty}^{AN}(x) = \Pr\left\{ \frac{a_n P_S N_A}{a_m P_A + 1 + d_n^{\alpha}} \le x \right\}. \tag{6.43}$$

After some further mathematical manipulations, the CDF of $F^{AN}_{B_n,\infty}$ for large antenna arrays can be obtained in the following lemma.

Lemma 9. *Assuming that user n is randomly located in the disc D_1 of Fig. 6.2 and $N_A \to \infty$, the CDF of $F^{AN}_{B_n,\infty}$ is given by*

$$F^{AN}_{B_n,\infty}(x) = \begin{cases} 0, x < \zeta_n \\ 1 - \frac{\left(\frac{a_n P_S N_A}{x} - a_m P_A - 1\right)^{\delta}}{R^2_{D_1}}, \zeta_n \le x \le \xi_n \\ 1, x \ge \xi_n \end{cases}, \tag{6.44}$$

where $\zeta_n = \frac{a_n P_S N_A}{R^{\alpha}_{D_1} + a_m P_A + 1}$ and $\xi_n = \frac{a_n P_S N_A}{a_m P_A + 1}$.

Similarly, based on (6.32),the CDF of the asymptotic $F^{AN}_{B_m,\infty}$ is given by

$$F^{AN}_{B_m,\infty}(x) = \Pr\left\{ \frac{a_m P_S N_A}{a_n P_S \left| \mathbf{h}_m \frac{\mathbf{h}_n^{\dagger}}{\|\mathbf{h}_n\|} \right|^2 + a_n P_A + 1 + d_m^{\alpha}} \le x \right\}. \tag{6.45}$$

After some further mathematical manipulations, the CDF of $F^{AN}_{B_m,\infty}$ for large antenna arrays is obtained using the following lemma.

Lemma 10. *Assuming that user m is randomly located in the ring D_2 of Fig. 6.2 and $N_A \to \infty$, the CDF of $F^{AN}_{B_m,\infty}$ is given by*

$$F^{AN}_{B_m,\infty}(x) = \begin{cases} 1, x \ge \zeta_{m1} \\ \frac{R^2_{D_2} - t_m^2 + b_1 e^{-\frac{a_m P_S N_A}{x a_n P_S}}}{R^2_{D_2} - R^2_{D_1}} \int_{R_{D_1}}^{t_m} r e^{\frac{r^{\alpha}}{a_n P_S}} dr, \zeta_{m2} < x \le \zeta_{m1} \\ \frac{b_1 e^{-\frac{a_m P_S N_A}{x a_n P_S}}}{R^2_{D_2} - R^2_{D_1}} \int_{R_{D_1}}^{R_{D_2}} r e^{\frac{r^{\alpha}}{a_n P_S}} dr, x < \zeta_{m2} \end{cases}, \tag{6.46}$$

where $b_1 = 2e^{\frac{a_n P_A + 1}{a_n P_S}}$, $t_m = \sqrt[\alpha]{\frac{a_m P_S N_A}{x} - a_n P_A - 1}$, $\zeta_{m1} = \frac{a_m P_S N_A}{R^{\alpha}_{D_1} + a_n P_A + 1}$, $\zeta_{m2} = \frac{a_m P_S N_A}{R^{\alpha}_{D_2} + a_n P_A + 1}$, and $\xi_m = \frac{a_m P_S N_A}{a_n P_A + 1}$.

Let us now turn the attention to the derivation of the Es' PDF in a large-scale antenna scenario. Using the theorem of large values, the following approximations can

be obtained: $\lim_{N_A\to\infty} I_{e,\infty}^{AN} = a_m\sigma_a^2\|\mathbf{h}_e\mathbf{V}_m\|^2 + a_n\sigma_a^2\|\mathbf{h}_e\mathbf{V}_n\|^2 \to P_A$. The asymptotic CDF of $F_{\gamma_{E_\kappa,\infty}^{AN}}$ associated with $N_A \to \infty$ is given by

$$F_{\gamma_{E_\kappa,\infty}^{AN}}(x) = \Pr\left\{\max_{e\in\Phi_e, d_e\geq r_p}\left\{\frac{a_\kappa P_S X_{e,\kappa}}{I_{e,\infty}^{AN} + d_e^\alpha}\right\} \leq x\right\} = E_{\Phi_e}\left\{\prod_{e\in\Phi_e, d_e\geq r_p} F_{X_{e,\kappa}}\left(\frac{(P_A + d_e^\alpha)\, x}{a_\kappa P_S}\right)\right\}. \tag{6.47}$$

Following the procedure used for deriving (6.11), this work applies the generating function and switches to polar coordinates. Then with the help of [125, Eq. (3.381.9)], (6.47) can be expressed as

$$F_{\gamma_{E_\kappa,\infty}^{AN}}(x) = \exp\left[-\frac{\mu_{\kappa 1}^{AN}\Gamma\left(\delta, \mu_{\kappa 2}^{AN} x\right)}{x^\delta} e^{-\frac{P_A x}{a_\kappa P_S}}\right]. \tag{6.48}$$

Taking derivative of (6.48), the PDF of $f_{\gamma_{E_\kappa,\infty}^{AN}}$ is obtained in the following lemma.

Lemma 11. *Assuming that the Es distribution obeys a PPP and that AN is generated at the BS, the E-exclusion zone has a radius of r_p, and $N_A \to \infty$, the PDF of $f_{\gamma_{E_\kappa,\infty}^{AN}}$ (where $\kappa \in \{m, n\}$) is given by*

$$\begin{aligned} f_{\gamma_{E_\kappa,\infty}^{AN}}(x) =& e^{-\frac{\mu_{\kappa 1}^{AN}\Gamma\left(\delta,\mu_{\kappa 2}^{AN} x\right)e^{-\frac{P_A x}{a_\kappa P_S}}}{x^\delta} - \frac{P_A x}{a_\kappa P_S}} \mu_{\kappa 1}^{AN} x^{-\delta} \\ &\times \left(\left(\mu_{\kappa 2}^{AN}\right)^\delta x^{\delta-1} e^{-\mu_{\kappa 2}^{AN} x} + \Gamma\left(\delta, \mu_{\kappa 2}^{AN} x\right)\left(\frac{P_A}{a_\kappa P_S} + \frac{\delta}{x}\right)\right). \end{aligned} \tag{6.49}$$

Remark 2. *The results derived in* (6.49) *show that the PDF of $f_{\gamma_{E_\kappa,\infty}^{AN}}$ is independent of the number of antennas N_A in the large antenna array analysis. This indicates that N_A has no effect on the channel of the Es, when the number of antennas is sufficiently high.*

Let us now derive the SOP for the large antenna array scenario. Using the results of **Lemma 10** and **Lemma 11**, based on (6.15), the SOP for user m can be expressed in the following theorem.

Theorem 14. *Assuming that the LUs and Es distribution obey PPPs, AN is generated*

at the BS, and $N_A \to \infty$, the SOP for user m is given by

$$P_{m,\infty}^{AN}(R_m) = 1 - e^{-\frac{\mu_{\kappa 1}^{AN}\Gamma\left(\delta,\mu_{\kappa 2}^{AN}\chi_{m1}\right)}{(\chi_{m1})^{\delta}}e^{-\frac{P_A\chi_{m1}}{a_\kappa P_S}}}$$
$$+ \frac{\mu_{m1}^{AN}b_1\Lambda_1}{R_{D_2}^2 - R_{D_1}^2}\int_0^{\chi_{m2}} e^{-\frac{\mu_{m1}^{AN}\Gamma\left(\delta,\mu_{m2}^{AN}x\right)e^{-\frac{P_A x}{a_m P_S}}}{x^{\delta}} - \frac{a_m P_S N_A}{\left(2^{R_m}(1+x)-1\right)a_n P_S} - \frac{P_A x}{a_m P_S}}\Xi_1 dx$$
$$+ \frac{\mu_{m1}^{AN}}{R_{D_2}^2 - R_{D_1}^2}\int_{\chi_{m2}}^{\chi_{m1}} e^{-\frac{\mu_{m1}^{AN}\Gamma\left(\delta,\mu_{m2}^{AN}x\right)e^{-\frac{P_A x}{a_m P_S}}}{x^{\delta}} - \frac{P_A x}{a_m P_S}}\left(R_{D_2}^2 - t_{m*}^2 + b_1 e^{-\frac{a_m P_S N_A}{\left(2^{R_m}(1+x)-1\right)a_n P_S}}\right)\Xi_1\Lambda_2 dx, \tag{6.50}$$

where $\Xi_1 = x^{-\delta}\left(\mu_{m2}^{AN}\left(\mu_{m2}^{AN}x\right)^{\delta-1}e^{-\mu_{m2}^{AN}x} + \Gamma\left(\delta,\mu_{m2}^{AN}x\right)\left(\frac{P_A}{a_m P_S} + \frac{\delta}{x}\right)\right)$, $\Lambda_1 = \int_{R_{D_1}}^{R_{D_2}} re^{\frac{r^\alpha}{a_n P_S}}dr$, $\Lambda_2 = \int_{R_{D_1}}^{t_{m*}} re^{\frac{r^\alpha}{a_n P_S}}dr$, $t_{m*} = \sqrt[\alpha]{\frac{a_m P_S N_A}{2^{R_m}(1+x)-1} - a_n P_A - 1}$, and $\chi_{m2} = \frac{\zeta_{m2}+1}{2^{R_m}} - 1$.

Similarly, using the results of **Lemma 9** and **Lemma 11**, as well as (6.17), the SOP for user n can be expressed in the following theorem.

Theorem 15. Assuming that the LUs and Es distribution obey PPPs, AN is generated at the BS and $N_A \to \infty$, the SOP for user n is given by

$$P_{n,\infty}^{AN}(R_n) = 1 - e^{-\frac{\mu_{n1}^{AN}\Gamma\left(\delta,\mu_{n2}^{AN}\chi_{n2}\right)}{(\chi_{n2})^{\delta}}e^{-\frac{P_A\chi_{n2}}{a_n P_S}}}$$
$$+ \mu_{n1}^{AN}\int_{\chi_{n1}}^{\chi_{n2}} e^{-\frac{\mu_{n1}^{AN}\Gamma\left(\delta,\mu_{n2}^{AN}x\right)e^{-\frac{P_A x}{a_n P_S}}}{x^{\delta}} - \frac{P_A x}{a_n P_S}}\Xi_2\left(1 - \frac{1}{R_{D_1}^2}\left(\frac{a_n P_S N_A}{2^{R_n}(1+x)-1} - a_m P_A - 1\right)^{\delta}\right)dx, \tag{6.51}$$

where $\chi_{n1} = \frac{\zeta_n+1}{2^{R_n}} - 1$, $\chi_{n2} = \frac{\xi_n+1}{2^{R_n}} - 1$,
and $\Xi_2 = x^{-\delta}\left(\left(\mu_{n2}^{AN}\right)^{\delta}x^{\delta-1}e^{-\mu_{n2}^{AN}x} + \Gamma\left(\delta,\mu_{n2}^{AN}x\right)\left(\frac{P_A}{a_n P_S} + \frac{\delta}{x}\right)\right)$.

Based on (6.50) and (6.51), the SOP for the selected user pair can be expressed as

$$P_{mn,\infty}^{AN} = 1 - \left(1 - P_{m,\infty}^{AN}\right)\left(1 - P_{n,\infty}^{AN}\right). \tag{6.52}$$

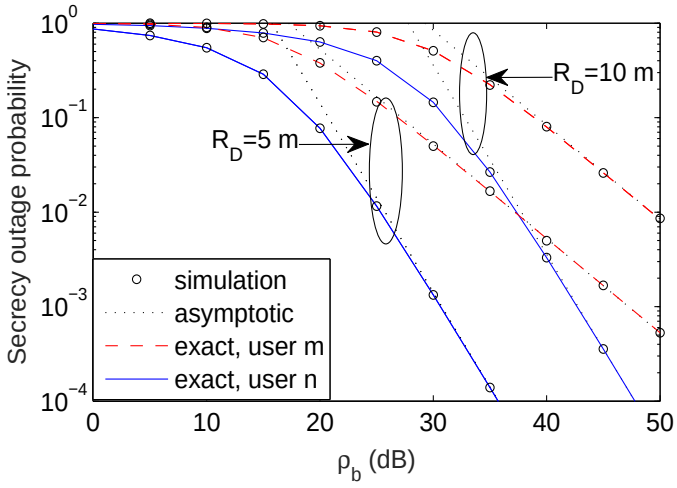

Figure 6.3: The SOP versus ρ_b, with $\rho_e = 10$ dB, $\alpha = 4$, $\lambda_e = 10^{-3}$, $M = 2$, $m = 1$, $n = 2$, and $r_p = 10$ m. The exact analytical results are calculated from (6.16) and (6.18). The asymptotic analytical results are calculated from (6.26) and (6.27).

6.4 Numerical Results

In this section, the numerical results are presented for characterizing the performance of large-scale networks. It is assumed that the power allocation coefficients of NOMA are $a_m = 0.6$, $a_n = 0.4$. The targeted data rates of the selected NOMA user pair are assumed to be $R_m = R_n = 0.1$ bit per channel use (BPCU).

6.4.1 Secrecy outage probability with channel ordering

In Fig. 6.3 to Fig. 6.5, the secrecy performance is investigated in conjunction with channel ordering, which correspond to the scenario considered in Section II.

Fig. 6.3 plots the SOP of a single user (m-th and n-th) versus ρ_b for different user zone radii. In this case, the number of NOMA users is set to $M = 2$. The curves represent the exact analytical SOP of both the m-th user and of n-th user derived in (6.16) and (6.18), respectively. The asymptotic analytical SOP of both the m-th and n-th users, are derived in (6.27) and (6.26), respectively. Monte Carlo simulations are

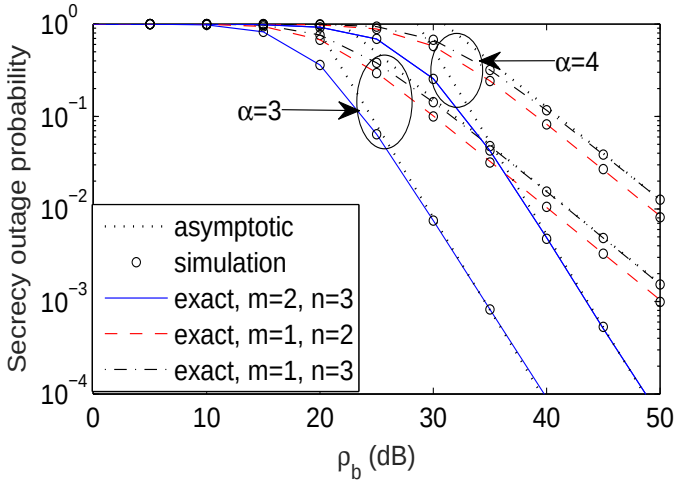

Figure 6.4: The SOP of user pair versus the transmit SNR ρ_b, with $\rho_e = 10$ dB, $\lambda_e = 10^{-3}$, $R_D = 10$ m, $M = 3$, and $r_p = 10$ m. The exact analytical results are calculated from (6.19). The asymptotic analytical results are calculated from (6.28).

used for verifying the derivations. Fig. 6.3 confirms the close agreement between the simulation and analytical results. A specific observation is that the reduced SOP can be achieved by reducing the radius of the user zone, since a smaller user zone leads to a lower path-loss. Another observation is that the n-th user has a more steep slope than the m-th user. This is due to the fact that $m < n$ and the m-th user as well as n-th user achieve a secrecy diversity order of m and n respectively, as inferred from (6.27) and (6.26).

Fig. 6.4 plots the SOP of the selected user pair versus the transmit SNR ρ_b for different path-loss factors. The number of NOMA users is set to $M = 3$. The exact analytical SOP curves are plotted from (6.19). The asymptotic analytical SOP curves are plotted from (6.28). It can be observed that the two kinds of dashed curves have the same slopes. By contrast, the solid curves indicate a higher secrecy outage slope, which is due to the fact that the secrecy diversity order of the user pair is determined by that of the poor one. This phenomenon is also confirmed by the insights in **Remark 1**.

Fig. 6.5 plots the SOP of the selected user pair versus r_p for different densities of the Es. One can observe that as expected, the SOP decreases, as the radius of the E-

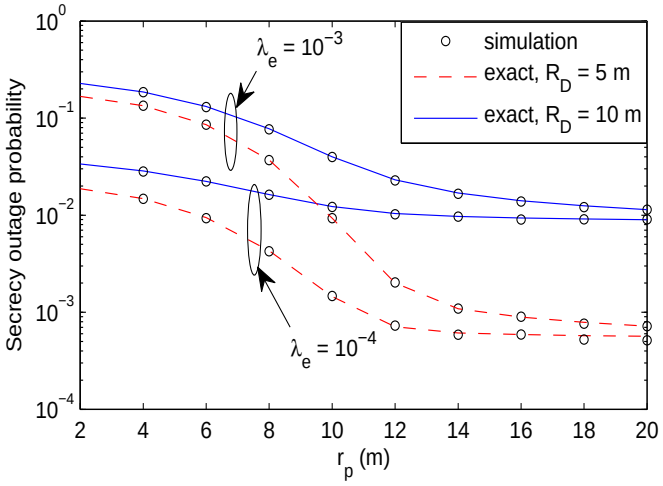

Figure 6.5: The SOP of user pair versus r_p, with $\rho_b = 50$ dB, $\rho_e = 40$ dB, $M = 2$, $m = 1$, $n = 2$, and $\alpha = 4$. The exact analytical results are calculated from (6.19).

exclusion zone increases. Another option for enhancing the PLS is to reduce the radius of the user zone, since it reduces the total path loss. It is also worth noting that having a lower E density λ_e results in an improved PLS, i.e. reduced SOP. This behavior is due to the plausible fact that a lower λ_e results in having less Es, which degrades the multiuser diversity gain, when the most detrimental E is selected. As a result, the destructive capability of the most detrimental E is reduced and hence the SOP is improved.

6.4.2 Secrecy outage probability with artificial noise

In Fig. 6.6 to Fig. 6.10, the secrecy performance in the presence of AN is investigated, which corresponds to the scenario considered in Section III.

Fig. 6.6 plots the SOP of user m and user n versus θ for different E-exclusion zones. The dashed and solid curves represent the analytical performance of user m and user n, corresponding to the results derived in (6.40) and (6.41). Monte Carlo simulations are used for verifying the derivations. Fig. 6.6 confirms a close agreement between the simulation and analytical results. Again, a reduced SOP can be achieved by increasing the E-exclusion zone, which degrades the channel conditions of the Es. Another obser-

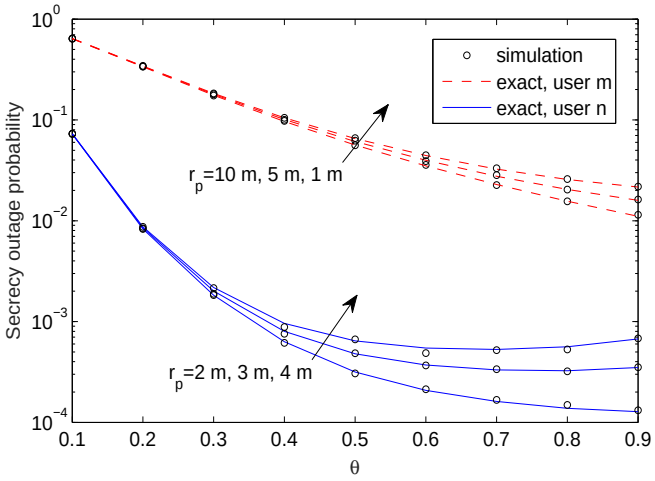

Figure 6.6: The SOP versus θ, with $\alpha = 4$, $R_{D_1} = 5$ m, $R_{D_2} = 10$ m, $\lambda_e = 10^{-4}$, $N_A = 4$, $\rho_t = 30$ dB. The exact analytical results are calculated from (6.40) and (6.41).

vation is that user n achieves a lower SOP than user m, which is explained as follows: 1) user n has better channel conditions than user m, owing to its lower path loss; and 2) user n is capable of cancelling the interference imposed by user m using SIC techniques, while user m suffers from the interference inflicted by user n. It is also worth noting that the SOP is not a monotonic function of θ. This phenomenon indicates that there exists an optimal value for power allocation, which depends on the system parameters. Actually, the optimal power sharing value θ^* can be analytically calculated by setting the first-order derivative of the SOP expressions with respect to θ to zero [130], which is however beyond the scope of this work.

Fig. 6.7 plots the SOP of user m and user n versus λ_e for different number of antennas. One can observe that the SOP decreases, as the E density is reduced. This behavior is caused by the fact that a lower λ_e leads to having less Es, which reduces the multiuser diversity gain, when the most detrimental E is considered. As a result, the distinctive capability of the most detrimental E is reduced and hence the secrecy performance is improved. It is also worth noting that increasing the number of antennas is capable of increasing the secrecy performance. This is due to the fact that $\|\mathbf{h}_m\|^2$ in (6.32) and $\|\mathbf{h}_n\|^2$ in (6.34) both follow $Gamma\,(N_A, 1)$ distributions, which is the benefit of the

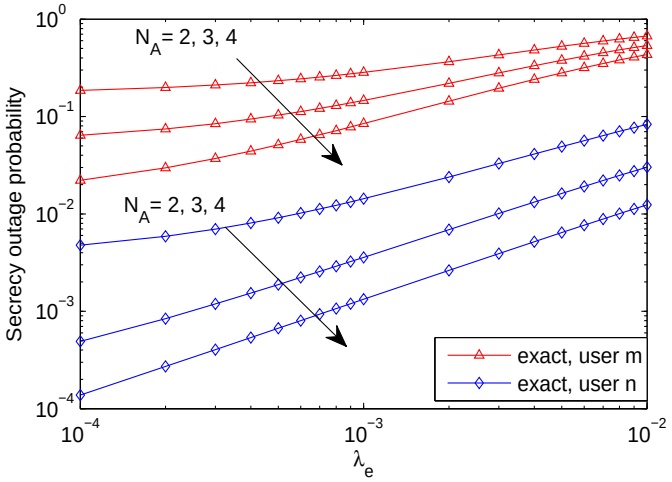

Figure 6.7: The SOP versus λ_e, with $\theta = 0.8$, $\alpha = 4$, $R_{D_1} = 5$ m, $R_{D_2} = 10$ m, $\rho_t = 30$ dB, $r_p = 4$ m. The exact analytical results are calculated from (6.40) and (6.41).

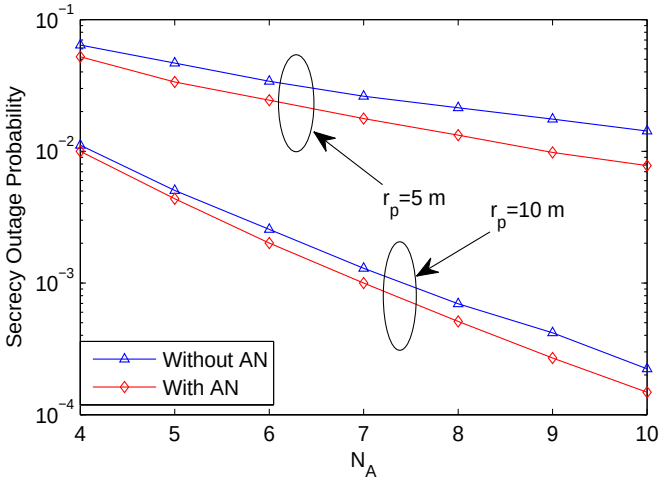

Figure 6.8: The SOP of the user pair versus N_A, with $R_{D_1} = 5$ m, $R_{D_2} = 10$ m, $\alpha = 3$, $\lambda_e = 10^{-3}$, $\rho_t = 30$ dB.

improved multi-antenna diversity gain.

Fig. 6.8 plots the SOP of the selected user pair versus N_A for different number of antennas. In this figure, the curves representing the case without AN are generated by setting $\theta = 1$, which means that all the power is allocated to the desired signal. In this case, the BS only uses beamforming for transmitting the desired signals and no AN is generated. The curves in the presence of AN are generated by setting $\theta = 0.9$. It is

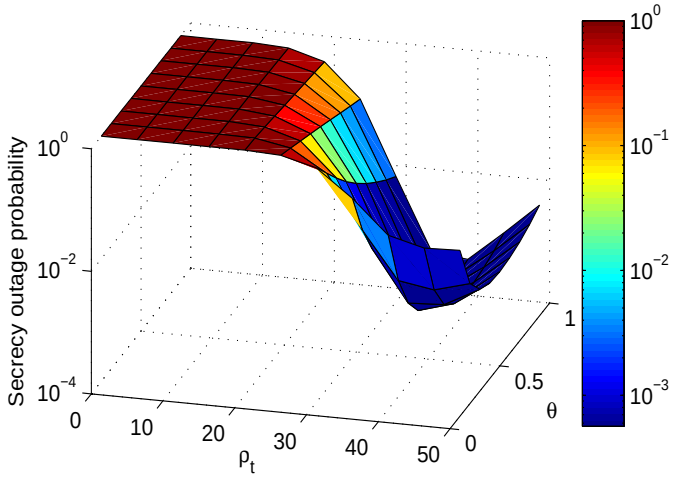

Figure 6.9: SOP of the user pair versus ρ_t and θ, with $N_A = 4$, $\alpha = 4$, $R_{D_1} = 5$ m, $R_{D_2} = 10$ m, $\lambda_e = 10^{-4}$, $r_p = 10$ m. The exact analytical results are calculated from (6.42).

shown that the PLS can be enhanced by using AN. This behavior is caused by the fact that at the receiver side, user m and user n are only affected by the AN generated by each other; By contrast, the Es are affected by the AN of both user m and user n. One can observe that the SOP of the selected user pair decreases, as the E-exclusion radius increases.

Fig. 6.9 plots the SOP of the selected user pair versus ρ_t and θ. It is observed that the SOP first decreases then increases as ρ_t increases, which is in contrast to the traditional trend, where the SOP always decreases as the transmit SNR increases. This behavior can be explained as follows. The SOP of the selected user pair is determined by user m. As ρ_t increases, on the one hand, the signal power of user m is increased, which improves the secrecy performance; On the other hand, user m also suffers from the interference imposed by user n (including both the signal and AN), because when ρ_t increases, the signal power of user n is also increased, which in turn degrades the secrecy performance. As a consequence, there is a tradeoff between ρ_t and the SOP. It is also noted that the power sharing factor θ also affect the optimal SOP associated with different values of ρ_t. This phenomenon indicates that it is of salient significance to select beneficial system parameters. Furthermore, optimizing the parameters ρ_t and

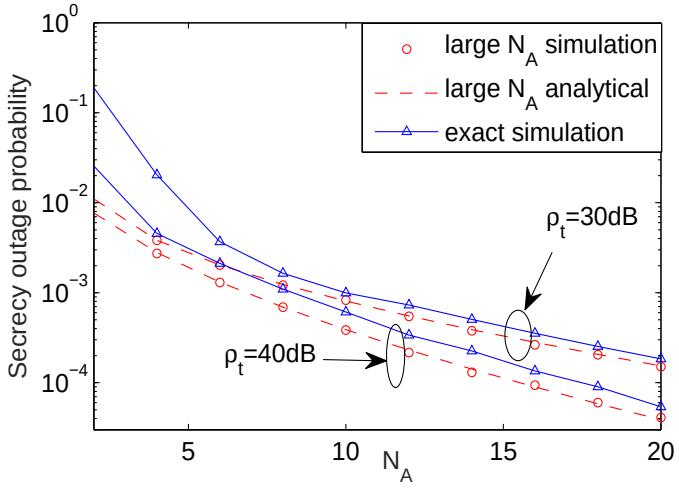

Figure 6.10: Large analysis for the SOP of user pair versus N_A, with $\theta = 0.8$, $R_{D_1} = 5$ m, $R_{D_2} = 10$ m, $\lambda_e = 10^{-4}$, $r_p = 5$ m. The asymptotic analytical results are calculated from (6.52).

θ is capable of further improving the SOP.

Fig. 6.10 plots the SOP of large antenna arrays of the selected user pair versus N_A parameterized by different transmit SNRs. The dashed curves represent the analytical SOP of the selected user pair, corresponding to the results derived in (6.52). It is observed that a close agreement between the theoretical analysis and the Monte Carlo simulations, which verifies the accuracy of the derivations. It is observed that as N_A increases, the approximation used in the analysis approaches the exact SOP. This phenomenon indicates that the asymptotic SOP derived converges to the exact values, when N_A is a sufficiently large number.

6.5 Summary

In this chapter, the secrecy performance of applying the NOMA protocol in large-scale networks was examined. Specifically, stochastic geometry based techniques were used for modeling both the locations of NOMA users and of the Es in the networks considered. Additionally, new analytical SOP expressions were derived for characterizing the system's

secrecy performance in both single-antenna and multiple-antenna scenarios. For the single-antenna scenario, the secrecy diversity order of the user pair was also characterized. It was analytically demonstrated that the secrecy diversity order was determined by that one of the user pair who had a poorer channel. For the multiple-antenna scenario, it was shown that the Es' channel quality is independent of the number of antennas at the BS for large antenna array scenarios. Numerical results were also presented for validating the analysis. It was concluded that the secrecy performance can be improved both by extending the E-exclusion zone and by generating AN at the BS. Optimizing the power sharing between the information-bearing signal and AN in the multiple-antenna aided scenario is capable of further improving the secrecy performance of the networks considered, which is a promising future research direction.

Chapter 7

Fairness of User Clustering in MIMO Non-orthogonal Multiple Access Systems

This chapter is organized as follows. The main contributions of this work is first introduced in 7.1. In Section 7.2, a cluster based MIMO-NOMA scenario is considered with applying a low complexity precoding design. In Section 7.3, a dynamic user allocation and power allocation problem is formulated. A two stage optimization approach is proposed to solve the formulated problem. The numerical results are presented in Section 7.4, which is followed by the conclusions in Section 7.5.

7.1 Introduction

A key feature of NOMA is the balanced tradeoff between throughput and user fairness. Different from [15] which considered the fairness issue in single-antenna scenarios, a dynamic user allocation and power optimization problem is investigated in this chapter, by considering the fairness issue in cluster-based MIMO-NOMA systems. Allocating

users into different clusters is a non-deterministic polynomial-time (NP)-hard problem, where exhaustive search yields optimal performance but with prohibitive complexity. The main contributions of this chapter are summarized in the following. From the standpoint of fairness, a two-step sub-optimal method is proposed for solving the dynamic user allocation problem. In the first step, the power allocation coefficients are optimized by invoking a bisection search based algorithm in order to maximize the SINR of the worst user in each cluster. In the second step, three efficient user allocation algorithms are proposed to seek a tradeoff between computational complexity and throughput of the worst user. The results of this chapter demonstrate that: 1) The proposed bisection search based power allocation algorithm is capable of efficiently enhancing the performance compared to the random power allocation scheme. 2) The three proposed user allocation algorithms can achieve a good throughput/complexity tradeoff in the considered cluster based MIMO-NOMA design.

7.2 System Model

A downlink MIMO NOMA scenario is considered, where a BS is equipped with M antennas, while K users are equipped with N antennas each. In order to implement NOMA in the considered MIMO scenario, the K users are further grouped into M clusters, where each cluster includes at least two users. It is assumed that the number of users and clusters are fixed. This assumption is motivated by the fact that these number are predetermined by the load of the networks. The number of users in each cluster is denoted as $\mathbf{L} = \{L_m\}, m = 1, \ldots, M$ with $L_m \geq 2$, and $K = \sum_{m=1}^{M} L_m$. The signals transmitted by the BS are given by

$$\mathbf{x} = \mathbf{P}\tilde{\mathbf{s}}, \tag{7.1}$$

where $\mathbf{P}$ is a $M \times M$ identity precoding matrix. This kind of precoding approach means that the BS can broadcasts the information of users' without any manipulation. By

doing so, the significant system overhead can be avoided. The $M \times 1$ vector $\tilde{\mathbf{s}}$ is given by

$$\tilde{\mathbf{s}} = \begin{bmatrix} \sqrt{\alpha_{1,1}} s_{1,1} + \cdots + \sqrt{\alpha_{1,L_1}} s_{1,L_1} \\ \vdots \\ \sqrt{\alpha_{M,1}} s_{M,1} + \cdots + \sqrt{\alpha_{M,L_M}} s_{M,L_M} \end{bmatrix} \triangleq \begin{bmatrix} \tilde{s}_1 \\ \vdots \\ \tilde{s}_M \end{bmatrix}, \tag{7.2}$$

where $s_{m,k}$ and $\alpha_{m,k}$ are defined as the transmitted information and the power allocation coefficient of the k-th user ($\{k = 1, \ldots, L_m\}$) in the m-th cluster, respectively.

The received signal at the k-th user in the m-th cluster is given by

$$\mathbf{y}_{m,k} = \mathbf{H}_{m,k}\mathbf{P}\tilde{\mathbf{s}} + \mathbf{n}_{m,k}, \tag{7.3}$$

where $\mathbf{H}_{m,k}$ is the $N \times M$ channel gain matrix from the BS to the k-th user in the m-th cluster, and $\mathbf{n}_{m,k}$ is an AWGN vector.

If denote $\mathbf{w}_{m,k}$ as the detection vector at the receiver, then the signal model can be expressed as

$$\mathbf{w}_{m,k}^H \mathbf{y}_{m,k} = \mathbf{w}_{m,k}^H \mathbf{H}_{m,k}\mathbf{P}\tilde{\mathbf{s}} + \mathbf{w}_{m,k}^H \mathbf{n}_{m,k}. \tag{7.4}$$

Denote the i-th column of $\mathbf{P}$ by $\mathbf{p}_i$. The signal model in (7.4) can be written as

$$\begin{aligned} \mathbf{w}_{m,k}^H \mathbf{y}_{m,k} = & \sum_{i=1, i\neq m}^{M} \mathbf{w}_{m,k}^H \mathbf{H}_{m,k} \mathbf{p}_i \tilde{s}_i + \mathbf{w}_{m,k}^H \mathbf{n}_{m,k} \\ & + \mathbf{w}_{m,k}^H \mathbf{H}_{m,k} \mathbf{p}_m \left(\sqrt{\alpha_{m,1}} s_{m,1} + \cdots + \sqrt{\alpha_{m,L_m}} s_{m,L_m} \right). \end{aligned} \tag{7.5}$$

In NOMA systems, the ordering of channel conditions is important for canceling interference between users in the same cluster using SIC. Without loss of generality, when implementing NOMA, channel gains and power allocation coefficients for the m-th

cluster are assumed to be ordered as

$$\left|\mathbf{w}_{m,1}^H \mathbf{H}_{m,1} \mathbf{p}_m\right|^2 \geq \cdots \geq \left|\mathbf{w}_{m,L_m}^H \mathbf{H}_{m,L_m} \mathbf{p}_m\right|^2. \tag{7.6}$$

To completely remove the inter-cluster interference, the detection matrices need to satisfy

$$\mathbf{w}_{i,k}^H \mathbf{H}_{i,k} \mathbf{p}_m = 0, \tag{7.7}$$

where $i \in \{1, \ldots, M, i \neq m\}$, as described in [14]. As such, for the k-th user in the i-th cluster, the constraints are rewritten as follows:

$$\mathbf{w}_{\mathrm{i},k}^H \underbrace{\left[\begin{array}{ccccccc} \mathbf{h}_{1,ik} & \cdots & \mathbf{h}_{i-1,ik} & \mathbf{h}_{i+1,ik} & \cdots & \mathbf{h}_{M,ik} \end{array} \right]}_{\widetilde{\mathbf{H}}_{i,k}} = \mathbf{0}, \tag{7.8}$$

where $\mathbf{h}_{i,ik}$ is the m-th column of $\mathbf{H}_{i,k}$, which has been removed. It is noted that $\tilde{\mathbf{H}}_{i,k}$ is a submatrix of $\mathbf{H}_{i,k}$ by removing column $\mathbf{h}_{i,ik}$. As such, the problem of finding the detection matrix is essentially to obtain the null space of $\tilde{\mathbf{H}}_{i,k}$. One possible approach is to adopt singular value decomposition (SVD) approach [131] as follows:

$$\mathbf{w}_{i,k} = \mathbf{U}_{i,k} \mathbf{z}_{i,k}, \tag{7.9}$$

where $\mathbf{U}_{i,k}$ contains all the left singular vectors of $\tilde{\mathbf{H}}_{i,k}$ corresponding to zero singular values, and $\mathbf{z}_{i,k}$ is a $(N - M + 1) \times 1$ normalized vector[1]. Normally there are many possible choices of $\mathbf{z}_{i,k}$ as the dimension of the null space is large. As a consequence, it is important to choose a good one. The choice of $\mathbf{z}_{i,k}$ in this work is to use the maximal radio combining (MRC)[2]. Adopting the similar approach as [14], a choice of $\mathbf{z}_{i,k}$ is given

[1]It is assumed that $N \geq M$ to ensure the existence of $\mathbf{w}_{i,k}$.

[2]Note that the choice of $\mathbf{z}_{i,k}$ can be further optimized with using the similar method in [25], which is out of the scope of this work.

by

$$\mathbf{z}_{i,k} = \frac{\mathbf{U}_{i,k}^H \mathbf{h}_{i,ik}}{\left|\mathbf{U}_{i,k}^H \mathbf{h}_{i,ik}\right|}. \tag{7.10}$$

By adopting the detection vector $\mathbf{w}_{m,k}$ at the receiver, the inter-cluster interference can be removed. Note that the identity precoding scheme in this work does not require the users to feedback their channel matrices to the base station. Instead, each user only needs to feedback one effective channel gain which is a scalar value, and therefore the amount of the required CSI feedback can be significantly reduced. As such, in the m-th cluster, the SINR for the k-th user ($1 \leq k \leq L_m$) to detect the j-th user ($k \leq j \leq L_m$) is given by

$$SINR_{m,k}^{j} = \frac{\left|\mathbf{w}_{m,k}^H \mathbf{h}_{m,mk}\right|^2 \alpha_{m,j}}{\sum_{l=1}^{j-1} \left|\mathbf{w}_{m,k}^H \mathbf{h}_{m,mk}\right|^2 \alpha_{m,l} + \left|\mathbf{w}_{m,k}\right|^2 \frac{1}{\rho}}, \tag{7.11}$$

where ρ denotes the transmit SNR. For the special case $k = j = 1$, the SINR can be simplified as

$$SINR_{m,1}^{1} = \rho \frac{\left|\mathbf{w}_{m,1}^H \mathbf{h}_{m,m1}\right|^2 \alpha_{m,1}}{\left|\mathbf{w}_{m,1}\right|^2}. \tag{7.12}$$

7.3 Problem Formulation and Proposed Optimization Methods

7.3.1 Problem Formulation

The objective of this work is to maximize the throughput of the worst user among all K users, by dynamically allocating users into different clusters. For each given combination of user allocation, in order to further improve the performance of MIMO-NOMA within each cluster, the power allocation coefficients are optimized according to instantaneous

channel conditions in each cluster. In addition, as aforementioned in Section II, each cluster accommodates at least two users. Taking into account above, the throughput of the system can be optimized by solving the following problem:

$$\max_{\Omega} \min_{\forall m} \left(\log_2 \left(1 + \max_{\boldsymbol{\alpha_m}} \min_{\forall k, \forall j} \left(SINR_{m,k}^{j} \right) \right) \right), \tag{7.13a}$$

$$\begin{aligned} s.t. \quad & \sum_{j=1}^{L_m} \alpha_{m,j} \leq \tfrac{L_m}{K}, \\ & \alpha_{m,j} \geq 0, j \in L_m. \end{aligned} \tag{7.13b}$$

where Ω is defined as the set of all user allocation combinations, $\boldsymbol{\alpha_m} = \{\alpha_{m,1}, \cdots, \alpha_{m,L_m}\}$, is the power allocation coefficient vector.

7.3.2 Proposed Optimization Methods

In order to solve the above non-convex optimization problem, the alternating optimization strategy is used in this work, which splits the throughput over j, k, $\boldsymbol{\alpha_m}$, m, and Ω into two steps:

7.3.2.1 Step 1

Fixing one combination of user allocation in Ω, and updating j, k, and $\boldsymbol{\alpha_m}$, the following sub-optimal problem can be solved:

$$\max_{\boldsymbol{\alpha_m}} \min_{\forall k, \forall j} \left(\mathbf{SINR_m} \left(\boldsymbol{\alpha_m} \right) \right) \quad s.t. \ (7.13b), \tag{7.14}$$

where $\mathbf{SINR_m}$ denotes all possible values of $SINR_{m,k}^{j}$, $\forall k, \forall j$ in the m-th cluster. Note that the max-min problem in (7.14) is not convex, which motives us to seek good equivalent transformations to make it tractable. Define the set $\mathbb{Q}_\Delta = \{\mathbf{SINR_m} \left(\alpha_\mathbf{m} \right) \geq \Delta, \Delta \in \mathbb{R}\}$ as the set of $\alpha_\mathbf{m}$ when the objective function is not smaller than Δ. Using the similar approach in [15], problem (7.14) can be prove to be quasi-concave. As such, (7.14) can

Algorithm 1 Optimization Algorithm for Solving (7.15)

Require:
Δ_{LB}, Δ_{UB}, ε.

while $\Delta_{UB} - \Delta_{LB} \geq \varepsilon$ **do**
  Update $\Delta = (\Delta_{UB} + \Delta_{LB})/2$;
  Calculate $\boldsymbol{\alpha_m}$ with the constraints in (7.15), by solving the convex problem;
  if feasible **then**
    $\boldsymbol{\alpha}^*_{\boldsymbol{m}} = \boldsymbol{\alpha_m}$; $SINR_{\min} = \Delta$;
    Update $\Delta_{LB} = \Delta$;
  else
    Update $\Delta_{UB} = \Delta$;
  end if
end while

Ensure: Output $SINR_{\min}$ and $\boldsymbol{\alpha}^*_{\boldsymbol{m}}$.

be equivalently transformed as

$$\begin{aligned} &\text{Find} && \boldsymbol{\alpha_m} \\ &s.t.\ (7.13b) && \text{and} \quad \left|\mathbf{w}_{m,k}^H \mathbf{h}_{m,mk}\right|^2 \alpha_{m,j} \geq \Delta J, \end{aligned} \tag{7.15}$$

where $J = \sum_{l=1}^{j-1} \left|\mathbf{w}_{m,k}^H \mathbf{h}_{m,mk}\right|^2 \alpha_{m,l} + |\mathbf{w}_{m,k}|^2 \frac{1}{\rho}$. It is implied that with the aid of appropriately bounding Δ, a bisection search based method can be effectively used to reduce the searching scope of possible SINRs for obtaining $\boldsymbol{\alpha_m}$. Note that (7.15) is linear programs can be solved with standard optimization solvers. In this work, the *cvx* tool is invoked to find the optimal $\boldsymbol{\alpha_m}$ by utilizing the *Mosek* solver. The details of solving (7.15) are illustrated in **Algorithm 1**. Here $SINR_{\min}$ is the minimum of $\mathbf{SINR_m}$, Δ_{UB} and Δ_{LB} are initialized as the upper bound and lower bound for $\mathbf{SINR_m}$, respectively, and ε is the tolerance. After obtaining the minimum value of $\mathbf{SINR_m}$ for the m-th cluster, the throughput of the worst user $\forall m$ can be calculated using (7.13a).

7.3.2.2 Step 2

The second step is to traverse all the combinations, which is a NP-hard problem. In order to lower the computational complexity, three efficient algorithms, named **Top-**

Algorithm 2 Top-down A Algorithm

Require:
K, $\mathbf{L}$, $\bar{\boldsymbol{L}} = sort\,(\mathbf{L}, descend)$, C_{th}, C_0, $m = 1$.

1: **while** $C_{m-1} > C_{th}$ **do**
2: Allocate $\bar{L}_m$ users randomly from $K - \sum_{p=1}^{m-1} L_p$ users to the cluster with m-th maximal number of users;
3: Update $m = m + 1$;
4: **if** $C_m < C_{th}$ **then**
5: Exhaustive search among the rest clusters;
6: Record the user allocation scheme, break;
7: **end if**
8: **end while**

Ensure: The corresponding user allocation scheme.

down A, **Top-down B**, and **Bottom-up** are proposed. The details of these algorithms are included in **Algorithm 2, 3, and 4**. In these algorithms, C_0 denotes the number of combinations for exhaustive search among all the users, while C_{th} denotes the threshold.

Top-down A: As shown in **Algorithm 2**, this algorithm begins from the cluster with largest number (denoted by $\bar{L}_1$) of users, where $\bar{L}_1$ users are randomly allocated to this cluster. Lately, the number of combinations C_1 is calculated and then C_1 is compared with the threshold, C_{th}. If $C_1 < C_{th}$, then exhaustive search is performed for the rest of the clusters, and return the obtained maximal throughput as the output. Otherwise, random user allocation for the cluster with the second maximal user number is continued, until the calculated combinations is less than C_{th}. The advantage of this algorithm is that it can reduce the complexity with the least decision times. This algorithm is suitable for the case when all the clusters have similar number of users.

Top-down B: As shown in **Algorithm 3**, initially, n users are randomly allocated to the cluster with the maximum number of users. Consequently, the number of combinations, C_1, is calculated, and compared with C_{th}. If $C_1 < C_{th}$, exhaustive search is performed among the rest of the clusters and the maximal throughput is obtained as the return value. Otherwise, n random users are allocated to the second sorted cluster. If $C_2 < C_{th}$, the obtained maximal throughput is returned. Otherwise, $n = n + 1$ is updated and the above user allocation scheme is performed until the calculated com-

Algorithm 3 Top-down B Algorithm

Require:
K, $\mathbf{L}$, $\bar{\boldsymbol{L}} = sort\,(\mathbf{L}, descend)$, C_{th}, C_0, $m = 1$, $0 < n < min\,(\mathbf{L})$.

```
while C_{m-1} > C_th do
  for m = 1 to M do
    Allocate n users randomly to the cluster with m-th maximal users number from K − (m − 1) × n users;
    Update m = m + 1;
    if C_m < C_th then
      Exhaustive search among the rest clusters;
      Record the user allocation scheme, break;
    end if
  end for
  Update n = n + 1;
end while
```

Ensure: The corresponding user allocation scheme.

binations is less than C_{th}. Finally, the corresponding throughput and the related user allocation scheme are output as return values. The advantage of this algorithm is that its complexity is the most controllable among the three.

Bottom-up: As shown in **Algorithm 4**, each cluster is randomly allocated with two users, as the starting point. Then, the cluster with the minimum user number is filled up randomly. After that the possible combination C_1 is calculated and it is compared with C_{th}. If $C_1 < C_{th}$, exhaustive search is used to allocate the remaining users to the remaining clusters in order to achieve maximal throughput for the worst users. Otherwise, the random user allocation is continued for the following clusters until the calculated combinations is less than C_{th}. The advantage of this algorithm is to guarantee that all clusters have some random search, and this is suitable for the case where the size of each cluster is significantly different.

7.3.3 Complexity of the proposed algorithms

Note that the complexity of this formulated problem contains two parts: 1) It can be easily observed that the complexity of solving (7.15) in *step 1* is linear to the number of users [15]. As a consequence, the computational complexity is $O\,(L_m)$. 2) The complexity

Algorithm 4 Bottom-up Algorithm

Require:

K, $\mathbf{L}$, $\tilde{\boldsymbol{L}} = sort\,(\mathbf{L}, ascend)$, C_{th}, C_0, $m = 1$.

1: **while** $C_{m-1} > C_{th}$ **do**
2: Allocate every two users into each cluster randomly.
3: Allocate $\tilde{L}_m - 2$ users randomly from $K - \sum_{p=1}^{m-1} L_p$ users to the cluster with m-th minimal number of users;
4: Update $m = m + 1$;
5: **if** $C_m < C_{th}$ **then**
6: Exhaustive search among the rest clusters;
7: Record the user allocation scheme, break;
8: **end if**
9: **end while**

Ensure: The corresponding user allocation scheme.

of solving (7.13a) in *step 2* is given by Table 7-A at the top of the next page, where r is the number of cluster which includes random search.

Table 7-A: Complexity of the proposed algorithms

Algorithm	Complexity
Exhaustive Search	$O\left(\frac{K!}{\prod_{m=1}^{M} L_m!}\right)$
Top-down A	$O\left(\frac{\left(K-\sum_{m=1}^{r}\bar{L}_m\right)!}{\prod_{m=r+1}^{M}\bar{L}_m!}\right)$
Top-down B	$O\left(\frac{(K-r\times n)!}{\prod_{m=1}^{r}\left(\bar{L}_m-n\right)!\prod_{m=r+1}^{M}\bar{L}_m!}\right)$
Bottom-up	$O\left(\frac{\left(K-\sum_{m=1}^{r}\tilde{L}_m-2(M-r)\right)!}{\prod_{m=r+1}^{M}\tilde{L}_m!}\right)$

7.4 Numerical Results

In this section, simulation results are presented to demonstrate the performance of the user allocation schemes, as described in Section III. In the simulations, it is assumed that the total number of users is $K = 9$, the number of clusters is $M = 3$, the number

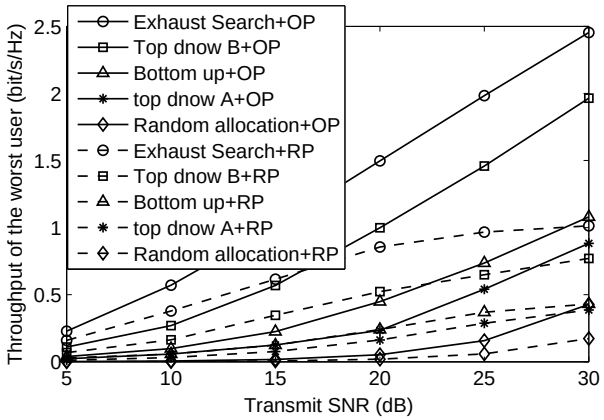

Figure 7.1: Optimized throughput of the worst user with different algorithms for user allocations under different transmit SNR.

of antennas at the BS and the receiver are assumed to be the same as $M = N = 3$, and each cluster contains $\mathbf{L} = \{4, 3, 2\}$ users. For simplicity, large scale path loss is not considered in this work and all the channel gains between the BS and users are assumed to be independent and identically complex Gaussian distributed, which is valid for many indoor scenarios. The initial values in Algorithm 1 are, $\Delta_{LB} = 0$, $\Delta_{UB} = 1000$, $\varepsilon = 10^{-4}$, and C_{th}= 200. The initial values of m are set as $m = 1$, in Algorithm 2, 3, and 4. The initial value of n is set as, $n = 1$, in Algorithm 3.

Fig. 7.1 shows the comparison of throughput for the worst case user among the three proposed algorithms and the exhaustive search with different transmit SNR. The solid curves represent the case with the optimal power allocation for each user within the cluster, while the dashed curves represent random power allocation which follows increasing order ($\alpha_{m,1} \leq \cdots \leq \alpha_{m,L_m}$) for each user. One can observe that the optimal power allocation achieves much better performance than random power allocation, which demonstrates the effectiveness of the proposed **Algorithm 1**. It is observed that the three proposed algorithms can achieve better performance than the random allocation scheme, and the performance of them follows the order of top-down B, bottom up, and top-down A.

Fig. 7.2 shows the fairness comparison between NOMA and OMA for the exhaustive

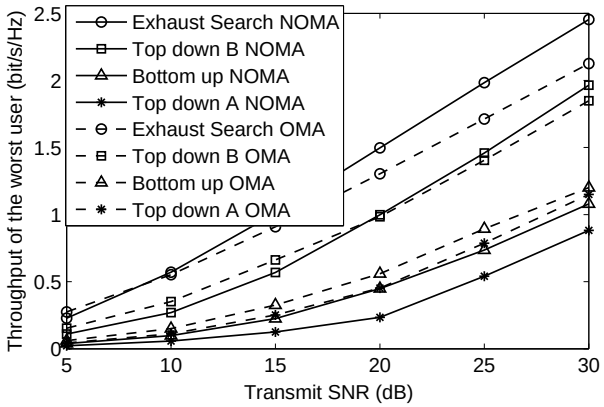

Figure 7.2: Comparison between NOMA and OMA of the proposed algorithms.

search and the three proposed algorithms. The solid curves represent NOMA, while the dashed curves represent OMA. It is observed that the exhaustive search and Top down B algorithms with NOMA outperform the corresponding ones with OMA, while the Bottom up and Top down B algorithms with OMA outperforms the corresponding ones with NOMA. This behavior can be explained as follows: the fairness in NOMA is more sensitive to the times of searching and system parameters. However, for the OMA scheme, since all the users are with the same power, reducing the time of searching will not affect much of the fairness performance. Therefore, it is concluded that by carefully designing the system parameters and choosing appropriate algorithm, NOMA can outperform OMA in term of fairness. Note that carefully selecting C_{th} and dynamically varying the number of clusters/users will further improve the performance of the considered MIMO-NOMA systems, which is out of the scope of this work. Fig. 7.3 shows the complexity comparison, measured by the number of combinations, among the exhaustive search and the three proposed algorithms under different thresholds C_{th}. One can observe that the exhaustive search algorithm requires highest combinations for user allocation as expected. For the proposed top-down A algorithm, the number of combinations reduces to ten, when the first cluster is filled up with four random users. With the lowest combination number, top-down A algorithm achieves the lowest throughput of the three proposed algorithms as shown in Fig. 7.1. It is worth noting that the proposed

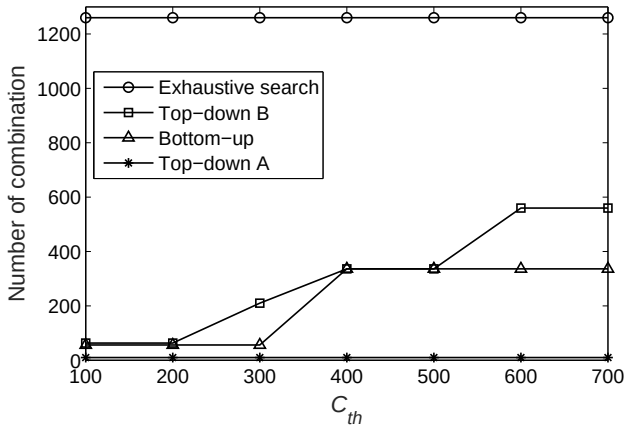

Figure 7.3: Number of combinations of different algorithms under different threshold C_{th}, SNR=30 dB.

top-down B and bottom-up algorithms require higher complexity for user allocation but their achieved throughput get more close to the exhaustive search algorithm. Combining the observations from Figs. 7.1 and 7.3, it is noted that there is a tradeoff between the achieved throughput of the worst user and the computational complexity. It is also worth noting that top-down B algorithm presents a good balance between achievable throughput of the worst user and the computational complexity.

7.5 Summary

In this chapter, a dynamic clustering optimization problem considering the fairness in MIMO-NOMA systems, was investigated. In order to solve this non-convex problem, a two-step optimization method was proposed. Three efficient suboptimal algorithms were proposed to reduce the computational complexity. To further improve the performance of the worst user in each cluster, power allocation coefficients were optimized by using bi-section search. Numerical results demonstrated that the proposed algorithms can achieve a good tradeoff between throughput and system complexity.

Chapter 8

Conclusions and Future Works

8.1 Contributions and Insights

This thesis concentrates on the NOMA in wireless networks, which is regarded as one promising technology in future 5G networks. The following three aspects are presented in this thesis: 1) The basic principles of NOMA is introduced, including the two key technologies—SC and SIC, information theoretic investigation of NOMA, mathematical demonstration of NOMA and the basic downlink/uplink NOMA transmission model; 2) The potential combination of NOMA with the emerging technologies such as SWIPT, cognitive radio and HetNets; and 3) The physical layer security enhancement and the fairness issue of NOMA have been utilized. The main contributions and insights are summarized as follows.

In Chapter 3, the application of SWIPT in NOMA networks was investigated. A new cooperative SWIPT NOMA protocol has been proposed, in which near NOMA users that are close to the source act as energy harvesting relays to help far NOMA users. Stochastic geometry is utilized to model the locations of NOMA users. Since the locations of users have a significant impact on the performance, three user selection schemes based on the user distances from the base station have been proposed. To

characterize the performance of the proposed selection schemes, closed-form expressions for the outage probability and system throughput were derived. These analytical results have demonstrated that the use of SWIPT will not jeopardize the diversity gain compared to the conventional NOMA. The proposed results confirmed that the opportunistic use of node locations for user selection can achieve low outage probability and deliver superior throughput in comparison to the random selection scheme. It was demonstrated that the performance of the proposed cooperative SWIPT NOMA protocol outperforms the non-cooperative NOMA scheme. It was also worth pointing that inappropriate choice of rate and power may lead the outage probability always be one.

In Chapter 4, fundamental questions were addressed when NOMA was applied to large-scale underlay CR networks with randomly deployed users. In order to characterize the performance of the considered network, new closed-form expressions of the outage probability have been derived using stochastic-geometry. More importantly, by carrying out the diversity analysis, new insights were obtained under the two scenarios with different power constraints: 1) fixed transmit power of the PTs, and 2) transmit power of the PTs being proportional to that of the secondary base station. It was analytically demonstrated that: 1) For the first scenario, a diversity order of m is experienced at the m-th ordered NOMA user; 2) For the second scenario, there is an asymptotic error floor for the outage probability. Simulation results have been provided to verify the accuracy of the derived results. A pivotal conclusion was reached that by carefully designing target data rates and power allocation coefficients of users, NOMA is capable of outperforming conventional orthogonal multiple access in underlay CR networks. The expressions reveal important design insights surrounding the impact of the primary network on the secondary network in cognitive radio NOMA networks.

In Chapter 5, the application of NOMA into K-tier HetNets has been investigated. A new promising transmission framework was proposed, in which massive MIMO is employed in macro cells and NOMA is adopted in small cells. For maximizing the biased average received power at mobile users, a massive MIMO and NOMA based user

association scheme was developed. In an effort to evaluate the performance of the proposed framework, analytical expressions for the spectrum efficiency of each tier have been derived using stochastic geometry. Simulation results were presented to verify the accuracy of the proposed analytical derivations and confirmed that NOMA is capable of enhancing the spectrum efficiency of the network compared to the OMA based HetNets. It is believed that the proposed framework will be a promising rewarding candidates in future 5G networks for its high spectrum efficiency, low complexity and better fairness/throughput tradeoff characteristics.

In Chapter 6, the physical layer security of NOMA was examined in large-scale networks with invoking stochastic geometry. Both single-antenna and multiple-antenna aided transmission scenarios were considered, where the BS communicates with randomly distributed NOMA users. In the single-antenna scenario, a protected zone around the BS is adopted to establish an eavesdropper-exclusion area with the aid of careful channel-ordering of the NOMA users. In the multiple-antenna scenario, artificial noise was generated at the BS for further improving the security of a beamforming-aided system. New exact expressions of the security outage probability have been derived for both single-antenna and multiple-antenna aided scenarios. It was demonstrated that 1) for the single antenna scenario, the analytical results derived demonstrated that the secrecy diversity order is determined by the specific user having the worse channel condition among the selected user pair; and 2) for the multiple-antenna scenario, the results derived indicated that the channels of the eavesdroppers are independent of the number of transmit antennas for sufficiently large antenna arrays. It was confirmed that the security performance of the NOMA networks can be improved by invoking the protected zone and by generating artificial noise at the BS.

In Chapter 7, a downlink MIMO NOMA communication scenario was considered. A dynamic user clustering problem was addressed from a fairness perspective. Three sub-optimal algorithms, namely top-down A, top-down B, and bottom up, have been proposed to realize different tradeoffs of complexity and throughput of the worst user.

Additionally, for each given user clustering case, the power allocation coefficients were further optimized for the users in each cluster by adopting a bisection search based algorithm. It is demonstrated that that the proposed algorithms can lower the complexity with an acceptable degradation on throughput compared with the exhaustive search method. One interesting conclusion is that top-down B algorithm can achieve the best tradeoff between complexity and throughput among the three proposed algorithms.

8.2 Future Works

8.2.1 Extensions of Current Works

In this subsection, the potential extensions of the current works in this thesis are described in the following.

8.2.1.1 Power Allocation in NOMA

Power controlling/allocation is an eternal research direction for each generation of networks, since the inappropriate allocating power among users will inevitably trigger energy consumption and also degrade the performance of the system throughput of the networks. Due to the fact that one of the key characteristics of downlink NOMA is to adopt SC at the transmitter, the power allocation issue is naturally existing in all NOMA scenarios. In Chapter 3—6, the power allocation coefficients at transmitters are fixed, and optimized power allocation is capable of further enhancing the performance of each considered NOMA scenario, which is worth researching in the future works.

8.2.1.2 Imperfect CSI

Current work in this thesis on NOMA mostly have relied on the perfect CSI assumption (e.g., in Chapter 3—6), which is difficult to realize, since sending more pilot signals to

improve the accuracy of channel estimation reduces the spectral efficiency. Therefore, it is important to study the impact of imperfect CSI on the reception reliability in NOMA systems. Another example of the strong CSI assumptions is that many NOMA protocols require the CSI at the transmitter, which can cause significant system overhead. However, the use of only a few bits of feedback is promising in NOMA systems, since obtaining the orders of users' channel conditions is sufficient for the implementation of NOMA in many applications. Therefore, investigating the existing considered NOMA systems with imperfect CSI would be more interesting on the standpoint of the implementation perspective.

8.2.2 Promising Future Directions on NOMA

In this subsection, some promising future directions in terms of NOMA are presented in the following.

8.2.2.1 Spectral-Energy Efficiency Tradeoff of NOMA

The recent research contributions of NOMA in terms of resource allocation mostly aims to maximize the system spectral efficiency (SE). However, the energy efficiency (EE) of NOMA systems—as one main concern in the state-of-the-art wireless communications—which is to the best of my knowledge, has not been investigated and still in its fancy. Thus, it is imperative to study the SE-EE tradeoff in NOMA systems. Besides, although the above literature addresses the issue of rate fairness, there is a lack of a general framework to model different types of rate fairness in resource allocation. As a consequence, investigating the spectral and energy efficiency tradeoff considering fairness issue is a promising future research direction and it is my undergoing topics.

8.2.2.2 D2D NOMA Communications towards 5G

Due to the recent rapid explosion in the demand of local area services in cellular networks, an emerging technology, namely D2D communication, was invoked to enable direct communications between devices without the assistance of cellular BSs [132]. The main advantages of integrating D2D communications into cellular networks are: i) It enables low-power transmission of proximity services to improve the energy efficiency; ii) It allows to reuse the frequency of the cellular networks in an effort to increase the spectral efficiency; and iii) It has penitential to facilitate new types of peer-to-peer (P2P) services [133]. Note that one of common features for both D2D and NOMA is to enhance the spectral efficiency by managing the interference among users in one resource block. Motivated by this, it is naturally to consider to investigate more intelligent joint interference management approaches, for fully exploiting the potential benefits of both D2D and NOMA, which is another my ongoing research work.

8.2.2.3 Novel Channel Estimation Design in Massive-MIMO-NOMA

In practical wireless communication system, obtaining the channel state information at the transmitter (CSIT) is not a trivial problem, which requires the pilot training process, especially in Massive-MIMO-NOMA systems. Massive-MIMO-NOMA enables large number of antennas be equipped at the BS, which provides large array gains or multiplexing gains for NOMA. However, large number arrays brings challenges for accurate channel estimation, the downlink pilot training overhead and the uplink CSI feedback overheard will become prohibitively large. Additionally, the channel coherence time and bandwidth limits the number of independent pilot available symbols [109]. Motivated by all the aforementioned reasons, a novel CSIT estimation design is more than necessary to support the Massive-MIMO-NOMA systems. By utilizing the joint sparsity of the user channel matrix, compressive sensing (CS) can be invoked as an effective approach to achieve low-cost channel estimation by reducing the training pilot symbols [134], as well

as to reduce the feedback overhead from receivers to the BS. In the CS based CSI estimation for Massive-MIMO-NOMA, a suitable measurement matrix is more than desired, by considering the universality, recovery complexity, speed minimal number of measurements required and implementation. More specifically, machine learning is supposed to be invoked for measurement matrix design and sparse domain selection in channel estimation for Massive-MIMO-NOMA, which is another valuable research topic.

8.2.2.4 Hybrid Multiple Access Design

It has been envisioned that future cellular networks will be designed by using more than one MA techniques, and this trend has also been evidenced by the recent application of NOMA to 3GPP-LTE. Particularly, MUST is a hybrid MA scheme between OFDMA and NOMA, where NOMA is to be used when users have very different CSI, e.g., one user close to the BS and the other at the cell edge. Therefore it is important to study how to combine NOMA with other types of MA schemes in future research works, including not only the conventional OMA schemes but also those newly developed 5G MA techniques.

8.2.2.5 Cross-layer Optimization of NOMA

Cross-Layer optimization is important to maximize the performance of NOMA in practice and meet the diversified demands of 5G, e.g, spectral efficiency, energy efficiency, massive connectivity, and low latency. For example, practical designs of coding and modulation are important to realize the performance gain of NOMA at the physical layer, and it is crucial to study how to feed these gains from the physical layer to the design of upper layer protocols. This cross-layer optimization is particularly important to NOMA which, unlike conventional MA schemes, takes the user fairness into consideration, which means that the issues related to user scheduling and pairing, power allocation, pilot and retransmission schemers design need to be jointly optimized. As such, the joint cross-layer optimization of NOMA can be an interesting research topic.

Appendix A

Proof in Chapter 3

A.1 Proof of Theorem 2

Substituting (3.4) and (3.12) into (3.22), the outage probability can be expressed as follows:

$$P_{\mathrm{A_i}} = \underbrace{\Pr\left(\gamma_{\mathrm{A_i,MRC}}^{x_{i1}} < \tau_1, \frac{\rho|h_{\mathrm{B_i}}|^2|p_{i1}|^2}{\rho|h_{\mathrm{B_i}}|^2|p_{i2}|^2 + 1 + d_{\mathrm{B_i}}^{\alpha}} > \tau_1\right)}_{\Theta_1} + \underbrace{\Pr\left(\gamma_{\mathrm{S,A_i}}^{x_{i1}} < \tau_1, \frac{\rho|h_{\mathrm{B_i}}|^2|p_{i1}|^2}{\rho|h_{\mathrm{B_i}}|^2|p_{i2}|^2 + 1 + d_{\mathrm{B_i}}^{\alpha}} < \tau_1\right)}_{\Theta_2}, \tag{A.1.1}$$

Θ_1 is expressed as

$$\Theta_1 = \Pr\left(Z_i < \frac{\tau_1 - \frac{\rho X_i |p_{i1}|^2}{\rho X_i |p_{i2}|^2 + 1}}{\eta\rho\left(Y_i - \varepsilon_{\mathrm{A}_i}\right)}, X_i < \varepsilon_{\mathrm{A}_i}, Y_i > \varepsilon_{\mathrm{A}_i}\right)$$

$$= \int_{D_\mathrm{B}}\int_{D_\mathrm{A}}\int_0^{\varepsilon_{\mathrm{A}_i}} \underbrace{\int_{\varepsilon_{\mathrm{A}_i}}^{\infty}\left(1 - e^{-\left(1+d_{\mathrm{C_i}}^{\alpha}\right)\frac{\tau_1 - \frac{\rho x|p_{i1}|^2}{\rho x|p_{i2}|^2+1}}{\eta\rho\left(y-\varepsilon_{\mathrm{A}_i}\right)}}\right) f_{Y_i}(y)\, dy}_{\Xi}$$

$$\times f_{X_i}(x)\, dx f_{W_{\mathrm{A_i}}}(\omega_{\mathrm{A_i}})\, d\omega_{\mathrm{A_i}} f_{W_{\mathrm{B_i}}}(\omega_{\mathrm{B_i}})\, d\omega_{\mathrm{B_i}}, \tag{A.1.2}$$

where $f_{X_i}(x) = \left(1 + d_{\mathrm{A_i}}^{\alpha}\right) e^{-\left(1+d_{\mathrm{A_i}}^{\alpha}\right)x}$, and $f_{Y_i}(y) = \left(1 + d_{\mathrm{B_i}}^{\alpha}\right) e^{-\left(1+d_{\mathrm{B_i}}^{\alpha}\right)y}$.

Based on (A.1.2), using $t = y - \varepsilon_{\mathrm{A}_i}$, Ξ is calculated as follows:

$$\Xi = \int_0^{\infty}\left(1 - e^{-\left(1+d_{\mathrm{C_i}}^{\alpha}\right)\frac{\tau - \frac{\rho x|p_{i1}|^2}{\rho x|p_{i2}|^2+1}}{\eta\rho t}}\right)\left(1 + d_{\mathrm{B_i}}^{\alpha}\right) e^{-\left(1+d_{\mathrm{B_i}}^{\alpha}\right)\left(t+\varepsilon_{\mathrm{A}_i}\right)} dt. \tag{A.1.3}$$

Applying [125, Eq. (3.324)], (A.1.3) is rewritten as follows:

$$\Xi = e^{-\left(1+d_{\mathrm{B_i}}^{\alpha}\right)\varepsilon_{\mathrm{A}_i}}\left(1 - 2\sqrt{\chi\Lambda}K_1\left(2\sqrt{\chi\Lambda}\right)\right), \tag{A.1.4}$$

where $\Lambda = \frac{\left(1+d_{\mathrm{B_i}}^{\alpha}\right)\left(1+d_{\mathrm{C_i}}^{\alpha}\right)}{\eta\rho}$ and $\chi = \tau_1 - \frac{\rho x|p_{i1}|^2}{\rho x|p_{i2}|^2+1}$.

The series representation of Bessel functions is used to obtain the high SNR approximation which is expressed as follows:

$$xK_1(x) \approx 1 + \frac{x^2}{2}\left(\ln\frac{x}{2} + c_0\right), \tag{A.1.5}$$

where $K_1(\cdot)$ is the modified Bessel function for the seconde kind, $c_0 = -\frac{\varphi(1)}{2} - \frac{\varphi(2)}{2}$, and $\varphi(\cdot)$ denotes the psi function [125].

To obtain the high SNR approximation of (A.1.4) and using (A.1.5), the following

express is obtained as

$$\Xi \approx -\chi\Lambda \left(\ln \chi\Lambda + 2c_0\right). \tag{A.1.6}$$

Substituting (A.1.6) into (A.1.2), (A.1.2) is rewritten as follows:

$$\Theta_1 = -\int_0^{\varepsilon_{\mathrm{A}_i}} \chi \int_{D_{\mathrm{A_i}}} \Lambda e^{-\left(1+d_{\mathrm{A_i}}^{\alpha}\right)x} \underbrace{\int_{D_{\mathrm{B_i}}} \left(1+d_{\mathrm{B_i}}^{\alpha}\right)\left(\ln \chi\Lambda + 2c_0\right) f_{W_{\mathrm{B_i}}}\left(\omega_{\mathrm{B_i}}\right) d\omega_{\mathrm{B_i}}}_{\Phi} f_{W_{\mathrm{A_i}}}\left(\omega_{\mathrm{A_i}}\right) d\omega_{\mathrm{A_i}} dx. \tag{A.1.7}$$

Since $d_{\mathrm{C_i}} = \sqrt{d_{\mathrm{A_i}}^2 + d_{\mathrm{B_i}}^2 - 2d_{\mathrm{A_i}}d_{\mathrm{B_i}}\cos\left(\theta_i\right)}$ and $R_{D_{\mathrm{C}}} \gg R_{D_{\mathrm{B}}}$, the distance can be approximated as $d_{\mathrm{A_i}} \approx d_{\mathrm{C_i}}$. Applying (3.16), Φ is calculated as follows:

$$\Phi \approx \frac{2}{R_{D_{\mathrm{B}}}^2} \int_0^{R_{D_{\mathrm{B}}}} \left(1+r^{\alpha}\right)\left(\ln m_0\left(1+r^{\alpha}\right) + 2c_0\right) r dr, \tag{A.1.8}$$

where $m_0 = \frac{\chi\left(1+d_{\mathrm{C_i}}^{\alpha}\right)}{\eta\rho} \approx \frac{\chi\left(1+d_{\mathrm{A_i}}^{\alpha}\right)}{\eta\rho}$.

For an arbitrary choice of α, the integral in (A.1.8) is mathematically intractable, Gaussian-Chebyshev quadrature is used to find the approximation. Then Φ can be approximated as follows:

$$\Phi \approx \frac{\omega_N}{2} \sum_{n=1}^{N} \left(\sqrt{1-{\phi_n}^2}\, c_n \left(\ln m_0 c_n + 2c_0\right)\left(\phi_n + 1\right)\right). \tag{A.1.9}$$

Substituting (A.1.9) into (A.1.7), (A.1.7) is rewritten as follows:

$$\begin{aligned}\Theta_1 =& -\frac{1}{\pi\left(R_{D_\mathrm{A}}^2 - R_{D_\mathrm{C}}^2\right)}\frac{\omega_N}{2}\int_0^{\varepsilon_{\mathrm{A}_i}}\int_{R_{D_\mathrm{C}}}^{R_{D_\mathrm{A}}}\int_0^{2\pi}\frac{\chi(1+r^\alpha)^2}{\eta\rho}e^{-(1+r^\alpha)x}\\ &\times\sum_{n=1}^{N}\left(\sqrt{1-{\phi_n}^2}c_n\left(\ln\frac{\chi\left(1+r^\alpha\right)}{\eta\rho}c_n+2c_0\right)\left(\phi_n+1\right)\right)r dr d\theta dx\\ =& -\frac{\omega_N}{R_{D_\mathrm{A}}^2 - R_{D_\mathrm{C}}^2}\int_0^{\varepsilon_{\mathrm{A}_i}}\frac{\chi}{\eta\rho}\sum_{n=1}^{N}\left(\phi_n+1\right)\sqrt{1-{\phi_n}^2}\\ &\underbrace{\int_{R_{D_\mathrm{C}}}^{R_{D_\mathrm{A}}} r(1+r^\alpha)^2 e^{-(1+r^\alpha)x}c_n\left(\ln\frac{\chi\left(1+r^\alpha\right)}{\eta\rho}c_n+2c_0\right)dr}_{\Delta}\,dx. \end{aligned}\tag{A.1.10}$$

Similarly as above, Gaussian-Chebyshev quadrature is used to find an approximation of Δ in (A.1.10) as follows:

$$\begin{aligned}\Delta \approx& \frac{\omega_K\left(R_{D_\mathrm{A}} - R_{D_\mathrm{C}}\right)}{2}\sum_{k=1}^{K}\sqrt{1-\psi_k^2}s_k(1+s_k^\alpha)^2\\ &\times e^{-\left(1+s_k^\alpha\right)x}c_n\left(\ln\frac{\chi\left(1+s_k^\alpha\right)}{\eta\rho}c_n+2c_0\right).\end{aligned}\tag{A.1.11}$$

Substituting (A.1.11) into (A.1.10), (A.1.10) is rewritten as follows:

$$\begin{aligned}\Theta_1 =& a_2\sum_{n=1}^{N}\left(\phi_n+1\right)\sqrt{1-{\phi_n}^2}c_n\sum_{k=1}^{K}\sqrt{1-\psi_k^2}s_k(1+s_k^\alpha)^2\\ &\times\underbrace{\int_0^{\varepsilon_{\mathrm{A}_i}}\chi e^{-\left(1+s_k^\alpha\right)x}\left(\ln\frac{\chi\left(1+s_k^\alpha\right)}{\eta\rho}c_n+2c_0\right)dx}_{\Psi},\end{aligned}\tag{A.1.12}$$

where $a_2 = -\frac{\omega_N\omega_K}{2\left(R_{D_\mathrm{A}}+R_{D_\mathrm{C}}\right)\eta\rho}$.

Similarly, Gaussian-Chebyshev quadrature is used to find an approximation of Ψ in (A.1.12) as follows:

$$\Psi \approx \frac{\omega_M\varepsilon_{\mathrm{A}_i}}{2}\sum_{m=1}^{M}\sqrt{1-\varphi_m^2}e^{-\left(1+s_k^\alpha\right)t_m}\chi_{t_m}\left(\ln\frac{\chi_{t_m}\left(1+s_k^\alpha\right)}{\eta\rho}c_n+2c_0\right).\tag{A.1.13}$$

Substituting (A.1.13) into (A.1.12), the following expression is obtained

$$\begin{aligned}\Theta_1 \approx & \zeta_1 \sum_{n=1}^{N} (\phi_n + 1) \sqrt{1 - {\phi_n}^2} c_n \sum_{k=1}^{K} \sqrt{1 - \psi_k^2} s_k (1 + s_k^{\alpha})^2 \\ & \times \sum_{m=1}^{M} \sqrt{1 - \varphi_m^2} e^{-(1+s_k^{\alpha}) t_m} \chi_{t_m} \left(\ln \frac{\chi_{t_m} (1 + s_k^{\alpha})}{\eta \rho} c_n + 2c_0 \right). \end{aligned} \tag{A.1.14}$$

Θ_2 can be expressed as follows:

$$\Theta_2 = \Pr\left(X_i < \varepsilon_{\mathrm{A}_i}\right) \Pr\left(Y_i < \varepsilon_{\mathrm{A}_i}\right). \tag{A.1.15}$$

The CDF of X_i for $\mathrm{A_i}$ is given by

$$\begin{aligned} F_{X_i}(\varepsilon) &= \int_D \left(1 - e^{-\left(1 + d_{\mathrm{A_i}}^{\alpha}\right)\varepsilon}\right) f_{W_{\mathrm{A_i}}}(\omega_{\mathrm{A_i}})\, d\omega_{\mathrm{A_i}} \\ &= \frac{2}{R_{D_{\mathrm{A}}}^2 - R_{D_{\mathrm{C}}}^2} \int_{R_{D_{\mathrm{C}}}}^{R_{D_{\mathrm{A}}}} \left(1 - e^{-(1+r^{\alpha})\varepsilon}\right) r dr. \end{aligned} \tag{A.1.16}$$

For an arbitrary choice of α, similarly to (3.19), Gaussian-Chebyshev quadrature is provided to find the approximation for the CDF of X_i. (A.1.16) is rewritten as follows:

$$F_{X_i}(\varepsilon) \approx \frac{\omega_K}{R_{D_{\mathrm{A}}} + R_{D_{\mathrm{C}}}} \sum_{k=1}^{K} \sqrt{1 - {\psi_k}^2} \left(1 - e^{-(1+s_k^{\alpha})\varepsilon}\right) s_k. \tag{A.1.17}$$

When $\varepsilon \to 0$, a high SNR approximation of the (A.1.17) is given by

$$F_{X_i}(\varepsilon) \approx \frac{\omega_K \varepsilon}{R_{D_{\mathrm{A}}} + R_{D_{\mathrm{C}}}} \sum_{k=1}^{K} \sqrt{1 - {\psi_k}^2} (1 + s_k^{\alpha}) s_k. \tag{A.1.18}$$

Substituting (A.1.18) and (3.19) into (A.1.15), the approximation for the general case

can be obtained as follows:

$$\Theta_2 \approx a_1 \sum_{n=1}^{N} \sqrt{1-{\phi_n}^2} c_n \left(\phi_n + 1\right) \sum_{k=1}^{K} \sqrt{1-{\psi_k}^2}(1+s_k^{\alpha}) s_k. \tag{A.1.19}$$

Combining (A.1.14) and (A.1.19), (3.23) can be obtained.

The proof is complete.

A.2 Proof of Corollary 2

For the special case $\alpha = 2$, and let $\lambda = \left(1 + r^2\right)$, (A.1.8) is rewritten as follows:

$$\begin{aligned} \Phi|_{\alpha=2} =& \frac{1}{R_{D_{\mathrm{B}}}^2} \int_1^{1+R_{D_{\mathrm{B}}}^2} \lambda \left(\ln m_{0^*} \lambda + 2c_0\right) d\lambda \\ =& \frac{\left(R_{D_{\mathrm{B}}}^2 + 2\right) \ln m_{0^*}}{2} + b_0, \end{aligned} \tag{A.2.1}$$

where $m_{0^*} = \frac{\chi\left(1+d_{\mathrm{C_i}}^2\right)}{\eta\rho} \approx \frac{\chi\left(1+d_{\mathrm{A_i}}^2\right)}{\eta\rho}$.

Substituting (A.2.1) and applying $\alpha = 2$ into (A.1.2), the following expression is obtained

$$\begin{aligned} \Theta_1|_{\alpha=2} = & -\frac{\left(R_{D_{\mathrm{B}}}^2 + 2\right)}{2\left(R_{D_{\mathrm{A}}}^2 - R_{D_{\mathrm{C}}}^2\right)\eta\rho} \int_0^{\varepsilon_{\mathrm{A}_i}} \chi \\ & \underbrace{\int_{R_{D_{\mathrm{C}}}}^{R_{D_{\mathrm{A}}}} r\left(1+r^2\right)^2 e^{-\left(1+r^2\right)x} \left(\ln \frac{\chi\left(1+r^2\right)}{\eta\rho} + b_0\right) dr\, dx}_{\Delta|_{\alpha=2}}. \end{aligned} \tag{A.2.2}$$

Note that the integral $\Delta|_{\alpha=2}$ in (A.2.2) is mathematically intractable. Gaussian-Chebyshev quadrature is used to find an approximation. Then $\Delta|_{\alpha=2}$ can be approxi-

mated as follows:

$$\Delta|_{\alpha=2} \approx \frac{\omega_K \left(R_{D_\mathrm{A}} - R_{D_\mathrm{C}}\right)}{2} \sum_{k=1}^{K} \sqrt{1-\psi_k^2} s_k \left(1+s_k^2\right)^2 e^{-\left(1+s_k^2\right)x} \left(\ln \frac{\chi\left(1+s_k^2\right)}{\eta\rho} + b_0\right). \tag{A.2.3}$$

Substituting (A.2.3) into (A.2.2), (A.2.2) is rewritten as follows:

$$\begin{aligned}\Theta_1|_{\alpha=2} = &- \frac{\omega_K \left(R_{D_\mathrm{B}}^2 + 2\right)}{4\left(R_{D_\mathrm{A}} + R_{D_\mathrm{C}}\right)\eta\rho} \sum_{k=1}^{K} \sqrt{1-\psi_k^2} s_k \left(1+s_k^2\right)^2 \\ &\times \underbrace{\int_0^{\varepsilon_{\mathrm{A}_i}} \chi e^{-\left(1+s_k^2\right)x} \left(\ln \frac{\chi\left(1+s_k^2\right)}{\eta\rho} + b_0\right) dx}_{\Psi|_{\alpha=2}}.\end{aligned} \tag{A.2.4}$$

Similarly, Gaussian-Chebyshev quadrature is used to find the approximation of $\Psi|_{\alpha=2}$ in (A.2.4) as follows:

$$\Psi|_{\alpha=2} \approx \frac{\omega_M \varepsilon_{\mathrm{A}_i}}{2} \sum_{m=1}^{M} \sqrt{1-\varphi_m^2} \chi_{t_m} e^{-\left(1+s_k^2\right)t_m} \left(\ln \frac{\chi_{t_m}\left(1+s_k^2\right)}{\eta\rho} c_n + b_0\right). \tag{A.2.5}$$

Substituting (A.2.5) into (A.2.4), the following expression is obtained

$$\begin{aligned}\Theta_1|_{\alpha=2} = &\zeta_2 \sum_{k=1}^{K} \sqrt{1-\psi_k^2} s_k \left(1+s_k^2\right)^2 \sum_{m=1}^{M} \sqrt{1-\varphi_m^2} \\ &\times \chi_{t_m} e^{-\left(1+s_k^2\right)t_m} \left(\ln \frac{\chi_{t_m}\left(1+s_k^2\right)}{\eta\rho} c_n + b_0\right).\end{aligned} \tag{A.2.6}$$

For the special case $\alpha = 2$, the CDF of X_i in (A.1.16) can be calculated as follows:

$$F_{X_i}(\varepsilon)|_{\alpha=2} = 1 - \frac{e^{-\left(1+R_{D_\mathrm{C}}^2\right)\varepsilon}}{\varepsilon\left(R_{D_\mathrm{A}}^2 - R_{D_\mathrm{C}}^2\right)} + \frac{e^{-\left(1+R_{D_\mathrm{A}}^2\right)\varepsilon}}{\varepsilon\left(R_{D_\mathrm{A}}^2 - R_{D_\mathrm{C}}^2\right)}. \tag{A.2.7}$$

Substituting (A.2.7) and (3.21) into (A.1.15), Θ_2 for the special case $\alpha = 2$ in exact

closed-form can be obtained as follows:

$$\Theta_2|_{\alpha=2} = \left(1 - \frac{e^{-\left(1+R_{D_\mathrm{C}}^2\right)\varepsilon_{\mathrm{A}_i}}}{\varepsilon_{\mathrm{A}_i}\left(R_{D_\mathrm{A}}^2 - R_{D_\mathrm{C}}^2\right)} + \frac{e^{-\left(1+R_{D_\mathrm{A}}^2\right)\varepsilon_{\mathrm{A}_i}}}{\varepsilon_{\mathrm{A}_i}\left(R_{D_\mathrm{A}}^2 - R_{D_\mathrm{C}}^2\right)}\right) \times \left(1 - \frac{e^{-\varepsilon_{\mathrm{A}_i}}}{R_{D_\mathrm{B}}^2\varepsilon_{\mathrm{A}_i}} + \frac{e^{-\left(1+R_{D_\mathrm{B}}^2\right)\varepsilon_{\mathrm{A}_i}}}{R_{D_\mathrm{B}}^2\varepsilon_{\mathrm{A}_i}}\right). \tag{A.2.8}$$

Combining (A.2.6) and (A.2.8), (3.24) can be obtained.

The proof is complete.

A.3 Proof of Theorem 4

Conditioned on the event that the numbers of users in group $\{\mathrm{A_i}\}$ and $\{\mathrm{B_i}\}$ satisfy $\mathrm{V} = N_\mathrm{A} \geq 1, N_\mathrm{B} \geq 1$, the outage probability for $\mathrm{A_{i*}}$ by applying $X_{i^*} \to X_i$, $Y_{i^*} \to Y_i$, and $Z_{i^*} \to Z_i$ in (A.1.1) is expressed as

$$P_{\mathrm{A}_{\mathrm{i}^*}} = \underbrace{\Pr\left(\frac{\rho X_{i^*}|p_{i1}|^2}{\rho X_{i^*}|p_{i2}|^2+1} < \tau_1, \frac{\rho Y_{i^*}|p_{i1}|^2}{\rho|p_{i2}|^2 Y_{i^*}+1} < \tau_1 \middle| \mathrm{V}\right)}_{\Theta_2^*} + \underbrace{\Pr\left(Z_{i^*} < \frac{\tau_1 - \frac{\rho X_{i^*}|p_{i1}|^2}{\rho X_{i^*}|p_{i2}|^2+1}}{\eta\rho\left(Y_{i^*} - \varepsilon_{\mathrm{A}_i}\right)}, X_{i^*} < \varepsilon_{\mathrm{A}_i}, Y_{i^*} > \varepsilon_{\mathrm{A}_i} \middle| \mathrm{V}\right)}_{\Theta_1^*}, \tag{A.3.1}$$

where $X_{i^*} = \frac{|h_{\mathrm{A_i}}|^2}{1+d_{\mathrm{A_{i^*}}}^\alpha}$, $Y_{i^*} = \frac{|h_{\mathrm{B_i}}|^2}{1+d_{\mathrm{B_{i^*}}}^\alpha}$, and $Z_{i^*} = \frac{|g_i|^2}{1+d_{\mathrm{C_{i^*}}}^\alpha}$. Here $d_{\mathrm{A_{i^*}}}$, $d_{\mathrm{B_{i^*}}}$, and $d_{\mathrm{C_{i^*}}}$ are distances from the BS to $\mathrm{A_{i^*}}$, from the BS to $\mathrm{B_{i^*}}$, and from $\mathrm{A_{i^*}}$ to $\mathrm{B_{i^*}}$, respectively.

Since $R_{D_\mathrm{C}} \gg R_{D_\mathrm{B}}$, the distance can be approximated as $d_{\mathrm{A_{i^*}}} \approx d_{\mathrm{C_{i^*}}}$. Using a similar approximation method as that used to obtain (A.1.2), Θ_1^* is calculated as follows:

$$\Theta_1^* = -\int_0^{\varepsilon_{\mathrm{A}_i}} \chi \int_{R_{D_C}}^{R_{D_\mathrm{A}}} \frac{\left(1+r_\mathrm{A}^\alpha\right)^2}{\eta\rho} e^{-\left(1+r_\mathrm{A}^\alpha\right)x} \Phi^* f_{d_{\mathrm{A_{i^*}}}}(r_\mathrm{A})\, dr_\mathrm{A} dx, \tag{A.3.2}$$

where
$\Phi^* = \int_0^{R_{D_\mathrm{B}}} (1+r_\mathrm{B}^\alpha) \left(\ln \chi \frac{(1+r_\mathrm{B}^\alpha)(1+r_\mathrm{A}^\alpha)}{\eta\rho} + 2c_0 \right) f_{d_{\mathrm{B_{i^*}}}}(r_\mathrm{B})\, dr_\mathrm{B}$ and $f_{d_{\mathrm{A_{i^*}}}}$ is the PDF of the nearest A_{i^*}.

Similar to (3.33) and applying stochastic geometry within the ring D_A, $f_{d_{\mathrm{A_{i^*}}}}(r_\mathrm{A})$ is obtained as follows:

$$f_{d_{\mathrm{A_{i^*}}}}(r_\mathrm{A}) = \xi_\mathrm{A} r_\mathrm{A} e^{-\pi\lambda_{\Phi_\mathrm{A}}\left(r_\mathrm{A}^2 - R_{D_\mathrm{C}}^2\right)}, \tag{A.3.3}$$

where $\xi_\mathrm{A} = \frac{2\pi\lambda_{\Phi_\mathrm{A}}}{1-e^{-\pi\lambda_{\Phi_\mathrm{A}}\left(R_{D_\mathrm{A}}^2 - R_{D_\mathrm{C}}^2\right)}}$.

Substituting (A.3.3) and (3.33) into (A.3.2), and using the Gaussian-Chebyshev quadrature approximation, Φ^* can be expressed as follows:

$$\Phi^* \approx \frac{\xi_\mathrm{B}\omega_N R_{D_\mathrm{B}}}{2} \sum_{n=1}^{N} \sqrt{1-{\phi_n}^2}\,(1+c_{n*}^\alpha)\left(\ln m_{\mathrm{B}*}\,(1+c_{n*}^\alpha) + 2c_0\right) c_{n*} e^{-\pi\lambda_{\Phi_\mathrm{B}} c_{n*}^2}. \tag{A.3.4}$$

where $m_{\mathrm{B}*} = \frac{\chi\left(1+r_\mathrm{A}^\alpha\right)}{\eta\rho}$.

Substituting (A.3.4) into (A.3.2), the following expression is obtained

$$\Theta_1^* = -\frac{\xi_\mathrm{B}\xi_\mathrm{A}\omega_N R_{D_\mathrm{B}}}{2\eta\rho} \int_0^{\varepsilon_{\mathrm{A}_i}} \chi e^{-\left(1+r_\mathrm{A}^\alpha\right)x} \sum_{n=1}^{N} \sqrt{1-{\phi_n}^2}\,(1+c_{n*}^\alpha)\, c_{n*} e^{-\pi\lambda_{\Phi_\mathrm{B}} c_{n*}^2} \Delta^* dx, \tag{A.3.5}$$

where $\Delta^* = \int_{R_{D_C}}^{R_{D_\mathrm{A}}} \left(\ln \chi \frac{\left(1+r_\mathrm{A}^\alpha\right)}{\eta\rho}\,(1+c_{n*}^\alpha) + 2c_0 \right) (1+r_\mathrm{A}^\alpha)^2 r_\mathrm{A} e^{-\pi\lambda_{\Phi_\mathrm{A}}\left(r_\mathrm{A}^2 - R_{D_\mathrm{C}}^2\right)} dr_\mathrm{A}$.

Applying Gaussian-Chebyshev quadrature approximation to Δ^*, the following expression is obtained

$$\begin{aligned}\Delta^* \approx & \frac{\omega_K\left(R_{D_\mathrm{A}} - R_{D_\mathrm{C}}\right)}{2} \sum_{k=1}^{K} \sqrt{1-\psi_k^2}(1+s_k^\alpha)^2 \\ & \times \left(\ln \frac{\chi\,(1+s_k^\alpha)\,(1+c_{n*}^\alpha)}{\eta\rho} + 2c_0 \right) s_k e^{-\pi\lambda_{\Phi_\mathrm{A}}\left(s_k^2 - R_{D_\mathrm{C}}^2\right)}.\end{aligned} \tag{A.3.6}$$

Substituting (A.3.6) into (A.3.2), the following expression is obtained

$$\begin{aligned}\Theta_1^* =& b_5 \sum_{n=1}^{N} \sqrt{1-{\phi_n}^2}\,(1+c_{n*}^{\alpha}) c_{n*} e^{-\pi\lambda_{\Phi_\mathrm{B}} c_{n*}^2} \\ &\times \sum_{k=1}^{K} \sqrt{1-\psi_k^2}(1+s_k^{\alpha})^2 s_k e^{-\pi\lambda_{\Phi_\mathrm{A}}\left(s_k^2 - R_{D_\mathrm{C}}^2\right)} \\ &\times \underbrace{\int_0^{\varepsilon_{\mathrm{A}_i}} \chi e^{-\left(1+r_{\mathrm{A}}^{\alpha}\right)x} \left(\ln \frac{\chi\left(1+s_k^{\alpha}\right)\left(1+c_{n*}^{\alpha}\right)}{\eta\rho} + 2c_0\right) dx}_{\Psi^*},\end{aligned} \tag{A.3.7}$$

where $b_5 = -\frac{\xi_\mathrm{B}\xi_\mathrm{A}\omega_N\omega_K R_{D_\mathrm{B}}\left(R_{D_\mathrm{A}} - R_{D_\mathrm{C}}\right)}{4\eta\rho}$.

Applying Gaussian-Chebyshev quadrature approximation to Ψ^*, the following expression is obtained

$$\Psi^* \approx \sum_{m=1}^{M} \omega_M \frac{\varepsilon_{\mathrm{A}_i}}{2} \sqrt{1-\varphi_m^2} e^{-\left(1+s_k^{\alpha}\right)t_m} \chi_{t_m} \left(\ln \frac{\chi_{t_m}\left(1+s_k^{\alpha}\right)\left(1+c_{n*}^{\alpha}\right)}{\eta\rho} + 2c_0\right). \tag{A.3.8}$$

Substituting (A.3.8) into (A.3.7), the following expression is obtained

$$\begin{aligned}\Theta_1^* =& \varsigma^* \sum_{n=1}^{N} \sqrt{1-{\phi_n}^2}\,(1+c_{n*}^{\alpha})\, c_{n*} e^{-\pi\lambda_{\Phi_\mathrm{B}} c_{n*}^2} \sum_{k=1}^{K} \sqrt{1-\psi_k^2} \\ &\times (1+s_k^{\alpha})^2 s_k e^{-\pi\lambda_{\Phi_\mathrm{A}}\left(s_k^2 - R_{D_\mathrm{C}}^2\right)} \sum_{m=1}^{M} \sqrt{1-\varphi_m^2} \\ &\times e^{-\left(1+s_k^{\alpha}\right)t_m} \chi_{t_m} \left(\ln \frac{\chi_{t_m}\left(1+s_k^{\alpha}\right)\left(1+c_{n*}^{\alpha}\right)}{\eta\rho} + 2c_0\right).\end{aligned} \tag{A.3.9}$$

Conditioned on the number of users in group $\{\mathrm{A_i}\}$ and $\{\mathrm{B_i}\}$, Θ_2^* is obtained as follows:

$$\begin{aligned}\Theta_2^* &= \Pr\left(X_{i^*} < \varepsilon_{\mathrm{A}_i} \middle| N_\mathrm{A} \geq 1\right) \Pr\left(Y_{i^*} < \varepsilon_{\mathrm{A}_i} \middle| N_\mathrm{B} \geq 1\right) \\ &= F_{X_{i^*}}\left(\varepsilon_{\mathrm{A}_i}\right) F_{Y_{i^*}}\left(\varepsilon_{\mathrm{A}_i}\right).\end{aligned} \tag{A.3.10}$$

Similar to (3.34), the CDF of A_{i^*} is given by

$$F_{X_{i^*}}(\varepsilon) = \xi_{\mathrm{A}} \int_{R_{D_{\mathrm{C}}}}^{R_{D_{\mathrm{A}}}} \left(1 - e^{-\left(1+r_{\mathrm{A}}^{\alpha}\right)\varepsilon}\right) r_{\mathrm{A}} e^{-\pi\lambda_{\Phi_{\mathrm{A}}}\left(r_{\mathrm{A}}^2 - R_{D_{\mathrm{C}}}^2\right)} dr_{\mathrm{A}}. \tag{A.3.11}$$

Applying the Gaussian-Chebyshev quadrature approximation, the following expression is obtained

$$F_{X_{i^*}}(\varepsilon) \approx b_2 \sum_{k=1}^{K} \sqrt{1-{\psi_k}^2} \left(1 - e^{-(1+s_k^{\alpha})\varepsilon}\right) s_k e^{-\pi\lambda_{\Phi_{\mathrm{A}}} s_k^2}. \tag{A.3.12}$$

Substituting (A.3.12) and (3.35) into (A.3.10) and using a high SNR approximation, the following expression is obtained

$$\Theta_2^* \approx b_2 b_3 \sum_{k=1}^{K} \sqrt{1-{\psi_k}^2}(1+s_k^{\alpha}) s_k e^{-\pi\lambda_{\Phi_{\mathrm{A}}} s_k^2} \sum_{n=1}^{N} \left(\sqrt{1-{\phi_n}^2}\,(1+c_{n*}^{\alpha})\, c_{n*} e^{-\pi\lambda_{\Phi_{\mathrm{B}}} c_{n*}^2}\right). \tag{A.3.13}$$

Combining (A.3.13) and (A.3.7), (3.37) is obtained.

The proof is complete.

A.4 Proof of Theorem 5

The outage probability for $\mathrm{A}_{i'}$ by applying $X_{i^*} \to X_i$, $Y_{i^*} \to Y_i$, and $Z_{i^*} \to Z_i$ in (A.1.1) can be expressed as

$$\begin{aligned} P_{\mathrm{A}_{i'}} = & \underbrace{\Pr\left(\frac{\rho X_{i'}|p_{i1}|^2}{\rho X_{i'}|p_{i2}|^2+1} < \tau_1, \frac{\rho Y_{i^*}|p_{i1}|^2}{\rho|p_{i2}|^2 Y_{i^*}+1} < \tau_1 \middle| \mathrm{V}\right)}_{\Theta_2{}'} \\ & + \underbrace{\Pr\left(Z_{i'} < \frac{\tau_1 - \frac{\rho X_{i'}|p_{i1}|^2}{\rho X_{i'}|p_{i2}|^2+1}}{\eta\rho\left(Y_{i^*} - \varepsilon_{\mathrm{A}_i}\right)}, X_{i'} < \varepsilon_{\mathrm{A}_i}, Y_{i^*} > \varepsilon_{\mathrm{A}_i} \middle| \mathrm{V}\right)}_{\Theta_1{}'}, \end{aligned} \tag{A.4.1}$$

where $X_{i'} = \frac{\left|h_{\mathrm{A_i}}\right|^2}{1+d^{\alpha}_{\mathrm{A_{i'}}}}$ and $Z_{i'} = \frac{|g_i|^2}{1+d^{\alpha}_{\mathrm{C_{i'}}}}$. Here $d_{\mathrm{A_{i'}}}$ and $d_{\mathrm{C_{i'}}}$ are distances from the BS to $\mathrm{A_{i'}}$ and from $\mathrm{A_{i'}}$ to $\mathrm{B_{i^*}}$, respectively.

Since $R_{D_\mathrm{C}} \gg R_{D_\mathrm{B}}$, the distance can be approximated as $d_{\mathrm{A_{i'}}} \approx d_{\mathrm{C_{i'}}}$. Using a similar approximation method as that used to get (A.1.2), first ${\Theta_1}'$ is calculated as follows:

$$\begin{aligned}{\Theta_1}' = &- \int_0^{\varepsilon_{\mathrm{A}_i}} \chi \int_{R_{D_C}}^{R_{D_\mathrm{A}}} \frac{\left(1+r_\mathrm{A}^{\alpha}\right)^2}{\eta\rho} e^{-\left(1+r_\mathrm{A}^{\alpha}\right)x} \\ &\times \int_0^{R_{D_\mathrm{B}}} \left(1+r_\mathrm{B}^{\alpha}\right) \left(\ln\chi \frac{\left(1+r_\mathrm{B}^{\alpha}\right)\left(1+r_\mathrm{A}^{\alpha}\right)}{\eta\rho} + 2c_0\right) \\ &\times f_{d_{\mathrm{B_{i^*}}}}\left(r_\mathrm{B}\right) dr_\mathrm{B} f_{d_{\mathrm{A_{i'}}}}\left(r_\mathrm{A}\right) dr_\mathrm{A} dx, \end{aligned} \tag{A.4.2}$$

where $f_{d_{\mathrm{A_{i'}}}}\left(r_\mathrm{A}\right)$ is the PDF for the farthest $\mathrm{A_{i'}}$.

Similar to (3.33) and applying stochastic geometry within the ring D_A, the following expression is obtained $f_{d_{\mathrm{A_{i'}}}}\left(r_\mathrm{A}\right)$ as follows:

$$f_{d_{\mathrm{A_{i'}}}}\left(r_\mathrm{A}\right) = \xi_\mathrm{A} r_\mathrm{A} e^{-\pi\lambda_{\Phi_\mathrm{A}}\left(R_{D_\mathrm{A}}^2 - r_\mathrm{A}^2\right)}. \tag{A.4.3}$$

Conditioned on the number of $\mathrm{A_{i'}}$ and $\mathrm{B_{i^*}}$, the following expression is obtained

$$\begin{aligned}{\Theta_2}' &= \Pr\left(X_{i'} < \varepsilon_{\mathrm{A}_i} \middle| N_\mathrm{A} \geq 1\right) \Pr\left(Y_{i^*} < \varepsilon_{\mathrm{A}_i} \middle| N_\mathrm{B} \geq 1\right) \\ &= F_{X_{i'}}\left(\varepsilon_{\mathrm{A}_i}\right) F_{Y_{i^*}}\left(\varepsilon_{\mathrm{A}_i}\right). \end{aligned} \tag{A.4.4}$$

Following a similar procedure as that used to obtain Θ_1^* and Θ_2^* in Appendix B, ${\Theta_1}'$ and ${\Theta_2}'$ can be obtained. Then combining ${\Theta_1}'$ and ${\Theta_2}'$, the general case (3.42) is obtained. For the special case $\alpha = 2$, following a method similar to that used to calculate (3.38), (3.43) can be obtained.

The proof is complete.

Appendix B

Proof in Chapter 6

B.1 Proof of Lemma 3

To derive the CDF of F_{γ_B}, based on (6.2), the following expression can be formulated

$$F_{\gamma_B}(x) = \Pr\left\{\rho_b a_n |h_n|^2 \leq x\right\} = F_{|h_n|^2}\left(\frac{x}{\rho_b a_n}\right), \tag{B.1.1}$$

where $F_{|h_n|^2}$ is the CDF of the ordered channel gain for the n-th user.

Assuming $y = \frac{x}{\rho_b a_n}$, and using order statistics [124] as well as applying binary series expansion, the CDF of the ordered channels has a relationship with the unordered channels captured as follows:

$$F_{|h_n|^2}(y) = \varphi_n \sum_{p=0}^{M-n} \binom{M-n}{p} \frac{(-1)^p}{n+p} \left(F_{|\tilde{h}_n|^2}(y)\right)^{n+p}, \tag{B.1.2}$$

where $F_{|\tilde{h}_n|^2}$ is the CDF of unordered channel gain for the n-th user.

Based on the assumption of homogeneous PPP, and by relying on polar coordinates,

$F_{\left|\tilde{h}_n\right|^2}$ is expressed as

$$F_{\left|\tilde{h}_n\right|^2}(y) = \frac{2}{R_D^2}\int_0^{R_D}\left(1-e^{-(1+r^\alpha)y}\right)rdr. \tag{B.1.3}$$

However, it is challenging to arrive at an easily implemented insightful expression for $F_{\left|\tilde{h}_n\right|^2}(y)$. Therefore, the Gaussian-Chebyshev quadrature relationship of [120] is invoked for finding an approximation of (B.1.3) in the following form:

$$F_{\left|\tilde{h}_n\right|^2}(y) \approx \sum_{k=0}^{K} b_k e^{-c_k y}. \tag{B.1.4}$$

Substituting (B.1.4) into (B.1.2) and applying the multinomial theorem, the CDF $F_{|h_n|^2}$ of ordered channel gain is given by

$$F_{|h_n|^2}(y) = \varphi_n \sum_{p=0}^{M-n}\binom{M-n}{p}\frac{(-1)^p}{n+p}\sum_{\tilde{S}_n^p}\binom{n+p}{q_0+\cdots+q_K}\left(\prod_{k=0}^{K} b_k^{q_k}\right)e^{-\sum\limits_{k=0}^{K} q_k c_k y}. \tag{B.1.5}$$

Substituting $y = \frac{x}{\rho_b a_n}$ into (B.1.5), (6.4) can be obtained. The proof is complete.

B.2 Proof of Lemma 6

Based on (6.32), the CDF of $F_{B_m}^{AN}$ can be expressed as

$$\begin{aligned} F_{B_m}^{AN}(x) &= \Pr\left\{\gamma_{B_m}^{AN} \le x\right\} \\ &= \Pr\left\{\frac{a_m\sigma_s^2\|\mathbf{h}_m\|^2}{a_n\sigma_s^2\left|\mathbf{h}_m\frac{\mathbf{h}_n^\dagger}{\|\mathbf{h}_n\|}\right|^2 + a_n\sigma_a^2\|\mathbf{h}_m\mathbf{V}_n\|^2 + 1 + d_m^\alpha} \le x\right\}. \end{aligned} \tag{B.2.1}$$

It may be readily seen that $\|\mathbf{h}_m\|^2$ obeys a Gamma distribution having the parameters of $(N_A, 1)$. Hence the CDF of $\|\mathbf{h}_m\|^2$ is given by

$$F_{B_m}^{AN}(x) = 1 - e^{-x} \sum_{p=0}^{N_A-1} \frac{x^p}{p!}. \tag{B.2.2}$$

Denoting $X_m = \left|\mathbf{h}_m \frac{\mathbf{h}_n^\dagger}{\|\mathbf{h}_n\|}\right|^2, Y_m = \|\mathbf{h}_m \mathbf{V}_n\|^2$, based on (B.2.2), (B.2.1) can be rewritten as

$$\begin{aligned} F_{B_m}^{AN}(x) &= \Pr\left\{\|\mathbf{h}_m\|^2 \le x\nu\left(I_m^{AN} + \frac{1+d_m^\alpha}{a_n}\right)\right\} \\ &= 1 - \int_{D_2}\int_0^\infty \sum_{p=0}^{N_A-1} \frac{\left(\nu x\left(z_m + \frac{1+d_m^\alpha}{a_n}\right)\right)^p}{p!} \\ &= \left(e^{-\nu x z_m - \nu x \frac{1+d_m^\alpha}{a_n}}\right) f_{I_m^{AN}}(z_m)\, f_{D_2}(\omega_m)\, dz_m d\omega_m, \end{aligned} \tag{B.2.3}$$

where $\nu = \frac{a_n}{a_m P_S}$, $f_{I_m^{AN}}$ and f_{D_2} are the PDF of I_m^{AN} and D_2, respectively. Here $I_m^{AN} = \sigma_s^2 X_m + \sigma_a^2 Y_m$ and $f_{D_2}(\omega_m) = \frac{1}{\pi\left(R_{D_2}^2 - R_{D_1}^2\right)}$.

Applying a binary series expansion to (B.2.3), it is arrived at:

$$F_{B_m}^{AN}(x) = 1 - \sum_{p=0}^{N_A-1} \frac{\nu^p x^p}{p!} \sum_{q=0}^{p} \binom{p}{q} Q_1 \int_{D_2} e^{-\nu x \frac{1+d_m^\alpha}{a_n}} \left(\frac{1+d_m^\alpha}{a_n}\right)^{p-q} f_{D_2}(\omega_m)\, d\omega_m, \tag{B.2.4}$$

where $Q_1 = \int_0^\infty e^{-\nu x z_m} z_m^q f_{I_m^{AN}}(z_m)\, dz_m$. Note that the distance d_m is determined by the location of ω_m. Then changing to polar coordinates and applying a binary series expansion again, it is obtained

$$F_{B_m}^{AN}(x) = 1 - \frac{2e^{-\frac{\nu x}{a_n}}}{R_{D_2}^2 - R_{D_1}^2} \sum_{p=0}^{N_A-1} \frac{\nu^p x^p}{p!} \sum_{q=0}^{p} \binom{p}{q} Q_1 \frac{1}{a_n^{p-q}} \sum_{u=0}^{p-q} \binom{p-q}{u} \int_{R_{D_1}}^{R_{D_2}} r^{u\alpha+1} e^{-\nu x P_S r^\alpha} dr. \tag{B.2.5}$$

By invoking [125, Eq. (3.381.8)], the following expression is obtained

$$F_{B_m}^{AN}(x) = 1 - \frac{2e^{-\frac{\nu x}{a_n}}}{R_{D_2}^2 - R_{D_1}^2} \sum_{p=0}^{N_A-1} \frac{\nu^p x^p}{p!} \sum_{q=0}^{p} \binom{p}{q} Q_1 \frac{1}{a_n^{p-q}} \times \sum_{u=0}^{p-q} \binom{p-q}{u} \frac{\gamma\left(u+\delta, \frac{\nu x}{a_n} R_{D_2}^{\alpha}\right) - \gamma\left(u+\delta, \frac{\nu x}{a_n} R_{D_1}^{\alpha}\right)}{\alpha\left(\frac{\nu x}{a_n}\right)^{u+\delta}}. \tag{B.2.6}$$

Let us now turn the attention to the derivation of the integral Q_1 in (B.2.4) – (B.2.6). Note that X_m follows the exponential distribution with unit mean, while Y_m follows the distribution $Y_m \sim Gamma(N_A - 1, 1)$. As such, the PDF of $f_{I_m^{AN}}$ is given by [75]

$$f_{I_m^{AN}}(z_m) = \begin{cases} \frac{t_1}{e^{\frac{z_m}{P_S}}} \left(1 - \sum_{l=0}^{N_A-2} \frac{\left(\frac{N_A-1}{P_A} - \frac{1}{P_S}\right)^l z_m^l}{l! e^{\left(\frac{N_A-1}{P_A} - \frac{1}{P_S}\right) z_m}}\right), \theta \neq \frac{1}{N_A} \\ \frac{z_m^{N_A-1} e^{-\frac{z_m}{P_S}}}{{P_S}^{N_A}(N_A-1)!}, \theta = \frac{1}{N_A} \end{cases}, \tag{B.2.7}$$

where $t_1 = \frac{\left(1 - \frac{P_A}{(N_A-1)P_S}\right)^{1-N_A}}{P_S}$. Based on (B.2.7), and applying [125, Eq. (3.326.2)], Q_1 can be expressed as follows:

$$Q_1 = \begin{cases} \frac{t_1 \Gamma(q+1)}{\left(x\nu + \frac{1}{P_S}\right)^{q+1}} - \sum_{l=0}^{N_A-2} \frac{\frac{t_1}{l!}\left(\frac{N_A-1}{P_A} - \frac{1}{P_S}\right)^l \Gamma(q+l+1)}{\left(\nu x + \frac{N_A-1}{P_A}\right)^{q+l+1}}, \theta \neq \frac{1}{N_A} \\ \frac{\Gamma(q+N_A)}{{P_S}^{N_A}(N_A-1)!\left(\nu x + \frac{1}{P_S}\right)^{q+N_A}}, \theta = \frac{1}{N_A} \end{cases}. \tag{B.2.8}$$

Upon substituting (B.2.8) into (B.2.6), the CDF of $F_{B_m}^{AN}$ is given by (6.37).

B.3 Proof of Lemma 7

Based on (6.34), the CDF of $F_{B_n}^{AN}$ is expressed as follows:

$$\begin{aligned} F_{B_n}^{AN}(x) &= \Pr\left\{\|\mathbf{h}_n\|^2 \le x\vartheta\left(\frac{P_A}{N_A-1}Y_n + \frac{1+d_n^\alpha}{a_m}\right)\right\} \\ &= 1 - \sum_{p=0}^{N_A-1}\frac{\vartheta^p x^p}{p!}\sum_{q=0}^{p}\binom{p}{q}Q_3\int_{D_1} e^{-\frac{\vartheta x}{a_m}(1+d_n^\alpha)}\left(\frac{1}{a_m}(1+d_n^\alpha)\right)^{p-q} f_{D_1}(\omega_n)\, d\omega_n, \end{aligned} \quad \text{(B.3.1)}$$

where $\vartheta = \frac{a_m}{a_n P_S}$, $Q_3 = \int_0^\infty e^{-\vartheta x z_n} z_n^q f_{I_n^{AN}}(z_n)\, dz_n$, $f_{I_n^{AN}}$ and $f_{D_1}(\omega_n)$ are the PDF of I_n^{AN} and D_1. Here $I_n^{AN} = \frac{P_A}{N_A-1}Y_n, Y_n = \|\mathbf{h}_n\mathbf{V}_m\|^2$, and $f_{D_1}(\omega_n) = \frac{1}{\pi R_{D_1}^2}$. Upon changing to polar coordinates and applying [125, Eq. (3.381.8)], it is arrived at

$$F_{B_n}^{AN}(x) = 1 - \frac{\delta e^{-\frac{\vartheta x}{a_m}}}{R_{D_1}^2}\sum_{p=0}^{N_A-1}\frac{\vartheta^p x^p}{p!}\sum_{q=0}^{p}\binom{p}{q}Q_3 a_m^{q-p}\sum_{u=0}^{p-q}\binom{p-q}{u}\frac{\gamma\left(u+\delta, \frac{\vartheta x}{a_m}R_{D_1}^\alpha\right)}{\left(\frac{\vartheta x}{a_m}\right)^{u+\delta}}. \quad \text{(B.3.2)}$$

Finally turn the attention on Q_3. It is readily seen that I_n^{AN} obeys the Gamma distribution in conjunction with the parameter $\left(N_A - 1, \frac{P_A}{N_A-1}\right)$. Then the PDF of $f_{I_n^{AN}}(z_n) = \frac{z_n^{N_A-2} e^{-\frac{z_n(N_A-1)}{P_A}}}{\left(\frac{P_A}{N_A-1}\right)^{N_A-1}\Gamma(N_A-1)}$ can be obtained. Applying [125, Eq. (3.326.2)], Q_3 can be expressed as $Q_3 = \frac{\Gamma(N_A-1+q)}{\Gamma(N_A-1)\left(\frac{P_A}{N_A-1}\right)^{N_A-1}\left(\vartheta x + \frac{N_A-1}{P_A}\right)^{N_A-1+q}}$. Upon substituting Q_3 into (B.3.2), the CDF of $F_{B_n}^{AN}(x)$ is obtained as (6.38).

B.4 Proof of Lemma 8

Based on (6.36), the CDF of $F_{\gamma_{E_\kappa}^{AN}}$ can be expressed as

$$\begin{aligned} F_{\gamma_{E_\kappa}^{AN}}(x) &= \Pr\left\{\max_{e\in\Phi_e, d_e\geq r_p}\left\{\frac{a_\kappa P_S X_{e,\kappa}}{I_e^{AN}+d_e^\alpha}\right\}\leq x\right\} \\ &= E_{\Phi_e}\left\{\prod_{e\in\Phi_e, d_e\geq r_p}\int_0^\infty F_{X_{e,\kappa}}\left(\frac{(z+d_e^\alpha)\,x}{a_\kappa P_S}\right) f_{I_e^{AN}}(z)\,dz\right\}. \end{aligned} \tag{B.4.1}$$

Following a procedure similar to that used for obtaining (6.11), this work applies the generating function [115] and switches to polar coordinates. Then (B.4.1) can be expressed as

$$F_{\gamma_{E_\kappa}^{AN}}(x) = \exp\left[-2\pi\lambda_e\int_{r_p}^\infty r e^{-\frac{x}{a_\kappa P_S}r^\alpha} dr Q_2\right], \tag{B.4.2}$$

where $Q_2 = \int_0^\infty e^{-z\frac{x}{a_\kappa P_S}} f_{I_e^{AN}}(z)\,dz$. Applying [125, Eq. (3.381.9)], it is arrived at

$$F_{\gamma_{E_\kappa}^{AN}}(x) = \exp\left[-\frac{\mu_{\kappa 1}^{AN}\Gamma\left(\delta, \mu_{\kappa 2}^{AN}x\right)}{x^\delta}Q_2\right]. \tag{B.4.3}$$

Let us now turn the attention to solving the integral Q_2. Note that all the elements of $\mathbf{h}_e\mathbf{V}_m$ and $\mathbf{h}_e\mathbf{V}_n$ are independent complex Gaussian distributed with a zero mean and unit variance. The notation $Y_{e,m} = \|\mathbf{h}_e\mathbf{V}_m\|^2$ and $Y_{e,n} = \|\mathbf{h}_e\mathbf{V}_n\|^2$ are introduced. As a consequence, both $Y_{e,m}$ and $Y_{e,n}$ obey the $Gamma\,(N_A-1,1)$ distribution. Based on the properties of the Gamma distribution, the following expressions are obtained: $a_m\sigma_a^2 Y_{e,m} \sim Gamma\left(N_A-1, a_m\sigma_a^2\right), a_n\sigma_a^2 Y_{e,n} \sim Gamma\left(N_A-1, a_n\sigma_a^2\right)$. Then the sum of these two items I_e^{AN} obeys the generalized integer Gamma (GIG) distribution. According to [135], the PDF of I_e^{AN} is given by

$$f_{I_e^{AN}}(z) = (-1)^{N_A-1}\prod_{i=1}^{2}\tau_i^{N_A-1}\sum_{i=1}^{2}\sum_{j=1}^{N_A-1}\frac{a_{N_A-j,N_A-1}}{(j-1)!}(2\tau_i-L)^{j-(2N_A-2)}z^{j-1}e^{-\tau_i z}. \tag{B.4.4}$$

Upon substituting (B.4.4) into (B.4.3), as well as applying [125, Eq. (3.381.4)], after some further manipulations, the CDF of $F_{\gamma_{E_\kappa}^{AN}}$ is obtained as

$$F_{\gamma_{E_\kappa}^{AN}}(x) = \exp\left[\Omega \frac{\Gamma\left(\delta, x\mu_{\kappa 2}^{AN}\right)}{\sum_{p=0}^{j} \binom{j}{p} (x)^{p+\delta} (a_\kappa P_S)^{-p} \tau_i^{j-p}}\right]. \tag{B.4.5}$$

Upon setting the derivative of the CDF in (B.4.5), (6.39) can be obtained.

References

[1] C.-X. Wang, F. Haider, X. Gao, X.-H. You, Y. Yang, D. Yuan, H. Aggoune, H. Haas, S. Fletcher, and E. Hepsaydir, "Cellular architecture and key technologies for 5G wireless communication networks," *IEEE Commun. Mag.*, vol. 52, no. 2, pp. 122–130, 2014.

[2] K. S. Gilhousen, I. M. Jacobs, R. Padovani, A. J. Viterbi, L. A. Weaver Jr, and C. E. Wheatley III, "On the capacity of a cellular cdma system," *IEEE Trans. Veh. Technol.*, vol. 40, no. 2, pp. 303–312, 1991.

[3] J. Li, X. Wu, and R. Laroia, *OFDMA mobile broadband communications: A systems approach.* Cambridge University Press, 2013.

[4] Z. Ding, Y. Liu, J. Choi, Q. Sun, M. Elkashlan, C.-L. I, and H. V. Poor, "Application of non-orthogonal multiple access in LTE and 5G networks," *IEEE Commun. Mag.*, submitted. [Online]. Available: http://arxiv.org/abs/1511.08610

[5] Y. Saito, A. Benjebbour, Y. Kishiyama, and T. Nakamura, "System-level performance evaluation of downlink non-orthogonal multiple access (NOMA)," in *Proc. IEEE Annual Symposium on Personal, Indoor and Mobile Radio Communications (PIMRC)*, London, UK, Sept. 2013.

[6] Z. Ding, P. Fan, and H. V. Poor, "Impact of user pairing on 5G non-orthogonal multiple access," *IEEE Trans. Veh. Technol.*, to appear in 2016.

[7] Y. Saito, Y. Kishiyama, A. Benjebbour, T. Nakamura, A. Li, and K. Higuchi,

"Non-orthogonal multiple access (NOMA) for cellular future radio access," in *Proc. Vehicular Technology Conference (VTC Spring)*, Jun. Dresden, Germany, Jun. 2013, pp. 1–5.

[8] L. Dai, B. Wang, Y. Yuan, S. Han, C. l. I, and Z. Wang, "Non-orthogonal multiple access for 5G: solutions, challenges, opportunities, and future research trends," *IEEE Commun. Mag.*, vol. 53, no. 9, pp. 74–81, Sep. 2015.

[9] Z. Ding, Z. Yang, P. Fan, and H. V. Poor, "On the performance of non-orthogonal multiple access in 5G systems with randomly deployed users," *IEEE Signal Process. Lett.*, vol. 21, no. 12, pp. 1501–1505, 2014.

[10] Z. Ding, M. Peng, and H. V. Poor, "Cooperative non-orthogonal multiple access in 5G systems," *IEEE Commun. Lett.*, vol. 19, no. 8, pp. 1462–1465, 2015.

[11] A. Goldsmith, S. A. Jafar, I. Maric, and S. Srinivasa, "Breaking spectrum gridlock with cognitive radios: An information theoretic perspective," *Proceedings of the IEEE*, vol. 97, no. 5, pp. 894–914, 2009.

[12] J. G. Andrews, S. Buzzi, W. Choi, S. V. Hanly, A. Lozano, A. C. Soong, and J. C. Zhang, "What will 5G be?" *IEEE J. Sel. Areas Commun.*, vol. 32, no. 6, pp. 1065–1082, 2014.

[13] A. D. Wyner, "The wire-tap channel," *Bell Syst. Tech. J.*, vol. 54, no. 8, pp. 1355–1387, 1975.

[14] Z. Ding, F. Adachi, and H. V. Poor, "The application of MIMO to non-orthogonal multiple access," *IEEE Trans. Wireless Commun.*, vol. 15, no. 1, pp. 537–552, Jan. 2015.

[15] S. Timotheou and I. Krikidis, "Fairness for non-orthogonal multiple access in 5G systems," *IEEE Signal Process. Lett.*, vol. 22, no. 10, pp. 1647–1651, Oct. 2015.

[16] A. Benjebbour, A. Li, Y. Saito, Y. Kishiyama, A. Harada, and T. Nakamura, "System-level performance of downlink NOMA for future LTE enhancements," in *Proc. IEEE Global Commun. Conf. (GLOBECOM) Workshops)*, 2013, pp. 66–70.

[17] P. Xu, Z. Ding, X. Dai, and H. V. Poor, "A new evaluation criterion for non-orthogonal multiple access in 5G software defined networks," *IEEE Access*, vol. 3, pp. 1633–1639, 2015.

[18] M. Al-Imari, P. Xiao, M. A. Imran, and R. Tafazolli, "Uplink non-orthogonal multiple access for 5G wireless networks," in *Proc. of International Symposium on Wireless Communications Systems (ISWCS)*, Barcelona, Spain, Aug 2014, pp. 781–785.

[19] M. Al-Imari, P. Xiao, and M. A. Imran, "Receiver and resource allocation optimization for uplink NOMA in 5G wireless networks."

[20] S. Chen, K. Peng, and H. Jin, "A suboptimal scheme for uplink NOMA in 5G systems," in *Proc. of Wireless Commun. and Mobile Computing Confer. (IWCMC)*, Aug. 2015, pp. 1429–1434.

[21] N. Zhang, J. Wang, G. Kang, and Y. Liu, "Uplink nonorthogonal multiple access in 5G systems," *IEEE Commun. Lett.*, vol. 20, no. 3, pp. 458–461, Mar. 2016.

[22] K. Higuchi and A. Benjebbour, "Non-orthogonal multiple access (NOMA) with successive interference cancellation for future radio access," *IEICE Transactions on Communications*, vol. 98, no. 3, pp. 403–414, 2015.

[23] Q. Sun, S. Han, C.-L. I, and Z. Pan, "On the ergodic capacity of MIMO NOMA systems," *IEEE Wireless Commun. Lett.*, vol. 4, no. 4, pp. 405–408, Aug. 2015.

[24] J. Choi, "Minimum power multicast beamforming with superposition coding for multiresolution broadcast and application to NOMA systems," *IEEE Trans. Commun.*, vol. 63, no. 3, pp. 791–800, March 2015.

[25] Z. Ding, R. Schober, and H. V. Poor, "A general MIMO framework for NOMA downlink and uplink transmission based on signal alignment," *IEEE Trans. Wireless Commun.*, to appear in 2016.

[26] M. F. Hanif, Z. Ding, T. Ratnarajah, and G. K. Karagiannidis, "A minorization-maximization method for optimizing sum rate in the downlink of non-orthogonal multiple access systems," *IEEE Trans. Signal Process.*, vol. 64, no. 1, pp. 76–88, Jan. 2016.

[27] J. Choi, "On the power allocation for MIMO-NOMA systems with layered transmissions," *IEEE Trans. Wireless Commun.*, to appear in 2016.

[28] Z. Ding, L. Dai, and H. V. Poor, "MIMO-NOMA design for small packet transmission in the internet of things," *IEEE Access*, to appear in 2016.

[29] B. Kim, S. Lim, H. Kim, S. Suh, J. Kwun, S. Choi, C. Lee, S. Lee, and D. Hong, "Non-orthogonal multiple access in a downlink multiuser beamforming system," in *Proc. IEEE Military Commun. Conf., MILCOM*, 2013, pp. 1278–1283.

[30] S. Qureshi, H. Kim, and S. A. Hassan, "MIMO uplink NOMA with successive bandwidth division," in *Proc. IEEE Wireless Commun. and Networking Conf, MILCOM*, Doha, Qatar, Apr. 2016.

[31] L. Liu, C. Yuen, Y. L. Guan, and Y. Li, "Capacity-achieving iterative LMMSE detection for MIMO-NOMA systems," in *Proc. Inter. Conf. on Commun. (ICC)*, May 2016, Kuala Lumpur, Malaysia.

[32] K. Higuchi and Y. Kishiyama, "Non-orthogonal access with random beamforming and intra-beam sic for cellular MIMO downlink," in *Proc. IEEE Veh. Technol. Conf. (VTC Fall)*, 2013, pp. 1–5.

[33] A. Benjebbour, Y. Saito, Y. Kishiyama, A. Li, A. Harada, and T. Nakamura, "Concept and practical considerations of non-orthogonal multiple access (NOMA) for future radio access," in *Proc. IEEE Intelligent Signal Processing and Communications Systems (ISPACS)*, 2013, pp. 770–774.

[34] Z. Ding and H. V. Poor, "Design of massive-MIMO-NOMA with limited feedback," *IEEE Signal Process. Lett.*, to appear in 2016.

[35] J. Men and J. Ge, "Performance analysis of non-orthogonal multiple access in downlink cooperative network," *IET Commun.*, vol. 9, no. 18, pp. 2267–2273, 2015.

[36] ——, "Non-orthogonal multiple access for multiple-antenna relaying networks," *IEEE Commun. Lett.*, vol. 19, no. 10, pp. 1686–1689, Oct. 2015.

[37] Z. Ding, H. Dai, and H. V. Poor, "Relay selection for cooperative NOMA," *arXiv preprint arXiv:1604.00787*, 2016.

[38] J. Choi, "Non-orthogonal multiple access in downlink coordinated two-point systems," *IEEE Commun. Lett.*, vol. 18, no. 2, pp. 313–316, Feb. 2014.

[39] Y. Tian, A. Nix, and M. Beach, "On the performance of opportunistic NOMA in downlink comp networks," *IEEE Commun. Lett.*, to appear in 2016.

[40] J. B. Kim and I. H. Lee, "Non-orthogonal multiple access in coordinated direct

and relay transmission," *IEEE Commun. Lett.*, vol. 19, no. 11, pp. 2037–2040, Nov. 2015.

[41] Q. T. Vien, N. Ogbonna, H. X. Nguyen, R. Trestian, and P. Shah, "Non-orthogonal multiple access for wireless downlink in cloud radio access networks," in *Pro. of European Wireless Conference;*, May 2015, pp. 1–6.

[42] Q. Zhao and B. M. Sadler, "A survey of dynamic spectrum access," *IEEE Signal Process. Mag.*, vol. 24, no. 3, pp. 79–89, May 2007.

[43] Y. Dhungana and C. Tellambura, "Outage probability of underlay cognitive relay networks with spatially random nodes," in *Global Commun. Conf. (GLOBECOM)*, Dec 2014, pp. 3597–3602.

[44] K. Lee and A. Yener, "Outage performance of cognitive wireless relay networks," in *Proc. IEEE GLOBECOM*, 2006, pp. 1–5.

[45] J. Lee, H. Wang, J. G. Andrews, and D. Hong, "Outage probability of cognitive relay networks with interference constraints," *IEEE Trans. Commun.*, vol. 10, no. 2, pp. 390–395, 2011.

[46] T. Duong, P. L. Yeoh, V. N. Q. Bao, M. Elkashlan, and N. Yang, "Cognitive relay networks with multiple primary transceivers under spectrum-sharing," *IEEE Signal Process. Lett.*, vol. 19, no. 11, pp. 741–744, 2012.

[47] P. L. Yeoh, M. Elkashlan, K. Kim, T. Duong, and G. Karagiannidis, "Transmit antenna selection in cognitive MIMO relaying with multiple primary transceivers," *IEEE Trans. Veh. Technol.*, 2015.

[48] A. Adhikary, H. S. Dhillon, and G. Caire, "Massive-MIMO meets hetnet: Interference coordination through spatial blanking," *IEEE J. Sel. Areas Commun.*, vol. 33, no. 6, pp. 1171–1186, Jun. 2015.

[49] Q. Ye, O. Y. Bursalioglu, H. C. Papadopoulos, C. Caramanis, and J. G. Andrews, "User association and interference management in massive MIMO hetnets," *arXiv preprint arXiv:1509.07594*, 2015.

[50] W. Liu, S. Jin, C. K. Wen, M. Matthaiou, and X. You, "A tractable approach to uplink spectral efficiency of two-tier massive MIMO cellular hetnets," *IEEE Commun. Lett.*, vol. 20, no. 2, pp. 348–351, Feb. 2016.

[51] Y. Xu, H. Sun, R. Q. Hu, and Y. Qian, "Cooperative non-orthogonal multiple access in heterogeneous networks," in *Proc. IEEE Global Commun. Conf. (GLOBECOM)*, Dec. 2015, pp. 1–6.

[52] N. Shinohara, "Power without wires," *IEEE Microw. Mag.*, vol. 12, no. 7, pp. 64–73, Dec. 2011.

[53] "RF energy harvesting and wireless power for low-power applications." [Online]. Available: http://www.powercastco.com/PDF/powercast-overview%20(2012).pdf

[54] A. N. Parks, A. Liu, S. Gollakota, and J. R. Smith, "Turbocharging ambient backscatter communication," in *Proc. ACM conference on SIGCOMM*, 2014, pp. 619–630.

[55] R. Vullers, R. van Schaijk, I. Doms, C. V. Hoof, and R. Mertens, "Micropower energy harvesting," *Solid State Electron.*, vol. 53, no. 7, pp. 684–693, Apr. 2009.

[56] P. Cheng, S. He, F. Jiang, Y. Gu, and J. Chen, "Optimal scheduling for quality of monitoring in wireless rechargeable sensor networks," *IEEE Trans. Wireless Commun.*, vol. 12, no. 6, pp. 3072–3084, 2013.

[57] S. He, J. Chen, F. Jiang, D. K. Yau, G. Xing, and Y. Sun, "Energy provisioning in wireless rechargeable sensor networks," *IEEE Commun. Mag.*, vol. 12, no. 10, pp. 1931–1942, 2013.

[58] L. Varshney, "Transporting information and energy simultaneously," in *Proc. IEEE Int. Symp. Inf. Theory (ISIT)*, Toronto, ON, 2008, pp. 1612–1616.

[59] R. Zhang and C. K. Ho, "MIMO broadcasting for simultaneous wireless information and power transfer," *IEEE Trans. Commun.*, vol. 12, no. 5, pp. 1989–2001, 2013.

[60] A. A. Nasir, X. Zhou, S. Durrani, and R. A. Kennedy, "Relaying protocols for wireless energy harvesting and information processing," *IEEE Trans. Wireless Commun.*, vol. 12, no. 7, pp. 3622–3636, 2013.

[61] I. Krikidis, S. Sasaki, S. Timotheou, and Z. Ding, "A low complexity antenna switching for joint wireless information and energy transfer in MIMO relay channels," *IEEE Trans. Commun.*, 2014.

[62] Y. Liu, S. A. Mousavifar, Y. Deng, C. Leung, and M. Elkashlan, "Wireless energy harvesting in a cognitive relay network," *IEEE Trans. Wireless Commun.*, vol. 15,

no. 4, pp. 2498–2508, Apr. 2016.

[63] Z. Ding, I. Krikidis, B. Sharif, and H. V. Poor, "Wireless information and power transfer in cooperative networks with spatially random relays," *IEEE Trans. Wireless Commun.*, 2014.

[64] Z. Ding and H. Poor, "Cooperative energy harvesting networks with spatially random users," *IEEE Signal Process. Lett.*, vol. 20, no. 12, pp. 1211–1214, Dec 2013.

[65] P. D. Diamantoulakis, K. N. Pappi, Z. Ding, and G. K. Karagiannidis, "Wireless powered communications with non-orthogonal multiple access." [Online]. Available: http://arxiv.org/abs/1511.01291

[66] A. Mukherjee and A. Swindlehurst, "Robust beamforming for security in MIMO wiretap channels with imperfect CSI," *IEEE Trans. Signal Process.*, vol. 59, no. 1, pp. 351–361, Jan. 2011.

[67] Z. Ding, K. K. Leung, D. L. Goeckel, and D. Towsley, "On the application of cooperative transmission to secrecy communications," *IEEE J. Sel. Areas Commun.*, vol. 30, no. 2, pp. 359–368, Feb. 2012.

[68] Y. Liu, L. Wang, T. T. Duy, M. Elkashlan, and T. Duong, "Relay selection for security enhancement in cognitive relay networks," *IEEE Wireless Commun. Lett.*, vol. 4, no. 1, pp. 46–49, Feb. 2015.

[69] Y. Zou, X. Wang, W. Shen, and L. Hanzo, "Security versus reliability analysis of opportunistic relaying," *IEEE Trans. Veh. Technol.*, vol. 63, no. 6, pp. 2653–2661, Jul. 2014.

[70] Y. Liu, L. Wang, S. Zaidi, M. Elkashlan, and T. Duong, "Secure D2D communication in large-scale cognitive cellular networks: A wireless power transfer model," *IEEE Trans. Commun.*, vol. 64, no. 1, pp. 329–342, Jan. 2016.

[71] W. Liu, Z. Ding, T. Ratnarajah, and J. Xue, "On ergodic secrecy capacity of random wireless networks with protected zones," *IEEE Trans. Veh. Technol.*, to appear in 2016.

[72] E. Tekin and A. Yener, "The general Gaussian multiple-access and two-way wiretap channels: Achievable rates and cooperative jamming," *IEEE Trans. Inf. Theory*, vol. 54, no. 6, pp. 2735–2751, Jun. 2008.

[73] S. Goel and R. Negi, "Guaranteeing secrecy using artificial noise," *IEEE Trans. Wireless Commun.*, vol. 7, no. 6, pp. 2180–2189, Jun. 2008.

[74] X. Zhou and M. R. McKay, "Secure transmission with artificial noise over fading channels: Achievable rate and optimal power allocation," *IEEE Trans. Veh. Technol.*, vol. 59, no. 8, pp. 3831–3842, Oct. 2010.

[75] X. Zhang, X. Zhou, and M. R. McKay, "Enhancing secrecy with multi-antenna transmission in wireless ad hoc networks," *IEEE Trans. Inf. Forensics Security*, vol. 8, no. 11, pp. 1802–1814, Nov. 2013.

[76] Y. Zhang, H. M. Wang, Q. Yang, and Z. Ding, "Secrecy sum rate maximization in non-orthogonal multiple access," *IEEE Commun. Lett.*, to appear in 2016.

[77] T. M. Cover, "Broadcast channels," *IEEE Trans. Inf. Theory*, vol. 18, no. 1, pp. 2–14, 1972.

[78] T. M. Cover and J. A. Thomas, *Elements of information theory.* John Wiley & Sons, 2012.

[79] P. Bergmans, "Random coding theorem for broadcast channels with degraded components," *IEEE Trans. Inf. Theory*, vol. 19, no. 2, pp. 197–207, Mar. 1973.

[80] A. Carleial, "Interference channels," *IEEE Trans. Inf. Theory*, vol. 24, no. 1, pp. 60–70, Jan 1978.

[81] T. Cover and A. E. Gamal, "Capacity theorems for the relay channel," *IEEE Trans. Inf. Theory*, vol. 25, no. 5, pp. 572–584, Sep. 1979.

[82] A. J. Grant, B. Rimoldi, R. L. Urbanke, and P. A. Whiting, "Rate-splitting multiple access for discrete memoryless channels," *IEEE Trans. Inf. Theory*, vol. 47, no. 3, pp. 873–890, Mar. 2001.

[83] I. Csiszar and J. Korner, "Broadcast channels with confidential messages," *IEEE Trans. Inf. Theory*, vol. 24, no. 3, pp. 339–348, May 1978.

[84] S. Vanka, S. Srinivasa, Z. Gong, P. Vizi, K. Stamatiou, and M. Haenggi, "Superposition coding strategies: Design and experimental evaluation," *IEEE Trans. Wireless Commun.*, vol. 11, no. 7, pp. 2628–2639, Jul. 2012.

[85] J. G. Andrews, "Interference cancellation for cellular systems: a contemporary overview," *IEEE Trans. Wireless Commun.*, vol. 12, no. 2, pp. 19–29, Apr. 2005.

[86] P. Patel and J. Holtzman, "Analysis of a simple successive interference cancellation scheme in a ds/cdma system," *IEEE J. Sel. Areas Commun.*, vol. 12, no. 5, pp. 796–807, Jun. 1994.

[87] P. W. Wolniansky, G. J. Foschini, G. D. Golden, and R. A. Valenzuela, "V-blast: an architecture for realizing very high data rates over the rich-scattering wireless channel," in *International Symposium on Signals, Systems, and Electronics*, Sep. 1998, pp. 295–300.

[88] E. Gelal, J. Ning, K. Pelechrinis, T.-S. Kim, I. Broustis, S. V. Krishnamurthy, and B. D. Rao, "Topology control for effective interference cancellation in multiuser MIMO networks," *IEEE/ACM Trans. on Networking (TON)*, vol. 21, no. 2, pp. 455–468, 2013.

[89] C. Jiang, Y. Shi, Y. Hou, W. Lou, S. Kompella, and S. Midkiff, "Squeezing the most out of interference: An optimization framework for joint interference exploitation and avoidance," in *Pro. IEEE Inter. Conf. on Computer Commun. (INFOCOM)*, Mar. 2012, pp. 424–432.

[90] C. Xu, L. Ping, P. Wang, S. Chan, and X. Lin, "Decentralized power control for random access with successive interference cancellation," *IEEE J. Sel. Areas Commun.*, vol. 31, no. 11, pp. 2387–2396, Nov. 2013.

[91] J. Lee, J. G. Andrews, and D. Hong, "Spectrum-sharing transmission capacity with interference cancellation," *IEEE Trans. Commun.*, vol. 61, no. 1, pp. 76–86, Jan. 2013.

[92] R. G. Gallager, "Capacity and coding for degraded broadcast channels," *Problemy Peredachi Informatsii*, vol. 10, no. 3, pp. 3–14, 1974.

[93] R. Zhang and L. Hanzo, "A unified treatment of superposition coding aided communications: Theory and practice," *IEEE Commun. Surveys Tutorials*, vol. 13, no. 3, pp. 503–520, Mar. 2011.

[94] P. Bergmans, "A simple converse for broadcast channels with additive white gaussian noise (corresp.)," *IEEE Trans. Inf. Theory*, vol. 20, no. 2, pp. 279–280, Mar. 1974.

[95] S. L. Shieh and Y. C. Huang, "A simple scheme for realizing the promised gains

of downlink non-orthogonal multiple access," *IEEE Trans. Commun.*, to appear in 2016.

[96] J. So and Y. Sung, "Enhancing non-orthogonal multiple access by forming relaying broadcast channels." [Online]. Available: http://arxiv.org/abs/1510.07369

[97] Y. Liu, L. Wang, M. Elkashlan, T. Q. Duong, and A. Nallanathan, "Two-way relaying networks with wireless power transfer: Policies design and throughput analysis," in *Proc. IEEE Global Commun. Conf. (GLOBECOM)*, Dec. 2014, pp. 4030–4035.

[98] Z. Qin, Y. Liu, Y. Gao, M. Elkashlan, and A. Nallanathan, "Throughput analysis for compressive spectrum sensing with wireless power transfer," in *Proc. IEEE Global Commun. Conf. (GLOBECOM)*, Dec. 2015, pp. 1–6.

[99] S. A. Mousavifar, Y. Liu, C. Leung, M. Elkashlan, and T. Q. Duong, "Wireless energy harvesting and spectrum sharing in cognitive radio," in *Proc. IEEE Vehicular Technology Conference (VTC Fall)*, Sept 2014, pp. 1–5.

[100] Z. Ding, C. Zhong, D. W. K. Ng, M. Peng, H. A. Suraweera, R. Schober, and H. V. Poor, "Application of smart antenna technologies in simultaneous wireless information and power transfer," *IEEE Commun. Mag.*, vol. 53, no. 4, pp. 86–93, Apr. 2015.

[101] J. Mitola, "Cognitive radio—an integrated agent architecture for software defined radio," 2000.

[102] A. Goldsmith, S. A. Jafar, I. Maric, and S. Srinivasa, "Breaking spectrum gridlock with cognitive radios: An information theoretic perspective," *Proc. IEEE*, vol. 97, no. 5, pp. 894–914, May 2009.

[103] S. Haykin, "Cognitive radio: brain-empowered wireless communications," *IEEE J. Sel. Areas Commun.*, vol. 23, no. 2, pp. 201–220, Feb. 2005.

[104] Y. C. Liang, Y. Zeng, E. C. Y. Peh, and A. T. Hoang, "Sensing-throughput tradeoff for cognitive radio networks," *IEEE Trans. Wireless Commun.*, vol. 7, no. 4, pp. 1326–1337, April 2008.

[105] Z. Qin, Y. Gao, and C. G. Parini, "Data-assisted low complexity compressive spectrum sensing on real-time signals under sub-nyquist rate," *IEEE Trans. Wireless*

Commun., vol. 15, no. 2, pp. 1174–1185, Feb. 2016.

[106] Z. Qin, Y. Gao, M. Plumbley, and C. Parini, "Wideband spectrum sensing on real-time signals at sub-nyquist sampling rates in single and cooperative multiple nodes," *IEEE Trans. Signal Process.*, vol. 64, no. 12, pp. 3106–3117, June 2016.

[107] Z. Qin, L. Wei, Y. Gao, and C. G. Parini, "Compressive spectrum sensing augmented by geo-location database," in *IEEE Wireless Communications and Networking Conference Workshops (WCNCW),*, Mar. 2015, pp. 170–175.

[108] Z. Qin, Y. Gao, M. D. Plumbley, C. G. Parini, and L. G. Cuthbert, "Efficient compressive spectrum sensing algorithm for M2M devices," in *IEEE Global Conference on Signal and Information Processing (GlobalSIP)*, Dec 2014, pp. 1170–1174.

[109] E. Larsson, O. Edfors, F. Tufvesson, and T. Marzetta, "Massive MIMO for next generation wireless systems," *IEEE Commun. Mag.*, vol. 52, no. 2, pp. 186–195, Feb. 2014.

[110] H. Huh, A. M. Tulino, and G. Caire, "Network MIMO with linear zero-forcing beamforming: Large system analysis, impact of channel estimation, and reduced-complexity scheduling," *IEEE Trans. Inf. Theory*, vol. 58, no. 5, pp. 2911–2934, 2012.

[111] K. Hosseini, W. Yu, and R. S. Adve, "Large-scale MIMO versus network MIMO for multicell interference mitigation," vol. 8, no. 5, pp. 930–941, 2014.

[112] H.-S. Jo, Y. J. Sang, P. Xia, and J. G. Andrews, "Heterogeneous cellular networks with flexible cell association: A comprehensive downlink SINR analysis," *IEEE Trans. Wireless Commun.*, vol. 11, no. 10, pp. 3484–3495, 2012.

[113] Y. Liu, L. Wang, S. A. R. Zaidi, M. Elkashlan, and T. Q. Duong, "Secure D2D communication in large-scale cognitive cellular networks with wireless power transfer," in *Proc. Inter. Conf. on Commun. (ICC)*, 2015, pp. 4309–4314.

[114] M. Bloch, J. Barros, M. R. D. Rodrigues, and S. W. McLaughlin, "Wireless information-theoretic security," *IEEE Trans. Inf. Theory*, vol. 54, no. 6, pp. 2515–2534, June 2008.

[115] W. K. D. Stoyan and J. Mecke, *Stochastic Geometry and its Applications*, 2nd ed. John Wiley and Sons, 1996.

[116] H. ElSawy, E. Hossain, and M. Haenggi, "Stochastic geometry for modeling, analysis, and design of multi-tier and cognitive cellular wireless networks: A survey," *IEEE Commun. Surveys Tutorials*, vol. 15, no. 3, pp. 996–1019, Third 2013.

[117] M. Haenggi, *Stochastic geometry for wireless networks*. Cambridge University Press, 2012.

[118] Z. Qin, Y. Liu, Y. Gao, M. Elkashlan, and A. Nallanathan, "Throughput analysis of wireless powered cognitive radio networks with compressive sensing and matrix completion," 2016. [Online]. Available: http://arxiv.org/abs/1601.06578

[119] T. M. Cover and J. A. Thomas, "Elements of information theory 2nd edition," 2006.

[120] E. Hildebrand, "Introduction to numerical analysis," *NewYork, NY, USA: Dover,*, 1987.

[121] J. N. Laneman, D. N. Tse, and G. W. Wornell, "Cooperative diversity in wireless networks: Efficient protocols and outage behavior," *IEEE Trans. Inf. Theory*, vol. 50, no. 12, pp. 3062–3080, 2004.

[122] M. Haenggi, *Stochastic Geometry for Wireless Networks*. Cambridge, U.K.: Cambridge Univ. Press, 2012.

[123] J. Venkataraman, M. Haenggi, and O. Collins, "Shot noise models for outage and throughput analyses in wireless ad hoc networks," in *Military Commun. Conf. (MILCOM)*, 2006, pp. 1–7.

[124] H. A. David and N. Nagaraja, *Order Statistics*, 3rd ed. John Wiley, 2003.

[125] I. S. Gradshteyn and I. M. Ryzhik, *Table of Integrals, Series and Products*, 6th ed. New York, NY, USA: Academic Press, 2000.

[126] P. C. Pinto, J. Barros, and M. Z. Win, "Secure communication in stochastic wireless networkspart I: Connectivity," *IEEE Trans. Inf. Forensics Security*, vol. 7, no. 1, pp. 125–138, Feb. 2012.

[127] N. Romero-Zurita, D. McLernon, M. Ghogho, and A. Swami, "PHY layer security based on protected zone and artificial noise," *IEEE Signal Process. Lett.*, vol. 20, no. 5, pp. 487–490, May 2013.

[128] S. Shafiee and S. Ulukus, "Achievable rates in Gaussian MISO channels with

secrecy constraints," in *Proc. of IEEE International Symposium on Information Theory (ISIT)*, 2007, pp. 2466–2470.

[129] S. Goel and R. Negi, "Guaranteeing secrecy using artificial noise," *IEEE Trans. Wireless Commun.*, vol. 7, no. 6, pp. 2180–2189, Jun. 2008.

[130] N. Yang, M. Elkashlan, T. Duong, J. Yuan, and R. Malaney, "Optimal transmission with artificial noise in MISOME wiretap channels," *IEEE Trans. Veh. Technol.*, to appear in 2016.

[131] O. Benjamin, "The null space of a matrix," 2015. [Online]. Available: https://cseweb.ucsd.edu/classes/wi15/cse252B-a/nullspace.pdf

[132] G. Fodor, E. Dahlman, G. Mildh, S. Parkvall, N. Reider, G. Miklós, and Z. Turányi, "Design aspects of network assisted device-to-device communications," *IEEE Commun. Mag.*, vol. 50, no. 3, pp. 170–177, Mar. 2012.

[133] C. Ma, W. Wu, Y. Cui, and X. Wang, "On the performance of successive interference cancellation in D2D-enabled cellular networks," in *Pro. IEEE Inter. Conf. on Computer Commun. (INFOCOM)*, Apr. 2015, pp. 37–45.

[134] X. Rao and V. K. N. Lau, "Distributed compressive CSIT estimation and feedback for FDD multi-user massive MIMO systems," *IEEE Trans. Signal Process.*, vol. 62, no. 12, pp. 3261–3271, Jun. 2014.

[135] C. A. Coelho, "The generalized integer Gamma distribution a basis for distributions in multivariate statistics," *Journal of Multivariate Analysis*, vol. 64, no. 1, pp. 86–102, 1998.